CANADIAN THESES ON MICROFICHE

THÈSES CANADIENNES SUR MICROFICHE

National Library of Canada
Collections Development Branch

Canadian Theses on
Microfiche Service

Ottawa, Canada
K1A 0N4

Bibliothèque nationale du Canada
Direction du développement des collections

Service des thèses canadiennes
sur microfiche

NOTICE

The quality of this microfiche is heavily dependent upon the quality of the original thesis submitted for microfilming. Every effort has been made to ensure the highest quality of reproduction possible.

If pages are missing, contact the university which granted the degree.

Some pages may have indistinct print especially if the original pages were typed with a poor typewriter ribbon or if the university sent us an inferior photocopy.

Previously copyrighted materials (journal articles, published tests, etc.) are not filmed.

Reproduction in full or in part of this film is governed by the Canadian Copyright Act, R.S.C. 1970, c. C-30. Please read the authorization forms which accompany this thesis.

AVIS

La qualité de cette microfiche dépend grandement de la qualité de la thèse soumise au microfilmage. Nous avons tout fait pour assurer une qualité supérieure de reproduction.

S'il manque des pages, veuillez communiquer avec l'université qui a conféré le grade.

La qualité d'impression de certaines pages peut laisser à désirer, surtout si les pages originales ont été dactylographiées à l'aide d'un ruban usé ou si l'université nous a fait parvenir une photocopie de qualité inférieure.

Les documents qui font déjà l'objet d'un droit d'auteur (articles de revue, examens publiés, etc.) ne sont pas microfilmés.

La reproduction, même partielle, de ce microfilm est soumise à la Loi canadienne sur le droit d'auteur, SRC 1970, c. C-30. Veuillez prendre connaissance des formules d'autorisation qui accompagnent cette thèse.

THIS DISSERTATION
HAS BEEN MICROFILMED
EXACTLY AS RECEIVED

LA THÈSE A ÉTÉ
MICROFILMÉE TELLE QUE
NOUS L'AVONS REÇUE

NL 339 (r. 85/09)

Canada

UNIVERSITÉ D'OTTAWA
UNIVERSITY OF OTTAWA

To Sharon

PREFACE

The electrochemical hydrogen evolution reaction (h.e.r.) has served as a model system in the development of ideas on the kinetics of electrode processes. Theoretical and experimental investigations on the kinetics of the h.e.r. have raised two important general questions concerning the nature of heterogeneous coupled electron/atom transfer reactions.

The first relates to the nature of the activation process in proton discharge: in the elaborate treatment of Dogonadze, Kuznetsov and Levich, the required activation for proton discharge to occur was considered to arise from long-range fluctuations in solvent polarization, while earlier treatments based on the pioneering work of Gurney and of Butler involved a more specific thermal activation of an O-H bond in the solvated H_3O^+ ion that was undergoing discharge. Thus two rather different views on the nature of the activation process have been advanced.

The second question concerns the experimentally-observed temperature-dependence of the Tafel slope, b. In particular, b only rarely exhibits the conventionally-assumed temperature-dependence ($\sim RT/\alpha F$), and is usually found to be temperature-independent or to have some temperature-independent component. It has been noted that, formally, for b to be independent of temperature, the entropy of activation should be a function of electrode potential, and theoretical reasons for the origin of such an effect have been suggested.

In the present work, the kinetics of the h.e.r. at different

metal electrode surfaces and the electrochemical desorption of strongly bound H at Pt from different states of solvation of H_3O^+ were investigated. It is shown, from a consideration of the experimentally determined potential-dependence of the entropy and enthalpy of activation for the h.e.r. at Hg, that an "unconventional" temperature-dependence of b is in fact expected.

Some of the work described in this thesis has already been published or submitted for publication and other papers are in preparation as follows:

a) B.E. Conway and D.F. Tessier, "Comparison of the Kinetics of Cathodic H_2 Evolution from the Unhydrated H_3O^+ Ion and its Hydrated Form $H_9O_4^+$: Frequency Factor Effects and Modes of Activation", Int. J. Chem. Kinetics, 13(1981)925.

b) B.E. Conway, Lijun Bai and D.F. Tessier, "Data Collection and Processing of Open Circuit Potential-Decay Measurements Using a Digital Oscilloscope: Derivation of the H-Capacitance behaviour of H_2-evolving, Ni-based Cathodes", J. Electroanal. Chem., 161(1984)39.

c) B.E. Conway and D.F. Tessier, "Proton Discharge from the Unhydrated and Hydrated States of the H_3O^+ Ion at Electrodes: Frequency Factors and Activation Energy Differences", to be submitted.

d) B.E. Conway, D.F. Tessier and D.P. Wilkinson, "Experimental Evidence for the Potential-Dependence of Entropy of Activation in Electrochemical Reactions in Relation to The Temperature-Dependence of Tafel Slopes", in preparation.

e) D.F. Tessier and B.E. Conway, "The Problem of Correction for Ohmic Potential Drop in Linear Potential Sweep Experiments and the Derivation of s_o Values for Electrode Surface Processes", submitted for publication (Electrochim. Acta).

The following publications resulted from collaboration with colleagues in the Department of Chemistry during the author's stay at the University of Ottawa:

a) J. Mozota, B. Barnett, D. Tessier, H. Angerstein-Kozlowska and B.E. Conway, "The Use of a Minicomputer for Data Collection and Treatment in the Study of Electrochemical Surface Processes", Anal. Chim. Acta, 183(1981)191.

b) J. Mozota, B.E. Conway and D.F. Tessier, "A Computer-Based Programmable Waveform Generator", Anal. Chim. Acta, 141(1982)383.

c) B.A. Morrow and D.F. Tessier, "Velocity and Energy Distributions in Gases", J. Chem. Ed., 59(1982)193.

ACKNOWLEDGEMENT

I am grateful for the generous help and guidance which my research director, Prof. Brian E. Conway, has provided throughout the conduct of this work. His willingness to undertake novel non-electrochemical experiments in the course of the research has made my stay in the Electrochemistry Group an especially stimulating one. I am also grateful for having had the opportunity to participate actively in the introduction of a number of modern and powerful experimental techniques.

I wish to express my sincere thanks to :

My colleagues for enriching my time here in many ways;

The members of the support staff who cheerfully made so many things possible;

Jose Mozota, Brian Barnett, Halina Angerstein-Kozlowska, Wojtek Halliop, David Harrington, Lijun Bai and David Wilkinson for rewarding scientific, and other, collaborations;

Prof. B.A. Morrow and Richard McFarlane for their help in recording and interpreting Raman spectra, and for stimulating discussions;

Prof. J. Holmes, John Krause and Peter Burghers for the helpful suggestions and mass spectral analyses required for the ^{18}O labelling work;

Prof. I. Smith for solid state NMR measurements and the interpretation thereof;

The members of the thesis examination board, Professors M. J. Weaver (Purdue U.), K. J. Laidler (U. of Ottawa) and B. A. Morrow (U. of Ottawa), for their careful reading of the thesis and helpful discussion and suggestions;

The province of Ontario and the Natural Sciences and Engineering Research Council Canada for post-graduate scholarships.

I am grateful to my parents for fostering qualities in their children which have served us well in all of our undertakings.

Finally, I wish to express my heartfelt love and gratitude to Sharon, my wife, whose generous support, sacrifice and understanding have enabled this venture to be undertaken. It is she who has sustained our family these past years, while at the same time taking a degree in Classical Studies at the "other" university in Ottawa.

Joel and David, thank you too.

CONTENTS

LIST OF TABLES

LIST OF FIGURES

ABSTRACT

The mechanism of the activation process in coupled atom/electron transfer processes, such as is involved in the cathodic H_2 evolution reaction, is not yet well understood. In particular, two distinguishable modes of activation have been considered: " OH bond stretching" or "solvation shell reorganization". The work described in this thesis is designed to provide new results that may contribute to a better understanding of this problem by examination of the entropy and energy components of the free energy of activation in proton transfer and neutralization at electrodes, from the hydrated proton in two well-defined states.

Experiments are described in which the kinetics of the cathodic hydrogen evolution reaction (h.e.r.) from the unhydrated H_3O^+ ion in pure $CF_3SO_3^-H_3O^+$ are compared with those from a dilute (1 M) aqueous solution of CF_3SO_3H where the proton is mainly in a fully hydrated state as "$H_9O_4^+$". From the acid hydrate, which exists as the ionic compound $CF_3SO_3^-H_3O^+$, rates of H_2 evolution at Ni and Pt electrodes, measured at a given overpotential or expressed as exchange current densities, are between 3.5 and 20 times slower than those from the same electrolyte in dilute (1 M) aqueous solution. Allowing for the concentration differences in these two solution media and double-layer effects, a "slowness" factor for the h.e.r. in the $CF_3SO_3^-H_3O^+$ melt of ca. 9.4 and 216 times is indicated.

In the experimentally accessible range of current densities,

the rate of the h.e.r. at Hg in the $CF_3SO_3^-H_3O^+$ melt is greater than in 1 M aqueous CF_3SO_3H, e.g. at = -0.8 V RHE, by a factor of 60 times. The h.e.r. at Hg in 1 M aqueous CF_3SO_3H showed the usual Tafel slope of ca. 0.12 V, while in the $CF_3SO_3^-H_3O^+$ melt, a rather unusual (for the h.e.r. at Hg in acidic solution) value 0.09 V was found. Extrapolation of the linear Tafel relation for the h.e.r. at Hg in these two media indicates that, owing to the difference in Tafel slopes, the rates become equal at an overpotential of ca. 0.17 V. A relatively small H/D kinetic isotope effect (2.6 x) was found with the $CF_3SO_3^-H_3O^+/D_3O^+$ melt; the smaller distance of approach of the H_3O^+ ion to the electrode in the monohydrate melt than in 1 M CF_3SO_3H, especially at potentials where H_2 is evolved, together with the similar Tafel slopes in the H_3O^+ (D_3O^+) melt, does not indicate the presence of significant quantum-mechanical proton tunneling.

Apparent activation parameters were evaluated from the temperature-dependence of the steady-state polarization behaviour for the h.e.r from the two media of interest at the above metals. The activation parameters for steady-state hydrogen evolution at Hg, Ni, and Pt indicate that differences of heats of activation determine the relative rates of proton discharge in the two media.

By means of non-isothermal potential measurements, "true" activation parameters for the H_2 evolution reaction at Hg were derived as a function of electrode potential; it is shown that the true entropy of activation or the corresponding frequency factor for the proton discharge step in cathodic H_2 evolution is

appreciably potential-dependent, and not constant as usually assumed. This entropic component makes a significant contribution to the diminution of free energy of activation which is usually associated with change of electrode potential and attributed in previous work to an energy change due to the change of Fermi level.

This situation leads to an expected temperature-dependence of Tafel slopes, b, which is not that conventionally assumed viz, $b = 2.3 \pm RT/\beta F$. The actual behaviour is rather of the form $b = 2.3 \pm RT/(\beta_H + \beta_S T)$ where β_H and $\beta_S T$ are enthalpic and entropic components, respectively, of the overall symmetry factor, β, or transfer coefficient, α.

The observed behaviour shows that the effects of potential on electrode reaction rates are to be represented not as usually assumed by a simple variation of the Fermi level by "$\pm \Delta VF$" with a corresponding relative change of transition state energy by $\beta \Delta VF$, but in addition by an appreciable variation of the molecular state of the transition complex with change of field across the double-layer. The origin of such effects could be the changing solvational and solvent-structure environment of the double-layer due to potential-dependent solvent dipole orientation and changing volume fraction of solvated reactant ions in the interphase.

The kinetics of desorption of strongly bound H at Pt in the $CF_3SO_3^-H_3O^+$ melt and in 1 M aqueous CF_3SO_3H was investigated by means of linear potential sweep cyclic-voltammetry; this system allows an elementary electrosorption step to be studied, e.g.

independently of the continuous hydrogen evolution reaction. In this case, the measured values of s_o and hence rates for H desorption at Pt were ca. 10 x greater in the 1 M aqueous CF_3SO_3H than in the $CF_3SO_3^-H_3O^+$. Analysis of the derived apparent activation parameters for the desorption of H from Pt indicates that, unlike in the case of the h.e.r. mentioned above, this difference in rates is due primarily to frequency factor effects related to the entropy of activation. H/D kinetic isotope effects were also evaluated for H desorption from Pt.

^{18}O-labelling experiments indicate that, in the $CF_3SO_3^-H_3O^+$ melt, anodically evolved oxygen gas contains O atoms from H_3O^+ only; no oxygen originating in the oxy-anion $CF_3SO_3^-$ was detected. Gaseous products indicative of the anodic decomposition of the anion were not found. At constant electrode potential in $CF_3SO_3^-H_3O^+$, the kinetics of growth of sub-monolayer surface oxide film at Pt showed a linear oxide-charge vs log[time] growth curve similar to that found in dilute aqueous acid solution.

CHAPTER 1

INTRODUCTION

1. The H.E.R. as a Prototype Electrochemical Atom Transfer Reaction

The electrochemical hydrogen evolution reaction (h.e.r.) has often been regarded as a model for the investigation and kinetic treatment of more complex multistep electrode reactions[1,2]. Indeed, the fundamental understanding of interfacial charge transfer processes has gained from the study of this prototypical electrochemical atom transfer reaction and the basis of its treatments has found diverse applications in investigations of metal deposition, corrosion, organic electrode reactions, electrosorption processes, redox reactions and especially electrocatalysis. At first considered a simple model reaction, the h.e.r. has provided a variety of interesting and complex experimental and theoretical problems: the role of electron and proton tunneling processes, evaluation of kinetic isotope effects, the behaviour of adsorbed kinetically-involved intermediates, and the significance of widely varying kinetics dependent on electrode material and surface properties, solution composition, and anion and neutral molecule adsorption.

The h.e.r. was one of the first chemical processes to be treated by means of quantum mechanics[3] and served as an example for one of the earliest applications of activated complex theory to an heterogeneous reaction involving species in solution[4].

Recent developments in ideas concerning the nature of the the discharge step in coupled electron-atom transfer reactions

have centered on the solvated-proton discharge step in the h.e.r.

2. Problems Previously Addressed in Respect of the H.E.R.

(i) Consecutive Step Mechanisms and Tafel Slopes in Relation to H Coverage as f(V)

The electrochemical hydrogen evolution reaction at metal electrodes proceeds by the following possible steps:

(discharge, D) $M + H_3O^+(aq.) + e^- = MH_{ads} + H_2O$ (1-1)

$1-\theta_H \quad C_s \quad \text{at } V \quad \theta_H$

followed by the alternative succeeding desorption processes,

(electrochemical desorption, E) $MH_{ads} + H_3O^+ + e^- = M + H_2 + H_2O$ (1-2)

$1-\theta_H \quad C_s \quad \text{at } V \quad 1-\theta_H$

or

(heterogeneous chemical recombination, C) $MH_{ads} + MH_{ads} = H_2 + 2M$ (1-3)

$\theta_H \quad \theta_H \quad 1-\theta_H$

where θ_H is the fraction of the surface covered by adsorbed H, $(1-\theta_H)$ is the corresponding fraction of unoccupied metal sites, M, and C_s is an appropriate surface concentration of H_3O^+ ions, e.g. as determined by the state of ion distribution in the double-layer and V is the electrode potential. Analogous equations can be written for the h.e.r. from H_2O as the proton source, e.g., as in alkaline solution.

A number of additional reaction intermediates have also been proposed in the literature: the H_2^+ molecule ion[5], the hydride ion[6] H^-, the hydrated electron e_{aq}^- [7,8] and alkali metal atom intermediates[9,10] in solutions containing ions of such metals. The participation of H_2^+ is not well supported by experiment[10,11] while Conway[12,13] has shown that e_{aq}^- is unlikely to be important under ordinary polarization conditions in aqueous media. For

hydrogen evolution from aqueous acid solutions, H^- is too unstable to be regarded as a reaction intermediate[14].

An empirical equation due to Tafel[15] relates the current density, i, flowing in an electrochemical electron transfer reaction in terms of the overpotential, η, defined as the difference between the operating electrode potential, V, and the corresponding reversible value, V_{rev}; thus η ($= V - V_{rev}$) is given by

$$\eta = a + b \log(i) \qquad (1\text{-}4)$$

where b is the so-called Tafel slope and the associated transfer coefficient, α , is given by $\alpha = 2.3RT/bF$. The value of α for a given reaction depends on: a) the value of the symmetry factor β (see section (viii), p.55) if a charge transfer step is rate-determining; b) the type of sequence of steps in the reaction pathway and c) the potential-dependence of coverage of the surface by the reaction intermediates, e.g. adsorbed H in the h.e.r. Parsons[6] and Bockris[16] have derived b values and the related transfer coefficients* for limiting cases of the reaction scheme in eqns.(1-1,1-2,1-3); the resulting values of are shown in Table 1-1.

---

* can be related to the total number of electrons passed in the overall reaction or in the rate-controlling step through β and the stoichiometric number ν. This matter has been treated by Horiuti[17], Bockris[2] and by Gileadi[18].

Table 1-1

Transfer Coefficients for Various Mechanistic Routes in the H.E.R.

Mechanism*	α**	Conditions
$D^* + C$	0.5	low $\lvert\eta\rvert$
$D + C^*$	2.0	$\theta_H \ll 1$
$D^* + E$	0.5	--
$D + E^*$	1.5	$\theta_H \ll 1$
coupled $D^* + E^*$	0.5	--

* Rate-determining step. D = discharge, eqn.(1-1); E = electrochemical desorption, eqn.(1-2); C = heterogeneous chemical recombination, eqn.(1-3).
** Assuming $\beta = 0.5$ in charge transfer steps.

For both D, C mechanisms considered above, chemical desorption leads to a limiting current at sufficiently large cathodic overpotentials; practically, under these conditions, the potential-dependent E step becomes more facile and eventually provides an alternate and usually preferred path for the desorption of H_{ads} to give H_2.

Values of $\alpha > 0.5$ can arise depending on: a) the particular rate-determining step and b) the potential dependence of coverage of electroactive intermediates. Values of $\alpha < 0.5$ may arise with reactions proceeding at barrier-layer films which exhibit non-Ohmic charge transport through them.

The potential dependence of the coverage of, e.g. H will affect the overall rate equation; the potential dependence of equilibrium coverage can be represented to a first approximation by an electrochemical Langmuir isotherm[19],

$$\theta_H = \frac{KC \exp(-VF/RT)}{1 + KC \exp(-VF/RT)} \qquad (1\text{-}5)$$

where K is an equilibrium constant for adsorption of H and C is the concentration of H_3O^+ ions, as in H^+ discharge from aqueous solution; in eqn.(1-5), V is taken negative for a cathodic reaction such as discharge of H^+. This expression for the coverage corresponds to the case where the discharge step (D, eqn.(1-1)) is taken to be at quasi-equilibrium. At large cathodic V, the terms in θ_H or $(1-\theta_H)$ in the kinetic equations for the rate-determining step then are given by $\theta_H = KC \exp(-VF/RT)$, or $(1-\theta_H) = (KC)^{-1}\exp(VF/RT)$; thus terms in VF/RT arise in the rate expressions. For example, in the case of rate-determining electrochemical desorption (D, eqn.(1-2)), we have

$$\frac{d \log(i)}{d V} = \frac{\beta F}{RT} + \frac{d \log(\theta_H)}{d V} = \frac{\beta F}{RT} + \frac{1}{\theta_H}\frac{d\theta_H}{d V} \qquad (1\text{-}6)$$

where $d\theta_H/dV$ ($= C_\phi/Q$) will be recognized as the adsorption pseudocapacitance[20,21], C_ϕ, divided by the charge for monolayer coverage, Q, of electroactive adsorbed H. The Temkin isotherm which includes a θ-dependence of K in eqn.(1-5) through a factor $\exp(g\theta)$ yields an expression analogous to eqn.(1-6) for the Tafel slope of the form[22,23]

$$b = \frac{dV}{d \log(i)} = \frac{2.3RT}{F}\left| \beta + \frac{1-\theta_H}{1 + g\theta_H(1-\theta_H)} \right| \qquad (1\text{-}7)$$

In general, the Tafel slope will consist of a potential-dependent coverage term, in addition to the charge transfer factor related to β.

In the analysis of eqns.(1-1,1-2,1-3), steady-state

conditions of current and coverage can be considered, provided that the concentration of H_3O^+ and of H_2 are constant; thus a complete steady-state treatment[16] can be given for reaction (1-1) followed by the desorption steps in eqn.(1-2) and/or eqn.(1-3), including the back reaction for each of these steps. The required steady-state coverage, θ_{ss}, is then given by the requirement

$$d\theta_H/dt = 0$$
$$= k_1^V(1-\theta_H) - k_{-1}^V\theta_H - k_2^V\theta_H + k_{-2}^V(1-\theta_H) - k_3^V\theta_H + k_{-3}^V(1-\theta_H) \qquad (1-8)$$

which then yields

$$\theta_{ss} = \frac{-B + (B^2 - 4AC)^{1/2}}{2A} \qquad (1-9a)$$

where $A = k_3 - k_{-3}$

$B = k_1^V + k_{-1}^V + k_2^V + k_{-2}^V + 2k_{-3}$

$C = -k_1^V - k_{-2}^V - k_{-3}$

or, when the chemical recombination reaction (1-3) is omitted, θ_{ss} is given by

$$\theta_{ss} = (k_{-1}^V + k_{-2}^V) / (k_1^V + k_{-1}^V + k_2^V + k_{-2}^V) \qquad (1-9b)$$

where, for brevity, k_i^V has been used to refer to the product of potential-dependent rate constants and any applicable concentration for the i-th reaction, e.g. $k_i^V = k_i^o C_i \exp(\pm\beta VF/RT)$.

The steady-state current for an overall process involving passage of n electrons is then given by

$$i_{ss} = -nF[\, k_1^V(1-\theta_{ss}) - k_{-1}^V\theta_{ss} + k_2^V\theta_{ss} - k_{-2}^V(1-\theta_{ss})\,] \qquad (1-10)$$

where the contributions of the chemical recombination reaction (1-3), if included, are contained implicitly in the θ_{ss} values

(see eqns.(1-9a,1-9b)). This analysis leads to the expectation of limiting coverages as shown in Table 1-2 for sufficiently large cathodic or anodic polarizations.

Table 1-2

Limiting Values of H Coverage for Possible Mechanisms in the H.E.R.

Mechanism*	θ_H(cathodic)	θ_H(anodic)
D	1	0
E	0	1
DE	$k_1^o/(k_1^o + k_2^o)$	$k_{-2}^o/(k_{-2}^o + k_{-1}^o)$
DC	1	0
DEC	$k_1^o/(k_1^o + k_2^o)$	$k_{-2}^o/(k_{-2}^o + k_{-1}^o)$

* D = discharge, eqn.(1-1); E = electrochemical desorption, eqn.(1-2); C = chemical recombination, eqn.(1-3).

For the DE (and DEC) mechanism, limiting cathodic coverages, $\theta_H < 1$, will occur, depending on the relative values of the composite rate constants shown in Table 1-2. In practice, the concentration of H_2 is usually rather low (< 1 mM) and so back-reaction steps involving H_2 are expected to become mass-transport limited, especially at anodic overpotentials; this limitation is much less severe in other ion discharge reactions, e.g. Br^- ion discharge where appreciable Br_2 concentrations in a suitable solvent such as acetonitrile may be used. This solubility question aside, for a particular range of values of rate constants, it is even possible to have θ_H decrease upon going to more cathodic potentials, e.g. θ_H^{lim}(anodic) > θ_H^{lim}(cathodic), as shown for the

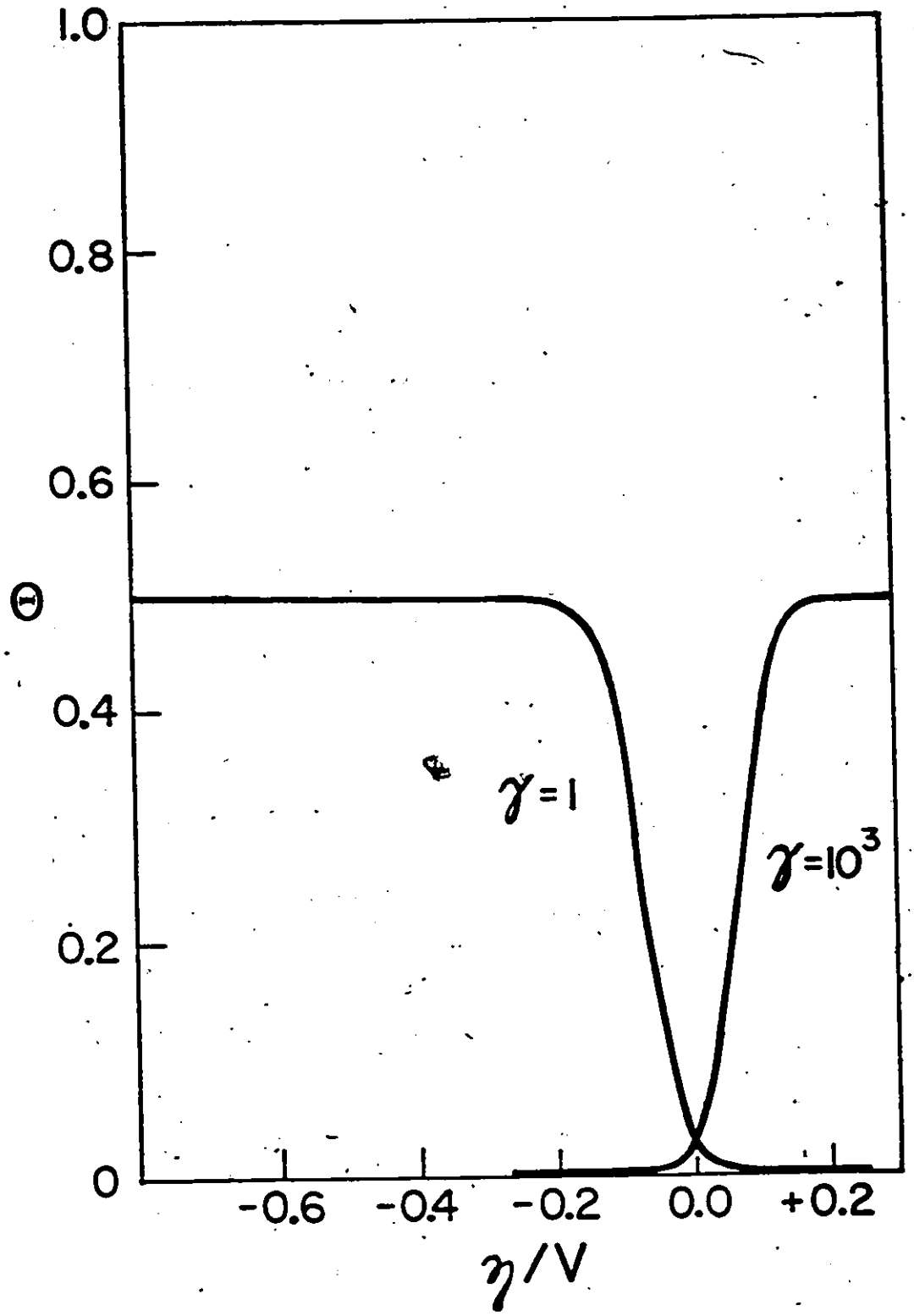

Fig.1-1 Variation of θ_{ss} in the DE mechanism with potential for various values of the rate parameters: $k_2^o/k_{-2}^o = 1000$ and $\gamma = k_2^o/k_1^o$

DE mechanism in Fig.1-1. It is interesting to note that this seemingly novel behaviour leads to a "negative" pseudo-capacitance, $Qd\theta_{ss}/dV$. Regardless of the choice of rate constants, the DE and DEC mechanisms (under activation control) lead to $b = \pm 2.3RT/\beta F$ at sufficiently anodic or cathodic potentials.

An additional feature of the DE mechanism arises in relation to the linear regions of the cathodic and anodic branches of the Tafel plot (cf. Fig.1-2): extrapolation of these linear regions, i.e., from appreciable magnitudes of η, gives an intersection point the potential of which differs from the reversible potential. An asymmetry in the respective curves as $\eta \to 0$, i.e., as $i \to 0$, is also evident in this figure. In contrast, the simple Butler-Volmer equation[24,25] for the current of an electrochemical reaction, viz.

$$i = zF\,[k_f \exp[\alpha VF/RT] - k_r \exp[-(1-\alpha)VF/RT]\,] \qquad (1\text{-}11)$$

leads to the usual intersection of the extrapolated cathodic and anodic log i vs V relations at the reversible potential.

In the DE mechanism, both reactions (1-1) and (1-2) involve the reduction of a proton from H_3O^+ to yield MH_{ads} (D, eqn.(1-1)) or H_2 (E, eqn.(1-2)), while the electrochemical desorption step (E) also involves breaking an $M\text{-}H_{ads}$ bond; considering the relative magnitudes of the energies of these bonds, one would expect, from a generalized Brønsted point of view, that the factors in θ_H and $(1-\theta_H)$ aside, the intrinsic rate of step E should be greater than that for step D since $E_{H-H} > E_{M-H}$.

The Tafel slope, b, or the related transfer coefficient α,

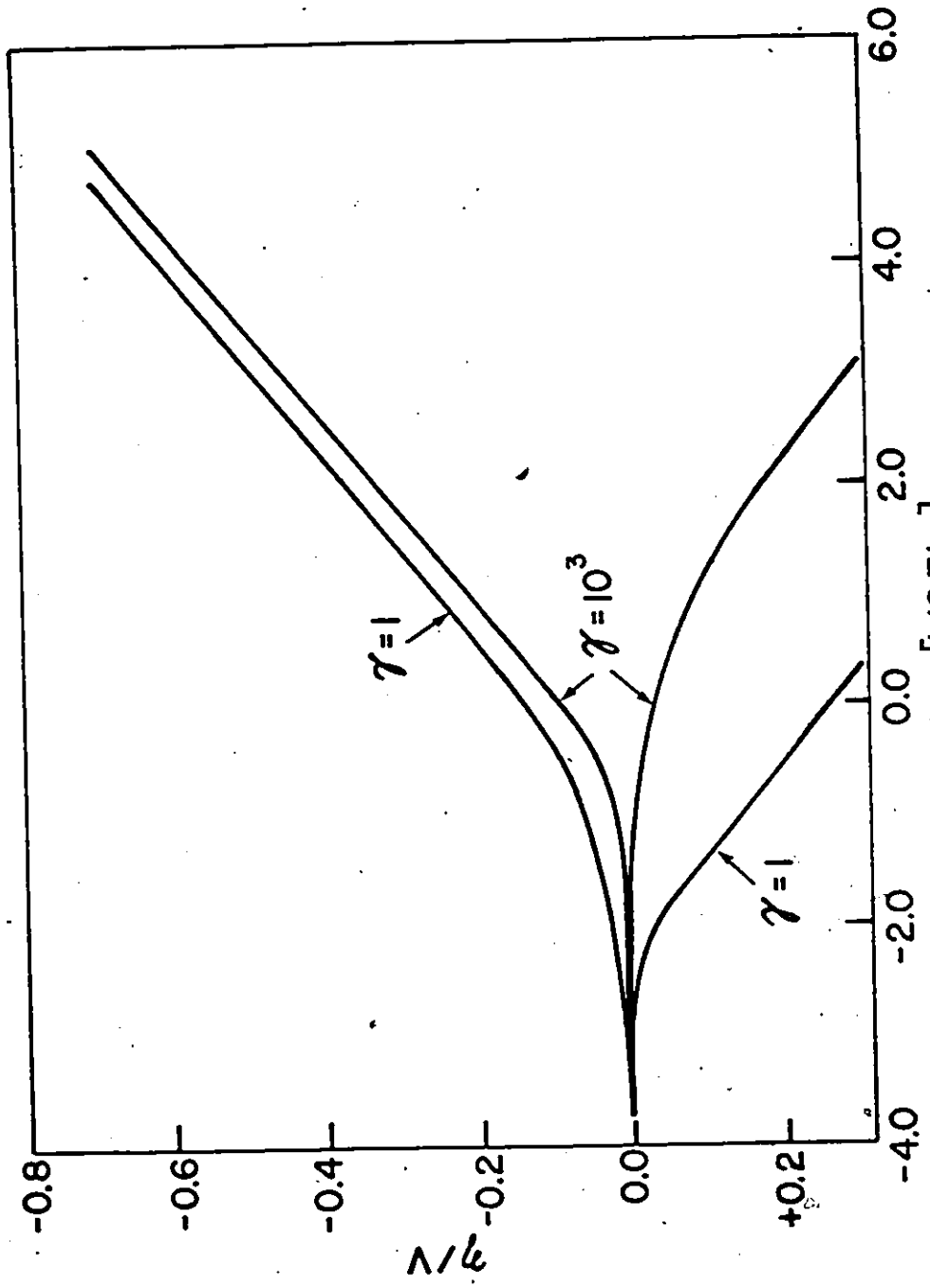

Fig.1-2 Cathodic and anodic branches of the Tafel plot for the DE mechanism (see Fig.1-1).

does not provide unique criteria for diagnosis of a mechanism for the h.e.r. in a particular system. The value $\alpha = 2$ expected for heterogeneous chemical recombination control is only observed over a limited potential range at Pt but this value may also arise from the effect of slow diffusion of H_2 away from this catalytic electrode as discussed by Breiter[26] and Schuldiner[27]. In the analogous anodic halogen evolution reactions, such Tafel behaviour characteristic of chemical recombination control is complicated by temperature- and potential-dependent halide adsorption as well as by the state of surface oxidation of the anode metal, e.g. Pt[28].

(ii) Relation of Mechanism and Rates (log i_o) to the Electron Work Function ϕ_M and Energy of H-Adsorption

The rate of the h.e.r., as characterized by the exchange current density, i_o, is found to vary over ca. 10 orders of magnitude, depending on the electrode metal used; thus there is considerable interest in identifying the metallic property(ies) which gives rise to this wide variation. In the 1920's, Ellingham and Allmand[29] and Bonhoeffer[30] noted that the overvoltages for the h.e.r. on different metals at a given current density varied periodically with atomic number. More recently, interest has focussed on the effect of the metal work function, ϕ_M, and of H-adsorption energy on this electrocatalytic behaviour[31,32,33,34].

From a consideration of an appropriate thermodynamic cycle, the effect of the work function, ϕ_M, on the free energy of reaction for electron transfer to an ion may be shown to be

given[35] by:

$$\Delta G^{\circ}_{R} = -zF\phi^{\circ}_{R} = z\phi_{M} - I + \delta(\Delta G^{\circ}_{s,ion}) \qquad (1\text{-}12)$$

where I and $\Delta G^{\circ}_{s,ion}$ refer to the ionization energy and solvation energies of the reactant/product ions, respectively. This direct dependence of ΔG°_{R} on ϕ_{M} gives rise to a change of $\beta z \Delta\phi_{M}$ in $\Delta G^{o\neq}$ as the electrode metal is changed, owing to a "vertical" shift of the potential energy curve of the initial state. However, $\Delta G^{o\neq} = \Delta G^{o\neq} - \Delta\phi^{\circ}_{R}zF$; but according to eqn.(1-12), $\Delta\phi^{\circ}_{R}$ is also determined by ϕ_{M}, so that the electrochemical standard free energy of activation is <u>independent</u> of the work function. Thus the observed correlation[32,33] between log i_{o} for the h.e.r. and the work function of the electrode metal must arise from an indirect effect.

Ruetschi and Delahay[36], and Conway and Bockris[32] showed that this behaviour paralleled the dependence of the H-adsorption energy on the work function of the metal. Some indication of the h.e.r. mechanism at various metals was deduced from the dependence of log i_{o} on the heat of H-adsorption[32]: a) in the case where $H^{+} + e_{M} + M = MH$ is the rate-determining step, a more favourable ΔH_{ads}, which stabilizes the final state, would result in a smaller activation energy; b) whereas if $H^{+} + e_{M} + MH = M + H_{2}$ or $2MH = 2M + H_{2}$ were the rate-determining steps, a more favourable ΔH_{ads}, which stabilizes the initial state, will give rise to a larger activation energy. Analogous arguments have been used to explain the experimentally observed relation between log i_{o} for the h.e.r. and the number of d-holes per atom in transition metal alloys[37].

Parsons[38] has considered a more general relation between the

exchange current for the h.e.r. and the heat of adsorption, for different assumed forms of the equilibrium adsorption isotherm for the overall reaction. A "volcano" relationship (reminiscent of those found in gas/solid heterogeneous catalysis) was found between log i_o and ΔH_{ads}, as shown in Fig.1-3. In the case of a Temkin[39] isotherm, log i_o can show a region of independence on H-adsorption energy.

In a more recent study, the relationship between log i_o and work function (using an updated set of critically-selected ϕ_M values[40]), Trasatti[33] has identified two groups of electrode metals: one group comprising all transition metals and sp metals with negatively charged surfaces, and a second group consisting only of sp metals with negatively charged surfaces. Similar behaviour was also noted in the associated correlation between log i_o and the heat of H-adsorption. (Note that heats of chemisorption usually decrease with coverage, so the "initial" heat of adsorption, as $\theta \to 0$, is considered).

The role of formation of solvated electrons as general intermediates in the h.e.r. and its relationship to the electrode metal work function has also been considered; except under conditions of very large cathodic overpotential, the participation of e^-_{aq} is not indicated[7,8].

Another indirect and usually weak effect of ϕ_M on log i_o may occur through a shift in the potential of zero charge and a related change in the structure of the electrical double-layer; in strong solutions or when anion adsorption arises, this effect may become significant.

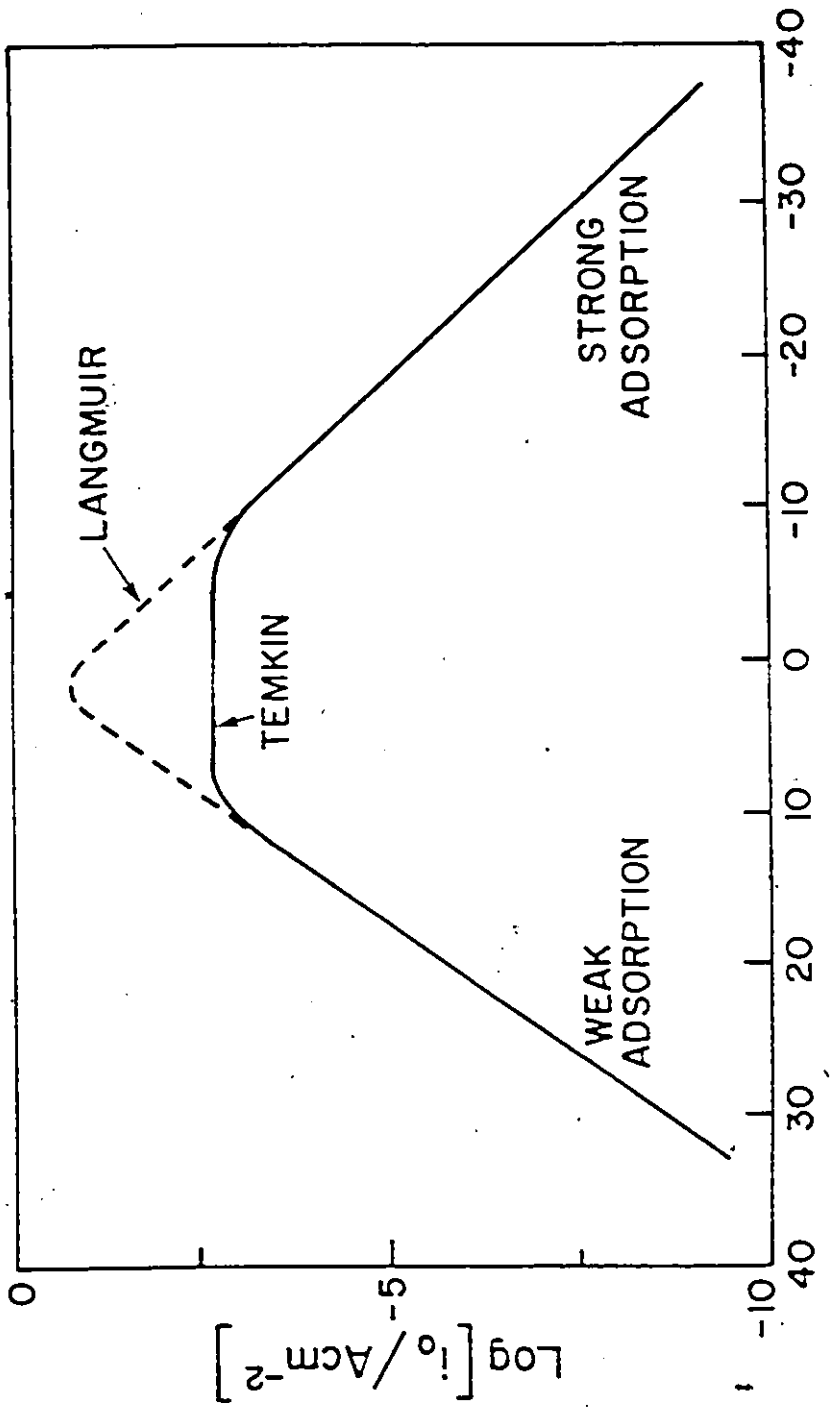

Fig.1-3 Theoretical relations between exchange current for the h.e.r. and standard free energy of adsorption (after Parsons[38])

(iii) Nature of e^- and H^+ Transfer Reaction

Reactions involving only the transfer of an electron, e.g. heterogeneous and homogeneous redox reactions, have been studied extensively. In these processes a single reaction coordinate in the sense of an energy profile is not obvious, unlike the case of atom-transfer reactions. Electron tunneling, as considered by Gurney[3] and Butler[24], constitutes the act of electron transfer. The required activation arises from solvational fluctuations which serve to bring the the reactants into a configuration intermediate between reactants and products, from (or to) which radiationless electron transfer can occur to yield the product state. The rates of these homogeneous and heterogeneous redox reactions have been treated theoretically by Libby[41], Hush[42], (R.A.) Marcus[43], Levich and Dogonadze[44] and others[45,46].

Proton discharge reactions at metal electrodes involve both electron transfer as in redox reactions, and H atom transfer to the electrode surface. Gurney[3] and Butler[24] treated this problem as a radiationless quantum-mechanical electron tunneling process. The specific atom transfer aspect of H^+ discharge led to the application of activated complex theory to this problem by Eyring, Glasstone and Laidler[4], Horiuti and Polanyi[47] and later, in more detail, by Parsons and Bockris[48], Conway and Bockris[49], and Despic and Bockris[50]. The concept of thermal solvational activation was implicit in these works. More recently, Dogonadze, Kuznetsov and Levich[51] have developed an elaborate theory of proton discharge based on activation via long-range fluctuations in solvation polarization; this work parallels

closely the theoretical treatments of redox reactions.

The question of the theory and mechanism of the activation process in the proton and coupled electron transfer step will be considered in some detail in the following Chapter.

3. Aspects of the H.E.R. Addressed in the Present Work

The present work is concerned with the comparative study of the discharge of, and hydrogen evolution from the unhydrated H_3O^+ ion in the state well characterized in strong acid "hydrates" which are oxonium ion (H_3O^+) salts of the acid anion[52,53,54], and from the aquo H^+ ion in solutions of the same acid in excess water. The temperature-dependence of the rates of the discharge step and of the h.e.r. are reported for different cathode metals; the resulting electrochemical activation parameters will be discussed in relation to the nature of the activation process and the temperature-dependence of the Tafel slope, b. Results on the temperature-dependence of the rate of the discharge step at Pt to yield strongly-bound H_{ads} (the so-called UPD H) are compared with the corresponding behaviour for steady-state H_2 evolution; H/D kinetic isotope effects for these processes are also reported.

CHAPTER 2

CRITICAL REVIEW OF THEORIES OF PROTON DISCHARGE IN THE H.E.R. AND THE STATE OF THE PROTON IN SOLUTION

1. Theories of Proton and Electron Transfer in the H.E.R.

The cathodic H_2 evolution reaction has come to be recognized as a prototype for consideration of mechanisms of electron charge-transfer processes at electrodes that also involve a coupled transfer of a neutralized atom. Other examples are the anodic evolution of halogens and metal deposition reactions from metal ion salt solutions. These type of processes are to be contrasted with the ionic redox reactions where both initial and final states of the electron transfer reaction at an electrode are solvated or ligand-complexed ions, e.g. $Fe^{3+}aq./Fe^{2+}aq.$, $Fe(CN)_6^{3-}/Fe(CN)_6^{4-}$, etc. In this chapter we examine the bases of various theories of proton and electron transfer in the h.e.r.

(i) Theory of Gurney

Following the phenomenological studies of the h.e.r. of Tafel[15] and of Bowden[55], the phenomenon of hydrogen overvoltage came to be associated variously with the formation of a thin film of gas, bubbles, or of a layer of oriented solvent dipoles in the course of the reaction[56]. In 1931, R.W. Gurney[3] published a quantum-mechanical theory of proton discharge which provided a basis for the understanding of the h.e.r. in cases where the electron transfer step is rate-determining. This paper became a landmark in the subject of electrode kinetics and the treatment of electron transfer at electrodes.

The central event in the process which this theory treats

consists in the quantum-mechanical tunneling of an electron in the metal surface to an acceptor state of equal energy in the solution. This transfer was considered to be radiationless in nature, e.g., it is consistent with the usual absence of photon emission from the products of electrochemical reactions. The essential condition (activation) for electron transfer to occur was identified with acquisition of the required energy in the thermal population of a rotational-vibrational band in solvated H_3O^+.

The relevant energy states are shown schematically in Fig.2-1 for the reduction of a cation (H_3O^+), in vacuum and in solution. The process considered is: $H_3O^+ + e(M) = H + H_2O$ where e(M) represents a state of electrons (see below) in the metal. In the vacuum case shown, electron transfer from an occupied level in the metal to the nearby acceptor state of equal energy is possible. For the particular case in solution, illustrated in Fig.2-1, the loss of electrostatic solvation energy, -W, upon neutralization causes an increase in potential energy of the final state and no electrons of appropriate energy are available in the metal; the availability of electrons of suitable energy in the metal depends on the applied potential. The energy of electrons in the metal is characterized by the Fermi level of the metal, ± the energy VF associated with the applied potential.

Gurney also considered the repulsive energy, R, of the product H / OH_2 pair; the energetic condition for electron tunneling to be able to occur is then

$$I - W - R \geq \phi + eV \qquad (2\text{-}1)$$

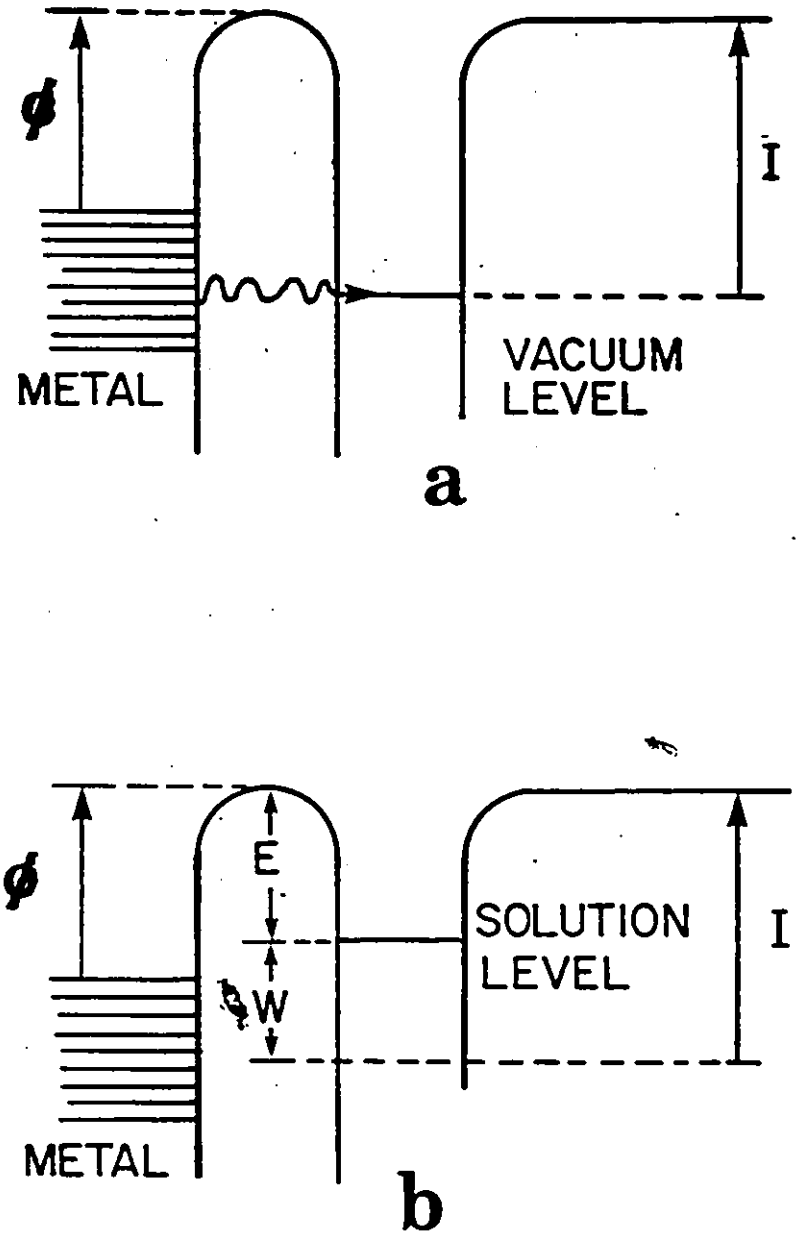

Fig.2-1 Energetics of ion neutralization at an electrode surface after Gurney (ref.3): a) ion in vacuum; b) ion in solution.

where I is the ionization energy of the resulting H atom and the quantity ϕ - eV is the energy of the Fermi level as modified by the arbitrary applied electrode potential, V, referred to above.

Thus Gurney [3] showed that the overpotential is not due to the progressive formation of an obstructive film but, rather, is a necessary and fundamental condition for electron transfer to occur.

The resulting expression for the total electrical current flowing across the interface is then of the form

$$I_{tot} \propto \int n(E,V)\, N(E,x)\, P(E,x)\, dE.dx \qquad (2\text{-}2)$$

In the evaluation of the above integral, Fermi-Dirac statistics were used to describe the population of electronic states, n(E,V) in the metal at the applied potential V. A continuous spectrum of rotation-vibration energy levels in the reacting ion was assumed, and $N(E,\bar{x})$, the number of ions at a mean distance $\bar{x}$ from the metal surface with a neutralization potential E (= W + R), was derived from a thermal Boltzmann distribution. The Gurney-Condon[57] result for tunneling through a rectangular barrier was used for the required electron tunneling probability, $P(E,\bar{x})$, in eqn.(2-2). The rectangular form of the barrier assumed in this work is probably inappropriate for moderate activation energies, 40 - 80 kJ mol^{-1}; better models for the form of the barrier were taken in later work.

The contributions of the ion solvation energy and of the H atom / water molecule repulsion are shown schematically in Fig.2-2. When the solvation contribution W shifts the initial bound state curve from EF to DG, the H / H_2O repulsion interaction decreases so that the change in W - R is greater than that in W. In Fig.2-

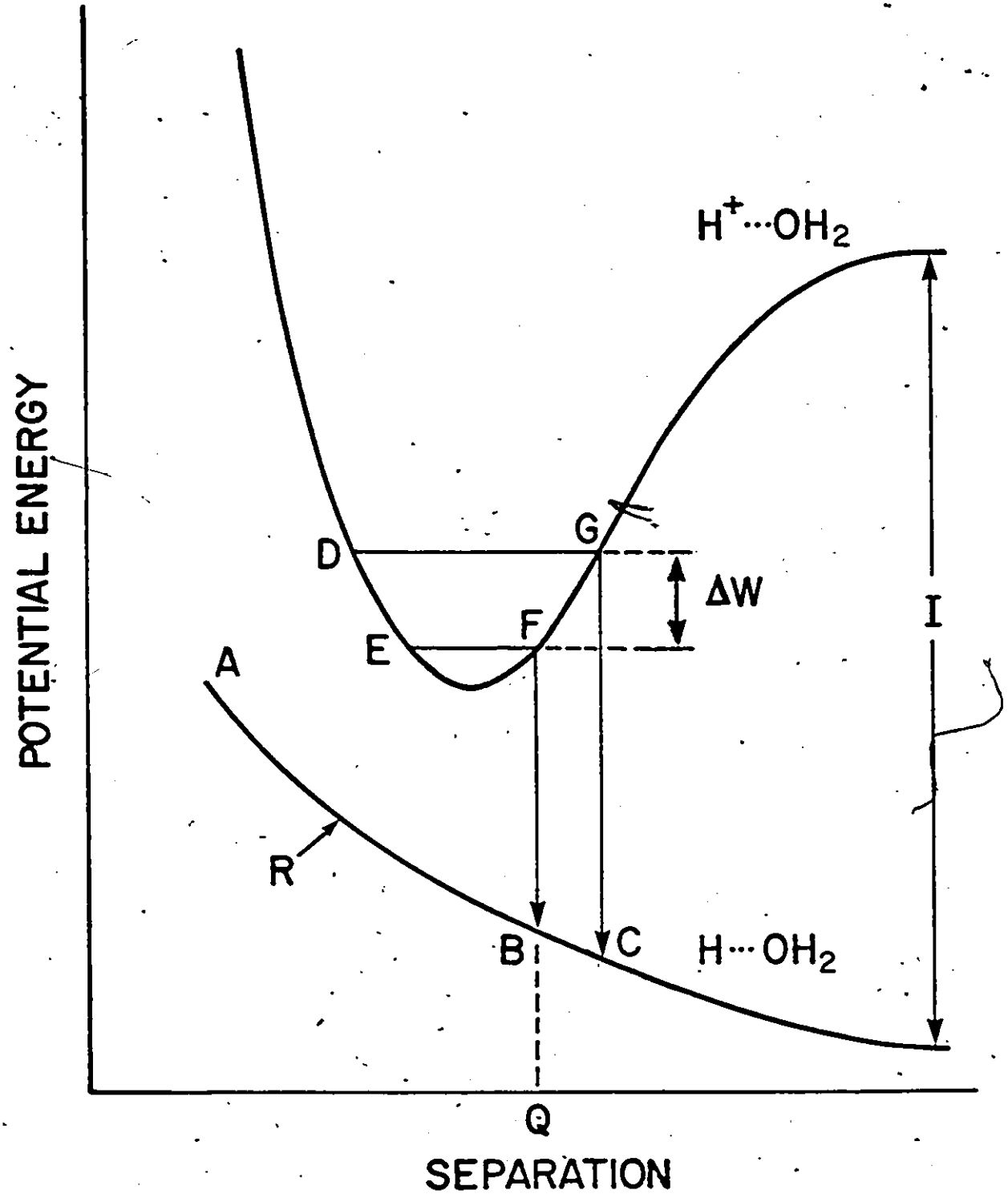

Fig.2-2 Effect of changes in ion solvation energy, W, on proton discharge according to the theory of Gurney[3].

2 from ref.3, Gurney omits the work function, ϕ_M, of the metal which determines the energy of the electron; inclusion of ϕ_M lowers curve DEFG yielding the familiar representation of intersecting initial and final state energy curves. As a first approximation in formulating $N(E,\bar{x})$, Gurney assumed $dW = \beta d(W-R)$ where $0 < \beta < 1$; thus β is determined by the relative slopes of the curves in Fig.2-2, which are effectively linearized in the region of interest.

The approximate integration[3] of eqn.(2-2) above was then shown to result in an equation of the form of the empirical Tafel relation given in eqn.(1-4).

Thus the explicit electron-tunneling theory of Gurney[3] for rate-limiting proton discharge in the h.e.r. accounted qualitatively for the potential-dependence of the rate of reaction and, significantly, showed that the overpotential required to cause a net current to flow was a consequence of the conditions required for a radiationless electron tunneling process to take place. Further, a theoretical basis of the symmetry factor, β, was provided intuitively in terms of the geometry of initial and final state energy curves. A clearer formulation of the significance of β was, however, apparent in Butler's subsequent treatment. Gurney's theory predicted activation energies for the proton discharge process that were much larger than those observed experimentally. The assumed final state of the H atom <u>free in solution</u> near the metal surface (rather than in an <u>adsorbed</u> state) was the origin of these large estimates.

(ii) Theory of Butler

Butler[24] improved on the Gurney theory by considering the product of proton discharge to be adsorbed H on the electrode surface. The final state energy then includes two additional components: a) a term for the adsorption energy of H bound at the metal surface, which was assumed to vary with distance in a manner similar to that in a diatomic hydride, and b) a term due to the H / OH_2 repulsion, R, as in Gurney's original treatment.

The condition for radiationless electron transfer then becomes

$$\phi + eV + R - A < I - L \qquad (2\text{-}3)$$

and the associated energy profile as a function of distance along the reaction coordinate is shown schematically in Fig.2-3. Curve BB represents the H / OH_2 final state, R, and curve CC consists of the sum of R and A representing the net energy of the bound M-H state adjacent to the H_2O left as the other product of electron transfer to H_3O^+. Inclusion of the H adsorption energy leads to a significant reduction in the required activation energy (for radiationless electron tunneling to occur) as measured by the change of the intersection point X to X' (Fig.2-3) and from estimates which Butler[24] made for the rate of the h.e.r. at a Ni electrode surface in comparison with that at Hg. Note that the representation of the level BB relative to AA is different from that in Gurney's figure.

Allowance for the energy of adsorption of the product H atom in Butler's treatment has two important consequences. First, significantly smaller activation energies are predicted than from the Gurney model, in better agreement with the experimental

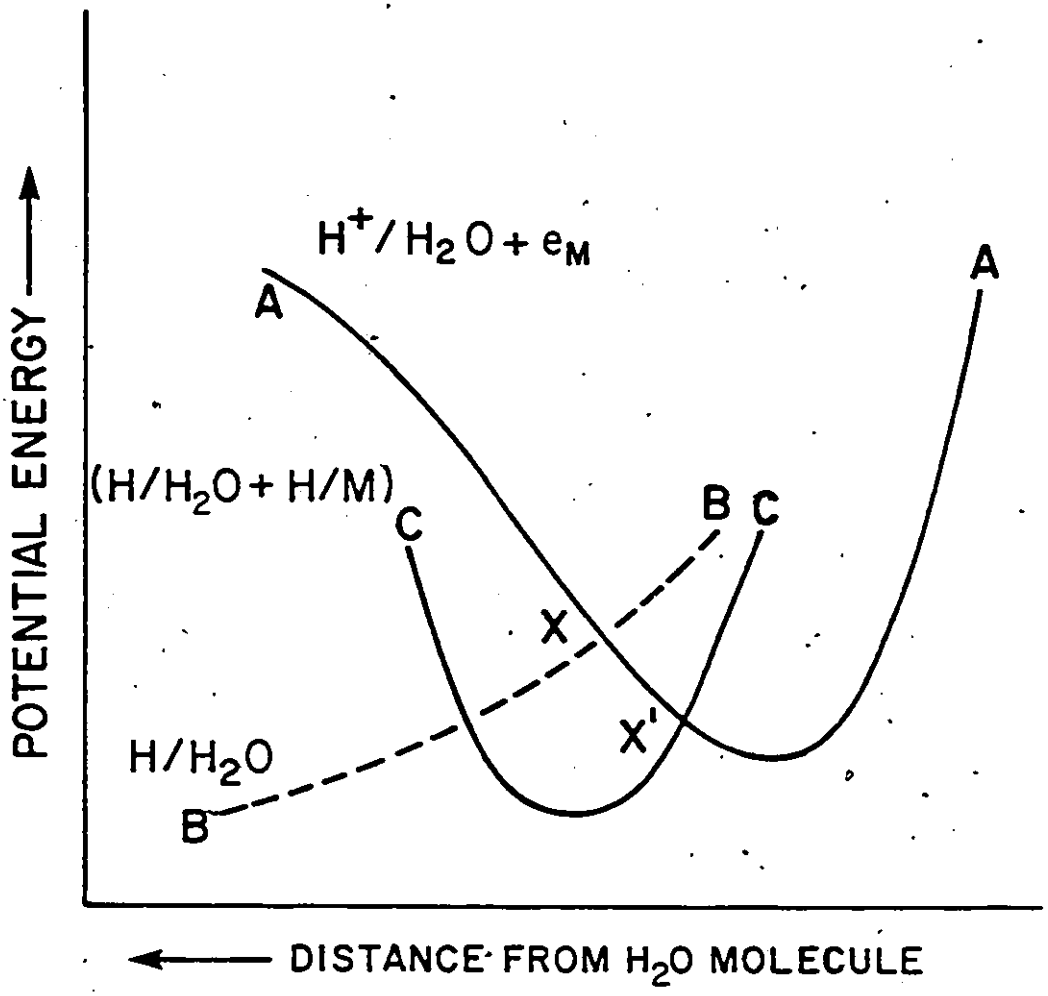

Fig.2-3 Effect of inclusion of H_{ads} on the energetics of proton discharge after Butler[24].

behaviour; of course, strong adsorption of H may lead to alternate steps in the overall h.e.r. being rate-determining (e.g. the reaction of H recombination at the surface) but the primary discharge of H onto electrode metal sites must always occur as an initial step in the h.e.r. Secondly, a basis was provided for explaining the extremely wide variation (ca. 10^9 x on going from Hg to Pt in aq. acid solution) in the standard rates of the h.e.r. at different electrode metals.

Introduction of a charge-transfer factor, α, in the rate expression for forward and backward directions of an electrode reaction was made explicitly by Volmer[25] and provided the first proper rationalization of the Tafel equation in terms of exponential dependence of reaction rates on potential, which, expressed logarithmically, gives the familiar form of the Tafel equation as $\eta = a + b \log i$ where η is the overpotential and b the Tafel slope, "$2.3RT/\alpha F$". Volmer's representation together with Butler's treatment of the energy profile along the reaction coordinate, has come to be known as the "Butler-Volmer" equation.

(iii) Construction of Detailed Energy Surfaces

The transfer of a proton from H_3O^+ to an adsorbed state on the electrode surface was viewed in early work of Horiuti and Polanyi[47] in terms of the gradual breaking of the H_2O-H^+ bond and the formation of a M-H bond; these authors were the first to point out that the energetics of the adsorption of H on the electrode surface would affect the rate of proton discharge. Ion neutralization was assumed implicitly to occur at the "crossing point" of the H_2O-H^+ and M-H energy curves, which in the Gurney

treatment, corresponds to some initial state of thermal activation of the H_3O^+ ion[3]. Calculations based on this approach and using suitably constructed energy profiles were first given by Butler and subsequently developed in more detail by Parsons and Bockris[48] for the discharge step, and by Conway and Bockris[49] in a theoretical study of the electrochemical desorption step ($e(M) + H_3O^+ + MH_{ads} = H_2 + H_2O$) from various metals, leading to an understanding of the relation of the kinetics of the h.e.r. to M-H bond energies.

Thermal activation of the reacting bond(s) in H_3O^+ was envisaged in this work; a Boltzmann distribution of H_3O^+ energies was employed in view of the near-continuum of energy states which results from the strong coupling of H_3O^+ in solution with surrounding water molecules (through H bonding and the electrostatic field of the ionic charge). These theoretical studies were useful in comparing reaction paths and assessing the effect of factors such as H adsorption energy, strength of H^+ solvation in various media and metal work function differences on rates of the h.e.r.[48,49,50]

An important problem was recognized in these papers[48,49,50]: how is the course of the activation process to be represented along a reaction coordinate when two rather different processes are involved simultaneously: ion neutralization and dehydration together with atom transfer <u>from</u> the ion in the Helmholtz plane in the double-layer <u>to</u> the electrode as an adatom? The ion dehydration process must be represented energetically by a multidimensional energy surface while the H^+ transfer from the H_3O^+ molecule ion can be represented, as in Butler's treatment,

in terms of O-H bond stretching in a quasi-diatomic molecule configuration, $H\text{-}OH_2$. In this early work[48,49,50], this problem was circumvented by taking, as an approximation, the whole solvation energy, W, of $H_3O^+_{aq}$ into account in the energy diagram representation, i.e. the proton affinity of H_2O (-786 kJ mol^{-1}) + the energy of hydration of H_3O^+ (viz. ca. 320 kJ mol^{-1}), and writing the course of change of W along the reaction coordinate in terms of a Morse-type function based on a force constant for the $H^+\text{-}OH_2$ interaction in H_3O^+ alone, the latter accounting for ca. 69% of W.

Quite apart from attempts to account for overpotential in electrode reactions through mechanistic treatments involving profiles of energy change of the particles in the course of an elementary act of the reaction, it is possible to understand the origins of overpotential in a quasi-thermodynamic way in terms of the thermodynamic treatment of irreversible processes.

At equilibrium, a classical reaction process is associated with some well defined standard free energy or "affinity" change and corresponding free energy of activation for the forward and backward directions of the process. In an electrode reaction, the electrochemical free energies of activation for forward and backward directions of the process are identical at equilibrium. In order for a net rate of a chemical reaction to occur, it is necessary to establish a diminution, δ, of the affinity change associated with the activation process to some new value $\Delta G^{\ddagger}_r - \delta G^{\ddagger}$ for the forward reaction. In an electrode reaction, the modulation quantity, $\delta G^{\ddagger}$, required to promote a net direction of

reaction is achieved by imposition of a potential, δV, different from the Nernst reversible value obtaining at equilibrium. In chemical reactions, the increment of affinity change must be introduced by a modulation in G due to a change of pressure or temperature (Eigen's procedures[58]), or to introduction of a non-equilibrium concentration, giving rise to a temporary difference in the chemical potential of reactant and product which quantities, at equilibrium, must be equal.

(iv) Role of Proton Tunneling

In any proton transfer process, the possibility of proton tunneling through the energy barrier must be considered; this arises on account of the wave-particle nature of matter according to the familiar de Broglie[59] relation

$$\lambda = h/p = h\ (2mE_k)^{-1/2} \qquad (2\text{-}4)$$

where p, m and E_k are respectively, the momentum, mass and kinetic energy of the particle, and the other symbols have their usual significance. Penetration through the energy barrier (and hence deviation from classical behaviour) is expected if the wavelength λ is comparable with the barrier width; for the proton with $E_k = kT$ and $T = 300$ K, one finds $\lambda = 10^{-8} - 10^{-9}$ cm which is comparable with the H^+ transfer distances along the reaction coordinate in chemical systems.

Bell[60] and Wigner[61] recognized that proton tunneling could play an important role in chemical reactions involving H and that this tunneling would lead to an H/D isotope effect in addition to that due to differences in zero-point energies. Subsequent calculations on H tunneling in the h.e.r. have paralleled closely

the general treatment of Bell[60].

Bell[60] calculated the effect of tunneling for a generalized proton transfer reaction using an Eckart[62] energy barrier function,

$$V(x) = \frac{A \exp(2\pi x/l)}{1 + \exp(2\pi x/l)} + \frac{B \exp(2\pi x/l)}{[1 + \exp(2\pi x/l)]^2} \qquad (2\text{-}5)$$

where 2l is the barrier width, A is the energy change in the reaction (cf. Fig.2-4) and the activation energy $E^{\ddagger}$ is related to B by $E^{\ddagger} = (A+B)^2/4B$ (=B/4 for a symmetrical barrier, viz. A=0). Note that the form of the Eckart barrier[62] is believed to be a good approximation to the barrier shape for simple atom/diatomic molecule processes, the potential profiles for which are usually based on Morse functions. Such a barrier shape is, of course, much more realistic than the rectangular barrier assumed by Gurney[3] in his treatment of electron tunneling. Providing that $B > h^2/8ml^2$, the permeability function for this barrier was given by Eckart[62] as

$$G(W) = \frac{\cosh[2\pi(\alpha+\beta)] - \cosh[2\pi(\alpha-\beta)]}{\cosh[2\pi(\alpha+\beta)] + \cosh[2\pi\delta]} \qquad (2\text{-}6)$$

where $\alpha = (2mW)^{1/2}l/h$, $\beta = [2m(W-A)]^{1/2}l/h$, $C=h^2/8ml^2$, $\delta = 1/2\,[(B-C)/C]^{1/2}$ and here W is the kinetic energy of motion of the "particle" representing the system which strikes the barrier. Assuming that G(W) = 1 for $W \geq E^{\ddagger}$, the rate of reaction is then derived by considering a Boltzmann distribution of proton energies, W, to give the relative number N/N_o of particles crossing the barrier:

$$N/N_o = (kT)^{-1} \int G(W) \exp(-W/kT)\, dW \qquad (2\text{-}7)$$

In subsequent work[63] using a parabolic energy barrier, the

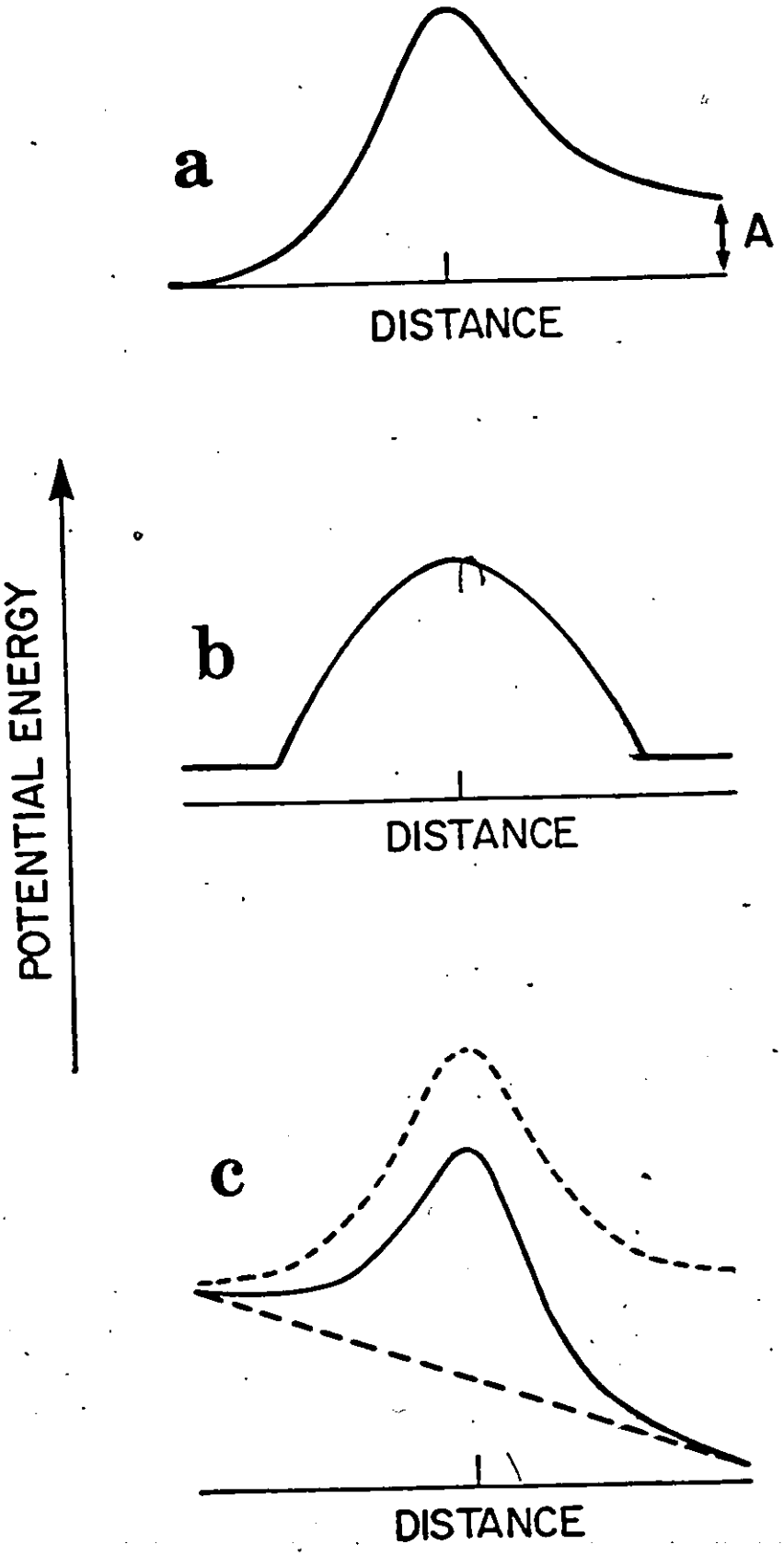

Fig.2-4 One-dimensional energy barriers: a) assymetrical Eckart; b) symmetrical truncated parabolic; c) symmetrical Eckart + linear potential gradient.

curvature at the saddle point was expressed in terms of a frequency $\nu^{\ddagger} = (\pi l)^{-1}(E^{\ddagger}/2m)^{1/2}$; the approximate ratio of quantum-mechanical transfer (solely due to tunneling) to classical transfer rate constants was found to be

$$k_{quant}/k_{class} = \mu/[2 \sin(\mu/2)] \qquad (2\text{-}8)$$

where $\mu = h\nu^{\ddagger}/kT$.

Using realistic values of the energy barrier width and height, and for various degrees of asymmetry (e.g. overall energy change in the reaction) with energy barriers of the forms described above, Bell[60,63] concluded that H tunneling could be significant in some chemical proton transfer processes. The principal experimental manifestation of H tunneling was concluded to be the observation of a temperature-dependent energy of activation, i.e. a deviation from the linear Arrhenius plot, and the approach to an almost constant rate at the lowest temperatures.

Bawn and Ogden[64] and Appelby and Ogden[65] discussed the contribution of proton tunneling in the proton discharge step of the h.e.r. along the lines of Bell's treatment referred to above. In these early calculations, the particular choice of energy barrier parameters and the neglect of differences in zero-point energy led to high values of the H/D separation factor*, S, (ca. 70), which do not agree with the values (ca. 7-10) that have been determined experimentally at several metals. However, Topley and Eyring[66] attributed the then known values of S primarily to zero-

* S for the h.e.r. from a dilute solution of "D^+" in H_2O is given by, S = [C(H,gas)/C(D,gas)]/[C(H,solution)/C(D,solution)].

point energy differences.

Christov has considered the role of proton tunneling systematically in a series of papers[67,68]. Both Eckart and parabolic energy barriers were used in studying the Tafel parameters and H/D separation factors, and their dependence on barrier parameters; in particular, the linear potential drop across the double-layer was considered to add, e.g., to the energy along the Eckart barrier as represented in Fig.2-4, and hence lead to potential-dependent rates.

The total current, i_T, associated with H^+ discharge was divided into two components

$$i_T = i_q + i_c \qquad (2\text{-}9)$$

corresponding to penetration through (i_q) and passage over (i_c; classical) the barrier. Both types of barrier led to Tafel behaviour over an appreciable range of potential[68]. With a parabolic barrier, the Tafel slope b was found to be greater than the classical value (ca. 2.3 RT/0.5F) at low temperatures where the tunneling route becomes important, and also to be independent of temperature; the rate similarly approached a limiting value while the model led to normal Arrhenius behaviour at higher temperatures (above 220 - 300 K). These deviations from classical behaviour (at low T) were less marked when Eckart barriers were used and the associated rates remained temperature-dependent in the classical way[68].

The experimental results of Post and Hiskey[69] for the rates of the h.e.r. at Hg from aq. HCl were used to adjust the barrier parameters[68]. Optimized values of 2d = 0.47 and 0.165 nm were found for the Eckart and parabolic energy barriers, respectively,

taking a barrier height = 1.6 x 10^{-17} J. Christov concluded that the parabolic barrier was more satisfactory since the value of 2d = 0.165 nm agreed with the double-layer thickness (0.175 nm) accepted at that time; this conclusion is, however, at variance with subsequently proposed models of the double-layer region, e.g. of Bockris, Devanathan and Muller[70]. Christov's neglect of the effects of zero-point energy differences in the initial and activated states was criticized by Bockris and Matthews[71].

Conway[72] evaluated the consequences of proton transfer occurring wholly by tunneling through an Eckart barrier and was the first to take the zero-point energy differences into account; the effect of a quantized distribution of H_2O-H^+ levels was also examined. An H/D mass dependence of the Tafel slope b was found when tunneling is important (cf. Fig.2-5); this behaviour was shown[72] to obtain for barrier widths of 2d = 0.05 to 0.15 nm and the mass effect on b was proposed as a diagnostic criterion for proton tunneling. At low and moderate overpotentials, respectively, classical Ohmic and Tafelian behaviour was found, while at high overpotentials, a limiting current was approached. A linear increase in b with temperature was found but the rate of decrease is less than that expected classically; thus a difference in b for H and D (Fig.2-5) was expected to be experimentally detectable.

Complementary experimental studies[73,74] on the h.e.r. at low temperatures in alcoholic HCl solutions did not show the expected characteristics, indicative of significant tunneling. From the results of detailed calculations, Conway and Salomon[73,75]

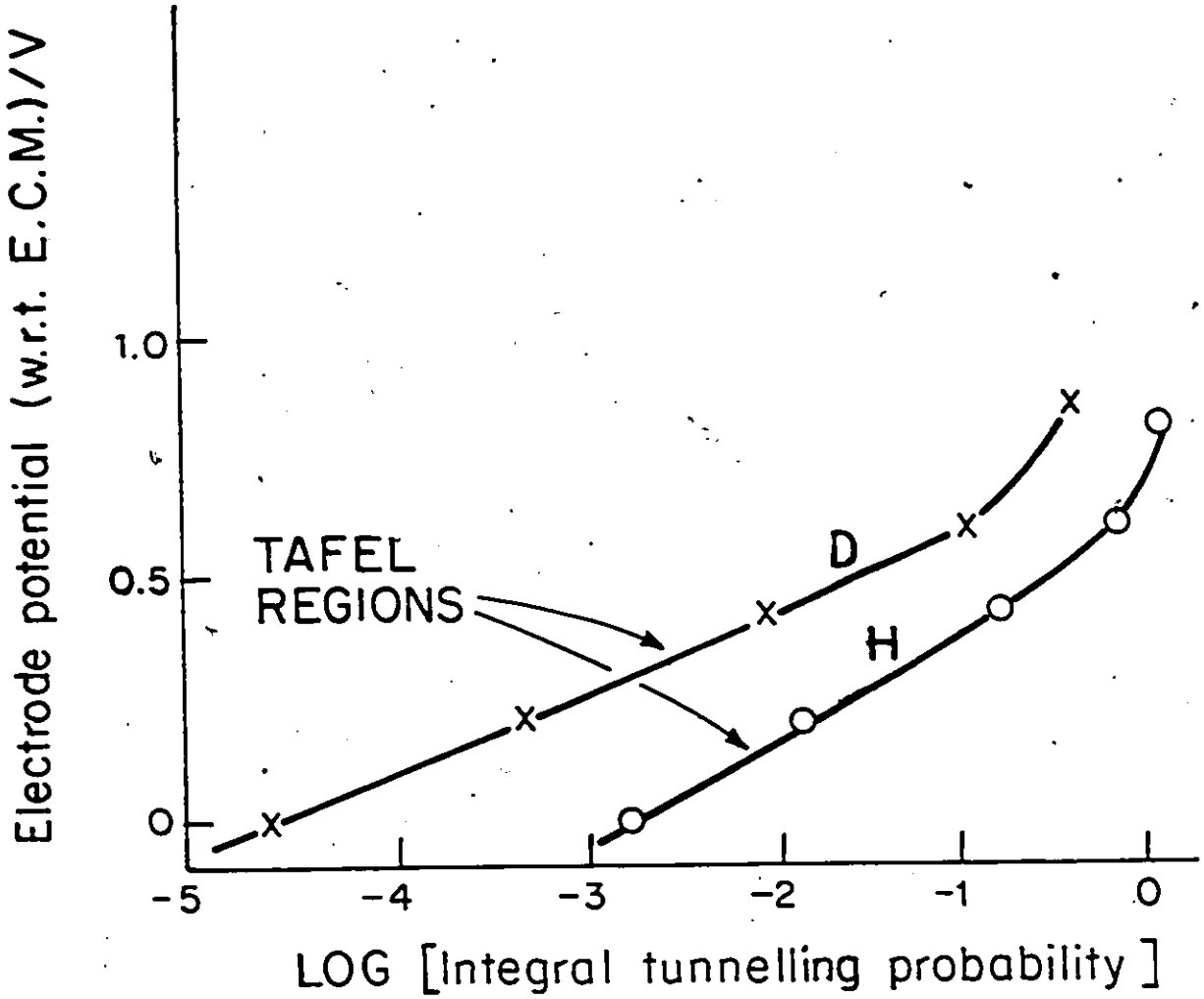

Fig.2-5 H/D isotope mass effect on Tafel slopes in the h.e.r. after Conway[72].

concluded that the isotope effects found in the h.e.r. could be explained satisfactorily from a consideration of zero-point energy difference effects.

Bockris and Matthews[71] reexamined the role of H^+ tunneling in the proton discharge process employing a range of temperatures and of parameters for an unsymmetrical Eckart barrier. A parallel classical + quantum-mechanical route for H^+ transfer was treated. Calculated currents corresponding to -0.5 to -1.0 V were extrapolated to 0.0 V in order to estimate exchange current densities in a manner like that used in the analysis of steady-state polarization measurements. The Tafel slope was found to be only a weak function of isotope mass and temperature, and hence not a very sensitive test for proton tunneling. However, rather large and improbable H^+ transfer distances (>ca. 0.2 nm) were considered, in accord with the BDM[70] model of a water-molecule covered electrode surface with hydrated cations located in the OHP beyond this inner water dipole layer. From an adjustment of the model parameters in order to reproduce the potential-dependence of the H/T separation factor, it was concluded that 69% of H^+ transfer at -1.0 V occurs by sub-barrier proton tunneling[71].

The predictions associated with various criteria for proton tunneling in proton discharge, including those expected to apply at low temperatures, have not been observed experimentally[73,75]; however, the potential-dependence of the separation factor has been attributed to a significant degree of proton tunneling[71]. Examples of tunneling in homogeneous (solid or liquid phase) proton transfer processes have been found and will be dealt with

further in a following section (and see Bell's monograph, ref.76, for a complete account).

(v) Non-Equilibrium Polarization Model of Proton Discharge

A substantial departure from the earlier approaches to the treatment of the activation process in electrochemical charge-transfer has originated from work on the mechanism of electron transfer in redox reactions, both homogeneous in solution and heterogeneous at electrodes. Early embodiments of the theory of such reactions took over the elements of polaron treatments of the creation of charges in dielectrics and thus were based on long-range polarization effects in the solvent medium caused by changes of charge on the ions of the redox system.

Such an approach has been the basis of treatments of the kinetics of charge-transfer in so-called outer-sphere redox reactions* as developed in the work of Libby[41], (R.J.) Marcus et al.[78], (R.A.) Marcus[43], and others[42,44]. Generally the activated state is viewed as requiring the reacting ions to approach each other, as in the treatment of Sacher and Laidler[79,80], and undergo environmental fluctuations in the solvating medium which satisfy the energy requirements for radiationless electron transfer to occur; an important component of this activation

* "Outer-sphere" redox reactions are those that are not mediated by sharing of an electron transfer facilitating ligand in the collision complex of the conjugate pair of redox ions. In the electrode situation, this implies a lack of specific adsorption of the reacting ions. Generally this has been interpreted as meaning that outer-sphere reactions at electrodes are associated with an activation process that involves only long-range polarization fluctuations but recent evidence, e.g. of Weaver[77], indicates that more specific ion-solvent structural interactions are involved which, in fact, is what would be expected.

process is said to result from long range, non-equilibrium polarization fluctuations. These constitute part of the so-called "reorganization energy" which is a major component of the activation energy. The theory of (R.A.) Marcus[43] has been particularly successful in the cross-correlation of homogeneous redox electron transfer rate constants, and has also yielded a simple theoretical relation between expected values of homogeneous and corresponding heterogeneous rates constants for a given reaction.

An elaborate treatment of proton discharge which stresses the role of fluctuations in solvent polarization in the activation process for the h.e.r. has been given by Dogonadze, Kuznetsov and Levich[51,81] (DKL); the treatment is an extension of the theoretical formalism for outer-sphere redox electron transfer reactions. In this theory of proton discharge, the motions of the electron, proton and solvent are considered in terms of three subsystems[81]:

a) The electron is considered as a "fast" quantum subsystem, relative to the time-scales of motions of the proton and solvent dipoles. Within the electrode surface, a Fermi distribution of electron energies is assumed

$$n(E) = [\exp((E-E_F)/kT)+1]^{-1} \qquad (2\text{-}10)$$

corresponding to an electron energy density which is a smooth function of E, e.g. that for a quasi-free electron was used. The final state of adsorbed H was taken to constitute a local, bound state energy level; this corresponds to a low surface coverage by H and to the absence of a surface band in the electron energy state spectrum as a result of adsorption. These conditions

correspond closely to the situation obtaining at the high overvoltage metals in acid solution, e.g. Hg, Pb.

b) The proton was viewed as a slower but still (vibrationally) quantized subsystem and considered to be strongly bound in both initial (H_3O^+) and final (MH_{ads}) states; only stretching modes normal to the surface were considered. Proton transfer was regarded as occurring by <u>tunneling</u> through an energy barrier to the metal surface. Discrete vibrational states were assumed for the initial $H_2O\text{-}H^+$ ($\nu_i = 5 \times 10^{14}\ s^{-1}$) and final adsorbed M-H ($\nu_a = 2 \times 10^{14}\ s^{-1}$) states; the former frequency corresponds to that expected for an isolated H_3O^+ ion, e.g. in the gas phase. Since both ν_i and $\nu_a > kT/h$ ($= 4 \times 10^{13}\ s^{-1}$), Dogonadze, Kuznetsov and Levich[51,81] concluded that H^+ exists only in the ground vibrational state in H_3O^+ in both initial and final states; this important but not necessarily correct conclusion indicated; in their discussion, the need for an activation process other than the usual (see below) thermal bond stretching one (which may itself involve varying degrees of proton tunneling, e.g. as in the treatment of Bell[60]) which implies vibrational activation. This conclusion is at variance with the considerable H_3O^+ vibrational band-broadening (e.g. see refs.82,83) which results from strong interactions with solvent dipoles in the condensed aqueous phase, as well as with the approaches of Gurney[3], Butler[24]; this point will be returned to below.

c) The solvent around the discharging H_3O^+ ion was treated as a classical subsystem and taken to consist of an inner-sphere of solvent dipoles performing small vibrations and of outer-

sphere solvent acting as a dielectric continuum, subject to thermal fluctuations of polarization. This representation is similar to that used in the treatment of outer-sphere redox reactions in the theories of Hush[42] and of Marcus[43] referred to above.

These three levels of processes that are involved in charge transfer in reactions also involving atom transfer correspond to the time scales distinguished by Kornyshev[84] in his treatment of solvation processes involving ions.

Two energy barriers in the process result from consideration of these three subsystems (electron, proton and solvent). The actual H^+ transfer is considered to occur by tunneling through an energy barrier along the proton coordinate normal to the electrode surface; the assumption, that is basic in this treatment, that only the ground vibrational states of H_3O^+ aq. and of $M\text{-}H_{ads}$ are populated led DKL to regard the activation process as involving only long-range fluctuations in solvent polarization outside the proton source, H_3O^+. These fluctuations along a multi-dimensional solvent coordinate activate the H_3O^+ initial state and permit proton tunneling to an adsorbed state of equal energy. The potential energy surfaces envisaged in this model for proton discharge are shown diagramatically in Fig.2-6. The activated state is reached along the solvent "coordinate", q, (while the H^+ coordinate is fixed -- corresponding to ground-state O-H vibration in H_3O^+) as a result of polarization fluctuations. From this activated state, proton tunneling is considered to occur directly to the ground vibrational level of MH_{ads}; then relaxation of the solvent yields the equilibrium

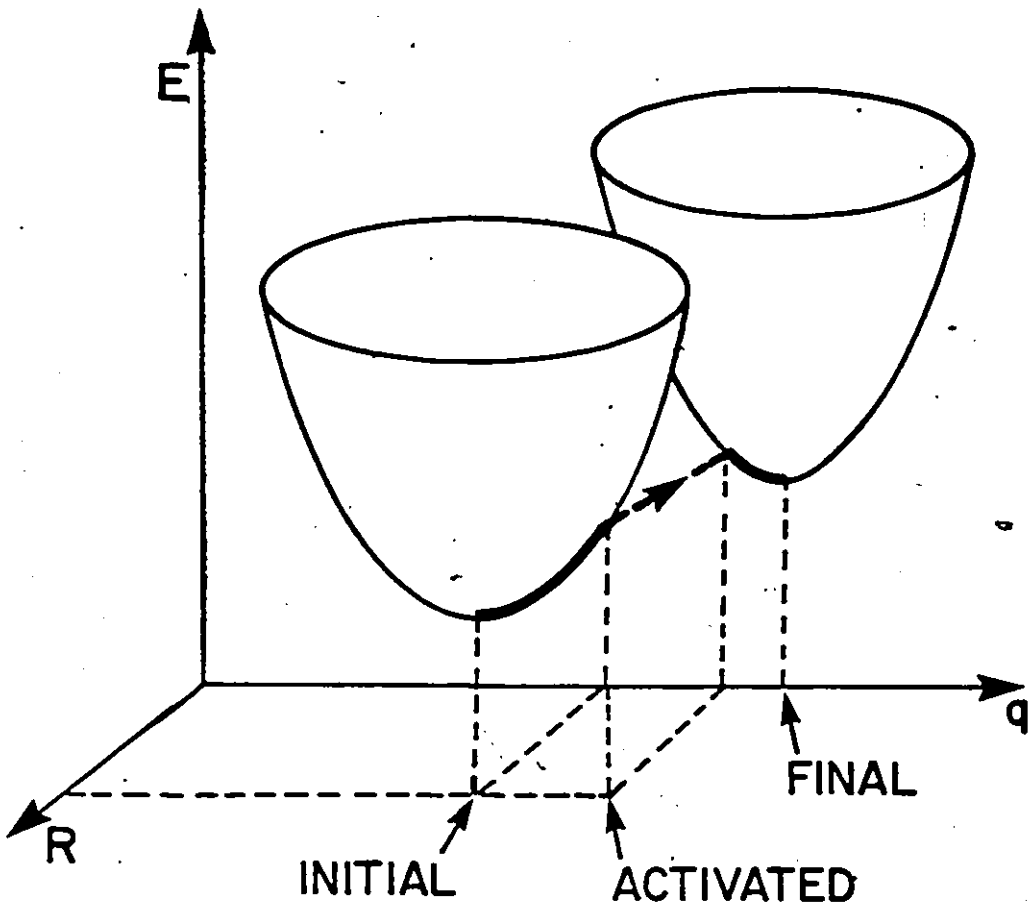

Fig.2-6 Schematic representation of the potential energy surface for H^+ discharge according to Dogonadze, Kuznetsov and Levich[81]: q = multi-dimensional solvent coordinate; R = proton coordinate; E = potential energy.

MH_{ads} + OH_2 final state (cf. Fig.2-6).

The rate of proton discharge is then written as

$$i = zF\, C(H_3O^+) \int n(E)\, \rho(E)\, P(E)\, dE \qquad (2\text{-}11)$$

where n(E) and ρ(E) are the Fermi distribution and electron density of states functions respectively, and P(E) is a thermally averaged transition probability.

The Born-Oppenheimer approximation was used to express initial- and final-state wavefunctions as a product of electron, proton and solvent harmonic oscillator wave-functions; DKL[81] justify this assumption for the proton relative to the solvent system by noting that the relevant vibrational frequencies for H_3O^+ and MH_{ads}, referred to above, are ca. 3 orders of magnitude higher than the frequencies of the solvent orientation (librational) modes.

Three kinetic regimes in the log[current] - potential (i.e. Tafel) relation result* from the DKL theory as illustrated in Fig.2-7. At very low overpotentials, so-called "activationless discharge"[85] (Fig.2-8) is predicted with a charge transfer coefficient $\alpha = 1$. At intermediate values of the overpotential, normal Tafel behaviour is found with $\alpha = 1/2$, while at high overpotentials, so-called "barrierless" ($\alpha = 0$) behaviour is seen (Fig.2-8). More detailed comparison with experimental activation energies requires accurate estimates of the reorganization energy which is not yet possible.

---

* Note that these limiting cases are not a unique consequence of the way DKL treat the activation process -- they can arise in other treatments such as those based on Butler's representation[24].

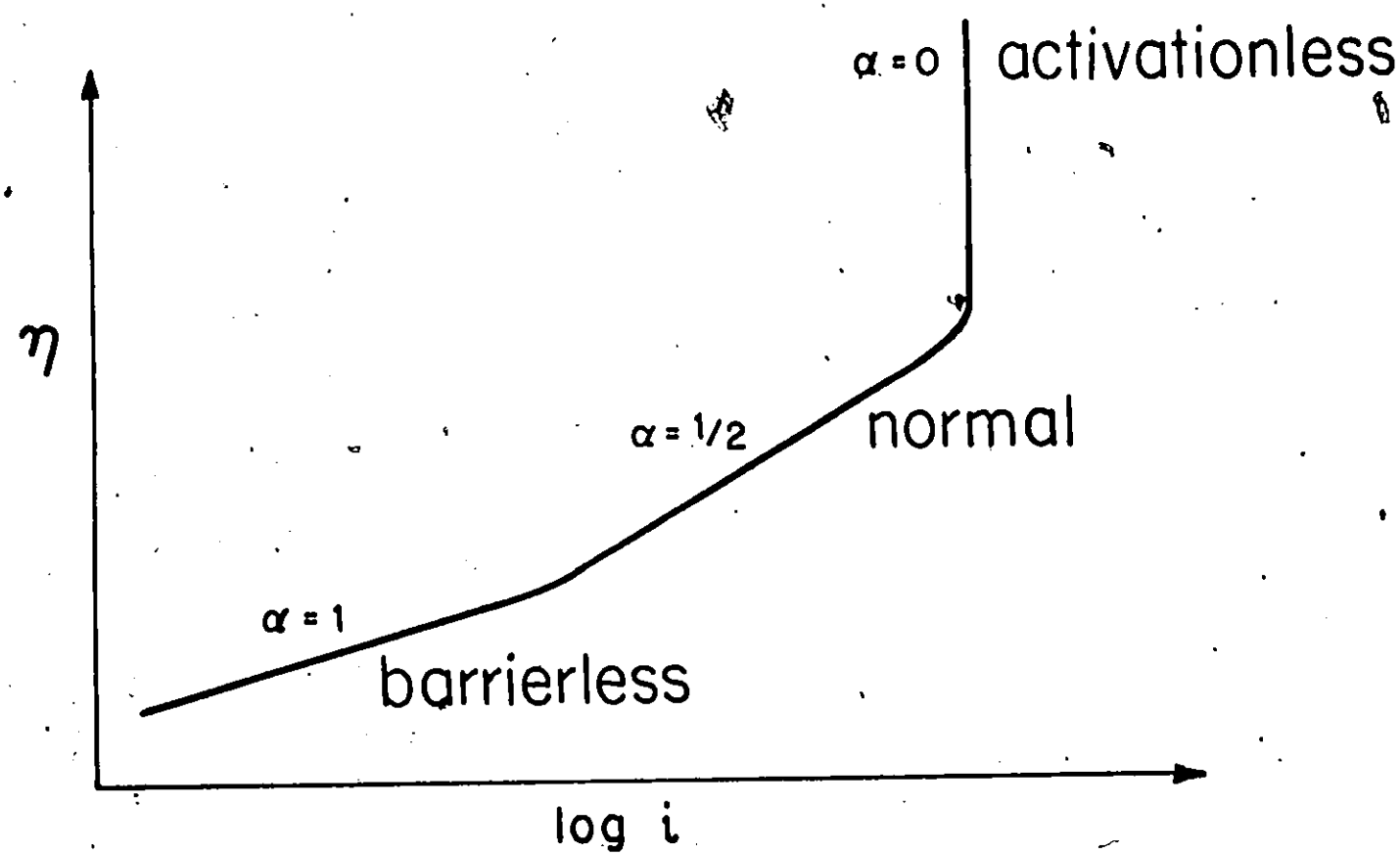

Fig.2-7 Schematic representation of range of Tafel behaviour according to the DKL model: activationless (a = 1), normal (a = 1/2) and barrierless (a = 0) discharge.

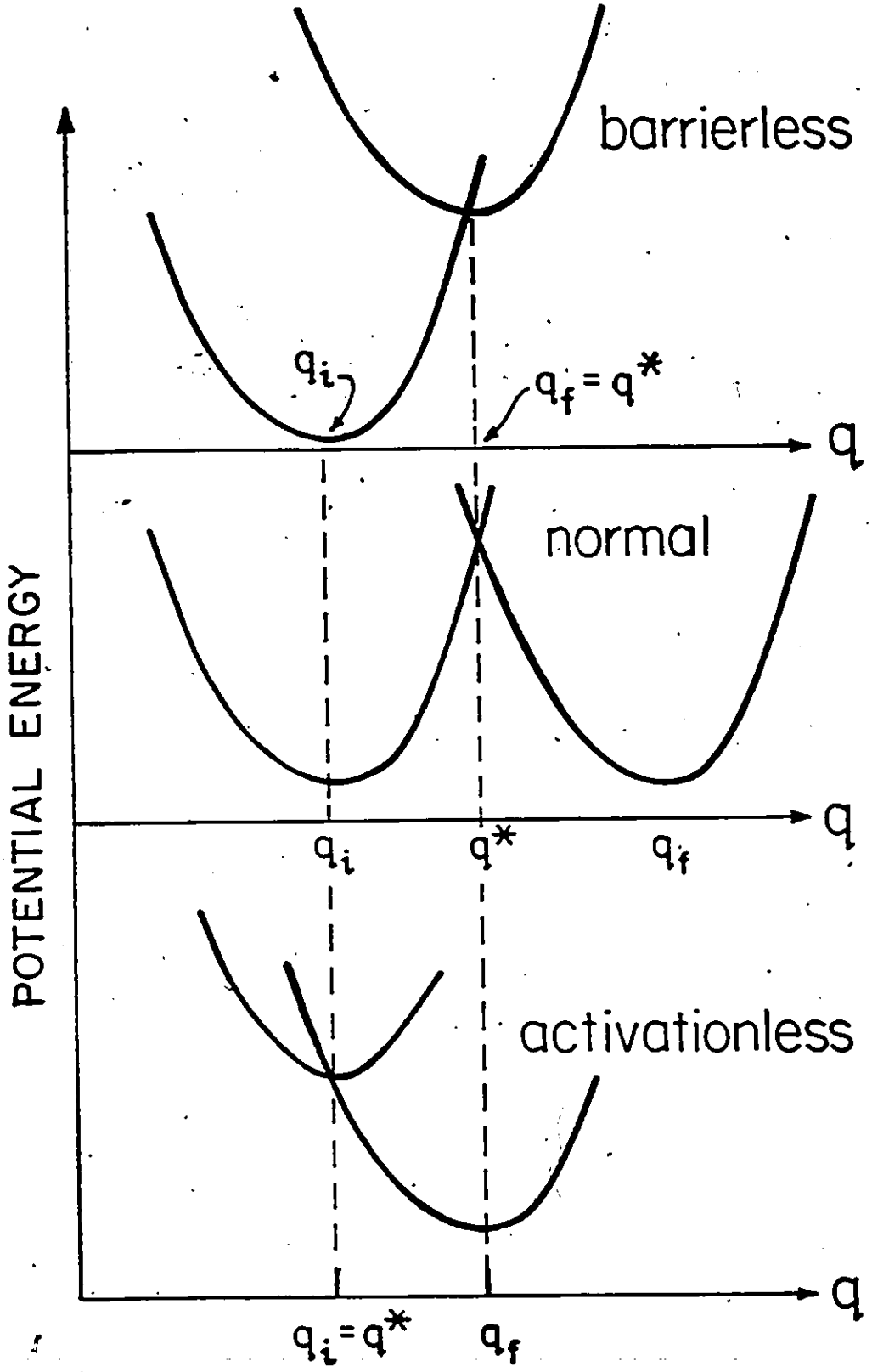

Fig.2-8 Limiting activation behaviour along the solvent coordinate for low (barrierless), moderate (normal) and high (activationless) overpotential.

Modifications and extensions of the basic DKL theory have been made in an effort to obtain agreement with experiment, e.g. the usually-found potential-independence of the transfer coefficient; these matters will be considered in a following section.

The DKL model deemphasizes the molecular mechanics of the activation of the H_3O^+ ion itself as an ion-in-solution problem and the way in which H becomes transferred (cf. ref.24) to an adsorption site on the electrode metal. An important deficiency of the DKL treatments is that they do not take into account the known manifold of lower energy "lattice modes"[82] associated with the hydrogen-bonded hydrated proton in aqueous solution, which are required to account for its high partial molar heat capacity[86]. The divergence of the DKL approach from the thermal bond-stretching models of activation in proton discharge originates from the view these authors take of the the vibrational state of H_3O^+ (i.e. widely spaced levels) in solution which led to the proposed alternate polarization fluctuation mode of activation.

A general point can also be made in regard to their view of the lack of vibrational activation in proton transfer from H_3O^+: in any reaction, even those that involve H or proton transfer, it seems there can always be a finite probability that reaction will occur through states corresponding to the high-energy side of the Boltzmann distribution for the system. This is the basis of the Arrhenius Law for reaction rates. Such energetic states can always arise with the probability $\exp(-E^{\ddagger}/RT)$ independently of the coarseness or otherwise of the structure of the vibrational

levels. As we have mentioned, in solution, especially in H bonded, associated solvents, the relatively coarsely quantized vibrational levels which "HX" molecules have in the gas phase ($h\nu = 40$ kJ mol^{-1}) become spread into vibration-libration bands having quite wide energies.

(vi) Developments of the DKL Model

The non-equilibrium polarization (DKL) model for the proton discharge process has been developed or examined in a number of theoretical and experimental investigations, particularly in order to: a) extend the predicted region of potential exhibiting normal Tafel behaviour[81], b) assess the agreement of the theoretical predictions with experiment in connection with the predicted limiting activationless and barrierless kinetic regimes[85], and c) determine the influence of the nature of the proton donor and solution medium on the kinetics of H^+ discharge[87]. Some of these developments will be outlined in the sections which follow.

(a) Potential-Dependence of the Transfer Coefficient, α

In the Marcus treatment of heterogeneous electron transfer rates, harmonic fluctuation of solvent polarization was the basis of the activation mechanism. On such a model, it can easily be shown that the potential-dependence of reaction rate involves a quadratic term in overpotential; thus an apparently potential-dependent α arises in the Tafel slope, so that a linear log form of the Tafel relation is not expected on the basis of the "harmonic" model. Various workers (see below) have attempted to detect the quadratic dependence of electrochemical

reaction rates on potential but only with limited success in often ambiguous experiments.

The effects of a number of factors on the potential-dependence of the transfer coefficient within the DKL[81] framework have been examined. Kharkats and Ulstrup[88], and also Dogonadze and Kuznetsov[89] considered the contribution to the transition probability due to the participation of excited vibrational levels of the proton and the associated anharmonicity; the bulk solvent beyond a central $H_9O_4^+$ ion was treated as a dielectric continuum. By a judicious adjustment of model parameters, Kharkats et al.[88] obtained a linear Tafel relation (b = 0.106 V decade^{-1}) over ca. 1 V in potential which was attributed to the inclusion of anharmonicity; the curvatures predicted using a harmonic potential for H_3O^+ were concluded to arise from the particular choice of the intramolecular potential function, and not as a consequence of the notion of distinct activation and tunneling barriers along the solvent and proton "coordinates". In these calculations, the limiting barrierless and activationless conditions were not reached.

In a photoelectron emission investigation of electrochemical desorption of H, a similarly linear a Tafel relation was obtained by Ovchinnikov et al.[90] by considering a linear dependence on separation for the potential energy for the MH_{ads} bond. More recently, Kuznetsov[91] has considered variations in charge on the adsorbed H in relation to the activation process in the H^+ ion discharge step; in this calculation, these variations in charge result from a modulation due to fluctuations in the medium

polarization (these same fluctuations along the solvent "coordinate" are those that activate the discharging particle in the DKL theory). Tafel plots showing the usual linear behaviour (b = 0.12 V) were found; however, for some values of the parameters considered in a LCAO description of the adsorbed state (or surface molecule), a non-monotonic variation in α with potential was found[91].

These theoretical investigations on the potential-dependence of α bring the DKL theory of proton discharge into closer agreement with the usually found linear Tafel behaviour; the inclusion of anharmonicity effects and excited vibrational levels in the initial H_3O^+ (cf. above and ref.88) seems the most promising approach which is, in fact, implicit in the earlier but less sophisticated treatments[48,49] based on Morse-function calculations of the barrier for proton transfer. However, the relatively wide spacing of vibrational energy levels assumed for the initial state (H_3O^+) seems at variance with the spectroscopic[82,92,93] and thermodynamic behaviour[86] of H_3O^+ in excess water -- H_3O^+ is not a "quantum molecule" in solution! It should be noted that there is some uncertainty as to the reason for the applicability of the Tafel law over such a wide range of overpotential, even in treatments based on a conventional thermal bond activation process (allowing for H^+ tunneling effects where indicated).

A potential-dependent transfer coefficient has been reported for the reduction of t-nitrobutane[94] and the oxidation in the Cr^{3+}/Cr^{2+} system[95]. In contrast,the reduction of chromium complexes in water exhibits a potential-independent transfer

coefficient[96] while the h.e.r. at Hg gives a constant transfer coefficient over ca. 9 decades of rate, i.e. over ca. 1.0 V with $\alpha = 0.5 \pm 0.05$.

(b) Limiting Activationless and Barrierless Behaviour

The experimental demonstration of a transition from $\alpha = 1$ (activationless) to $\alpha = 1/2$ (normal discharge) is hampered by a) the small currents which obtain at Hg at the required low overpotentials, b) the effects of the presence of trace quantities of depolarizing impurities, e.g. O_2, in solution at such low polarizations, and c) changes in the Ψ_1 potential and surface concentration of H_3O^+ ions near the potential of zero charge[97,98] especially when surface-active ions such as I^- are used in the supporting electrolyte as in Krishtalik's work[85]. Bowden et al.[99], in a careful experimental study of the h.e.r. in dilute acid solution at Hg, found linear Tafel behaviour with $\alpha = 1/2$ down to current densities in the nA range (V = -0.25 V RHE). Krishtalik[85,100] has reported an apparent transition from $\alpha = 1$ to $\alpha = 1/2$ at V = -0.5 V for the h.e.r. at Hg from, e.g. 6.0 M KI + 0.5 M HCl aq. solutions. However, these results were obtained only over about 1.5 decades in current density and may well be due, at least in some part, to anion adsorption and discreteness-of-charge effects in these very concentrated solutions of halides that are known to be strongly specifically adsorbed. Generally, for the h.e.r. at Hg and at other high overpotential metals in aqueous acid solution, linear Tafel behaviour (i.e., constant α) is found over four to nine decades in current density.

The transition from normal ($\alpha = 1/2$) to barrierless ($\alpha = 0$)

proton discharge has not been observed experimentally. In experiments at very high overpotentials, Krishtalik et al.[101] have reported estimates of probable limiting currents suggestive of barrierless discharge behaviour at Ag; the uncertain indications found in this work[101] are the result of severe solution resistance losses and mass transfer-limitations which occur in this regime of overpotential and which lead to limiting currents and correspondingly large Tafel slopes ($\alpha > 0$), which thus arise for essentially trivial reasons.

It should be emphasized that linear Tafel behaviour is the "rule", especially at Hg where a linear potential - log i relationship holds over ca. 9 decades in current density (or 1.0 V of overpotential) for the h.e.r. as mentioned above.

(c) Nature of the Medium and of the Proton Donor

In the DKL theory of proton discharge, considerable emphasis was placed on the role of the solution medium in bringing the H_3O^+ ion into a state from which proton tunneling to an adsorbed state of equal energy may occur. Krishtalik and coworkers[87,102,103,104] have examined this question in a series of papers on medium and bond-nature effects in proton discharge. Accordingly, apparent (at constant overpotential) activation energies and log[frequency factor] quantities were evaluated from steady-state polarization measurements for the discharge of $CH_3CN\text{-}H^+$ and H_3O^+ in acetonitrile solution at Hg[87,102]. The results were compared with previous results for discharge of aqueous H_3O^+ (see Table 2-1).

Table 2-1

Apparent Activation Energy and log [frequency factor] for Proton Discharge at Hg from Various Media (after Krishtalik et al.[87])

	CH_3CNH^+/CH_3CN	H_3O^+/CH_3CN	H_3O^+/H_2O
$E^{\neq}_{app}$/kJ mol^{-1}	18.2	18.2	21.9
log K	2.1	3.2	3.4*

* a value of 4.0 was cited by Titova and Krishtalik[102]

The difference in $E^{\neq}_{app}$ values obtained (regardless of the discharging ion) in CH_3CN and in H_2O was taken to indicate: a) a strong dependence of the activation process on the solution medium, and b) an independence of the nature of the bond (N-H^+ or O-H^+) being ruptured; the similarity in bond lengths in the CH_3CN-H^+ and H_2O-H^+ was considered to give rise to nearly identical solvational environments. However, Khan[105] has pointed out that, on the basis of the DKL approach, significantly different free energies of activation should be expected owing to the different radii of the CH_3CNH^+ (0.25 nm) and H_3O^+ (0.14 nm) ions.

This criticism not withstanding, this line of investigation initiated by Krishtalik seems promising in the study of the nature of the activation process in proton discharge. In the light of the recent work of Weaver[77], wherein the absolute metal-solution potential difference was fixed by means of non-isothermal cell measurements, it would be useful to investigate, e.g. "true" activation parameters and H^+ donor effects under conditions of constant field, rather than at constant

overpotential. Research along these lines is currently in progress in this laboratory[106].

(vii) Relation to Homogeneous Proton Transfer

Strong similarities exist between proton (and electron) transfer to electrode surfaces and proton transfer between solution species. These commonalities relate principally to the dependence of proton transfer rates on overall free energy changes[107] and to the participation of proton tunneling in these related processes[76].

Brønsted and Pedersen[108] first related the effectiveness of a catalyst to its acid/base strength by the relation

$$k_A = G_A K^{\alpha} \qquad (2\text{-}12)$$

where k_A is the catalytic rate constant for acid catalysis, K is the dissociation constant for the acid and α is the so-called Brønsted coefficient, analogous to the transfer coefficient α in electron-transfer processes at electrodes. G_A and α are often constant for a series of structurally similar catalysts and given solvent and temperature. This relation applies to direct proton transfer reactions of the type

$$AH^+ + B = A + HB^+ \qquad (2\text{-}13)$$

Noting that $\Delta G^o = -RT \ln (K)$ and taking logarithms, eqn.(2-12) can be rewritten as

$$\ln k_A = -\alpha \Delta G^o/RT + \ln G_A \qquad (2\text{-}14)$$

This equation, the so-called Brønsted relation, was the first linear free energy relationship to be formulated and was interpreted in terms of potential energy diagrams by Horiuti and Polanyi[109] and by Bell[110]. The situation is shown schematically

in Fig.2-9 in terms of intersecting energy curves for AH^+ and HB^+ in eqn.(2-13). In this figure, curve B_2 is "shifted" to curve B_1 on account of a change in free energy $\Delta RT \ln K$ associated with a change of acidity constant. This brings about a reduction in the free energy of activation $G_1^{\ddagger} - G_2^{\ddagger} = (1-\alpha)\Delta RT \ln K$ and a corresponding increase in rate in according to eqn.(2-14) above.

The connection between the Brønsted relation and the kinetics of electrochemical proton transfer was pointed out by Brønsted and Ross-Kane[111] and treated further by Frumkin[112] and Conway[113]. Thus changes in electrode potential in the heterogeneous case are equivalent to changes in acidity constant in homogeneous proton transfer as shown comparatively in Fig.(2-9); as a consequence of a change in applied potential, the free energy of activation for electrochemical proton transfer is modified according to

$$\Delta\bar{G}^{o\ddagger} = \Delta G^{o\ddagger} \pm (1-\alpha)\Delta VF \qquad (2\text{-}15)$$

where $\Delta\bar{G}^{o\ddagger}$ is the electrochemical free energy of activation and $(1-\alpha)$ is the charge transfer symmetry factor which is usually found to be constant over a wide range of potential. In contrast, in the homogeneous case, the Brønsted coefficient is found to vary appreciably with $\Delta \log K$ in a number of systems[107]. This is because, in the electrochemical case, changes of electric energy ΔVF change principally the Fermi level energy of electrons in the metal without changing appreciably the form of the molecular potential function of the proton donor, e.g. H_3O^+, at the electrode interface. On the other hand, for homogeneous proton transfer between a series of acids and bases, change e.g. of acid (HA) strength (pK_a) is usually associated with a

Fig.2-9 Comparison of a) the effect of change of base strength $\Delta RT \ln K$, in a homogeneous Brønsted acid-base proton-transfer process in terms of a free energy profile diagramme with b) the effect of an electrode potential change ΔV on the potential-energy profile and activation energy for a heterogeneous electrochemical proton-transfer process with chemisorption.

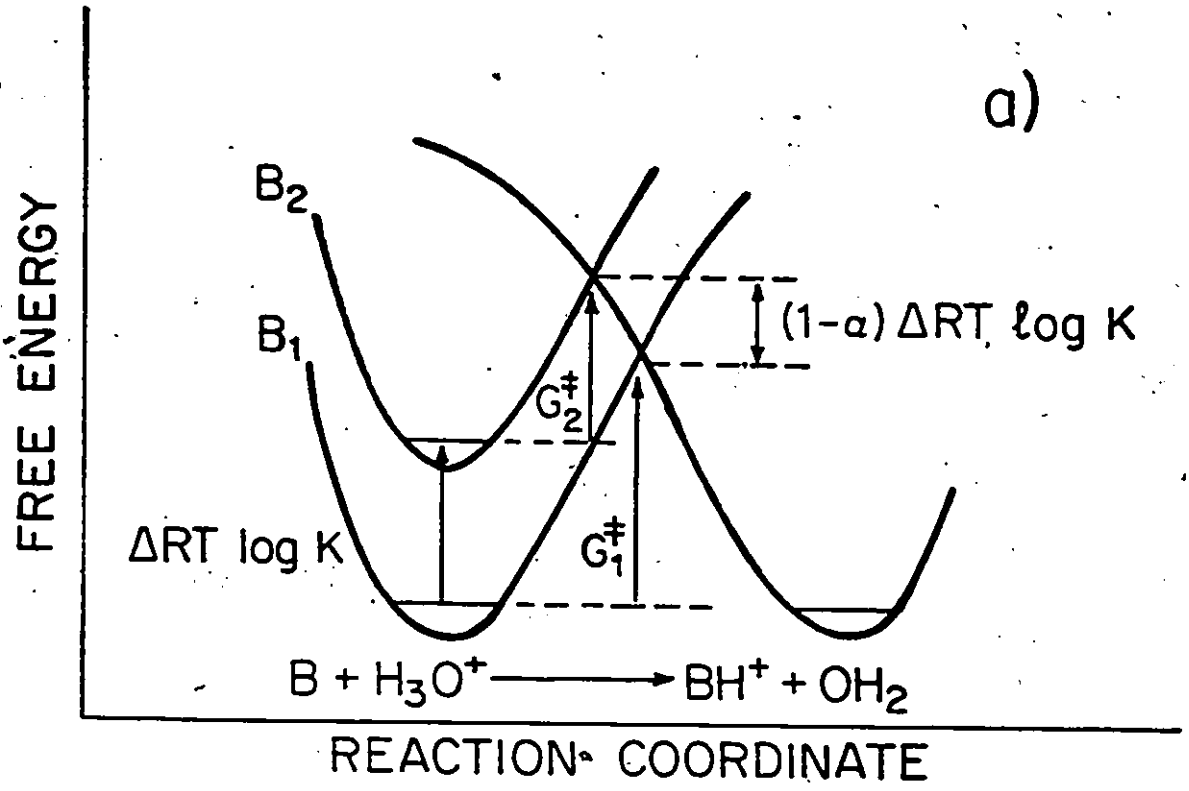
a)
FREE ENERGY
B_2
B_1
$(1-\alpha)\,\Delta RT\,\ell og\,K$
$G_2^{\ddagger}$
$\Delta RT\ log\ K$
$G_1^{\ddagger}$
$B + H_3O^+ \longrightarrow BH^+ + OH_2$
REACTION COORDINATE

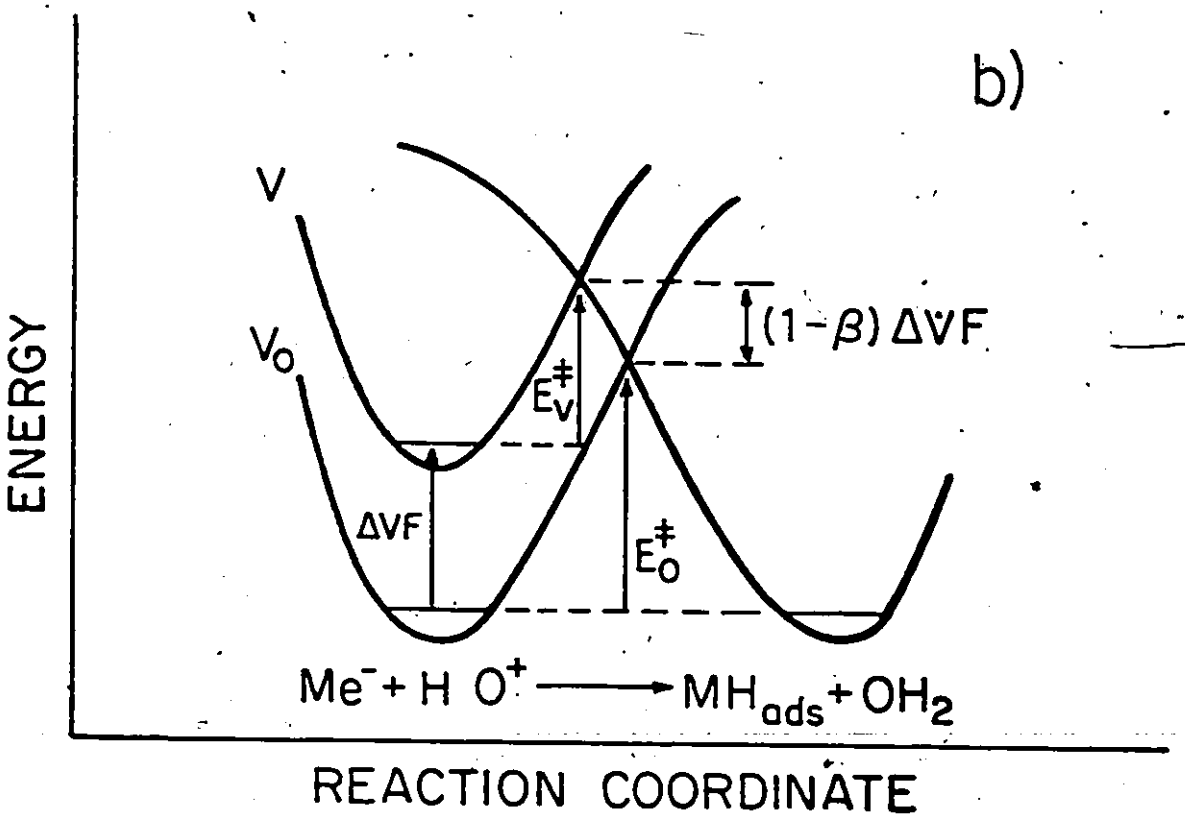
b)
ENERGY
V
V_o
$(1-\beta)\,\Delta VF$
$E_V^{\ddagger}$
ΔVF
$E_o^{\ddagger}$
$Me^- + H\ O^+ \longrightarrow MH_{ads} + OH_2$
REACTION COORDINATE

change of A-H bond strength and associated force constant, so that the potential profiles for the course of the reaction (as in Fig.2-9) also change their form as their relative energy level, determined by $\Delta RT \log K_a$, is changed in a series of proton donors.

Later, however, we show from results obtained in the course of the present work that the entropy of activation in the h.e.r. is experimentally observed to vary with electrode potential, a situation of great interest in the kinetics of the h.e.r. and other electrochemical atom-transfer reactions.

Homogeneous proton transfer reactions may also involve H tunneling[76] and a number of striking examples have been discovered. Bell[114] found the first clear evidence of proton tunneling in a study of the Arrhenius parameters and H/D kinetic isotope effect in proton abstraction from 2-ethoxycarbonylcyclopentanone. More recently the participation of H tunneling has been shown in the proton abstraction reaction ($\cdot CH_3 + CH_3CN = CH_4 + \cdot CH_2CN$) of photochemically generated methyl radicals in the solid state[115,116]; the rate of reaction was followed by monitoring the e.s.r. spectra of the reactant $\cdot CH_3$ and product $\cdot CH_2CN$ radicals. At 77 K, $k_H/k_D > 28000$ for the reaction[116] was found, which exceeds the maximum value $k_H/k_D = 1500$ predicted on the basis of differences in zero point energies.

The participation of proton tunneling has also been indicated by significant curvature in Arrhenius plots, e.g. in the isomerization of 2,4,6-tri-t-butylphenyl[117] which involves the intramolecular transfer of an H atom; the H/D kinetic isotope

effect (k_H/k_D = 13000 at 123 K) further indicated the presence of tunneling in this system.

Low temperature measurements of electrochemical proton transfer are limited by the freezing point of the electrolyte solutions commonly employed. Conway and Salomon's investigations on the h.e.r. down to 163 K used CH_3OH and C_2H_5OH. The use of solid electrolytes should allow the range of temperatures accessible to study to be extended, although mass transport and electrolyte conductivity effects may be limiting. Stimming and Schmickler[118] have recently used solid $HClO_4 \cdot 5.5H_2O$ at temperatures down to 123 K in an exploratory voltammetric study of surface processes and of the Fe^{3+}/Fe^{2+} redox couple at Pt; diffusion coefficients and exchange current densities for the redox reactions were determined as a function of temperature. This work and a subsequent investigation[119] on the h.e.r. from this frozen electrolyte demonstrate the feasibility of direct low-temperature electrochemical investigations, e.g. of the role of proton tunneling in proton discharge.

(viii) The Symmetry Factor β

The significance of the symmetry factor, β , derived from the Tafel slopes for electron-transfer reactions has been discussed in terms of the effect of changes in electrode potential in the various theories of electron transfer[35,120]. It is necessary to distinguish the "symmetry factor" (β) from the "transfer coefficient" (α). β refers to the potential-dependence of the rate of an electron transfer step (elementary reaction) while α applies to the potential-dependence of the rate of the overall

reaction. Thus α derived directly from the Tafel relation may result from several elementary steps, e.g. involving the potential-dependence of coverage by any adsorbed intermediates involved in the reaction sequence -- see eqns.(1-6), (1-7) in the overall reaction. In some cases, the electron transfer step may be rate-determining, e.g. for the h.e.r. at Hg, and hence $\alpha \equiv \beta$. General expressions for α for the h.e.r. when a single step in the overall reaction is clearly rate-determining have been given in the literature[6,16] and were discussed in a previous section.

In the context of activated complex theory, changes in applied potential are considered as modifying the electrochemical free energy of activation according to

$$\Delta \bar{G}^{o\neq} = \Delta G^{o\neq} - \beta VF \qquad (2\text{-}16)$$

where β is a barrier symmetry factor and V is the metal-solution potential difference. A simple interpretation[2] of the significance of β can be given by manipulating the energy profile diagram shown schematically in Fig.2-10. The applied potential shifts the initial state energy curve for $M + H^+ + e^-$ (Fig.2-10) by an amount VF; this results in a change $(1-\beta)VF$ in the relative energy of the transition state and in a change βVF in the activation energy for the forward reaction. For symmetrical energy curves which are approximately linear in the region of intersection and have similar slopes, it is obvious from Fig.2-10 that $\beta = 0.5$ for appreciable changes in V. Such a relation between activation energy and the energetics of the overall reaction is analogous to the Brønsted[108] relation, e.g. for homogeneous proton transfer. Since the effect of potential is primarily to change the Fermi level of electrons in the metal by

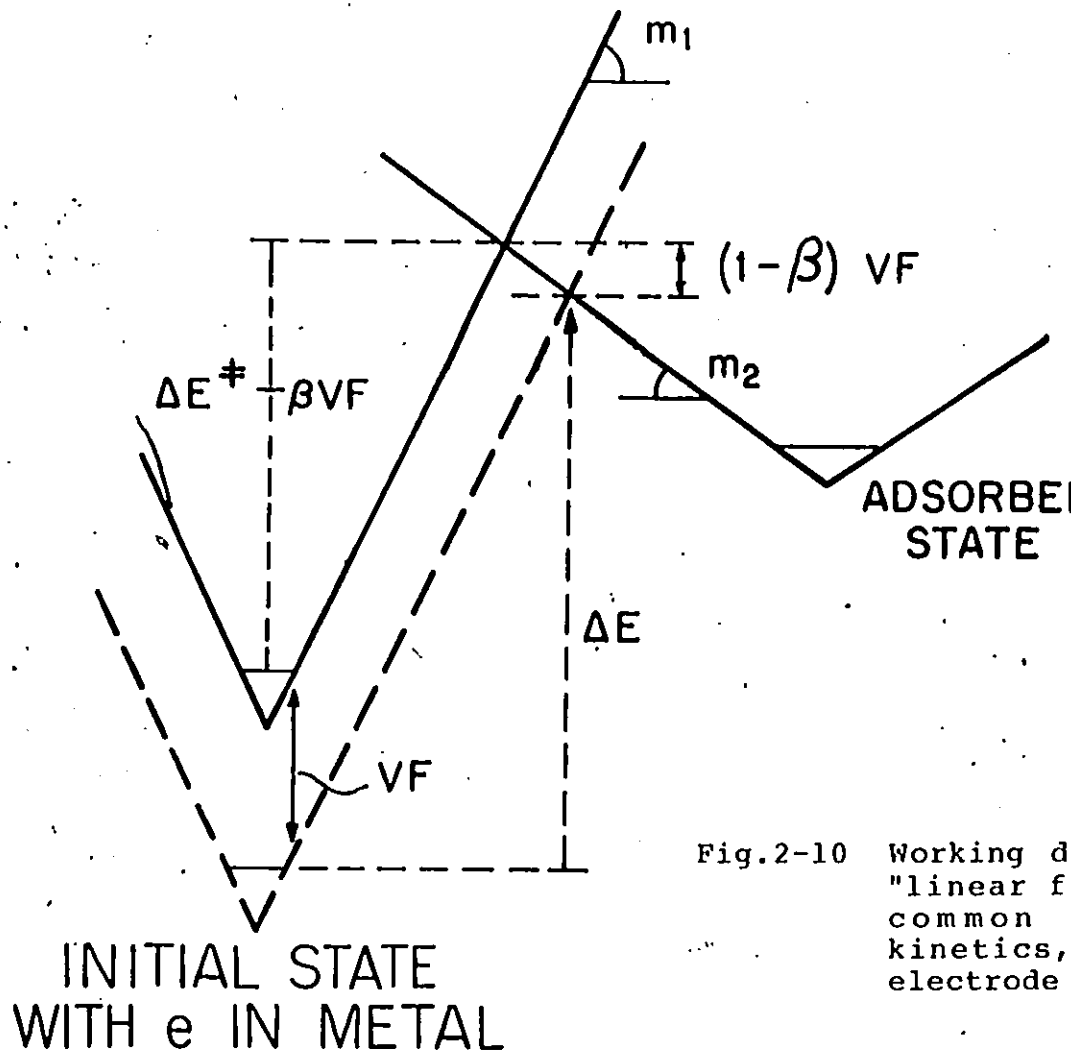

Fig.2-10 Working diagrammes showing how the "linear free energy relationship", common in electrode process kinetics, arises from changes in electrode potential.

eV, leaving the form of the energy surface essentially unchanged, such "linear free energy relationships" for electrode processes are often linear over wide ranges of change of energy (potential). Of course, this energy profile representation is an oversimplification since the course of activation in a charge-transfer process involves fluctuations in the reacting ion's solvation shell, in addition to the physical transfer of an atom down a single coordinate as in Cl_2 evolution or in the h.e.r.; for the proton transfer, proton tunneling[76] must also be considered, as was mentioned earlier.

In ionic redox processes which do not involve atom transfer, Hush[42,121] has identified β with the fractional charge transferred in forming the activated complex. Symmetrical heterogeneous redox reactions, e.g., $Fe(CN)_6^{3-}/Fe(CN)_6^{4-}$, then should have $\beta = 0.5$, in the absence of differences in specific adsorption of the ions of the conjugate redox pair[122]. This representation also gives an indication of the relative electrical and structural similarity of the activated state with respect to initial and product states. β may also be taken as a measure[50,18] of the "distance" along the reaction coordinate at which the activated complex occurs and hence as the fraction of the potential difference across the Helmholtz layer through which the electron charge is transferred to the activated state. Conway[123] has pointed out that if <u>both</u> fractional charge transfer <u>and</u> the local field at the activated complex are considered simultaneously, then $\beta = 0.25$ would result (a conclusion inconsistent with experiment), assuming nearly symmetrical

behaviour in both cases; this was taken to imply that electron transfer occurs by electron tunneling, as proposed by Gurney[3] to a suitably activated reacting particle.

In the present work, the form and temperature-dependence of for the h.e.r. at Hg will be considered in the light of true activation parameters.

(ix) Synopsis of Remaining Problems with the H.E.R.

The following problems remain incompletely or unsolved:

a) a clear indication of proton tunneling in the h.e.r. at some metals. This requires work at temperatures lower than those hitherto reached, with evaluation of the Arrhenius plots and H/D isotope effects down to such temperatures;

b) the mechanism of activation in the h.e.r. -- "bond stretching" or H_3O^+ solvation shell reorganization;

c) evaluation of the entropy of activation as a function of electrode potential and hence the temperature dependence of Tafel slopes;

d) clearer evaluation of the effect of varying proton source and proton-acceptor solvent on the kinetics of the proton discharge step in the h.e.r.; and

e) evaluation of the behaviour of overpotential-deposited H species that are kinetically-involved intermediates in steps of the h.e.r. at appreciable faradaic currents.

Several of the above topics are the subject of the work described in this thesis. Others, d) and e), are also under investigation in this laboratory by various co-workers.

2. Temperature Dependence of the Tafel Slope, b

The temperature-dependence of the Tafel slope, b, is intimately connected with the origin and nature of the effect of potential on electron transfer rates at electrodes and, in the particular case of the h.e.r., with the molecular aspects of coupled electron and atom transfer. We hence consider this important question in some detail in this section, as it will have a bearing on the discussion of some of the results to be given later.

The potential-dependence of the rates of many electrochemical electron transfer reactions is adequately described by the Tafel relation (eqn.1-4); the so-called Tafel slope, b, is conventionally written as

$$b = 2.3RT/\alpha F \qquad (2\text{-}17)$$

where α is the transfer coefficient ($\equiv \beta$ in some cases) and the other symbols have their usual significance. Such an expression for b occurs implicitly in the widely used Butler-Volmer[24,25] equation for the rate of an electrochemical charge transfer reaction. The representation of the Tafel slope as $RT/\alpha F$ arises from the supposition that some fraction, α (ca. 0.5), of the applied overpotential serves to modify the free energy of activation $\Delta G^{\ddagger}$ which appears in an Arrhenius expression for the electrochemical rate constant. In particular, some fraction of the applied potential has usually been assumed to modify the enthalpy or energy of activation for the process through a change of the Fermi level of electrons in the metal by $\pm\Delta VF$; the entropy of activation has been assumed implicitly to be independent of electrode potential[120] but very little discussion

on the significance and behaviour of the entropy of activation of electrode reactions is to be found in the electrochemical literature, except recently (ref.77).

The widely adopted form of b given above indicates that for α sensibly constant, b should be proportional to temperature. However, following the early work of Stout[124] on the anodic decomposition of azide ion, it has been found experimentally that b is rarely represented with respect to its temperature-dependence by the commonly assumed relation shown above. In particular, b is often found to be independent of temperature or to contain a temperature-independent component, implying temperature-dependence of the symmetry factor (or transfer coefficient) itself.

Since variation of the energy of activation with potential, as referred to above, can lead to only a classical linear variation of b with T through the Boltzmann factor $\exp[\pm\beta\Delta VF/RT]$, it is clear that there exists a major hiatus in the fundamental understanding of the mechanism and molecular mechanics of the process of activation in electron and atom transfer in electrode processes. Thus, the problem of the temperature-dependence of the Tafel slope[74,123] is central to an understanding of the effects of potential on the rates and mechanism of activation in electron transfer reactions.

Relatively few detailed investigations of the temperature-dependence of b have been made. Bockris and Parsons[48,125] and subsequently Conway, MacKinnon and Tilak[74] examined the variation of b over a wide range of temperature. A full critical review of

details and examples of this problem has been given recently by Conway[123].

Bockris and Parsons[48,125] and Bockris, Parsons and Rosenberg[126] found an "unconventional" temperature-dependence of b in the h.e.r. at Hg in methanolic HCl between ca. 276 and 303 K; at lower temperatures, b apparently varied in the conventional way with T, although the derived values of β showed some scatter.

Consideration of this and of more recent work[13] indicates that the "unconventional" dependence does not arise from incidental impurity effects. Bockris and Parsons[48] suggested that the temperature-dependence of b for the h.e.r. at Hg could result from an expansion of the inner region of the double-layer with temperature, although this effect was found to be of insufficient magnitude to account for the "unconventional" experimental behaviour. They also noted that, formally, for b to be independent of T, the entropy of activation, $\Delta S^{\ddagger}$, should be a function of electrode potential, but this point was not pursued further until the study of Conway, MacKinnon and Tilak[74], who examined this matter quantitatively and suggested theoretical reasons for the origin of such an effect on $\Delta S^{\ddagger}$.

Post and Hiskey[69] investigated the h.e.r. at Hg in aq. HCl over the temperature range 270 - 360 K and found an "unconventional" temperature-dependence of b; their b values are shown in Fig.2-11 along with the conventional b (=2.3RT/0.5F). The results of Conway, MacKinnon and Tilak[74] for the h.e.r. at Hg in methanolic HCl over the range 180 - 335 K are also shown in Fig.2-11; it is evident from this plot that eqn.(2-17) for b as f(T) does not apply. The temperature-dependence of b is better

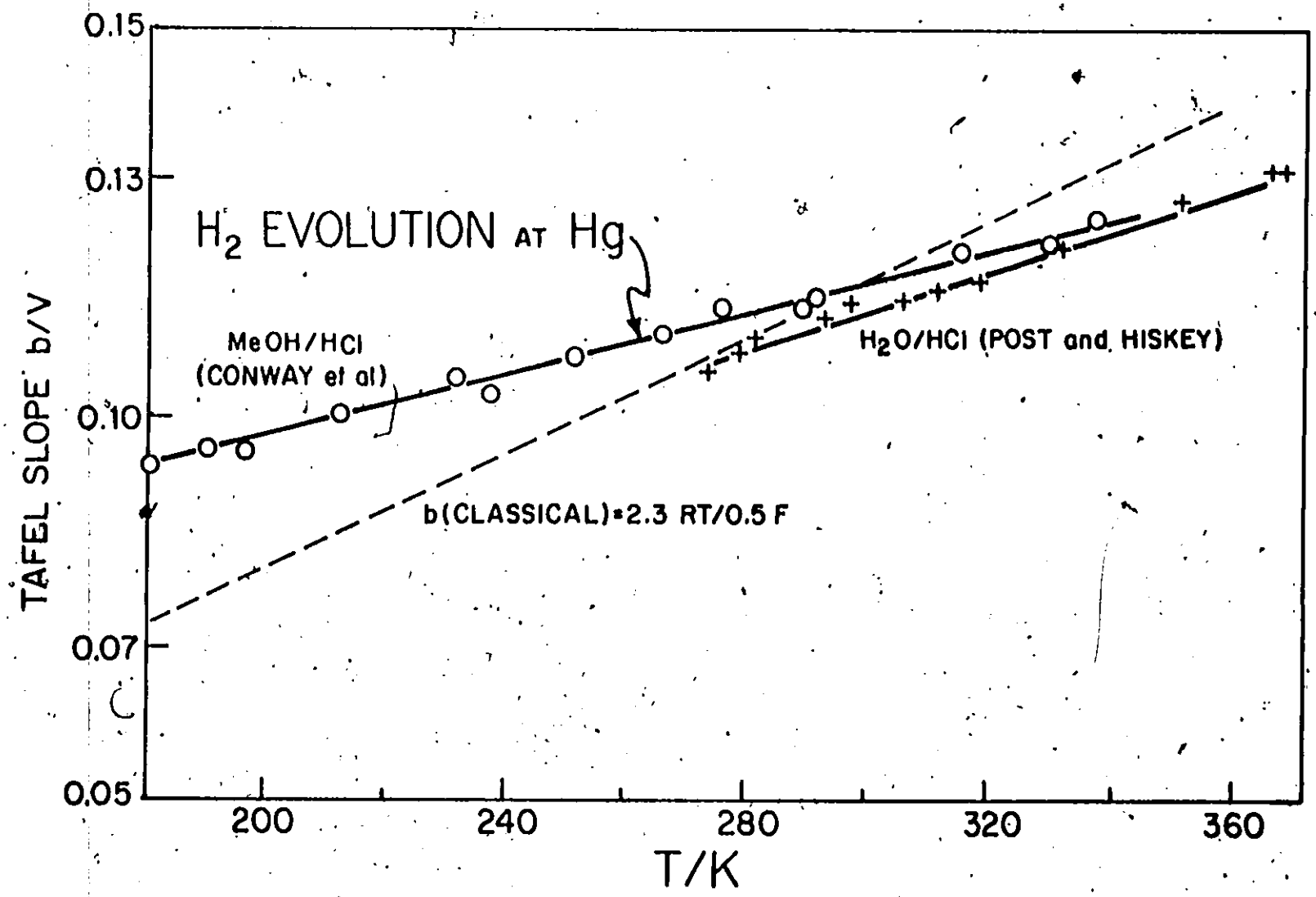

Fig.2-11 Temperature-dependence of b for the h.e.r. at Hg from aqueous[69] and methanolic[73,75] solutions of HCl.

represented by an empirical equation of the form[74]

$$b = 2.3RT/\beta'F + K \qquad (2\text{-}18)$$

where β' is the symmetry factor which is derived from the derivative of b w.r.t. T

$$db/dT = 2.3R/\beta'F \qquad (2\text{-}19a)$$

$$\beta' = (2.3R/F) / (db/dT) \qquad (2\text{-}19b)$$

rather than from a given single value of b at a particular temperature, assuming the conventional form of b, eqn.(2-17). Note that for the h.e.r. at Hg from acidic solutions, the proton discharge step is generally considered to be rate-determining (but see Horiuti et al., ref.127) so that $\alpha \equiv \beta$.

As a consequence of the linear dependence of b on T shown in Fig.2-11, β' is a constant with T but may differ significantly from the conventional $\beta = 0.5 \pm 0.05$ usually obtained using eqn.(2-17) at T near 298 K. It would appear then that for the h.e.r., it is incorrect to evaluate a temperature-independent β from eqn.(2-17) at some particular temperature T since, in fact, eqn.(2-17) does not adequately represent the form of b with T. Conway[123] has called attention to the remarkable coincidence that β evaluated from eqn.(2-17) at "room temperature", ca. 298 K, turns out to be very near the conventional value of 0.5 . Yeager[128] has emphasized a similar point in discussing experimental results for O_2 reduction at Pt in H_3PO_4 over a wide temperature range. If β is considered to be temperature-dependent, then the relation between β and β' from eqns.(2-17) and (2-18) is

$$\beta = \beta'[\ 1 + \beta' KF/RT\ ] \qquad (2\text{-}20)$$

so that β is apparently temperature-dependent. An increase in β, with temperature, evaluated according to eqn.(2-17), has been noted in earlier work.

In a following chapter of the present thesis, an alternate expression for the temperature-dependence of b will be deduced from an analysis of the experimental activation parameters for the h.e.r. at Hg in acidic media.

A temperature-independent b was reported by Stout[124] for the anodic evolution of N_2 from the discharge of azide ion at Pt in aqueous solutions; this corresponds to α being apparently linear in T. Qualitatively, this case may be expected to differ from that for the h.e.r. since here the detailed mechanism and N_3 radical participation or other adsorbed intermediates is not known; alternatively, the azide oxidation may be viewed as a limiting case of the empirical relation in eqn.(2-18) where $K >> 2.3RT/\beta'F$. Although very little is known about the surface electrochemistry in azide discharge, this reaction probably occurs on a Pt surface covered or partially covered by surface OH or O species (see ref.129); this is the situation in anodic halogen evolution[129] and in carboxylate anion[130] discharge from aqueous solutions. The state of the Pt surface itself will be temperature-dependent[131] and hence complicate the identification of a single reason for the independence of b on temperature.

Conway, MacKinnon and Tilak[74] reported a temperature-independent Tafel slope for the anodic Br_2 evolution reaction at C in CH_3CN; it was concluded that in this relatively unstructured solvent, the "unconventional" temperature-dependence of b cannot be attributed to changes in the structural factor[132] in the

solvation of the reactant ion. A possible contribution to the entropy of activation from potential- and temperature-dependent solvent orientation in the inner region of the double-layer was suggested in ref.74; this question was examined in terms of the BDM[70] 2-state model of solvent dipole orientation in the double-layer.

Appleby[133] and later Yeager et al.[128] have found b to be constant (with temperature) for O_2 reduction at Pt and Os in H_3PO_4 over a 220 K and a 115 K range of T, respectively. The values of α derived from b by means of eqn.(2-17) are shown in Fig.2-12[128]; clearly α is temperature-dependent, corresponding to the "unconventional" behaviour of b. This example shows that this type of behaviour may also arise for a reduction reaction as well as for anodic processes where the coverage of surface oxide at, e.g. Pt, may be considerable. Yeager[128] has stressed the importance of the temperature-dependence of α to the understanding of the effect of applied potential on the rates of electrode processes.

3. State of the Proton in Solution

In considering the molecular mechanism and mechanics of discharge of H^+ from aqueous acid solutions, it is obvious that the state of the reactant proton in solution is a matter of major importance.

(i) Solvation Energetics and its Relevance to the Topics Treated in (1) Above

The initial-state energy curve for H^+ discharge in relation

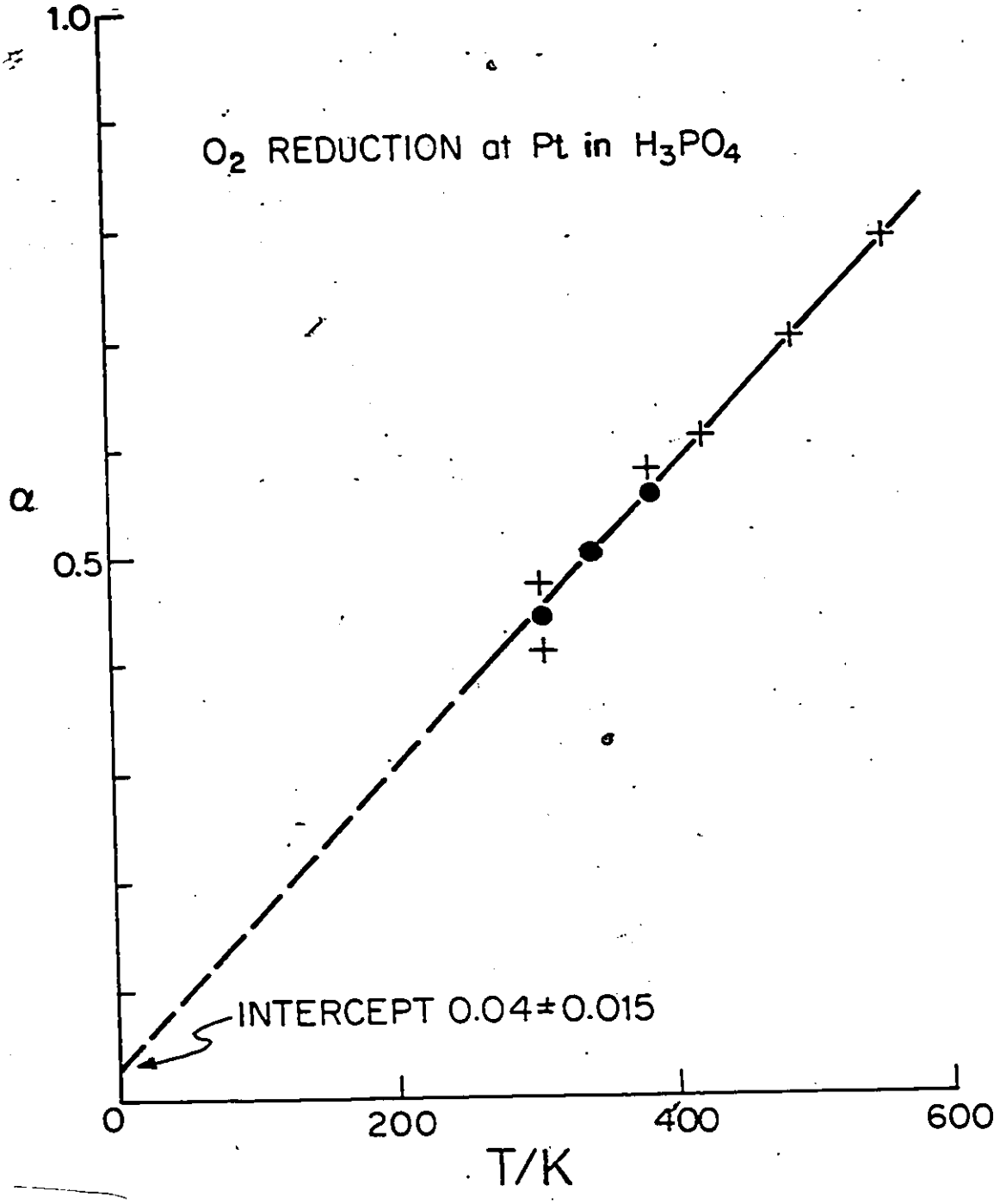

Fig.2-12 Transfer coefficient as a function of temperature for O_2 reduction at Pt in H_3PO_4 (ref.128).

to the Brønsted relation should be "shifted" by changes in proton solvation energy, as well as by changes in energy of the electron through changes in electric potential. Accordingly, changes in the state of solvation of the proton change the free energy of activation by α times the free energy change of the initial state; this might be expected to give rise to large differences in rates of proton discharge (and hence for the h.e.r.). However, Krishtalik[134] has shown that hydrogen overpotentials in a number of non-aqueous solutions differ very little, and that no simple quantitative relation exists between these values and the corresponding proton solvation energies in these media. This situation is peculiar to electrochemical Brønsted relations and is due to an exactly equivalent but opposite change of the metal-solution potential difference at the reversible potential with changes in solvation energy of the reacting ion; since electrochemical kinetic measurements are usually compared at constant overpotential, these two effects change the free energy of activation to equal but opposite extents and so no net primary effect is expected according to the Brønsted relation[108]. In practice, however, some changes in free energy of activation can occur due to changes in the energy surface or transition state other than those predicted by Brønsted effects based on shifting initial-state energy curves "up" or "down" on the energy scale.

It is of some interest to compare the rates of electrochemical reactions at constant metal-solution potential difference, and, e.g. vary a) the proton source, b) the solvent, or c) the temperature.

a) The work of Krishtalik[87] on the rates of the h.e.r. from

H_3O^+ or CH_3CNH^+ in CH_3CN suggests an approach for varying the proton source while keeping ϕ_{M-S} constant: thus kinetic measurements can be made for various proton donors (in a given solvent) and compared with respect to a reference electrode which is reversible to, say, the anion of the acid, or to an ion of a supporting electrolyte. Provided that the proton donors are chosen so as to leave the reference electrode potential essentially unchanged (i.e., there are only minor effects of these modifications on the activity coefficients, as with the use of a supporting electrolyte), then to a good "chemical" approximation, ϕ_{M-S} at the working electrode may be taken as constant. Under these conditions, a comparison of the proton discharge kinetics will reflect changes due to the specific solvational state of H^+. A kinetic investigation employing this approach in the study of the h.e.r. from series of N-alkyl ammonium salts is currently in progress in this laboratory[106].

b) Considerably more uncertainty arises in attempting to fix ϕ_{M-S} while changing the solvent. Here a reference electrode which is reversible to some ion other than the proton source is required and in addition, ϕ^R_{M-S} for this reference electrode must be independent of the solvent used (or at least amenable to a suitably accurate solvation energy correction, e.g. based on solvent dielectric constant). The drastic change in medium effect on ϕ_{M-S} resulting from a change of solvent makes this approach rather unreliable for use in electrochemical kinetic studies.

c) The question of practically fixing ϕ_{M-S} while varying the

temperature has been addressed by Weaver[77] and will be considered in some detail in a following section of this thesis.

(ii) Existence of H_3O^+

The H_3O^+ ion is indicated as the possible cationic species in aqueous solutions of strong acids; the "chemical" existence of free H^+ (a sub-atomic particle) in water is extremely unlikely[83]. Early evidence for the existence of a specific oxonium species arose from Goldschmidt's work[135] on acid-catalyzed esterifications, and from Bagster and Cooling's[136] investigations of the conductivities of solutions of HBr in SO_2 with the addition of small amounts of H_2O.

More direct evidence for the existence of H_3O^+ has been obtained from proton n.m.r. studies on the monohydrates of strong acids (e.g. H_2SO_4, HNO_3, HCl and $HClO_4$) by Richards and Smith[137] and by Kakiuchi et al.[138]. The line shapes in solid state proton n.m.r. of the monohydrates depend on the geometrical arrangement of the interacting nuclei[139]; the observed three-band spectrum is consistent only[137,138] with a trigonal pyramidal structure, H_3O^+, analogous to NH_3. $CF_3SO_3H.H_2O$ has been shown[140] to be a similar salt: $H_3O^+CF_3SO_3^-$. The structures of these acid monohydrates have, in some cases, also been determined by X-ray[141,142,143] and neutron diffraction[144]; the expected, nearly trigonal, (C_{3v}) pyramidal geometry of H_3O^+ was confirmed.

Mass spectrometry has been used in the study of H_3O^+ and of higher complexes of H^+ with two, three, four or more water molecules[145] in the gas phase. The work of Kebarle and Godbole[146] showed the presence of hydrated protons up to

$H^+(H_2O)_5$; the most abundent ion is H_3O^+ and $H_9O_4^+$ is apparently not significantly more stable than the other species. The enthalpies of successive stages of proton hydration and the kinetics of complex formation can also been studied by this method.

In the liquid aqueous phase, early investigations failed to yield an observable characteristic vibrational spectrum for H_3O^+ ions[147]; this was attributed to the supposed short lifetime of H_3O^+ associated with the "anomalous" mobility exhibited by the proton in aqueous solution. However, Conway, Bockris and Linton[148] made kinetic calculations on the mechanism of proton mobility and predicted a significant lifetime for the H_3O^+ ion. Falk and Giguere[82] succeeded in characterizing the H_3O^+ and corresponding D_3O^+ species by i.r. spectroscopy in concentrated aqueous solutions of strong acids; bands were observed corresponding to those which had been assigned previously to H_3O^+ in crystalline "acid hydrates". Thus the chemical existence of H_3O^+ in aqueous solutions is well established.

Sherman[149] calculated the proton affinity of water, $P(H_2O)$, associated with the reaction

$$H_2O + H^+ = H_3O^+ + P(H_2O) \qquad (2\text{-}20)$$

by means of energy cycles for oxonium and ammonium perchlorate, taking the crystal lattice energy of these two isomorphous salts to be equal; a value of $P(H_2O) = 761$ kJ mol^{-1} was found, which was revised, in the light of more modern thermodynamic data, to 786 kJ mol^{-1} by Sokolov[150]. The related standard free energy change[151] for the gas phase protonation of H_2O is -677 kJ mol^{-1}.

(iii) $H_9O_4^+$ in aqueous Solution

The proton affinity of H_2O[150] and the best estimates for the enthalpy of hydration of the proton[152] indicate a hydration energy of H_3O^+ in excess water of -355 to -330 kJ mol^{-1}; the nature of this residual hydration of H_3O^+ in water has been considered with regard to hydrogen bonding and formation of the H-bonded complex[86,153] $H_9O_4^+$. This species is one of several stable gas phase species studied by mass spectrometry[145,146] and is consistent with estimates of the primary coordination number[154] of H_3O^+. The large partial molar heat capacity of H^+_{aq} and its temperature-dependence can only be explained according to Ackermann[86] in terms of the complex hydrated ion, $H_9O_4^+$, and not by the structure H_3O^+ alone. The configuration around the H_3O^+ ion is envisaged as an almost tetrahedral $H_9O_4^+$ primary solvation shell as shown in Fig.2-13; as a result of this configuration, rapid exchange of H^+ can occur between the central H_3O^+ and the three H-bonded H_2O molecules, yielding a kind of delocalization of H^+ on a somewhat longer time scale than that for an OH vibration[151].

The nature of $H_9O_4^+$ in excess water and of the additional coordinated water molecule (Fig.2-13) determine the molecular mechanics of processes such as "anomalous" proton conduction and electrochemical proton discharge.

(iv) Overall Solvation of H^+

From the foregoing discussion, it will be seen that three stages in proton hydration can be identified: a) protonation of an H_2O molecule in the gas phase to form a stable molecule ion,

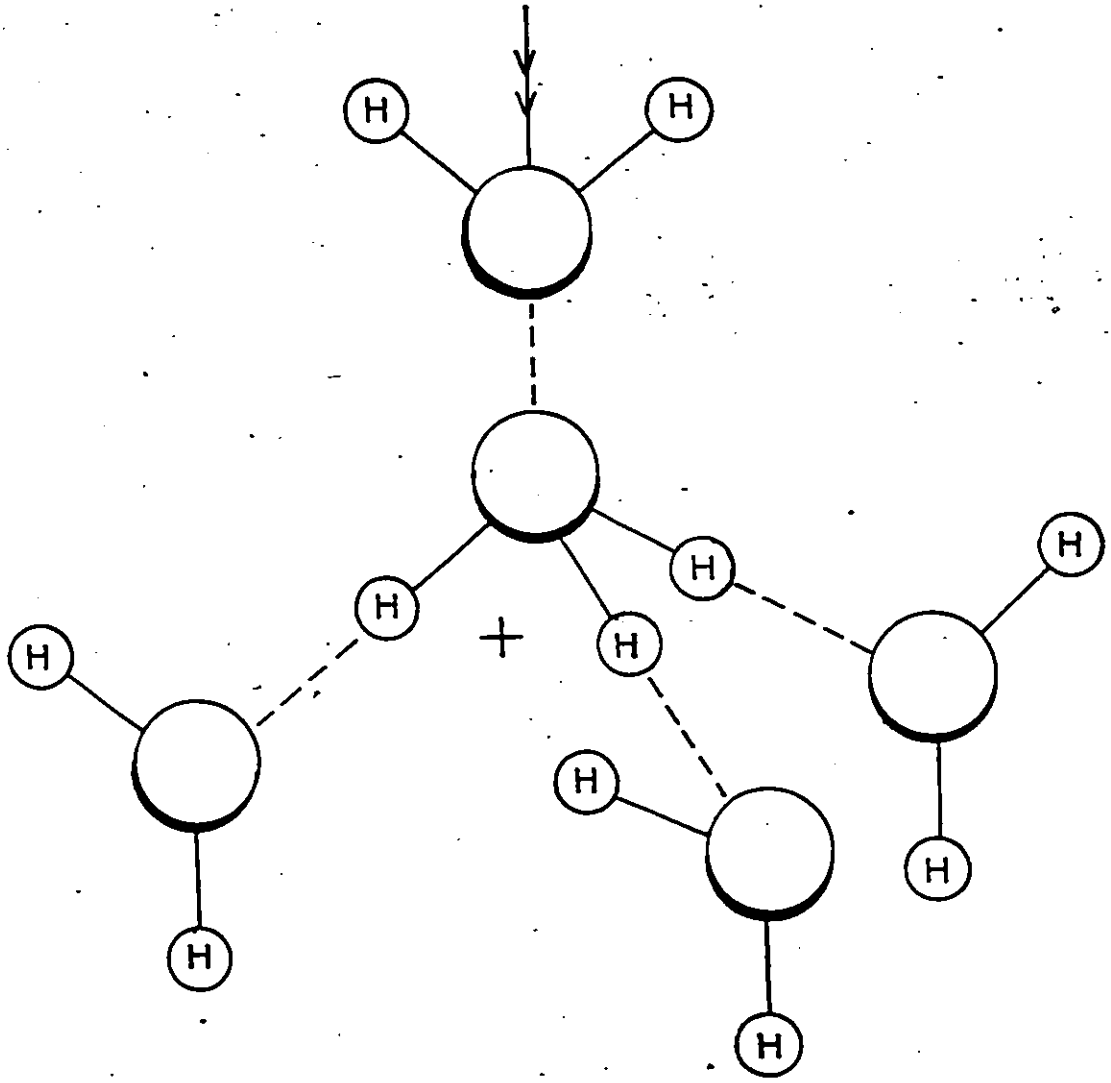

Fig.2-13 Configuration of the $H_9O_4^+$ ion with extra electrostatically bound H_2O molecule.

H_3O^+, b) the specific hydration of H_3O^+, e.g. with three H_2O molecules giving the labile H-bonded $H_9O_4^+$ complex, and c) the further hydration of this charged complex associated with long-range dielectric polarization.

For absolute heats of solvation of the H^+ ion to be derived from experimental data, some extra-thermodynamic principle for division of the observed enthalpy of solution for a salt must be introduced. A critical review of such procedures which are based, e.g. on consideration of inner-sphere ion-dipole and ion-quadrupole interactions in addition to a Born-type solvent polarization, has been given by Conway[155]. Lister, Nyburg and Poyntz[156] give a value for the absolute heat of hydration of H^+ as -1096 kJ mol^{-1}, using the extrapolation procedure of Halliwall and Nyburg[157] for doubly charged complex ions. Combining this result with the value for the absolute entropy of H^+, derived from its individual partial molar entropy in aqueous solution, gives the free energy of hydration of the proton as -1079±29 kJ mol^{-1}.

The strongly hydrogen bonded state of H_3O^+ in excess water is reflected in broad bands in the vibrational spectrum, and the above-mentioned large and classical heat capacity; this may be expected to influence the nature of the activation and molecular mechanics in electrochemical proton discharge as will be discussed later.

CHAPTER 3

EXPERIMENTAL PROCEDURES

1. Choice of Methods

a) In the evaluation of heats of activation and frequency-factor data for the h.e.r. and d.e.r. steady-state current-density vs overpotential information was required over a range of temperatures. A computer-controlled steady-state measurement procedure was used in that part of the work.

b) In corresponding evaluations of the kinetic behaviour of adsorbed H and D ionization, linear-potential-sweep experiments were conducted over a wide range of sweep-rates (s) to evaluate the reversibility parameter[158], s_o, with corrections for the uncompensated resistance effect (see below) at high s values.

c) Computer-controlled experimentation and data-collection procedures were used where appropriate and the requisite data handling and reduction software developed. And

d) A new method of data acquisition and processing for open-circuit potential-decay measurements was developed with Bai and leads to information on the adsorption pseudocapacitance and coverage behaviour of the kinetically significant intermediates in the h.e.r.

2. Choice of Systems

The monohydrate of CF_3SO_3H provides a source of protons in the unhydrated H_3O^+ state, from which the proton discharge reaction can be studied. Dilute (1 M) aqueous CF_3SO_3H in which the proton exists as the extensively hydrated "$H_9O_4^+$" species (cf. ref.86) was used in the comparative study of the role of the

state of the proton source in the kinetics of the h.e.r. and of the ionization of adsorbed H at Pt. The thermal stability of the anion, as well as its inactivity as a redox reagent, facilitates the purifcation of the CF_3SO_3H by distillation. The relatively inert salts of CF_3SO_3H are increasingly replacing the corresponding perchlorates, especially in studies in non-aqueous solvents, since the latter salts can cause the violent oxidation of these solvents.

The h.e.r. was studied comparatively at Pt, where the electrochemical desorption of H is usually the rate-determining step, and at Hg, where the coupled electron/atom transfer step is generally believed to be rate-determining. The anodic desorption of under-potentially deposited H at Pt provided an opportunity to study directly an elementary reaction involving electron transfer with single atom transfer. Hydrogen evolution at Ni was also of interest due to the possible formation of an hydride phase in the electrode surface, which has been indicated at cathodic potentials in a number of electrolytes.

3. Preparation of Reagents and Solutions

Experiments were conducted in 1 M aqueous CF_3SO_3H and in the ionic liquid monohydrate of CF_3SO_3H, made up in pyrodistilled[159] or triply distilled water. H/D kinetic isotope effects were also evaluated using CF_3SO_3D in redistilled D_2O (99.8% from Atomic Energy of Canada Ltd.). The D_2O is very free from impurities owing to its method of production from repetitive electrolysis and re-synthesis of water from $H_2/HD/D_2$ by combustion in oxygen.

(i) $\underline{CF_3SO_3^-H_3O^+}$ and 1M aq. $\underline{CF_3SO_3H}$

The CF_3SO_3H used in the preparation of the monohydrate was distilled at atmospheric pressure (b.p. 435 K) in a N_2 stream. After addition of a stoichiometric quantity of H_2O, the $CF_3SO_3^-H_3O^+$ formed was twice distilled in an all-glass apparatus at reduced pressure (b.p. 355 K, P < 130 Pa) and collected in Pyrex collection ampoules which were immediately sealed under vacuum for subsequent use in the runs.

Aqueous solutions, 1 M in the trifluoromethanesulfonic acid, were made up from the "monohydrate" in pyrodistilled water. In these solutions, the proton exists in the normal, fully aquated state that has been represented as "$H_9O_4^+$".

(ii) $\underline{CF_3SO_3^-D_3O^+}$ and 1M $\underline{CF_3SO_3D}$ (in $\underline{D_2O}$)

Trifluoromethanesulfonic anhydride was prepared by dehydration of the acid with "P_2O_5" and redistilled with a further small quantity of "P_2O_5". $CF_3SO_3^-D_3O^+$ was prepared from the acid anyhydride by reaction with the required stoichiometric amount of D_2O. It was then purified twice by vacuum distillation as described above for $CF_3SO_3^-H_3O^+$. 1 M CF_3SO_3D in D_2O was made up from this material by addition of the required quantity of redistilled D_2O.

(iii) $\underline{CF_3S^{18}O_3H}$ and $\underline{CF_3S^{18}O_3^-H_3O^+}$

Partially labelled $CF_3S^{18}O_3H$ was prepared by reaction of trifluoromethanesulfonic anhydride (prepared as above) with a stoichiometric amount of $H_2{}^{18}O$ (MSD Isotopes, Merck Frosst Canada Inc.). The isotopic composition of the product was verified by mass-spectrometry and confirmed by Raman spectroscopy.

The correspondng ^{18}O-labelled monohydrate was prepared immediately prior to its use by reaction of the ^{18}O-labelled acid with an equimolar quantity of isotopically normal water.

The ^{18}O-labelled acid and monohydrate so prepared were used without further purification in studies to elucidate the nature of the counter-electrode (anode) reaction in the monohydrate "melt".

(iv) Gases

Electrolytic grade hydrogen gas was passed through a conventional purification train consisting of a drying agent, molecular sieve, an oven containing Cu turnings and palladized asbestos at 623 K, and charcoal traps maintained at liquid nitrogen temperature. Deuterium gas was freed from oxygen and other contaminants in a smaller but otherwise similar gas train to that used for hydrogen. H_2 and D_2 gas were bubbled in the working and reference electrode compartments during steady-state polarization experiments.

Nitrogen gas was treated as above, except that only Cu turnings were used in the heated oven. A bright metallic state of the Cu turnings was maintained by periodic regeneration of the Cu by passage of H_2 through the oven.

4. Electrodes

(i) Reference Electrodes

A platinized Pt hydrogen reference electrode (RHE) in the same solution as that under study was employed. In the polarization measurements, the entire electrochemical cell,

including the reference electrode, was maintained at each temperature of interest. This is of importance for the subsequent discussion of the results and their quantitative interpretation. Non-isothermal cell reference electrode measurements were made in separate experiments to establish, to a good approximation, the temperature derivative of the H_2 electrode potential (cf. ref.160).

In some of the transient measurements, a Pt probe reference electrode was also provided within the working electrode compartment; its potential with respect to the RHE could be monitored. This probe must be used instead of, or in conjunction (using a capacitative shunt) with, the RHE in order to avoid errors due to reference-circuit impedance at high frequencies or sweep-rates in potentiodynamic experiments.

(ii) Pt Electrodes

Pt electrodes were made from polycrystalline drawn Pt wire electrodes (Johnson Matthey, high purity grade) as in other work[158]. Samples of the Pt wire were degreased by refluxing in acetone in a Soxhlet-type extractor for 12 h and then sealed in soft glass electrode holders. The Pt electrodes were then maintained in 98% sulphuric acid. Just prior to runs, these electrodes were washed repetitively in pyrodistilled water. Conditioning cycles of potential change between +0.05 and +1.2 - 1.35 V RHE were applied prior to the kinetic runs.

Small Pt disk electrodes were fabricated using a diamond saw to cut sections of a Pt wire previously sealed in soft glass; the disks were then etched briefly in aqua regia before use.

(iii) Hg Electrodes

Electrodes having a mercury surface were made by amalgamation of a gold wire by electroplating with Hg. The amalgamated surface was then dipped in 3x distilled polarographic grade liquid Hg to produce a liquid Hg film on the electrode. These Hg-film electrodes on Au always gave lower overpotentials for the h.e.r. than on pure Hg.

Experiments were conducted also on a pool electrode of pure liquid Hg contained in a siliconized Pyrex cup.

(iv) Ni Electrodes

Ni electrodes were made of 0.038 cm diameter high-purity grade Ni wires (Johnson Matthey & Mallory Co.). The Ni wire samples were heated and sealed in protective glass bulbs in a stream of purified hydrogen, as described in earlier papers[161]. The glass bulbs were broken in situ in the cell with a suitable negative potential applied before rupturing the bulbs.

(v) Electrode Area

Estimates of the electrode surface areas were made in order to compute real current densities for use in comparing the rates at different metals or under different conditions.

The real area of the Pt electrodes was determined from the adsorbed H ionization charge. A fractional coverage of H species equal to 1 was assumed to obtain at 0.0 V RHE in 0.5 M sulfuric acid, as in previous work[158]. This coverage of under-potentially deposited H corresponds to a charge of 210 $\mu C\ cm^{-2}$ (ref.162).

The geometrical area of the smooth liquid Hg and Hg-film

electrodes surfaces was used and identical Hg pools were employed throughout this part of the work. A consistent preparation technique was used for the Ni electrodes and the electrochemical rates were compared on the basis of the resulting geometrical areas.

5. Experimental Cells and Temperature Control

The all-glass electrochemical cells employed were soaked periodically in concentrated CrO_3 - H_2SO_4 solution and then rinsed and soaked in triply distilled water. The cells were then stored filled with 98% sulfuric acid which was discarded and the cell rinsed repeatedly and soaked in pyrowater before each experiment. Just prior to runs in $CF_3SO_3^-H_3O^+$, the cell was dried in an oven (400 K) for several hours. All auxiliary glass apparatus which came into contact with the test solutions was cleaned in the above manner.

The steady-state polarization and transient experiments were conducted in pyrex cells requiring as little as 30 ml of electrolyte. Separate working, reference, and counter electrode compartments were provided; the Pt counter electrode was placed directly in the working electrode compartment for the cyclic-voltammetry measurements. This type of cell, which could be immersed in a temperature-controlled water bath, is shown in Fig.3-1a.

A counter electrode compartment, which could be inserted into the working compartment through the cell top, isolated the working electrode from the counter electrode reaction products by means of a ground glass conical plug (see Fig.3-1b).

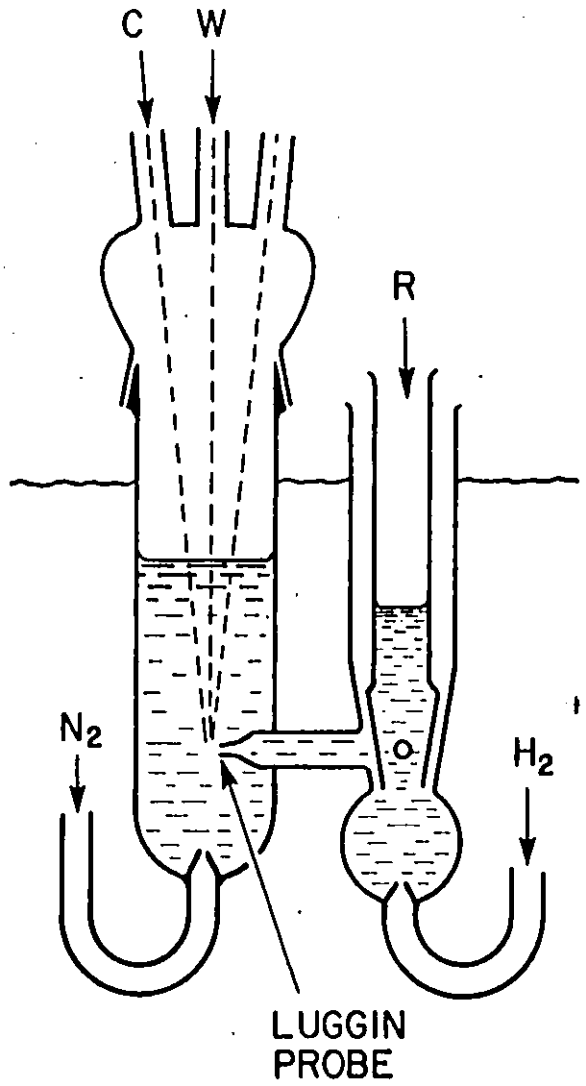

a

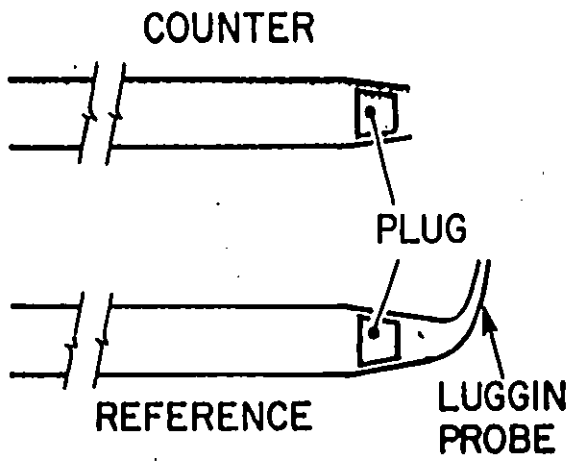

b

Fig.3-1 Electrochemical cells and electrode compartments: a) immersible isothermal electrochemical cell; b) compact counter and reference electrode compartments with ground glass plug separators.

A similar compartment equipped with a Luggin probe was sometimes used in place of the separate reference electrode compartment shown in Fig.3-1a, thereby minimizing the volume of electrolyte required and reducing the reference-circuit impedance. The use of these insertable reference and counter electrode compartments also allowed the resulting one-compartment cell to be conveniently water jacketed for temperature control purposes.

Non-isothermal reference electrode measurements were made using the cell shown in Fig.3-2. The thermal liquid junction was established in a 1 cm x 0.8 cm i.d. tube between water jacketed compartments; provision was made for using a salt bridge in the region of this thermal junction. A thermostated fluid (water or water/ethylene glycol) was circulated through each water jacket.

A small (4 ml) two- compartment pyrex cell for the collection of gaseous products from a Pt anode (ca. 1 cm^2) into evacuated bulbs was used in the ^{18}O labeling work. This cell could be immersed in a thermostated bath.

A commercially available thermostated ($\pm$ 0.05 K) water bath was used for experiments in the range of 273 - 258 K. An ethylene glycol/water mixture was sometimes used as a heat exchange fluid in order to extend the upper temperature limit to ca. 423 K.

6. Instrumentation

The potential of the working electrode was controlled using a PAR 173 potentiostat and the resulting current measured either by means of a precision resistance box (Leeds and Northrup) in

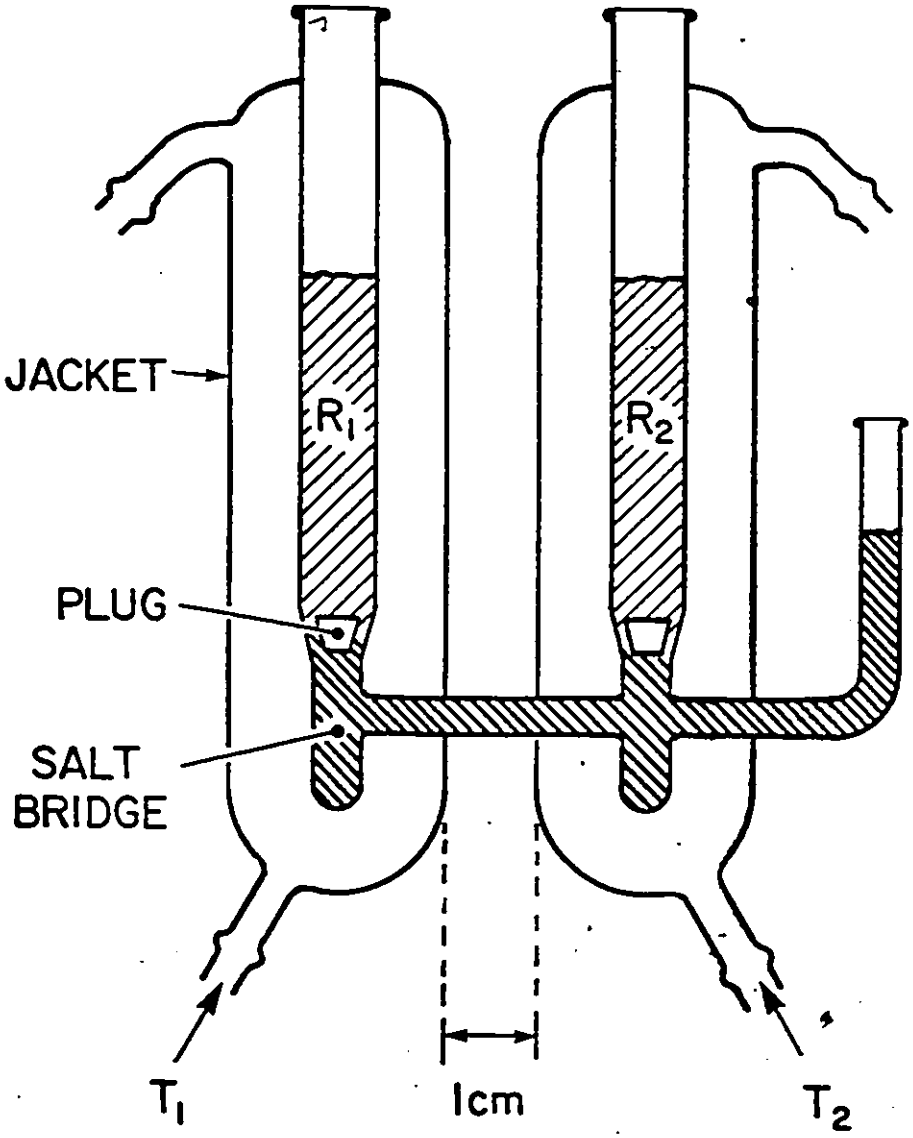

Fig.3-2 Water jacketed non-isothermal reference electrode cell with provision for a salt bridge in the region of the thermal liquid junction.

series with the counter electrode or by means of a suitable digital multimeter. The potential of the working electrode vs the RHE was measured by means of a high-impedance electrometer probe supplied with the potentiostat or using an auxiliary cathode follower.

Steady-state polarization measurements were made by holding the potential constant at selected values for ca. 10 s before recording the current; a computer-based data acquisition and treatment system was developed and used as described in detail in Chapter 4. The uncompensated solution resistance was measured by the interrupt method (and verified by a.c. impedance in some cases), and the observed overpotentials were corrected accordingly.

A Kepco current source was used in the open-circuit potential decay measurements in conjuction with a Hg-wetted reed relay and a Nicolet 2090 (or 3090) digital oscilloscope. A new procedure for analyzing the decay results is described in Chapter IV; the method allows the pseudocapacitance behaviour of adsorbed intermediates to be studied, in the presence of large steady-state currents.

A TACUSSEL type GSATP arbitrary function generator was employed for producing complex potential programmes in the s_o and oxide growth measurements by cyclic-voltammetry. Dynamic IR_u compensation was used at the highest sweep-rates. The resulting I-E profiles could be integrated numerically on a PDP 11/34 or HP87 computer.

Raman spectra of CF_3SO_3H solutions were recorded in capillary tubes using a Yvon-Jobin (model HG2) spectrometer and a

argon ion laser. I.r. spectra were measured on a Perkin-Elmer (model 283) spectrometer, using NaCl windows.

Some of the positive ion mass spectra, used in the analysis of the ^{18}O labelling experiments, were measured on a AEI MS-902S instrument. The ^{18}O isotopic content of water samples in these experiments was measured by both positive and negative ion mass spectroscopy on a VG-ZAB, spectrometer.

7. Computer Procedures and Data Acquisition

During the course of the work, a number of in-house computer-controlled experimental procedures and data acquisition and processing techniques were developed. These will be separately described in some detail in Chapter 4 which follows.

CHAPTER 4

COMPUTER PROCEDURES RELATED TO ELECTROCHEMICAL MEASUREMENTS

Early applications of digital computers in electrochemical surface science were concerned primarily with performing calculations on relatively small data sets, or in numerical simulations; subsequently, data acquisition and experiment control systems for use in electrochemical investigations were developed and applied in a number of areas, e.g., in studies using various transient techniques, in a.c. impedance work and in Laplace transform analysis[163].

Until relatively recently, a single computer was still commonly used to control most aspects of an experimental system: data acquisition by digital-to-analog conversion (DAC), event triggering and timing, data reduction and display, etc. For example, in previous work in this laboratory (see ref.164), a minicomputer was used in the application of linear potential sweep cyclic-voltammetry to the study of electrochemical surface processes at noble metal electrodes.

In recent years, it has become feasible to incorporate one (or more) dedicated microcomputers where indicated, into any laboratory instrument, thereby creating a peripheral device capable of performing complex and exacting measurements. This trend has given rise to a variety of new (or improved) and useful instruments for use in electrochemical experiments, e.g., frequency response analysers for a.c. impedance work, fast digitizing oscilloscopes with novel triggering features useful in transient studies, auto-ranging digital multimeters for steady-

state (or slowly varying) work, precise DAC and function generator units, temperature regulators, etc., and also yielded versatile computer peripherals, e.g., digital plotters and large capacity mass storage devices.

In the present chapter, a description will be given of recent computer procedures and simulation results which were developed in our laboratory during the course of this work; the techniques involving the computer-controlled acquisition of experimental data generally employed the versatile instrumental components referred to above.

1. Computer Control and Data Acquisition in Steady State Polarization (Tafel) Experiments

Useful information on the kinetics of electrode processes may be obtained from measurements of the steady-state current resulting from controlled but varied applied potential. The general form of the associated log i vs V relation (the so-called Tafel plot), and in particular, its slope, can be diagnostic of the reaction mechanism operative in the electrode process; the extrapolated exchange current densities further serve to characterize the kinetics of the process. Recently, Conway et al.[165] have combined steady-state polarization and open-circuit potential decay results and derived information concerning the pseudocapacitance and surface coverage of adsorbed intermediates in an electrode reaction.

In practice, the steady-state currents at a given applied potential may be attained gradually, or vary slowly (seconds to hours) in time, e.g., as a result of progressive changes in the

state of the electrode surface through film formation, self-inhibition, or as a result of impurities in solution. Such behaviour yields hysteresis or memory effects as the electrode is cycled through a series of holding potential values, as i vs V is monitored.

An automated data acquisition system for making steady-state polarization measurements offers a number of advantages. First, a large number of i-V pairs may be measured conveniently; this permits the characteristic Tafel slopes and exchange current densities to be more accurately determined[166]. This large number of data points also facilitates the derivation of the pseudocapacitance behaviour of reaction intermediates, when considered in conjunction with open-circuit potential decay data from separate experiments (see Section 3)[167].

Secondly, an automated data acquisition system lends itself favourably to the use of a well-defined consistent potential holding and potential changing procedure. This is especially useful in dealing with time-dependent hysteresis, described above; as will be discussed below, a reproducible initial surface state may be achieved in certain cases by suitable potential modulation, prior to the measurement of each i-V pair.

Thirdly, an automated system facilitates the processing and display of the experimental results, as well as the comparison of these latter with the predictions of possible physical models.

A number of the different potential programmes employed in the present steady-state polarization work are shown in Fig.4-1. Programmes a) or b) were used repetitively for the evaluation of reproducibility or hysteresis behaviour; programme c)

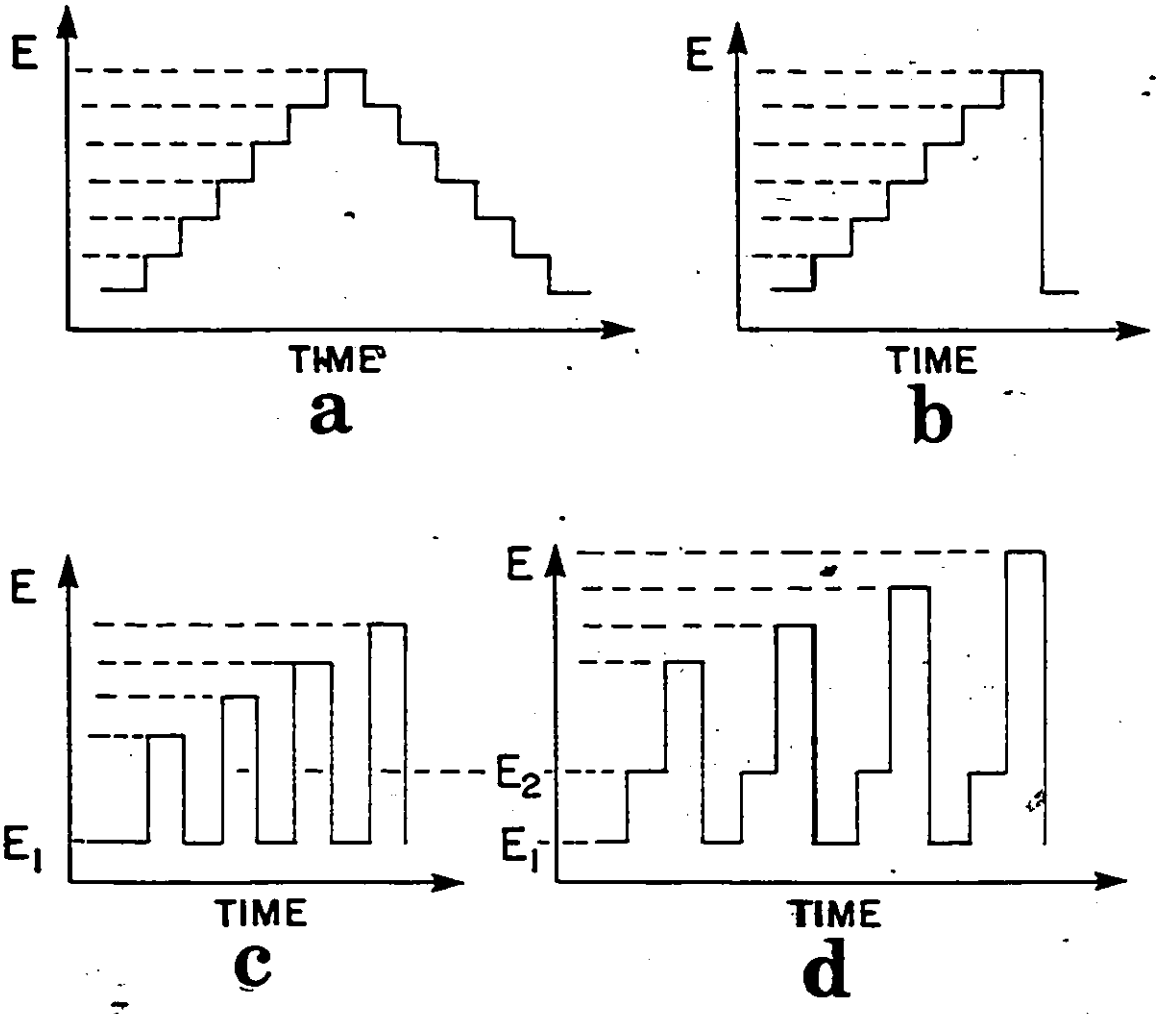

Fig.4-1 Potential programmes for use in steady-state polarization measurements (see the text for a detailed description).

incorporates a surface conditioning segment (holding at potential E_1) between successive measurements. Alternatively, two surface conditioning potential holding periods at E_1 and E_2 are shown in d); at Pt, this scheme permits the removal of an interfering surface species at a potential $V = E_1$, say by the formation of a surface oxide layer, followed by the reduction (removal) of this film at $V = E_2$, before proceeding to the next i-V measurement. In this way, a reproducible initial surface state may be obtained.

The measurement system also allows for the acquired i-V data, and any associated parameters or derived quantities, to be displayed and stored. For example, the Tafel plots of V vs log i could be displayed on a CRT or on paper during the course of the experiment; this permits various diagnostic trends (diffusion currents, IR_u effects, ...) which are evident from the Tafel plots to be assessed as the experiments proceed. A straightforward implementation of other plotting schemes was also possible, depending on the nature of the system under study, e.g., the V vs $i^{1/2}$ behaviour may be of particular interest in certain cases.

The relatively large amount of acquired and stored data was treated numerically and displayed either graphically or in tabular form. In the present context, useful transformations such as accounting for the back reaction in Tafel plots, correcting for the effect of uncompensated solution resistance, adding a d.c. offset value to the overpotential values, and calculating Tafel and activation parameters, could be made.

These features were incorporated into a data acquisition system which was assembled and used in the steady-state polarization measurements.

(i) Hardware

The controller consisted of an HP87 or HP86B laboratory computer equipped with 128K bytes of additional RAM, a system monitor for use in machine language programming, serial (RS-232C) and parallel (HP-IB / IEEE-488) interfaces, double sided double density flexible disk mass storage (HP 82901M), a digital graphics plotter (HP 7470A), a daisy-wheel printer (HP 2602A), and plotter and assembler software ROM's. Communication between the controller and the instruments and other peripheral devices employed the HP-IB interface; this allowed up to fifteen devices to be interconnected at one time.

An HP-IB-compatible digital-to-analog converter (Kepco, model SN488-122) was used to supply the desired potential to the external control input of a potentiostat; this DAC gave 13 bit resolution over $\pm$1 V or $\pm$10 V, which corresponds to a minimum potential increment of 0.2 mV and 2.4 mV, respectively (linearity error $\pm$ 1/2 LSB).

The current resulting from the applied potential was monitored by means of an HP-IB-compatible digital multimeter (DMM) (Keithley, model 195A); the autoranging feature allowed for continuous measurement over the several decades in current of interest, thus avoiding the need for controller- or user-implemented sensitivity selection. In the experiments to be described in the following chapter, the actual potential between

the working and reference electrodes was also monitored.

The potentiostat, cathode follower and additional instruments used are described in the experimental section. A block diagram of the experimental set-up is given in Fig.4-2; also included in this figure is an optional digital oscilloscope, e.g., for the determination of the uncompensated solution resistance by the interrupt method, or for use in open-circuit potential decay measurements (see following sections).

(ii) Software

The time scale involved in steady-state polarization measurements, as well as the nature of the peripheral instruments allowed the driving program and the associated subroutines to be written in high level HP BASIC programming language. However, an assembler was also available for improving program performance, e.g., in speeding up the decoding of large (4 or 8K element) data sets from digital oscilloscopes. Whenever possible, the built-in capabilities of the on-line measuring instruments were used, e.g., the triggering and display cursor features of the digital oscilloscopes, and data logging function of the DMM's.

An outline of the programme appears in Fig.4-3; the main programme consists of a menu by means of which various data acquisition, storage, retrieval, display, and numerical processing tasks may be performed. Some effort was made to facilitate the ongoing addition of features to the initial programme, i.e., new potential-step programmes, sampling sequences, or data handling procedures; in addition, advantage could be taken of the HP calculator mode operation, during

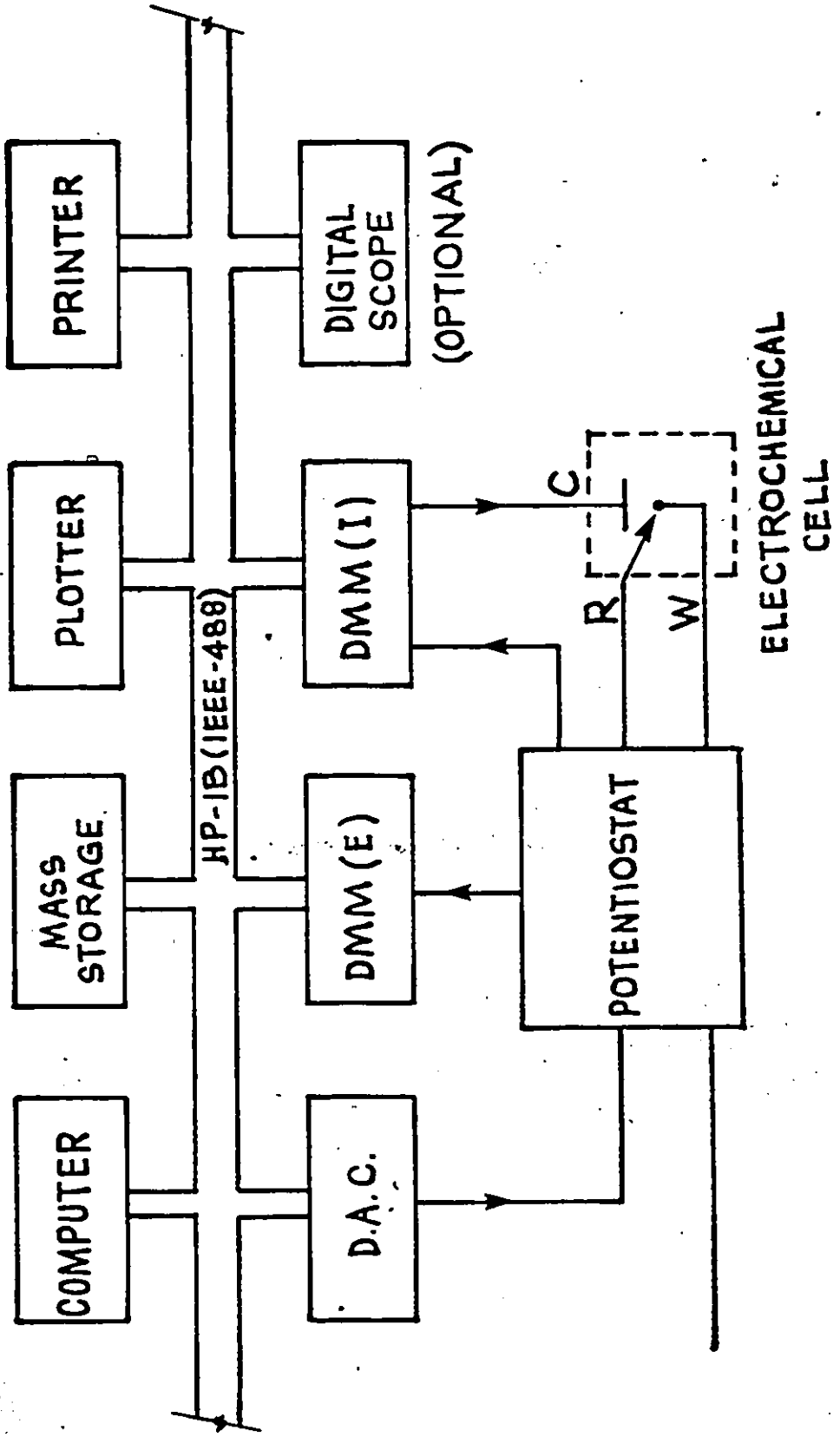

Fig.4-2 Schematic diagram of the experimental set-up used in the steady-state polarization measurements.

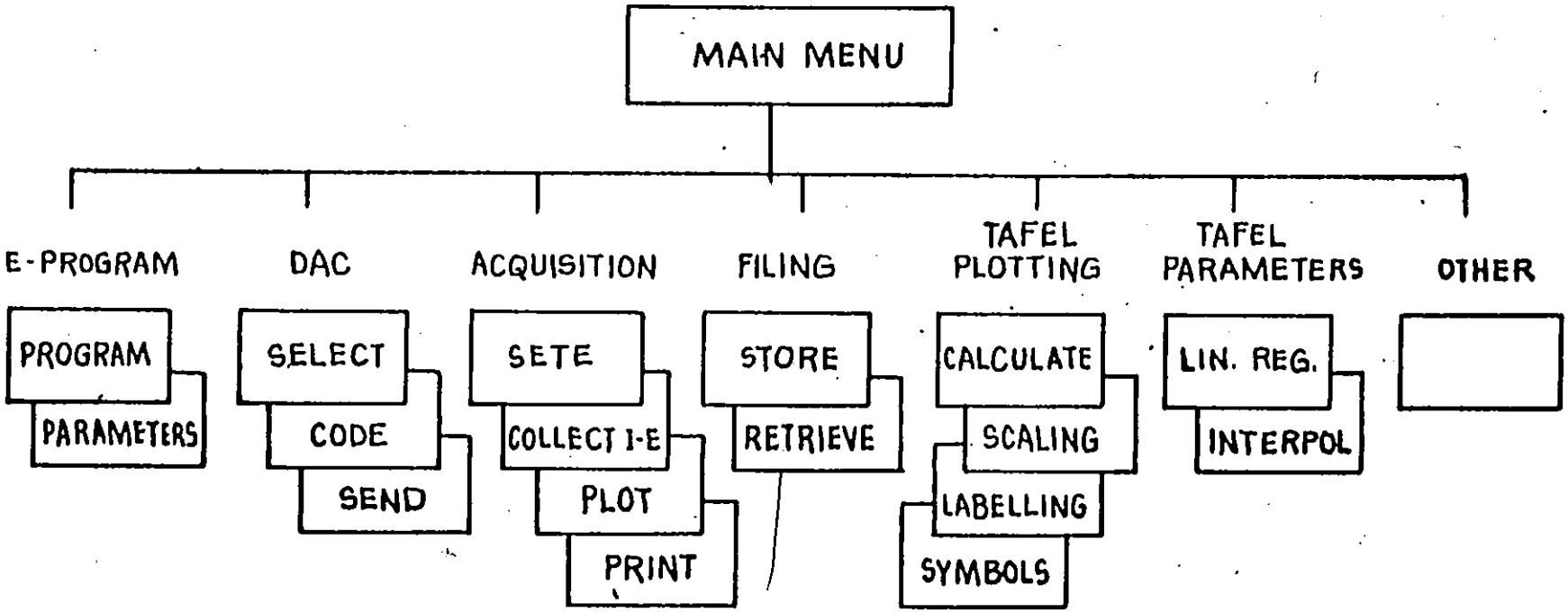

Fig.4-3 Outline of data acquisition programme used in the steady-state polarization measurements.

temporary programme suspension, for "one-off" manipulations involving the electrochemical cell, experimental results or peripheral devices.

(iii) Operation

The use of DMM's (sampling time ca. 200 ms) and of the interfacing arrangement described above resulted in a minimum holding time at a given potential of ca. 1 s (see below for rapid potential/current decay measurements). Holding times of 10 - 30 s were used in the steady-state polarization measurements.

Preliminary experimental results could optionally be displayed graphically during data acquisition and not stored in memory, enabling the development of a continuous indefinite record of, e.g., start-up behaviour (compare the use of conventional storage oscilloscopes in the set up of fast transient measurements, such as in cyclic-voltammetry).

In the present work, potential programmes a) and b) of Fig.4-1 were employed in a repetitive fashion. Additional potential programmes developed in the course of this work are currently in use in other experimental investigations in this laboratory.

2. Compensation for Solution Resistance

In many experiments in interfacial electrochemistry, the measurement of the relative potential drop between an electrode and the solution side of the electrical double-layer is of interest. When a net current is passed across such an interface, a potential-sensing probe placed near the electrode surface measures a finite potential drop, IR_u, in the solution, in

addition to the desired interfacial potential difference.

A unique R_u may be associated with this potential drop in solution provided a symmetrical current field exists about the test electrode surface, e.g., for a spherically or cylindrically symmetrical arrangement of electrodes where the potential-sensing probe introduces a negligible perturbation. This situation is realizable practically through appropriate electrochemical cell design, and can be represented by the equivalent circuit of Fig.4-1. Although the magnitude of R_u can be reduced by increasing the electrolyte conductivity, the effect of the residual R_u is still evident when large currents are passed (and hence large IR_u values arise).

The effect of the so-called uncompensated resistance, R_u, may range from the introduction of a constant shift in the observed potential, e.g., when I and R_u are constant, to the introduction of a variable shift in potential when I or R_u (or both) vary in time. A number of dynamic and post-factum IR_u compensation and correction techniques have been developed in order to overcome this common problem (e.g., see ref.168).

(i) Uncompensated Solution Resistance and Steady-State Polarization Measurements

From a knowledge of the value of R_u (assumed constant), the actual overpotential at the OHP, V, in a steady-state polarization measurement, is given by

$$V = V_{obs} - IR_u \qquad (4\text{-}1)$$

where V_{obs} is the observed potential. In a practical way, it is desirable that the IR_u correction be small compared to V_{obs} in

order to obtain reliable values of V.

If Tafel behaviour obtains, then

$$V_{obs} = b \log I/I_o + IR_u \qquad (4\text{-}2)$$

so that the solution potential drop across R_u is shown to be more strongly dependent on I than the overpotential component which is only logarithmic in I. Thus the IR_u term eventually dominates the V_{obs} behaviour over less than one decade in current; nevertheless, such IR_u corrections are useful in extending the range of overpotential (or current) accessible to study.

In the present work, R_u was determined primarily by the interrupt method which involves opening the current-carrying circuit by means of a fast mercury-wetted reed relay (or other suitable relay), and following the open-circuit potential decay behaviour of the test electrode using a suitable oscilloscope. The potential decay across the interfacial impedance, $Z_{interface}$, in Fig.4-4 is generally rather slower (i.e. the associated decay time t_F is larger) than that across R_u which is practically instantaneous and hence $V_{IR} = IR_u$ can be measured directly. R_u is deduced from the slope of a V_{IR} vs I plot which is usually linear and passes through the origin; such behaviour indicates that a unique constant R_u is applicable.

Two principal difficulties may mitigate the determination of R_u by this method. First, a finite capacitance, C_x, due to the measuring system (leads and cathode follower) effectively short-circuits the solution side of R_u to ground. This introduces another time constant, t_x, (= R_uC_x) which slows the decay of potential across R_u and may obscure the IR_u component, unless $t_F >> t_x$. t_x may be reduced by minimizing R_uC_x, e.g., by the use of

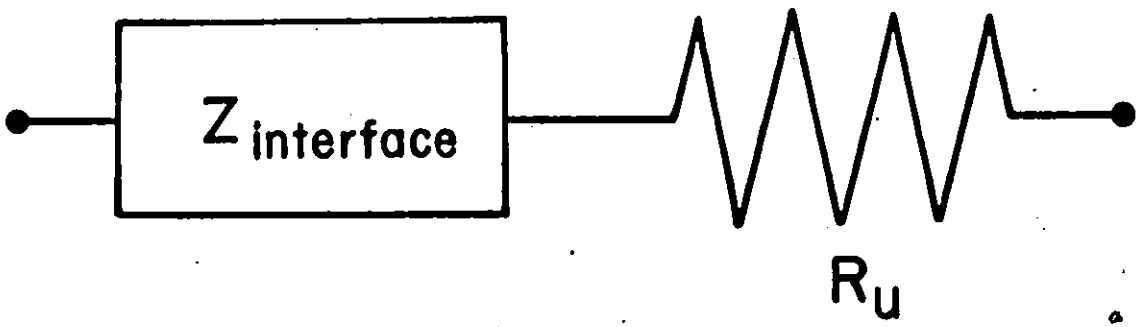

Fig.4-4 General equivalent circuit for an electrode/solution interface and associated solution resistance, R_u.

short shielded cabling and a suitable cathode follower.

Secondly, if the kinetics of the electrode process which discharges the double-layer are very fast, then the associated time constant, t_F, will be very small and the requirement that $t_F >> t_X$ may no longer be satisfied. This intrinsic time constant, coupled with the finite bandwidth of the measuring equipment (including leads), may make the interrupt method inapplicable in some situations.

The interrupt technique has also been applied in this laboratory to the linear potential scan case, where the potential decay upon interruption of the sweep in the potential region of a surface process (oxide deposition) was measured[169]. The resulting R_u values compared well with those deduced from a.c. impedance measurements in the double-layer region.

In the a.c. impedance method, R_u is deduced from the overall impedance (and its frequency dependence) for the equivalent circuit of Fig.4-4. This is easily done if a potential interval is available for which $Z_{interface}$ consists only of the double-layer capacitance, since in this case, the real part of the total complex impedance gives R_u directly.

In the present work, the interrupt method was employed in the determination of R_u and the Tafel relations were corrected accordingly; a.c. impedance measurements yielded identical values of R_u. It should be noted that if formation of a thick surface film occurs, or if the solution conductivity changes with time, then R_u will also vary. In addition, in transient experiments where V is varied, i.e., linearly, in time, the IR_u component

will not be constant and a post-factum IR_u correction will not generally be valid in deducing the behaviour obtaining where $R_u = 0$. This problem, as well as the possibility for dynamic compensation or correction, will be discussed in the following section.

(ii) Uncompensated Ohmic Drop in LPS Voltammetry and the Derivation of s_o Values For Electrode Surface Processes

It is the purpose of this section to examine the effect of R_u on linear potential scan (LPS) I vs V profiles for a one-electron surface process. In particular, the derivation of the kinetically significant reversibility parameter[158], s_o, from LPS results where $R_u \neq 0$, will be considered with a view to distinguishing spurious IR_u effects from kinetically significant irreversibility effects that are to be quantitatively evaluated in such experiments. The method was used to evaluate s_o data for H ionization at Pt in 1 M aqueous CF_3SO_3H and in the melt $CF_3SO_3^- H_3O^+$ (see Chapter 5, Section 4).

Stonehart, Kozlowska and Conway[170] made the first calculations on the effect of the IR_u drop on the form of linear potential sweep (LPS) I vs V relationships for an electrode surface process, in their case one involving oxide film reduction, e.g., at Pt, and showed how characteristic distortions of the I vs V profile can arise, depending on the magnitude of R_u. Later, de Tacconi, Calandra and Arvia[171] considered a similar problem and also applied their treatment to Pt surface oxide reduction. IR_u effects are particularly significant in the LPS study of thick-film processes involving battery electrode

materials[172], e.g., in the formation and reduction of $PbSO_4$, $PbCl_2$ and in the oxidation of Zn in alkaline solutions[173].

More recently, Rouillier and Laviron[174] have treated the problem of evaluation of surface rate constants (k) by the LPS method of Angerstein-Kozlowska and Conway[158] (which gives the reversibility parameter[158], s_o, value related to i_o and k) when IR_u drop is significant, particularly at high sweep-rates, s V s^{-1}. The latter authors recognized the necessity for taking into account the IR_u drop in LPS I vs V profiles, particularly with respect to the correct evaluation of peak potentials, V_p, for surface processes which are required as a function of log s in the evaluation of s_o and of the Tafel slope for the surface process from V_p vs log s plots[158]. In their work at Pt, Angerstein-Kozlowska and Conway made automatic IR_u compensation, employing the Tacussel instrument. The IR_u correction or compensation is, of course, increasingly necessary with increasing sweep-rate since, for a surface process, $I \propto Cs$ where C is the total capacitance (double-layer + adsorption pseudocapacitance[20]) of the electrode interface. Sweep-rates up to 500 V s^{-1} were used in the s_o evaluations for surface processes at Pt[158].

The present section is concerned with the effect of a fixed uncompensated solution resistance on the kinetic behaviour of electrochemical surface processes under LPS conditions. In particular, the effects of R_u on the LPS I vs V profiles, and on the associated apparent potential and the actual potential sweep-rate will be considered. These considerations are relevant to the accurate evaluation of the kinetics of H discharge and

ionization at Pt from H_3O^+, in the $CF_3SO_3^-H_3O^+$ melt, and H^+_{aq}, in 1 M CF_3SO_3H, treated in Chapter 5 of this thesis.

(a) Formulation of the Kinetic Problem

Consider the following electrochemical 2-dimensional surface process subject to a linear potential scan:

$$\underset{1-\theta}{M} + \underset{c_o}{A^-} \underset{k_{-1}}{\overset{k_1}{\rightleftharpoons}} \underset{\theta}{MA} + e^- \qquad (4\text{-}3)$$

where θ is the fractional coverage of the surface by an adsorbed species A, c_o is the concentration of A^- in the outer-Helmholtz plane (OHP), and the fractional surface concentration of metal sites, M, is represented by the quantity $(1-\theta)$.

In the absence of mass-transport limitations and of diffuse double-layer effects, the net current density for reaction (4-3) is given[158,21] by

$$I(t) = Q\, d\theta/dt = Qk\,[(1-\theta)\exp(V/b) - \theta\exp(-V/b)] \qquad (4\text{-}4)$$

where V is the potential referred to that for which $\theta = 1/2$, $b = RT/\beta F$ or $RT/(1-\beta)F$, i.e., when β, the charge-transfer symmetry factor is 1/2, and Q is the charge required for formation or desorption of a monolayer of A on M in reaction (4-3).

At any instant in a LPS experiment, the potential driving reaction (4-3) is given by

$$V(t) = (V_o + st) - R_u I(t) \qquad (4\text{-}5a)$$

$$= (V_o + st) - R_u Q(d\theta/dt) \qquad (4\text{-}5b)$$

where s is the applied sweep-rate and R_u is the uncompensated solution resistance. Taking eqns.(4-5a,b) into account, the net current in eqn.(4-4) becomes

$$I(t) = Q d\theta/dt = Qk\,[\,(1-\theta)\exp[(V_o + st - R_u Q d\theta/dt)/b] - \theta\exp[-(V_o + st - R_u Q d\theta/dt)/b]\,] \qquad (4\text{-}6)$$

The variable difference in the apparent electrode potential ($V_o + st$) compared with that actually obtaining at the OHP (viz. $V_o + st - R_u I(t)$), due to the influence of IR_u drop, results in a time-dependent actual potential sweep rate:

$$dV(t)/dt = s - R_u dI(t)/dt \qquad (4\text{-}7a)$$

$$= s - R_u Q d^2\theta/dt^2 \qquad (4\text{-}7b)$$

In the limit $R_u \to 0$, the constant formal sweep rate, s, is of course recovered. It should be noted that the actual and formal sweep rates also become equal when $d^2\theta/dt^2 = 0$, that is, at the maximum in the I vs t (or I vs $V_{apparent}$) profile. The quantity $d^2\theta/dt^2$ can be obtained by conventional operations on eqn.(4-6):

$$\frac{d^2\theta}{dt^2} = \frac{sf - 2b\, d\theta/dt\, \cosh(V/b)}{b/k + R_u\, Qf} \qquad (4\text{-}8)$$

where $f = \exp(V/b) - 2\theta\sinh(V/b)$ and hence the actual sweep-rate behaviour can be investigated for various assumed values of the uncompensated solution resistance, given $(t,\theta,d\theta/dt)$ satisfying eqn.(4-6).

Formally then, eqn.(4-6) can be solved for a wide range of s/k and R_u values, and the resulting kinetic behaviour considered in terms of the various diagnostic parameters which serve to characterize an electrochemical surface process[158,175]. In the case of $R_u = 0$, the response of reaction (4-3) to the LPS varies from quasi-reversible behaviour for small s/k ($<5 \times 10^{-3}$) to irreversible behaviour for large s/k ($>5 \times 10^{-1}$)[158]. This

transition at a characteristic sweep-rate s_o[158,176] is accompanied by (a) a change to an asymmetric I vs V profile; (b) a decrease in peak pseudocapacitance $C_{\phi,p}$ (= I_p/s), to ca. 0.73 of the value obtaining under reversible conditions; and, (c) a linear increase in peak potential with log(s)[158,21,175], characterized by the Tafel slope of the surface process.

An analysis of the I vs V peak shapes and peak potentials has been given by de Tacconi et al. for reaction (4-3) under LPS conditions ($R_u \neq 0$) for the quasi-reversible and irreversible cases[171]. In these limiting cases, larger R_u values give rise to peak broadening, and increase in θ_p reflecting the asymmetry of the resulting peaks and a shift of peak potentials, as shown in a previous publication[170]. The effect of a constant double-layer capacitance in addition to a finite R_u has, under reversible conditions, also been considered elsewhere[177].

More recently[174], Rouillier and Laviron have shown that the uncompensated solution resistance may cause a surface process operating in the quasi-reversible sweep-rate regime to exhibit I vs V peak-shape and peak-potential behaviour similar to that expected under irreversible conditions at sweep-rates > s_o (cf. ref.158). In the above work[174], the importance of distinguishing spurious IR_u effects from kinetically significant behaviour was emphasized and illustrated by means of calculations and with reference to the behaviour of selected experimental systems.

In the present section, the results of a numerical solution of the general kinetic eqn.(4-6) will be given, particularly in connection with the dependence of the actual V_p and the sweep-rate on R_u.

(b) Method of Calculation

Many systems of rate equations arising in chemical kinetics exhibit so-called "stiffness"[178,179] and require the use of stiffly stable algorithms in their solution[180]. The advent in the early 1970's of software packages implementing such algorithms has enabled the majority of stiff problems to be solved quite routinely[180,181].

Equation (4-4) exhibits stiffness for small values of s/k (<ca. 10^{-3} - 10^{-2}) corresponding to the quasi-equilibrium regime of reaction (4-3) under LPS conditions. The use of non-stiff methods results in an unstable numerical solution as s/k decreases over the several decades of variation of s that are of interest.

In the present work, an algorithm based on that of Gear[181] was employed to solve eqn.(4-6) for (t,θ) or correspondingly (V,θ) directly. However, owing to the implicit nature of eqn.(4-6) with respect to $d\theta/dt$, evaluation of the required quantity $d\theta/dt$ cannot be performed by simple substitution. Instead, an iterative procedure must be used to determine $d\theta/dt$ for given (t,θ) according to eqn.(4-6) at each step in the numerical solution.

All calculations were performed in extended precision on a PDP-11/34 computer, and selected results plotted using a graphics package developed in house.

For the purpose of calculation, the following values of the kinetic parameters were selected: $k = 1\ s^{-1}$, $Q = 2.2 \times 10^{-4}$, $= 1/2$, and $V^{o} = 0.0V$. Values of R_u were then chosen so as to give

rise to appreciable R_u effects (e.g. ca. 100 mV shift in V_p due to R_u) in the quasi-reversible, intermediate and irreversible kinetic regimes, respectively.

(c) I vs V Profiles and Peak Potentials

The effect of R_u on the I vs V profiles at an intermediate value of $s/k = 5 \times 10^{-2}$ is illustrated in Fig.4-5. It is seen that the broadening and the asymmetry of these profiles for large R_u, as well as the shift in peak potential and decrease in peak current, I_p, qualitatively resemble the behaviour characteristic of quasi-reversible or irreversible conditions[158,171], depending on s/k.

Fig.4-6a shows the dependence of the apparent peak potential ($= V_o + st_p$) on R_u over several decades of the value of s/k. The actual magnitudes of R_u in Ohms given in Fig.4-6 are not of special numerical significance but are linked to the arbitrary choice of the other kinetic parameters as indicated above. By making R_u sufficiently large, substantial deviation from the unperturbed, $R_u = 0$, case may, of course, be obtained. In all cases, however, the region of increase in peak potential due to R_u shows some curvature when compared with the linear V_p vs log(s/k) behaviour for irreversible conditions when $R_u = 0$. In considering the V_p vs log(s) behaviour in an actual experimental situation, this curvature could provide an indication that the surface process under study is not operating in the irreversible kinetic regime, i.e., $s < s_o$.

The sweep-rate dependence of the formal peak adsorption pseudocapacitance, $C_{\phi,p}$ (= I_p/s), shown in Fig.4-6b provides a

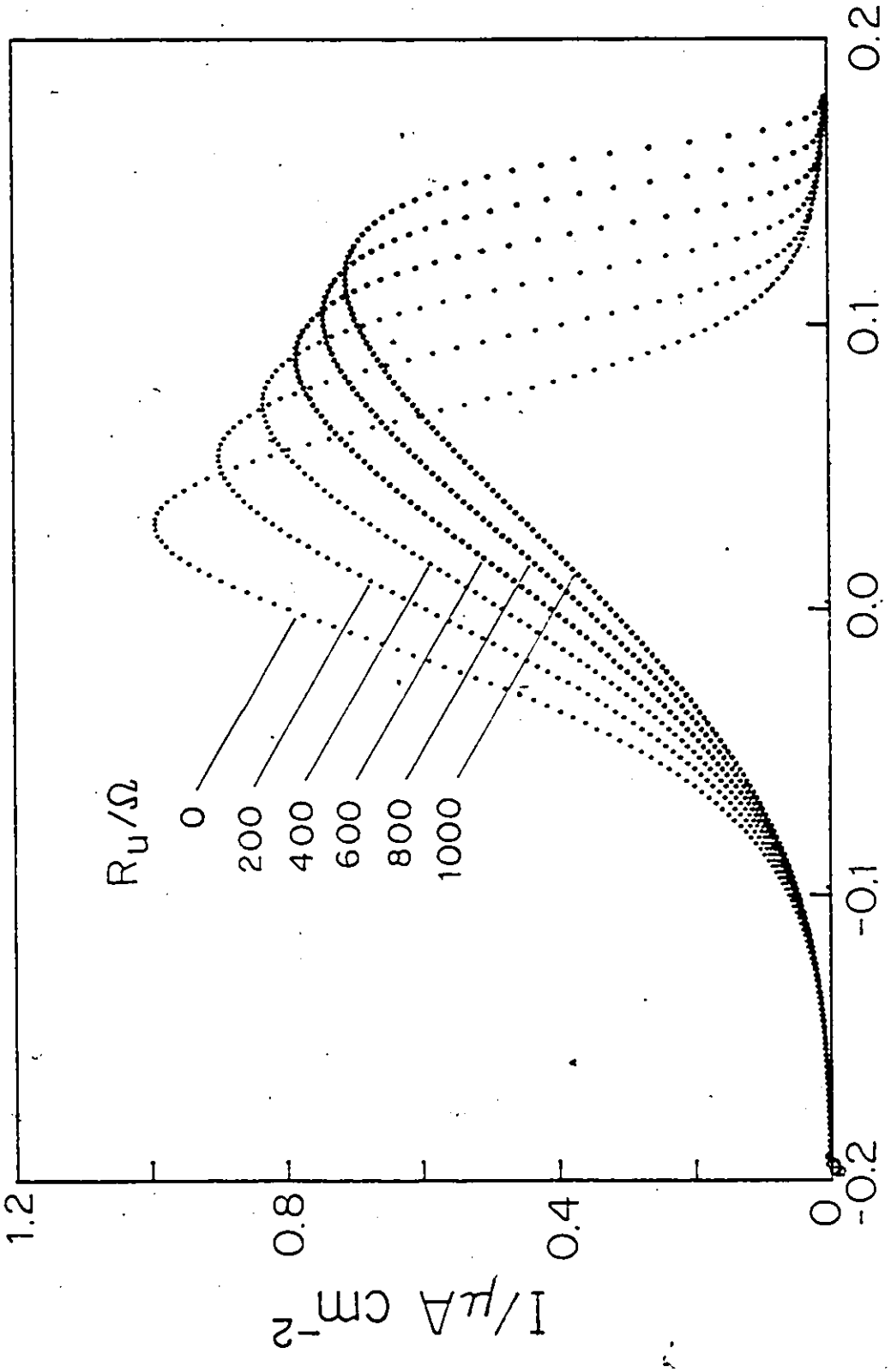

Fig.4-5 Current vs potential profiles for reaction (4-3) under LPS conditions ($s/k = 5 \times 10^{-3}$) for various values of R_u.

Fig.4-6 Dependence of a) apparent peak potential and b) apparent peak adsorption pseudocapacitance on log s for various values of R_u.

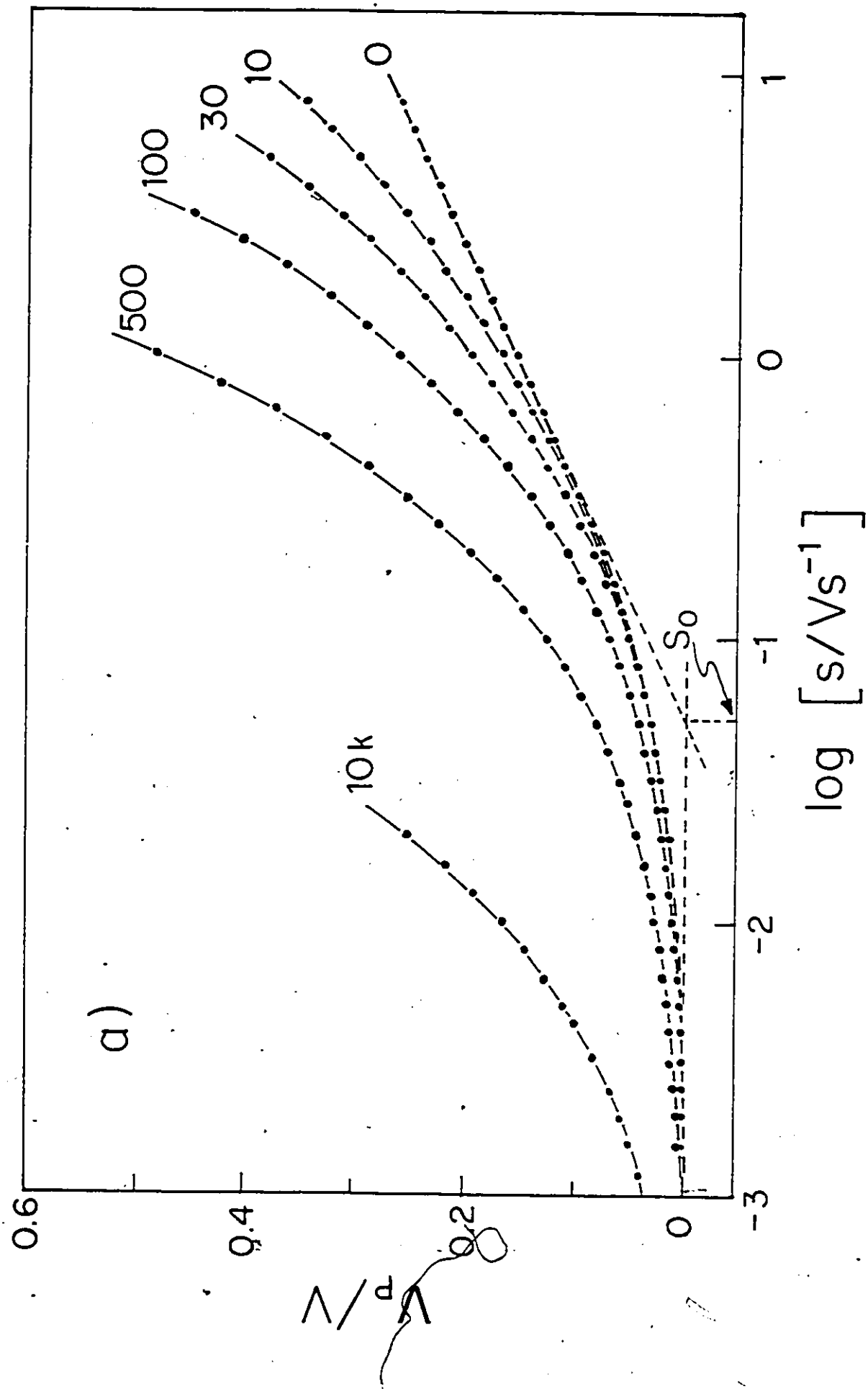
a)
0
10
30
100
500
10k
S_0
log [s/Vs^{-1}]
1
0
-1
-2
-3
0.6
0.4
0.2
0
V_p/V

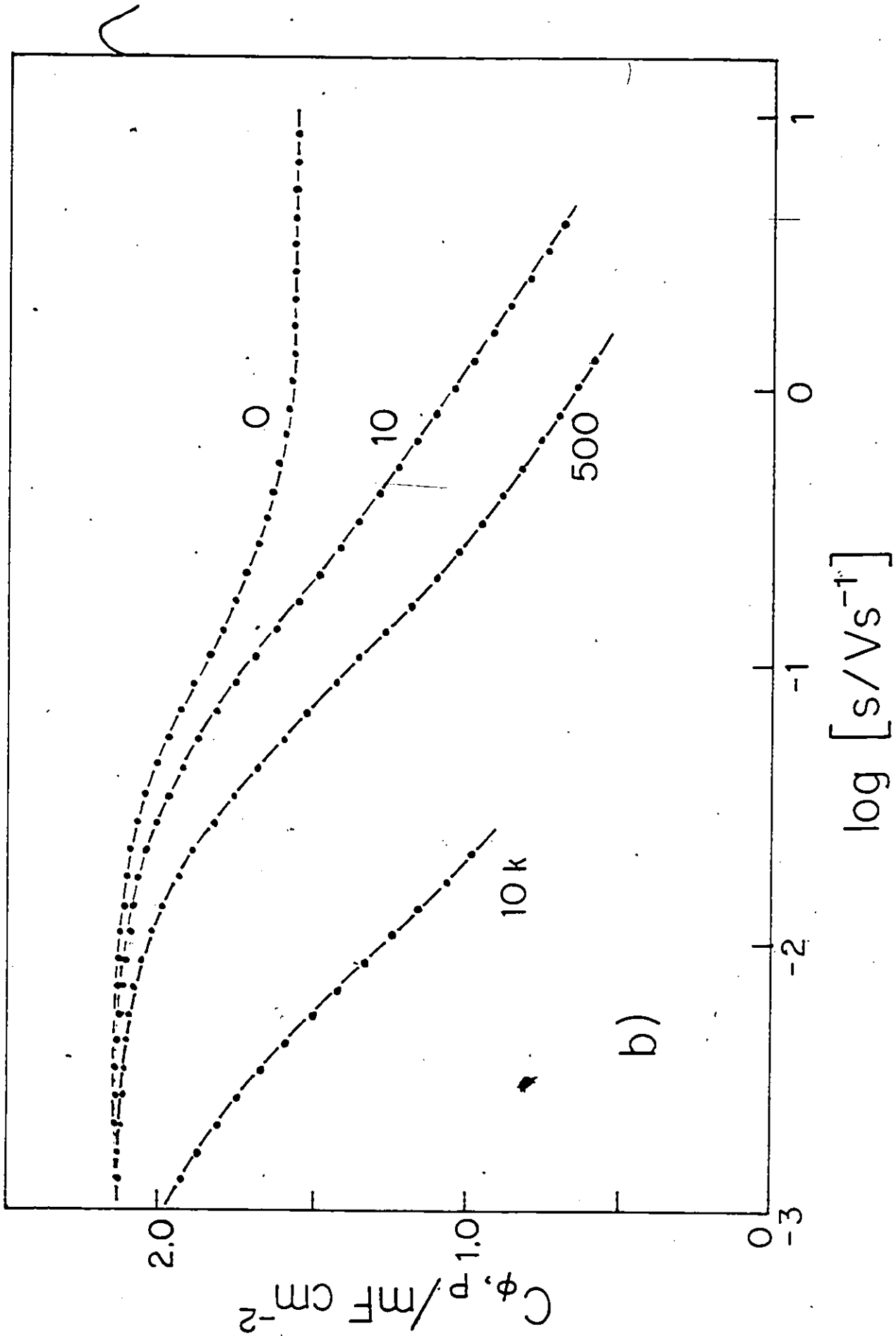
0
10
500
10 k
b)
2.0
1.0
0
-3
-2
-1
0
1
log [s/Vs^{-1}]
$C_{\phi,p}$/mF cm^{-2}

more discriminating check on the origin of observed progressive changes in V_p with log s. When $R_u > 0$, the value of $C_{\phi,p}$ decreases more markedly with log s and does not reach a constant value as required for a genuine transition to the irreversible kinetic regime (cf. $R_u = 0$ in Fig.4-6b). Thus, even when the value of R_u is not known, i.e., when using dynamic IR_u compensation, the $C_{\phi,p}$ vs log s behaviour may be used to distinguish changes due to IR_u effects.

When both R_u and $C_{\phi,p}$ for reversible conditions are known, a practical sweep-rate below which IR_u compensation will not be needed, may be estimated by requiring that $C_{\phi,p,rev} \times s \times R_u < \Delta V$ where ΔV is the maximum acceptable deviation in potential due to IR_u effects.

Under irreversible conditions, the peak potential is given by,

$$V_o + st_p - R_u I_p = b \ln(s/bk) \qquad (4\text{-}9a)$$

or

$$V_{p,app} - R_u I_p = b \ln(s/bk) \qquad (4\text{-}9b)$$

The right-hand side of eqns.(4-9a) or (4-9b) is just the actual peak potential expected under irreversible conditions when $R_u = 0$. Thus a simple transformation of the observed peak potentials (i.e., by subtraction of $R_u I_{p,observed}$) to yield the true peak potentials (corresponding to $R_u = 0$ and $dV/dt = s$) is possible, provided that R_u is known. This latter requirement may be realizable in systems when an a.c. impedance-, or circuit interrupt-determination of R_u is possible or has been made.

In practice, the sweep-rate above which reaction (4-3)

proceeds irreversibly, and hence eqns.(4-9a) or (4-9b) apply, is not known, a priori, nor is it unambiguously determinable when R_u is sufficiently significant that IR_u at sweep rates around or > s_o is comparable with the shift of V_p with log s due to kinetic irreversibililty effects.

The result of performing the simple transformation implicit in eqns.(4-9a,b) on the apparent V_p is shown in Fig.4-7 for the cases of reaction (4-3) occurring in the quasi-reversible, reversible, and intermediate kinetic regimes. In the reversible region, the transformed V_p values still lie above those for R_u = 0 but, with increasing log(s/k), and hence irreversibility, the V_p's eventually coincide with the data on the unperturbed, R_u = 0, curve according to eqns.(4-9a,b).

Under reversible conditions, relations analogous to eqns.(7a,b) can be derived:

$$V_{p,app} - I_p R_u - b \ln\left[\left(\frac{Qs}{2bI_p}\right)^{1/2} + \left(\frac{Qs}{2bI_p} - 1\right)^{1/2}\right] = V_{p,R=0} = 0 \qquad (4\text{-}10a)$$

or

$$V_{p,app} - I_p R_u - \frac{b}{2} \ln\left[\frac{\theta_p}{1-\theta_p}\right] = V_{p,R=0} \qquad (4\text{-}10b)$$

in terms of the current, I_p, or the surface coverage, θ_p, at the maximum in the I vs V profiles. Comparison of eqn.(4-9b) and eqn.(4-10a) shows that, under reversible conditions, an additional term in I_p is required in order to transform $V_{p,apparent}$ (for $R_u \neq 0$) to yield V_p corresponding to R_u = 0. The practical use of eqns.(4-10a,b) is limited by the complexity of eqn.(4-10a) in I_p, through practical difficulties in the estimation of θ_p, in eqn.(4-10b), and by the relative magnitudes

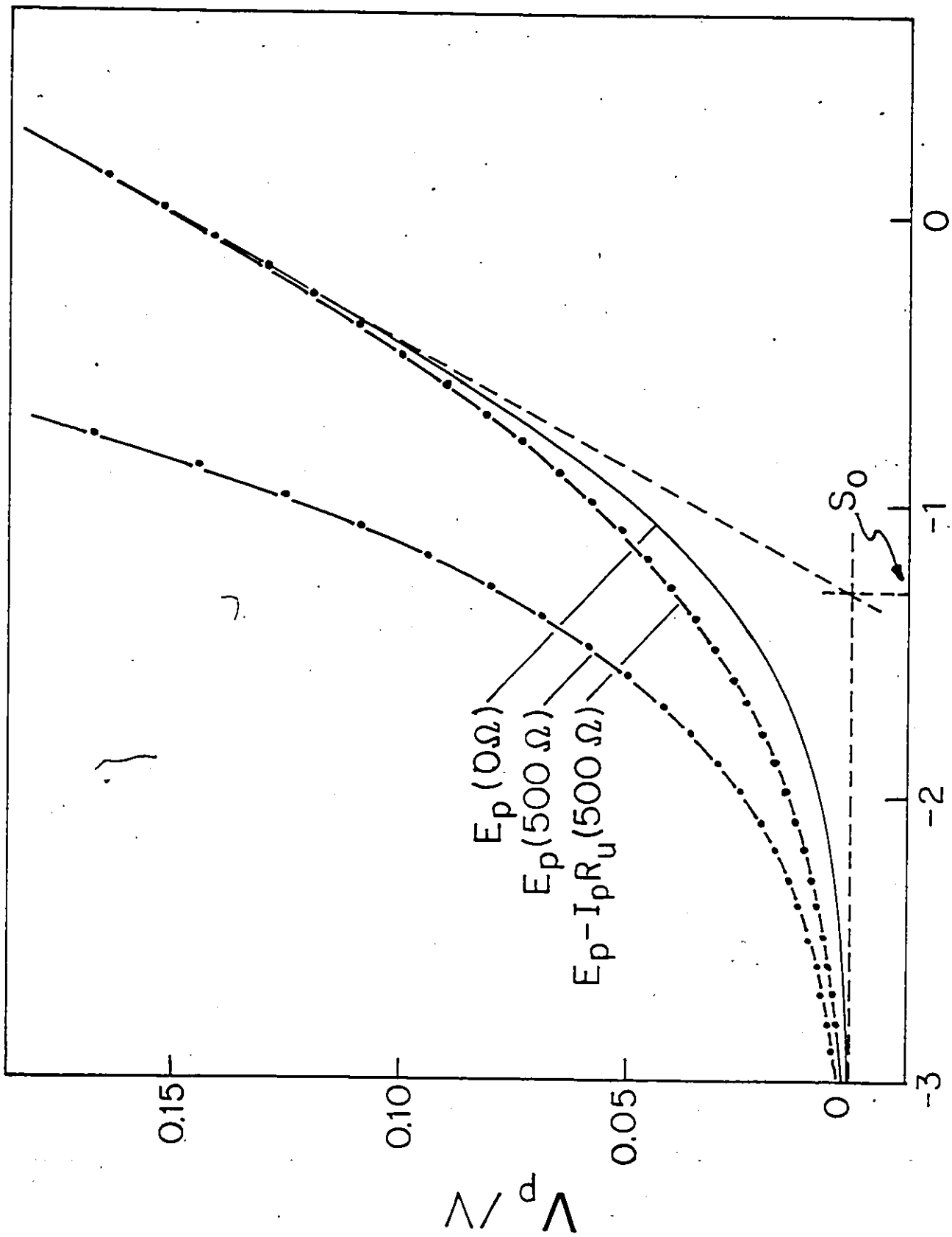

Fig.4-7 Effect of the transformation $V_{p,app} - I_p R_u$ [cf. eqns.(4-9a,b)] on the peak potential vs log s behaviour.

of the shift in V_p and IR_u mentioned above.

(d) Potential and Sweep-rate at the OHP

The time dependence of the actual potential drop, V(t), across the electrical double-layer can be evaluated using eqn.(4-7) and the numerical solution of eqn.(4-6) for θ and $d\theta/dt$. The resulting actual V(t) as a function of the apparent applied potential (proportional to time) is shown in Fig.4-8a for the case $s/k = 5 \times 10^{-2}$. As the current due to reaction (4-3) increases, V(t) falls below the programmed value of $V_o + st$; beyond the peak in the I vs V profile, V(t) eventually becomes equal to $V_o + st$ as the current for the surface process vanishes when $\theta \to 1$. (A residual double-layer charging current, $I_{dl} = C_{dl} s$, of course, remains but is not of interest here.) Clearly, as R_u increases, the extent of the deviation of V(t) from the programmed value of the potential difference increases.

The effect of R_u on the actual potential sweep-rate, $dV(t)/dt$, is evidently quite pronounced, as shown in Fig.4-8b. The actual potential sweep-rate first falls below the overall s as currents due to reaction (4-3) vanish as $\theta \to 1$ or 0. The $dV(t)/dt$ curve crosses the $dV(t)/dt = s$ line at the peak in the I vs t profile, according to eqn.(4-6). The very sharp increase and subsequent decrease in $dV(t)/dt$ beyond the peak corresponds to the very rapid decay of current beyond I_p, when R_u is significant. In the presence of substantial uncompensated solution resistance, the actual potential sweep-rate, effective at the electrode interface, is seen to differ significantly from s.

Fig.4-8 a) Effect of R_u on the potential at the OHP for reaction (4-3) under LPS conditions;

b) The potential sweep-rate at the OHP (= dV(t)/dt) for various values of R_u.

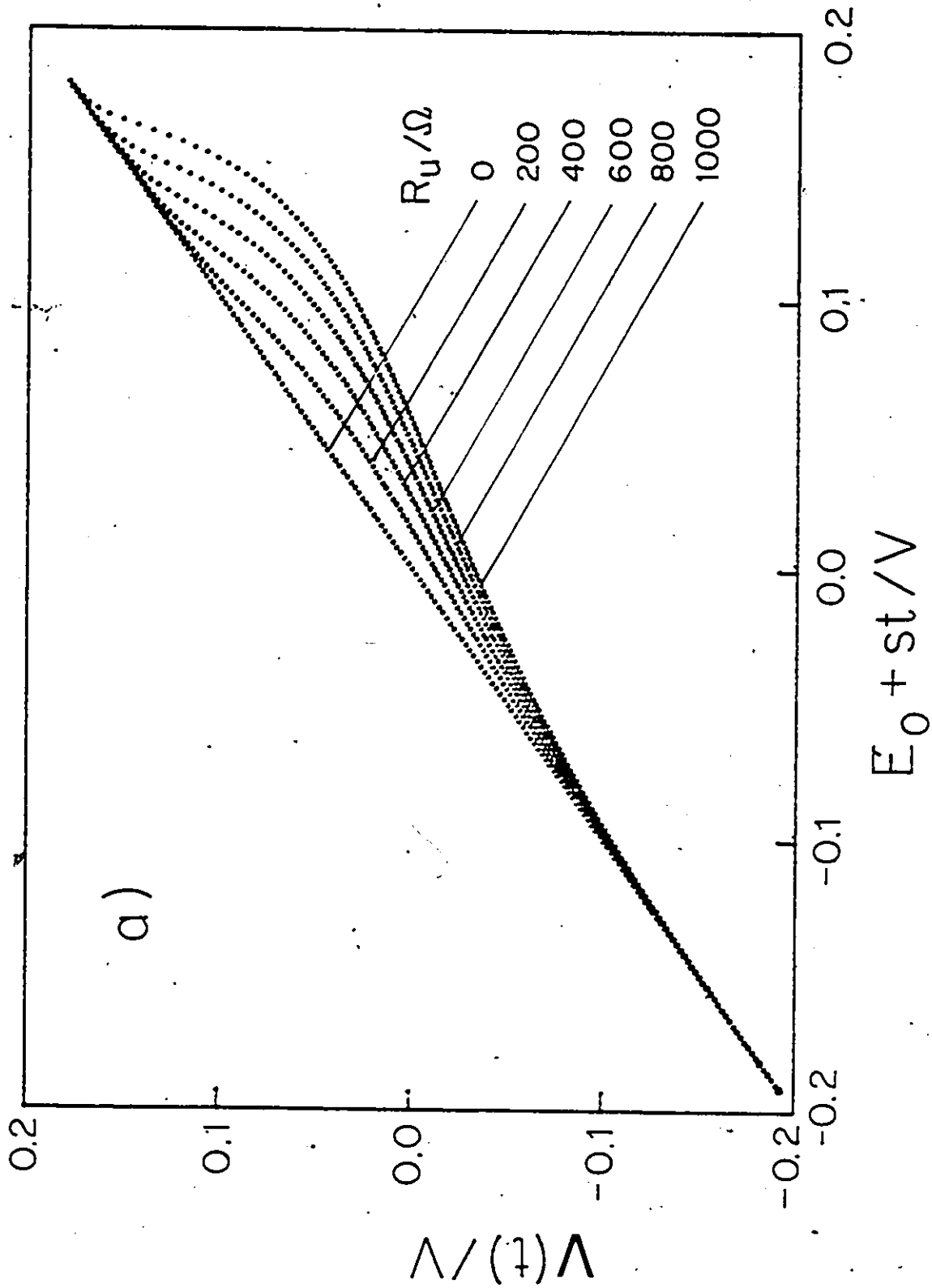
a)
R_u/Ω
0
200
400
600
800
1000
$V(t)/V$
$E_0 + st/V$
0.2
0.1
0.0
-0.1
-0.2

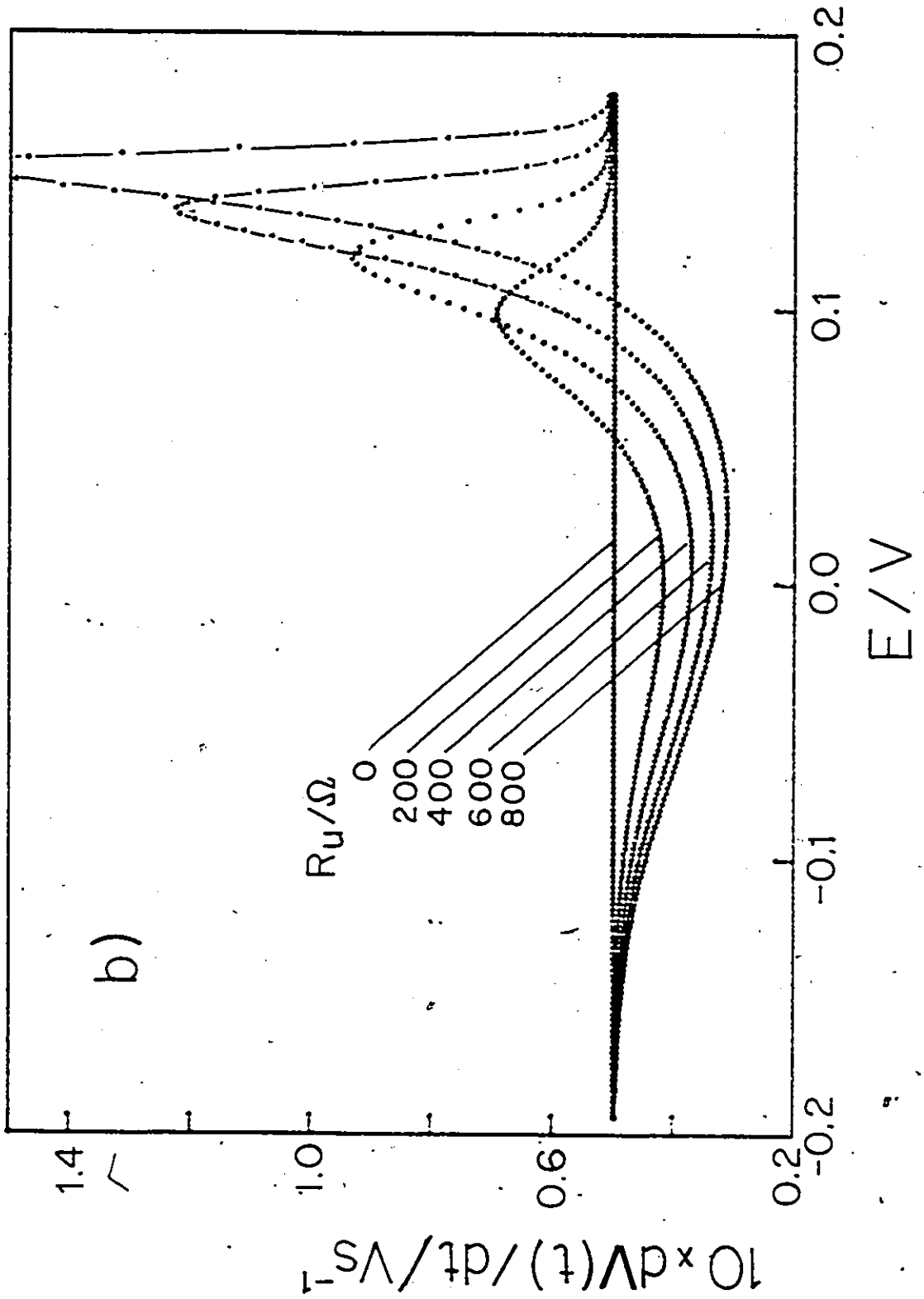
b)
R_u/Ω
0
200
400
600
800
E / V
0.2
0.1
0.0
-0.1
-0.2
$10 \times dV(t)/dt/vs^{-1}$
1.4
1.0
0.6
0.2

Given an observed I vs $V_{apparent}$ profile, and the knowledge of R_u, both V(t) and dV(t)/dt could be evaluated numerically in order to assess the effect of the uncompensated solution resistance.

(e) Adsorption Pseudocapacitance

The variation in dV(t)/dt is important in deriving the adsorption pseudocapacitance, C_ϕ = I/(dV/dt), which will only coincide with C_ϕ = I/s at the peak in the I vs V profile. In addition, the observed potentials (for each I-value) may be corrected according to eqn.(4-5) to yield actual V(t) data; of course, an important result of the present analysis is that the actual potential programme which obtains at the OHP will not be a linear potential sweep and so the resulting peak shapes will still differ from those which would be observed were dV(t)/dt = constant, e.g., for R_u = 0.

The effect of taking account of the actual relative interfacial potential drop and of its rate of change with time on the C_ϕ vs V profiles is shown in Fig.4-9. Curve A represents the adsorption pseudocapacitance, C_ϕ (=I/s) for the unperturbed R_u = 0 case for $s/k = 5 \times 10^{-2}$ (i.e. in the intermediate kinetic regime[158]). The analogous result for an R_u taken as 800 Ohms (a large and improbable value) is also shown as curve B; the I vs V profile is shifted to higher $V_{apparent}$ and broadened. Correcting the apparent potential [according to eqn.(4-5)] at each point along profile B yields the I(t)/s vs V(t) curve denoted as C in Fig.4-9. The resulting peak potential does not coincide wih that for the R_u = 0 case as expected for the intermediate regime of

Fig.4-9 Pseudocapacitance, C_{ϕ}, for R_u = 800 Ohms: a) reference R_u = 0 case; b) C'_{ϕ} (= i/s) vs V_{app}; c) C'_{ϕ} vs $V_{app} - IR_u$; d) $I(t)/(dV(t)/dt)$ vs $V_{app} - IR_u$.

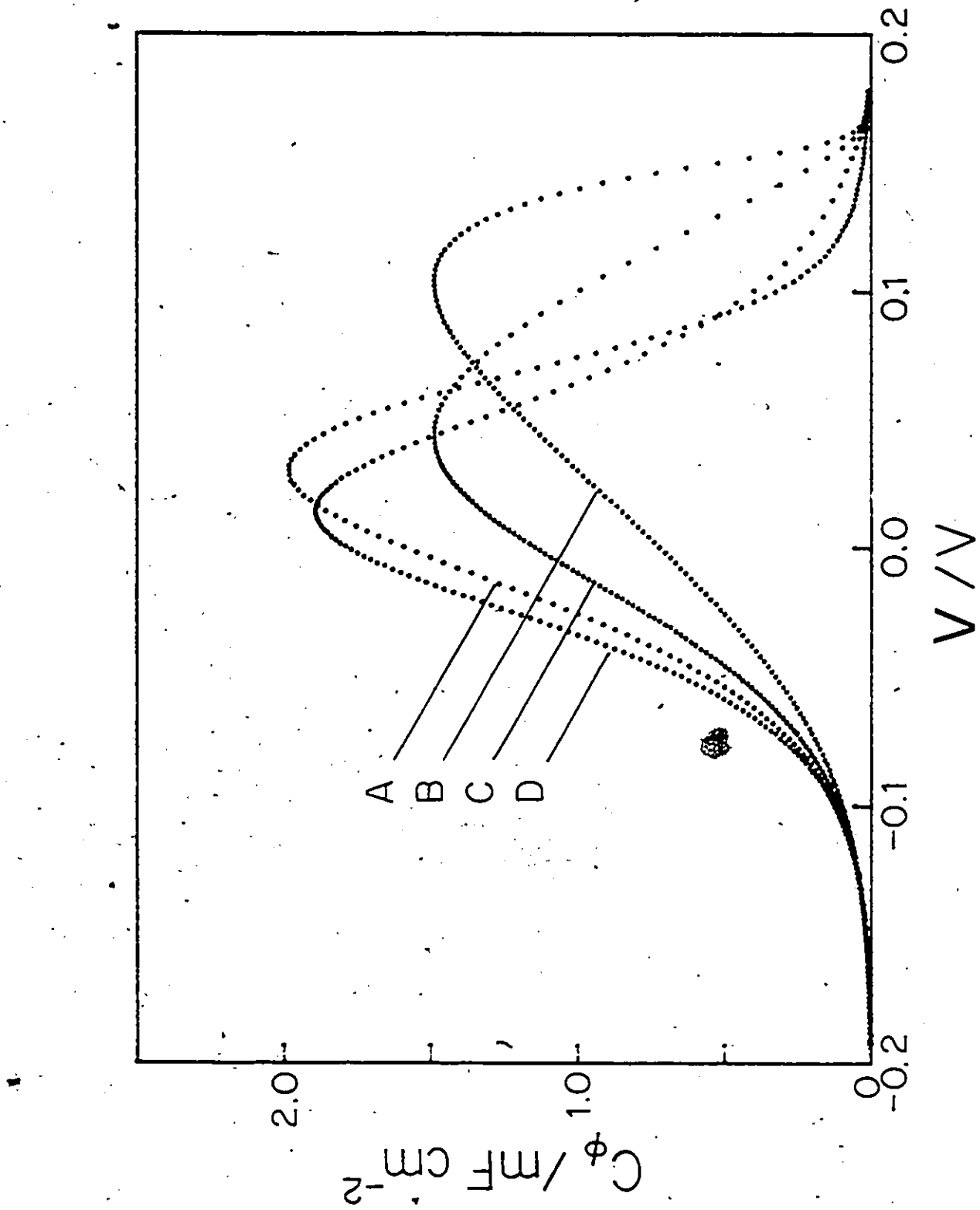
A
B
C
D
0.2
0.1
0.0
−0.1
−0.2
V / V
2.0
1.0
C_ϕ /mF cm^{-2}

kinetic reversibility.

The programmed value of the potential sweep-rate, s, was used in calculating C_ϕ in curve C, but the actual sweep-rate, dV(t)/dt, varies considerably in the potential region of the peak. Curve D shows C_ϕ = I(t)/(dV(t)/dt) vs V(T). The asymmetry in the C_ϕ profile for R_u = 800 Ohms is seen to be reduced and the C_ϕ at the peak is increased, although it is still smaller than the value of $C_{\phi,p}$ for R_u = 0. In addition, the potential at the maximum in the actual C_ϕ vs V profile resulting from this calculation arises at a less positive potential than in the R_u = 0 case and differs from the actual potential of the maximum current (or the corresponding $C_{\phi,apparent}$). Curve C in Fig.4-9 then corresponds to the shape of the actual I(t) vs V(T) profile (since constant s was used here), while curve D gives the actual instantaneous C_ϕ [=I(t)/(dV(t)/dt)] behaviour.

We have mentioned that the figure of R_u = 800 Ohms is an improbably large one, taken only for illustrative purposes (given the assumed kinetic parameters, see (b) above). In most practical situations, the R_u experimentally encountered is rarely in excess of 20 Ohms.

In general, the potentials of the maxima in I(t) and I(t)/(dV(t)/dt) will differ. In the particular case of irreversible kinetic conditions ($s > s_o$), the $V_{p,apparent}$ for the I(t) maximum transforms to give $V_p(R_u = 0)$, while the pseudocapacitance quantity, I(t)/(dV(t)/dt), has a maximum at a different potential.

(f) Conclusions

When uncompensated solution resistance is significant, it gives rise to distorted I vs V profiles for surface processes under LPS conditions owing to the associated distortion of the potential programme which is effectively applied at the OHP. Significant deviations in the potential, and especially in the potential sweep-rate, result in correspondingly distorted C_{ϕ} vs V(t) traces.

Under irreversible conditions, the observed $V_{p,apparent}$ values which are required for relating to log s in order to characterize the kinetics of the surface process, can be transformed simply according to eqns.(4-9a,b) to yield the peak potential obtaining when $R_u = 0$. In the quasi-reversible regime of kinetic behaviour ($s < s_o$) (where I(t) values are relatively small and hence IR_u losses are less significant), this transformation does not apply. However, in a practical application, where IR_u effects are not significant if s is sufficiently small, a reliable estimate of $V_{p,reversible}$ may be obtained; at higher sweep-rates in the regime of kinetic irreversibility, the above transformation will hold. Thus, some estimate of the kinetically significant transition sweep-rate, s_o (the reversibility parameter), may still be made. Of course, as with the analogous correction of steady-state "Tafel-plots", the uncertainty associated with the above procedure increases as the I_pR_u correction becomes comparable with the actual shift in peak potential due to kinetic irreversibility of the surface process under study.

In practical applications of the LPS method of Angerstein-

Kozlowska and Conway[158] in the study of the kinetics of electrode surface processes, it is important to distinguish observed changes in V_p with log s due to the onset of kinetic irreversibility[158,175] from those due to IR_u effects[174]. Changes in V_p with log s, due to the latter effects, give rise to somewhat curved V_p vs log s plots; the present calculations show that in this case, the associated $C_{\phi,p}$ ($=I_p/s$) does not attain a constant value (= 0.73 $C_{\phi,p,rev}$) as expected for reaction (1) operating in the irreversible kinetic regime, i.e., for $s > s_o$[158,175]. It is important to note that the application of this $C_{\phi,p}$ criterion does not require a knowledge of the value of R_u; this may be especially advantageous when the use of dynamic IR_u compensation results in an unknown residual uncompensated solution resistance.

3. Collection and Processing of Open-Circuit Potential Decay Measurements

The open-circuit potential decay behaviour upon interruption of a steady-state current yields information on the mechanistic and pseudocapacitance characteristics of an electrode reaction[165]. In reactions involving adsorbed intermediates, an adsorption pseudocapacitance component, C_ϕ, of the total interfacial capacitance occurs, and reflects the potential dependence of the fractional coverage, θ, of such intermediates.

The determination of the coverage, θ, of an electrode surface by some electroactive intermediate can also be investigated by galvanostatic pulse or cyclic-voltammetry; however, when significant continuous faradaic currents are

passing, these techniques prove difficult or unreliable.

For example, consider the conditions for observing a peak in a LPS voltammetry experiment due to a surface electrosorption process in the presence of an <u>independent</u> continuous faradaic process:

$$\text{(electrosorption)} \quad A^- + M = MA + e^- \qquad (4\text{-}11)$$

$$\text{(continuous process)} \quad Red = Ox + e^- \qquad (4\text{-}12)$$

where MA represents an adsorbed species. Assuming that process (4-11) is operating in the reversible kinetic regime of sweep-rate, s, the overall current is given by the sum of the components

$$\begin{aligned} i_T &= i_1 + i_2 \\ &= QFks/RT\ [\exp(-VF/2RT) + k\ \exp(VF/RT)]^{-2} \\ &\quad + i_o[\exp(\beta VF/RT) - \exp(-(1-\beta)VF/RT)] \end{aligned} \qquad (4\text{-}13)$$

where Q is the charge for a monolayer of adsorbed MA and β is the symmetry factor (assumed = 1/2 below). Fig.4-10 shows the corresponding i_T/s <u>vs</u> V behaviour for a number of values of V^o_2, the reversible potential of process (4-12) relative to the potential for which $\theta = 1/2$ in reaction (4-11). Clearly the strongly potential-dependent component i_2 may completely obscure the component of the total current due to the surface process (4-11). The existence of a peak (or at least of an inflection point) in the I <u>vs</u> V profile requires that $di_T/dV = 0$ and this results in a maximum potential V_{max}, relative to V^o_2, for which a peak may be expected.

This condition is represented in the V_{max} <u>vs</u> log (i_o/s) plot of Fig.4-11. In this figure, for given log (i_o/s), a discernable

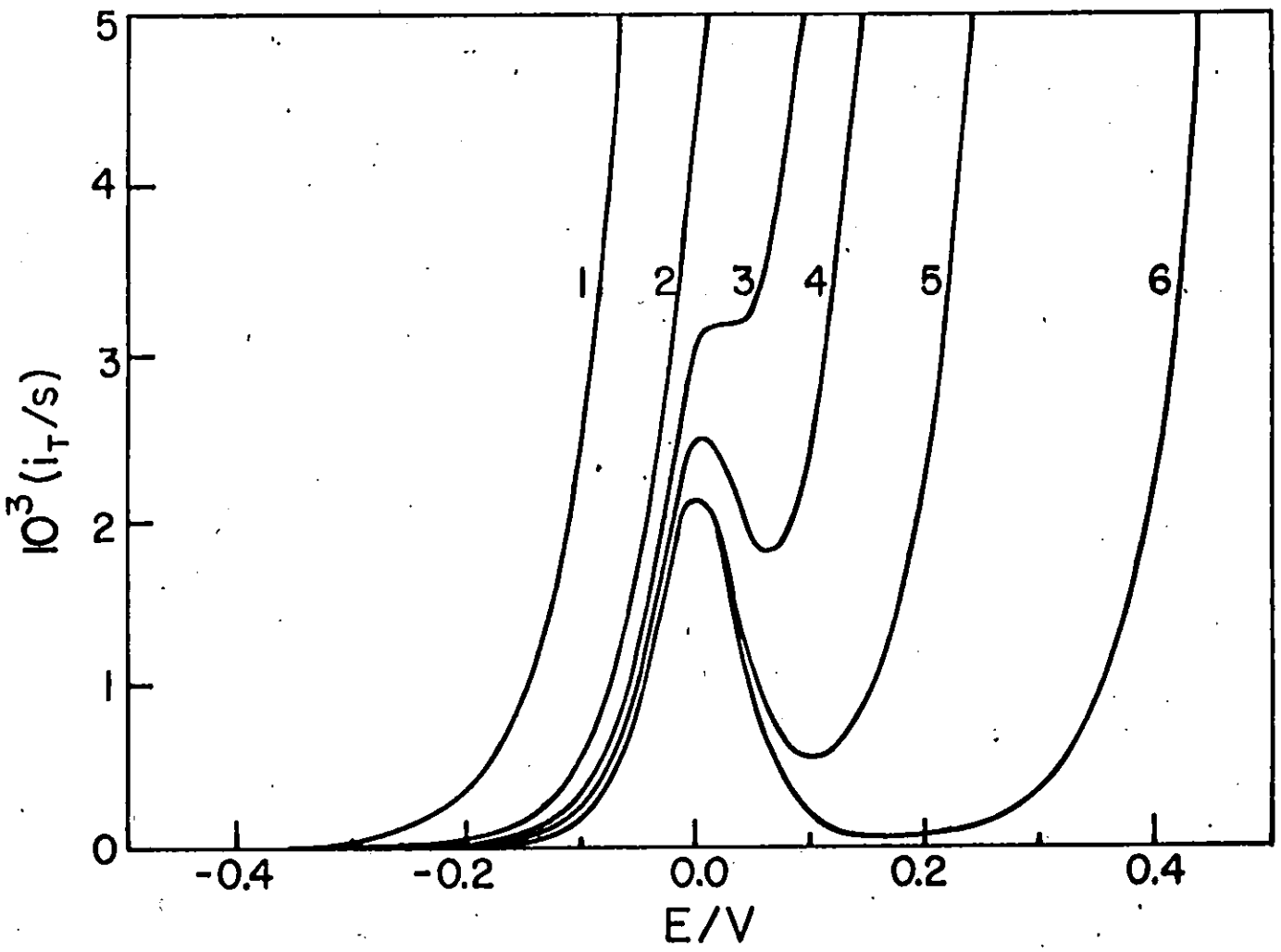

Fig.4-10 Cyclic-voltammogram for parallel continuous and surface faradaic processes at various values of E_2^o, the reversible potential of reaction (4-10) relative to the potential for which $\theta = 1/2$ in reaction (4-9); E_2^o = 1) -0.5; 2) -0.4; 3) -0.35; 4) -0.3; 5)-0.2 and 6) 0.0 V.

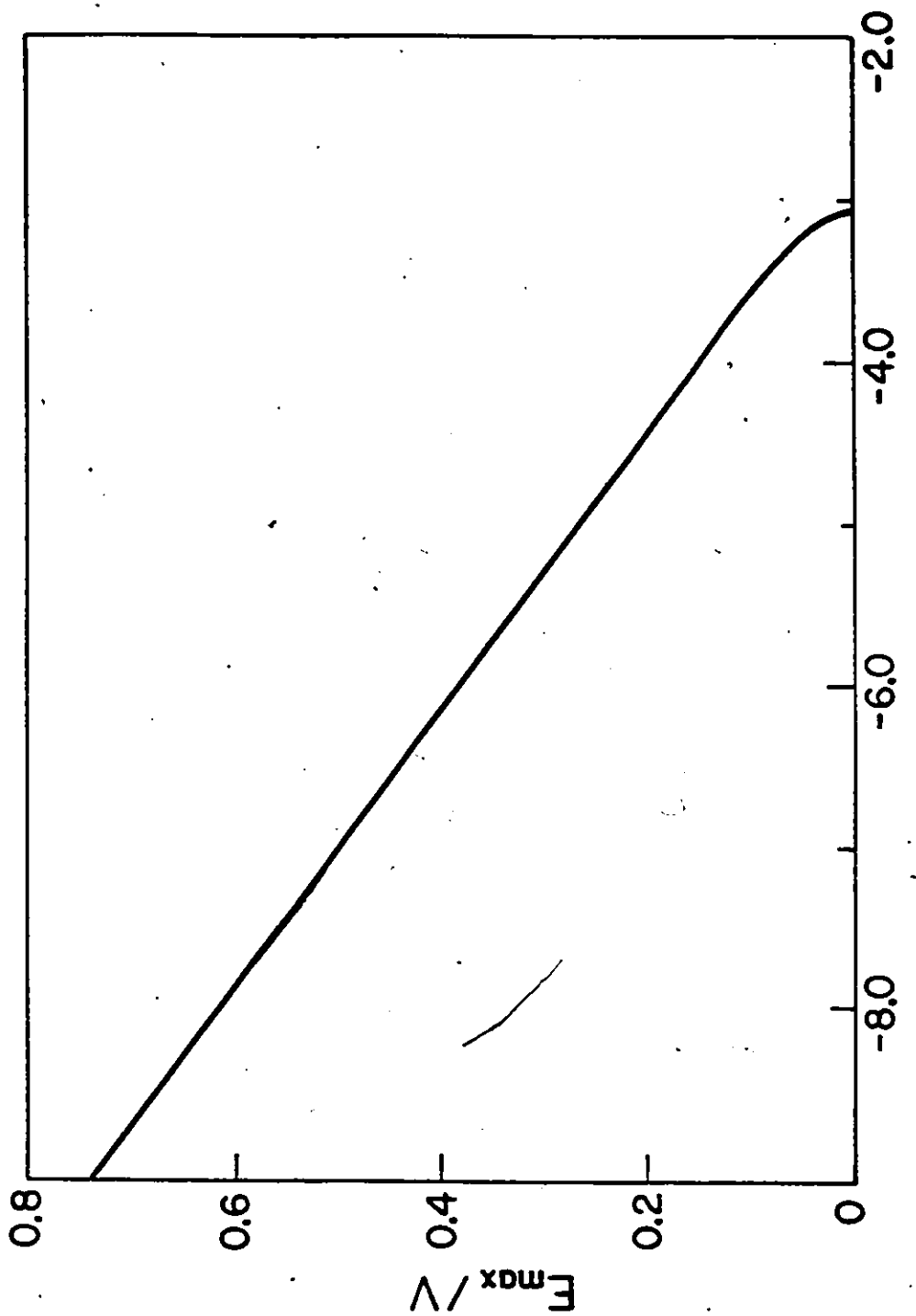

Fig.4-11 Conditions for the existence of a peak in the cyclic-voltammogram for parallel continuous and surface processes.

peak is only expected at potentials below the indicated curve; for given i_o, an increase in s, and hence a decrease in $\log(i_o/s)$, extends the accessible potential range. This is a result of the linear dependence of the current due to process (4-11) under LPS conditions compared with the sweep-rate independent current response of reaction (4-12). This masking of the overall current severly restricts the use of the LPS method for the detection of electrosorbed species in the presence of large continuous faradaic currents. If the surface species is an intermediate in the continuous faradaic reaction itself, limiting coverages of $<\cdot 1$ can be shown (see Chapter 1) to occur for certain mechanistic schemes and their detection by LPS will be rendered still more difficult.

In the present section, a data collection and processing procedure will be described for the evaluation of the capacitance behaviour from open-circuit potential decay results, which avoid the problems outlined above*.

Upon interruption of a steady-current through an interface, the discharge of the double-layer capacitance via the faradaic process under study obeys the relation

$$-C(V)dV/dt = i(V) \qquad (4\text{-}14)$$

where C is the total interfacial capacitance ($= C_{dl} + C_{\phi}$) at a potential V, and i(V) is the corresponding potential-dependent faradaic current (see Fig.4-4 for an equivalent circuit representation of this situation). The usual procedure for an electrode process showing linear Tafel behaviour and constant C

* The work to be reported here is in collaboration with Lijun Bai and is based on a joint paper with him.

is to replace $i(V)$ with $i_o \exp(\beta VF/RT)$ and integrate:

$$-V(t)/b = \ln(t + \tau) + \ln(i_o/bC) \qquad (4\text{-}15)$$

where $\tau = bC/i(V_o)$.

Thus $V(t)$ is then linear in $\log(t + \tau)$, which at long times, $t >> \tau$, reduces to $\log(t)$. In such a case where C is assumed constant, τ must be estimated or only the data for which $t >> \tau$ used. When C includes a significant potential-dependent adsorption pseudocapacitance, C_ϕ, in addition to the usual double-layer capacitance, $C_{d.l.}$, two limiting types of behaviour can arise. At low coverage, θ, when C_ϕ increases exponentially with V, $dV/d(\log t)$ is greater than the steady-state $dV/d(\log i)$; as $\theta \to 1$, C_ϕ decreases exponentially with V, $dV/d(\log t)$ is less than the corresponding $dV/d(\log i)$ [182,183,184]

The procedure developed for dealing with open-circuit potential decay data deals directly with the fundamental differential relation in eqn.(4-14) above. Rather than assuming an arbitrary form for $i(V)$ or $C(V)$ as indicated above, the decay data were used to establish information about $C(V)$ and hence about C_ϕ itself due to kinetically significant adsorbed intermediates.

Thus, the first derivative (dV/dt) of the potential-time decay data was calculated numerically from the experimentally observed $V(t)$ behaviour. This could be done accurately using a laboratory computer, given the large data records (4096 or 8192 data points), spanning more than three decades in time, which are obtained by using a digital oscilloscope to record directly the course of the potential decay digitally. Thus, for $i(V) = i_o$

$\exp(V(t)/b)$ in eqn.(4-14),

$$\ln(-dV/dt) = \ln i_o - \ln C(V) + V(t)/b \qquad (4\text{-}16)$$

whence plots of $\ln(-dV/dt)$ vs $V(t)$ can be made and $C(V)$ deduced from a knowledge of the Tafel parameters log i_o and b obtained from the experimental steady-state polarization behaviour.

For overpotential values significantly less than 75 mV, the back reaction component of i(V) becomes significant. Inclusion of this component in a manner analogous to that used for the correction of steady-state polarization results for the back reaction, yields

$$\ln\left[\,[1-\exp(V(t)F/RT)]^{-1}(-dV/dt)\,\right] = \ln i_o - \ln C(V) + V(t)/b \qquad (4\text{-}17)$$

analogous to eqn.(4-16) above; the correction factor $[1 - \exp(V(t)F/RT)]^{-1} \to 1$ for large V and eqn.(4-16) is recovered. This technique was applied by Conway et al.[165] in a study of the electrocatalytic properties of Ni-based cathode materials for the h.e.r. in alkaline solutions. Thus, direct information concerning the pseudocapacitance behaviour can be obtained by means of eqn.(4-14) along with the dV/dt and Tafel i-V quantities derived from open-circuit potential decay and steady-state polarization experiments.

A more general treatment of the decay data involves the use of the actual (i.e. not necessarily Tafelian) i(V) data from automated steady-state polarization measurements in the derivation of C(V); this removes the restriction to reactions exhibiting Tafel log i - V relationships. In this way i(V) and dV/dt from separate experimental measurements can be combined according to

$$C(V) = i(V)/(-dV/dt) \qquad (4\text{-}18)$$

in order to derive the interfacial capacitance behaviour. The results of this analysis of the h.e.r. at a mercury cathode at high overpotentials were shown to be consistent with a constant double-layer capacitance.

In recent work, Conway and Bai[185] have investigated the adsorption pseudocapacitance associated with the h.e.r. for a number of electrode materials and solution pH conditions, using the above method. The presence of over-potentially deposited ("OPD") H (in contrast to the well-known under-potentially deposited ("UPD") H at potentials anodic to the reversible h.e.r. potential) was demonstrated at Ni and Ni-Mo alloy electrodes, and also at Pt. The absence of a significant adsorption pseudocapacitance at a Au cathode, and at Hg as above, was expected from other work, and its observation confirmed the validity of the treatment and analysis of the open-circuit potential decay results given above.

Thus, the utilization of a fast digitizing oscilloscope in the acquisition of open-circuit potential decay data, and of an automated steady-state polarization system, has yielded very useful information on the pseudocapacitance and coverage due to adsorbed intermediates, in the potential regime where large continuous faradaic currents are passing. The accurate numerical calculation of $dV(t)/dt$ from the observed $V(t)$ values, which is essential for the satisfactory application of this new potential decay method, was only possible because of the dense sampling (in time) of potential values that could be achieved. By this method, the uncertainties and/or neglect of short time data

traditionally associated with the constant of integration, τ, in eqn.(4-15) were avoided and direct information concerning the total interfacial capacitance was derived from the V vs t data. From the derived C_ϕ vs V data, the coverage or changes of coverage of the ad-species involved in the reaction can be calculated as f(V) by integration of the experimentally determined C_ϕ vs V profile.

4. Other Applications and Procedures

A brief mention of other laboratory computer applications arising from this work follows:

a) An arbitrary waveform generator for use in cyclic-voltammetry was realized by means of a programme-controlled DAC for generating repetitive wave forms consisting of potential ramp, hold, and step segments. This generator was implemented on a PDP 11/34 laboratory minicomputer, fitted with a suitable DAC and real-time clock (see ref.186 for a detailed description). In an earlier related application[164], a PDP 11/34-based data acquisition and treatment system was developed for use in the study of electrochemical surface processes by LPS voltammetry.

b) A Solartron 1172 frequency response analyser was available for a.c. impedance measurements and a complementary software package was developed. This enabled the remote automatic control of this instrument and the storage of relevant experimental results; for example, impedance measurements at several frequencies could be made automatically at a number of desired electrode potentials and the results displayed graphically or in tabular form. Complex-plane analyses could

also be performed.

c) A subroutine library was developed for plotting results on the PDP 11/34 system through a DAC to an x-y plotter. In using the HP87 (or HP86B) laboratory computer, a commercially available graphics software package and graphics plotter were used.

CHAPTER 5

RESULTS AND DISCUSSION

1. Significance of $\Delta H^{\ddagger}$ and Frequency Factors in Electrochemical Kinetic Measurements

Experimental determinations of heats of activation ("activation energies") and of the associated frequency factors (related to entropies of activation) provide a useful characterization of the kinetics of chemical reactions and often a basis for critical interpretations of mechanisms. The Arrhenius equation for the temperature-dependence of a chemical rate constant, k, is of the form

$$k = A \exp[-E_a/RT] \qquad (5\text{-}1)$$

where A is the frequency factor and E_a is the experimental heat of activation. In the context of activated complex theory, the enthalpy, $\Delta H^{\ddagger}$, and entropy, $\Delta S^{\ddagger}$, of activation are derived in the usual way[187] from the values of E_a and A, respectively.

The determination of a single pair of these activation parameters provides little information on the mechanistic details of an electrochemical process. However, for the same overall reaction (e.g. the h.e.r.) occurring at different metal surfaces, differences of true activation energies and ratios of frequency factors can be evaluated and these may be related to progressive changes in electrode metal properties[37] for a given mechanism, or else signal a change in mechanism; for example, Conway, Beatty and DeMaine[37] have compared the activation parameters for the h.e.r. on a series of Cu-Ni alloys and related them to progressive changes in electronic properties of the alloy

electrodes.

Activation parameters are also useful as diagnostic criteria for the participation of proton tunneling in H/D isotopic substitution studies, e.g. of the h.e.r. at Hg^{73}. In the present work, consideration of the potential-dependence of these activation parameters will be shown to bear on the question of the temperature-dependence of the Tafel slope, b, or symmetry factor, β, referred to in Chapter 2.

(i) Temperature Dependence of the Reversible Potential

The significance of activation energies in the case of electrochemical reactions is obscured by the fact that they are deduced from measurements of current densities at constant electrode potential referred to a reversible reference electrode in the system. Alternatively, activation energies can be deduced from the temperature coefficient of overpotential (with respect to some reference electrode) at constant current density. In both approaches, the absolute metal-solution potential difference at the reference electrode varies with temperature in a thermodynamically inaccessible manner.

Although the standard value of the potential of the hydrogen electrode is conventionally taken as zero at all temperatures, the potential of the reference electrode used, e.g. the hydrogen electrode, will actually vary with temperature on account of the associated entropy change in the half-cell reaction

$$H_3O^+ + e^- = H_2O + 1/2H_2 \qquad (5\text{-}2)$$

which, like any half-cell or single ion property, is inaccessible to direct thermodynamically-unambiguous determination. If the

reference electrode is maintained at a constant temperature while that of the working electrode is varied, then an unknown irreversible thermal liquid-junction potential is included in the measured potential. Conditions under which this non-isothermal cell arrangement may be used to advantage in fixing the metal-solution potential difference will be considered in the following section, as they lead to fairly reliable means of evaluating the true $\Delta H^{\ddagger}$ for an electrode reaction.

As a result of this variation in the absolute potential of the reference electrode with temperature, so-called apparent heats of activation result from Arrhenius plots at constant overpotential. Temkin[188] first treated the problem of the relation between the apparent and true, i.e. at constant metal-solution potential difference, heats of activation*.

A more direct analysis was given by Conway[35] as follows: at a given ionic concentration, the electrochemical rate constant $\bar{k}$ for an ion neutralization reaction may be written as

$$\bar{k} = kT/h \exp [-\Delta G^{o\ddagger}/RT] \exp [-\beta z \Delta\phi F/RT] \qquad (5\text{-}3)$$

where $\Delta\phi$ is the metal-solution potential difference, β is the symmetry factor, $\Delta G^{o\ddagger}$ is the standard chemical free energy of activation, i.e., at $\Delta\phi = 0$, and the other symbols have their usual significance. Eqn.(5-3) can be expressed in terms of the constituent true enthalpy, $\Delta H^{o\ddagger}$, and entropy, $\Delta S^{o\ddagger}$, of activation at $\Delta\phi = 0$, and ϕ_R, the metal-solution potential difference at the reversible potential:

$$\bar{k} = kT/h \exp [\Delta S^{o\ddagger}/R] \exp [-\Delta H^{o\ddagger}/RT] \exp [\beta z(\phi_R + \eta)F/RT] \qquad (5\text{-}4)$$

ϕ_R may be expressed in terms of the standard potential ϕ_R^o and

* The terms "real" and "ideal" have been used by Weaver[77].

hence in terms of $-\Delta G^{o}/zF$ where ΔG^{o} refers to the standard free energy change for the half-cell reaction under reversible conditions.

The quantity $d(\log \bar{k})/d(1/T)$ at $\eta = 0$ $(i = i_o)$ is then

$$-\frac{\Delta H^{o\ddagger}}{R} - \frac{zF\beta}{RT}\frac{d\,\phi_R^o}{d(1/T)} - \frac{zF\beta\phi_R^o}{R} \qquad (5\text{-}5a)$$

or,

$$-\frac{\Delta H^{o\ddagger}}{R} + \frac{\beta T\Delta S^{o}}{R} + \frac{\beta\Delta G^{o}}{R} \qquad (5\text{-}5b)$$

where the term in kT/h has been neglected and $\Delta S^{o\ddagger}$ and $\Delta H^{o\ddagger}$ are assumed, to a first approximation, to be independent of temperature.

Then,

$$\left[\frac{d(\log \bar{k})}{d(1/T)}\right]_{\eta=0} = -[\Delta H^{o\ddagger} - \beta\Delta H^{o}]/R \qquad (5\text{-}6)$$

if ΔS^{o} for the half-cell reaction is independent of T. Hence, in the absence of changes in double-layer and surface coverage effects, $d(\log i_o)/d(1/T)$, which corresponds to $[d(\log \bar{k})/d(1/T)]_{\eta=0}$, yields the experimentally accessible apparent heat of activation

$$E_a = \Delta H^{o\ddagger} - \beta\Delta H^{o} \qquad (5\text{-}7)$$

at the reversible potential ($\eta = 0$). In practice, β may also be a function of temperature as discussed by Conway, MacKinnon and Tilak[74] and so eqn.(5-7) can also contain a term dependent on $d\beta/d(1/T)$.

The use of eqn.(5-7) in the determination of $\Delta H^{o\ddagger}$ requires that ΔH^{o} be estimated by an extra-thermodynamic calculation, assuming β to be known from the Tafel slope. This calculation

for a metal deposition process involves the cycle[189].

$$\begin{array}{ccccc} & M^{z+}_{(g)} & + & ze^-_{(g)} & \xrightarrow{-I(M,z+)} & M_{(g)} \\ \Delta H^o(s,M^{z+}) \uparrow & & & \uparrow z\phi_e & & \uparrow -\Delta H_{sub} \\ & M^{z+}_{(s)} & + & ze^-_{(M)} & \xrightarrow{\Delta H^o} & M \end{array}$$

where

$$\Delta H^o = -\Delta H^o(s,M^{z+}) + z\phi_e - I(M,z^+) - \Delta H_{sub} \qquad (5\text{-}8)$$

and $\Delta H^o(s,M^{z+})$ is the heat of solvation of the M^{z+} ion, $I(M,z+)$ is the ionization energy of M to M^{z+}, ΔH_{sub} is the heat of sublimation of M and ϕ_e is the electron work function of M. Values of the single-ion solvation enthalpy, $\Delta H^o(s,M^{z+})$, are not known to better than 20 - 40 kJ mol^{-1} [157] so that the true $\Delta H^{o\ddagger}$ could not be calculated very precisely from the experimentally determined E_a. Consequently, the true frequency factor $e(kT/h)\exp[\Delta S^{o\ddagger}/R]$ in eqn.(5-4) cannot be accurately determined by this method. However, as noted above, <u>differences</u> in heats of activation or <u>ratios</u> of frequency factors may still be reliably derived, e.g. for a given reaction on a series of metals.

(ii) <u>Use of Non-Isothermal Cells</u>

In order to determine "true" electrochemical activation parameters independent of the temperature-dependence of the reference electrode potential (eqn.5-5a), it is necessary to fix the metal-solution potential difference at the various temperatures of interest; this requires the application of some extra-thermodynamic assumption or principle, e.g. the cycle in the previous section, or avoidance, experimentally, of variation of temperature of the reference electrode. This problem arises as the result of the experimental inaccessibility of the absolute

potential difference across a single metal-solution interface. The significance of this difficulty in the evaluation of heats of activation of electrode processes was first treated by Temkin[188], as referred to above. A similar situation obtains in the study and assignment of the physical properties of single ions in solution[190]; a critical survey of proposed schemes for "splitting" various physico-chemical properties of salts among the constituent ions may be found in refs.155,191. One useful method which has been used involves the measurement of potential differences across non-isothermal cells[192,193] coupled with suitable extra-thermodynamic interpretations or assumptions.

In studies of the half-cell reaction entropies of transition metal redox couples, Weaver et al.[160] have made use of potential measurements on non-isothermal reference electrode cells[192,194]; this method has also been applied to the study of temperature effects on the rates of redox processes at electrode surfaces[77]. In this method, the following type of cell, shown for the H^+/H_2 reference half-cell, is used[77]:

$$\underset{\leftarrow\text{-------}}{Cu \mid Pt \mid H^+,H_2} \;\|\; KCl(3.5M) \mid \underset{\leftarrow\text{----- }T_1\text{(fixed) -----}\rightarrow}{KCl(3.5M)} \;\|\; \underset{\leftarrow\text{----- }T_2\text{(varied) -----}\rightarrow}{H^+,H_2} \mid Pt \mid Pt \mid \underset{T_1}{Cu}$$

where the thermal liquid junction is established within the KCl salt bridge and Cu lead wires are used. The overall cell potential, E_{cell}, is then given by

$$E_{cell} = \phi_{tj} + \phi_{tc} + \Delta\phi_{1j} + \Delta\phi^{\circ}_{M} \qquad (5\text{-}9)$$

where ϕ_{tj} is the thermal liquid junction potential difference in the salt bridge, ϕ_{tc} is the analogous thermal potential difference in the Pt metal conductor, and $\Delta\phi_{1j}$ and $\Delta\phi^{\circ}_{M}$ are the differences in isothermal liquid junction potentials and Galvani

metal-solution potential drop at the electrode surfaces, respectively. Of interest here is the quantity $\Delta\phi_M^o$ by means of which the scales of overpotential corresponding to the h.e.r. reaction at different temperatures may be compared; if the first three quantities in eqn.(5-9) are known or can be estimated, then $\Delta\phi_M^o$ may be obtained from potential measurements on such a non-isothermal cell.

Estimates of the values of the absolute Thompson coefficient for a number of metals indicate that $d\phi_{tc}/dT$ is of the order of a few microvolts per K [193]; for the temperature range 273 - 373 K, $d\phi_{tc}/dT$ for Pt is ca. 6 $\mu V\ K^{-1}$ [160]. For variations in temperature of 30 - 40 K, the associated ϕ_{tc} will be much smaller than the corresponding changes in $\Delta\phi_M^o$ and may, to a good approximation, be neglected. The use of a suitable salt bridge, usually made of a concentrated solution of a salt with ions of equal mobility, reduces $\Delta\phi_{lj}$ to negligibly small values. As will be seen below, the salt bridge may be eliminated in certain cases where $d\phi_{tj}/dT$ is small for the solution used with the particular reference electrode under study but generally it is desirable to include it.

The temperature coefficient of the thermal liquid junction potential, $d\phi_{tj}/dT$ is $\leq 50\ \mu V\ K^{-1}$ for most electrolytes; in addition, this thermodynamically inaccessible quantity is only a weak function of temperature[195,196,197]. The larger $d\phi_{tj}/dT$ values found for strongly acidic or basic media[194], parallel the large isothermal liquid junction potentials which can arise with solutions (of different concentration) of H^+ or OH^- ions. The

non-isothermal salt bridge arrangement described above, made of concentrated KCl, has been used by de Bethune et al.[194] in order to minimize $d\phi_{tj}/dT$ (and hence ϕ_{tj}) in the study of entropies of half-cell reactions; the use of this device is especially required when dealing with acidic solutions where the high mobility of the proton is involved. Using this salt bridge electrolyte, $d\phi_{tj}/dT \leq 20\ \mu V\ K^{-1}$ and probably considerably smaller[192,194].

The effect of such an uncertainty in the thermal liquid junction potential on a Tafel plot of steady-state electrode kinetic polarization results can be estimated from a "worst case" calculation: consider a temperature change $\Delta T = 35$ K and $d\phi_{tj}/dT = 20\ \mu V\ K^{-1}$ giving a maximum contribution of $35K \times 20\ \mu V\ K^{-1}$, = 0.7 mV to the assigned overpotential. If a Tafel slope of 120 mV/decade is assumed, then this represents $0.7/120 = 5.8 \times 10^{-3}$ decades in the current, i.e., a "worst case" deviation of ca. 1%; this is quite acceptable in the study of the kinetics of electrode processes.

In the light of the above discussion, the overall non-isothermal potential is then approximately given by,

$$E_{cell} = \Delta\phi_M^{\circ} \qquad (5\text{-}10)$$

This then yields the required $\Delta\phi_M^{\circ}$ by means of which the interfacial Galvani potential difference at a test working electrode may be fixed while the temperature is varied. In this way, electrochemical activation parameters, independent of the temperature variation of the equilibrium potential, may be rather reliably derived from experimental polarization measurements at various temperatures, as in Weaver's work[77].

(iii) Effect of Variation of Surface Coverage on Heat of Activation

In processes involving an adsorbed intermediate, the surface coverage, θ, generally varies with temperature, even at fixed metal-solution potential difference, and makes a contribution to the apparent energy of activation. This effect is unimportant when the kinetic data are derived from regions of potential where the surface is fully covered ($\theta = 1$) or bare ($\theta = 0$), and for moderate changes in temperature.

Considering the cathodic direction of the three usual steps in the h.e.r. (cf. eqns.(1-1,1-2,1-3)), the corresponding cathodic exchange current density may be written as

(discharge) $$i_o = k_1 C(1-\theta) \exp[-\Delta G_1^{o\ddagger}/RT] \exp[-\phi_R/b] \quad (5\text{-}11)$$

(electrochemical desorption) $$i_o = k_2 C\theta_H \exp[-\Delta G_2^{o\ddagger}/RT] \exp[-\phi_R/b] \quad (5\text{-}12)$$

(atom recombination) $$i_o = k_3 \theta^2 \exp[-\Delta G_3^{o\ddagger}/RT] \quad (5\text{-}13)$$

where the "k" terms include constants but not free energies of activation. In any of these cases, $d(\log i_o)/d(1/T)$ will involve a θ-term $d(\log \theta)/d(1/T)$ or $d \log(1-\theta)/d(1/T)$ in addition to the $\Delta H^{o\ddagger}$ terms in $\Delta G^{o\ddagger}$ and $d\phi_R/d(1/T)$ discussed above.

For quasi-equilibrium conditions in the proton discharge step, the electrochemical Langmuir isotherm gives for a given state of adsorption of H

$$\theta_H = \frac{K_1 C \exp[-\phi_R F/RT]}{1 + K_1 C \exp[-\phi_R F/RT]} \quad (5\text{-}10)$$

where K_1 is the "chemical" part of the electrochemical equilibrium constant at the reversible potential ϕ_R and is related to the standard free energy of adsorption of H. At low

coverage at the reversible potential, ϕ_R,

$$\theta \equiv K_1 C \exp[-\phi_R F/RT] \quad (5\text{-}15a)$$

$$\equiv C \exp[-\Delta G^\circ_H/RT] \exp[-\phi_R F/RT] \quad (5\text{-}15b)$$

whence

$$d \log(\theta_H)/d(1/T) = -\Delta H^\circ_H/R - F/RT \; d\,\phi_R/d(1/T) - F\phi_R/R \quad (5\text{-}16)$$

For the proton discharge step, the resulting expression (low coverage) for the apparent heat of activation is given by[189]

$$d \log(i_o)/d(1/T) = -[\Delta H^{o\ddagger} + \Delta H^\circ_{ads} - \beta\Delta H^\circ]/R \quad (5\text{-}17a)$$

$$= -[E_a + \Delta H^\circ_{ads}]/R \quad (5\text{-}17b)$$

where ΔH°_{ads} is the heat of adsorption at the reversible potential and is usually a negative quantity. Thus the apparent heat of activation could be negative when $E_a + \Delta H^\circ_{ads} < 0$; such behaviour has been reported for H_2 evolution at Pb[74].

The foregoing example will serve to illustrate the importance of the "θ" factor in determining activation parameters in the h.e.r. At Hg where $\theta \ll 1$ and the discharge step is rate determining, these complications are not encountered. It should be noted that even where "true" heats of activation are determined, e.g. by means of non-isothermal cell measurements in order to fix the metal-solution potential difference, the intrinsic temperature-dependence of the "chemical" part of the adsorption equilibrium constant will still make a contribution.

Formally, it would be desirable to normalize exchange current data with respect to a coverage factor (θ or 1-θ), as was done in the publication of Devanathan[198], but in practice θ may not be accurately known; however, the potential-dependent values of θ that can be derived from open-circuit potential decay

measurements may allow this normalization to be performed (see Chapter 4 and refs.165,167).

(iv) Heat of Activation in Relation to Proton Tunneling

It was noted in a previous section that the involvement of proton tunneling in the h.e.r. might be demonstrable in kinetic behaviour examined at sufficiently low temperatures. At such temperatures the Arrhenius plot is expected to show some curvature if tunneling is occurring, in a manner analogous to that known for homogeneous proton transfer processes[76].

The following effects of tunneling are to be expected, especially at low temperature:

a) The activation energy, E_a^*, when tunneling is significant should be less than the classical value E_a; however, in the absence of reliable *a priori* theoretical calculations of the energy barrier height, this prediction cannot usefully be tested in practice.

b) The frequency factor A^* should depend on temperature and be less than the classical A; this test is impracticable except at the lowest temperatures. The fact that tunneling leads to low rather than high values of A^* is illustrated by the schematic plot of log $\bar{k}$ *vs* 1/T in Fig.5-1. The value of log A is equal to the extrapolated ($1/T \to 0$) intercept of this plot, and for measurements over a finite temperature range, $A^* < A$ will result owing to the curvature in the plot.

c) In H/D kinetic isotope studies, $E_D^* - E_H^*$ should be larger than the appropriate difference in zero point energies; this requires a detailed knowledge of the properties of initial and

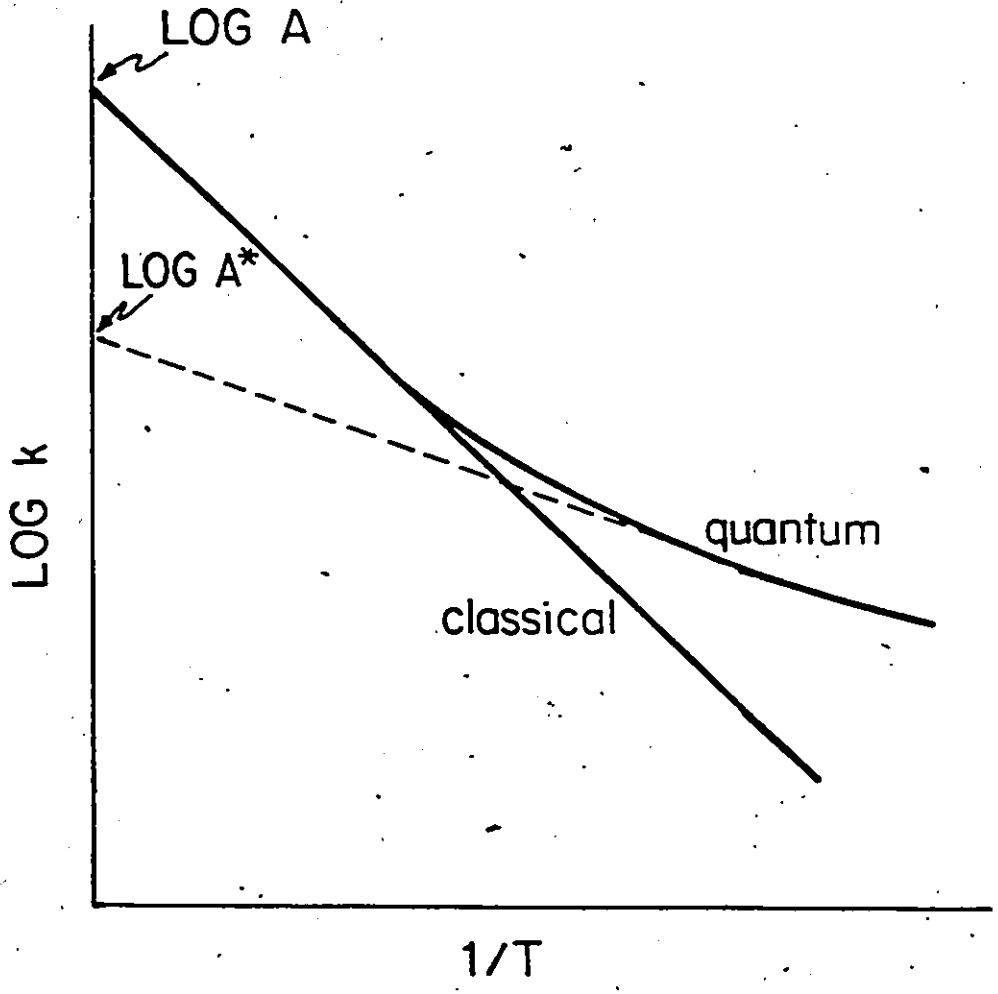

Fig.5-1 Schematic Arrhenius plot showing the effect of proton tunneling.

activated states, but evaluation of $E_D^* - E_H^*$ may be indicative of tunneling if the latter effect is considerable.

d) When tunneling is important, $A_H^* < A_D^*$. This is a useful criterion for tunneling since activated complex theory predicts A_H^*/A_D^* in the range 0.5 - 1.0, with values close to unity being probable. Thus experimental values of A_H^*/A_D^* substantially less than 0.5 can provide evidence for an appreciable degree of tunneling.

These predictions concerning activation parameters for proton transfer also apply to homogeneous reactions; in electrochemical H^+ transfer the temperature dependence of the Tafel slope provides another diagnostic criterion of the participation of proton tunneling[72], apart from other complications mentioned earlier.

2. Comparative Rates and Apparent Activation Parameters for the H.E.R. from 1M CF_3SO_3H and $CF_3SO_3^-H_3O^+$

Comparative steady-state polarization measurements were made at several temperatures in the range 313 - 348 K for proton discharge from pure $CF_3SO_3^-H_3O^+$ and in the range 298 - 348 K for the 1 M aq. CF_3SO_3H solutions; Hg, Ni and Pt electrodes were used.

The slopes of electrochemical Arrhenius plots of log i vs T^{-1} at constant overpotential (with respect to the reversible hydrogen electrode in the same solution and at the same temperature as the working electrode) can be used to derive apparent heats of activation in the usual way (see the previous section).

Ratios of frequency factors ($A(H^+_{aq})/A(H_3O^+)$) for the

h.e.r. were also derived; these ratios are "apparent" quantities owing to the different value and temperature-dependence of the absolute potential of the reference electrode in the dilute 1 M CF_3SO_3H and ca. 10.8 M $CF_3SO_3^-H_3O^+$ melt. This is to be contrasted with conditions in the work of Conway et al.[37] referred to in a previous section, where the solution composition was kept constant and the electrode material varied; in this latter case, assuming identical temperature-independent transfer coefficients, the $\alpha F \Delta H_R^o$ terms in eqn.(5-7) cancel when the difference of apparent heats of activation (or ratio of frequency factors) is taken. The important question of a suitable basis for comparison of "true" activation parameters for the h.e.r. from the monohydrate melt and dilute aqueous CF_3SO_3H solution will be considered in a subsequent section.

(i) State of H^+ as H_3O^+ in $CF_3SO_3^-H_3O^+$

Trifluoromethanesulfonic acid (CF_3SO_3H) is a very strong acid[199] which forms a monohydrate salt $CF_3SO_3^-H_3O^+$ (m.p. 307 K[53]); the melt of this monohydrate provides a medium in which to study the chemical and physical properties of the H_3O^+ ion in the absence of further hydration[140]. The physical properties of the system CF_3SO_3H/H_2O have been investigated by Corkum and Milne[52] while the structure of the ionic solid has been determined by means of X-ray and neutron diffraction by Lundgren et al.[143,144]

The 300MHz ^1H NMR spectrum of the solid monohydrate was determined in the present work and appears in Fig.5-2; the 3-peaked spectrum is unambiguously characteristic of an H_3O^+ salt with trigonal symmetry of the H^+ cation rather than of a

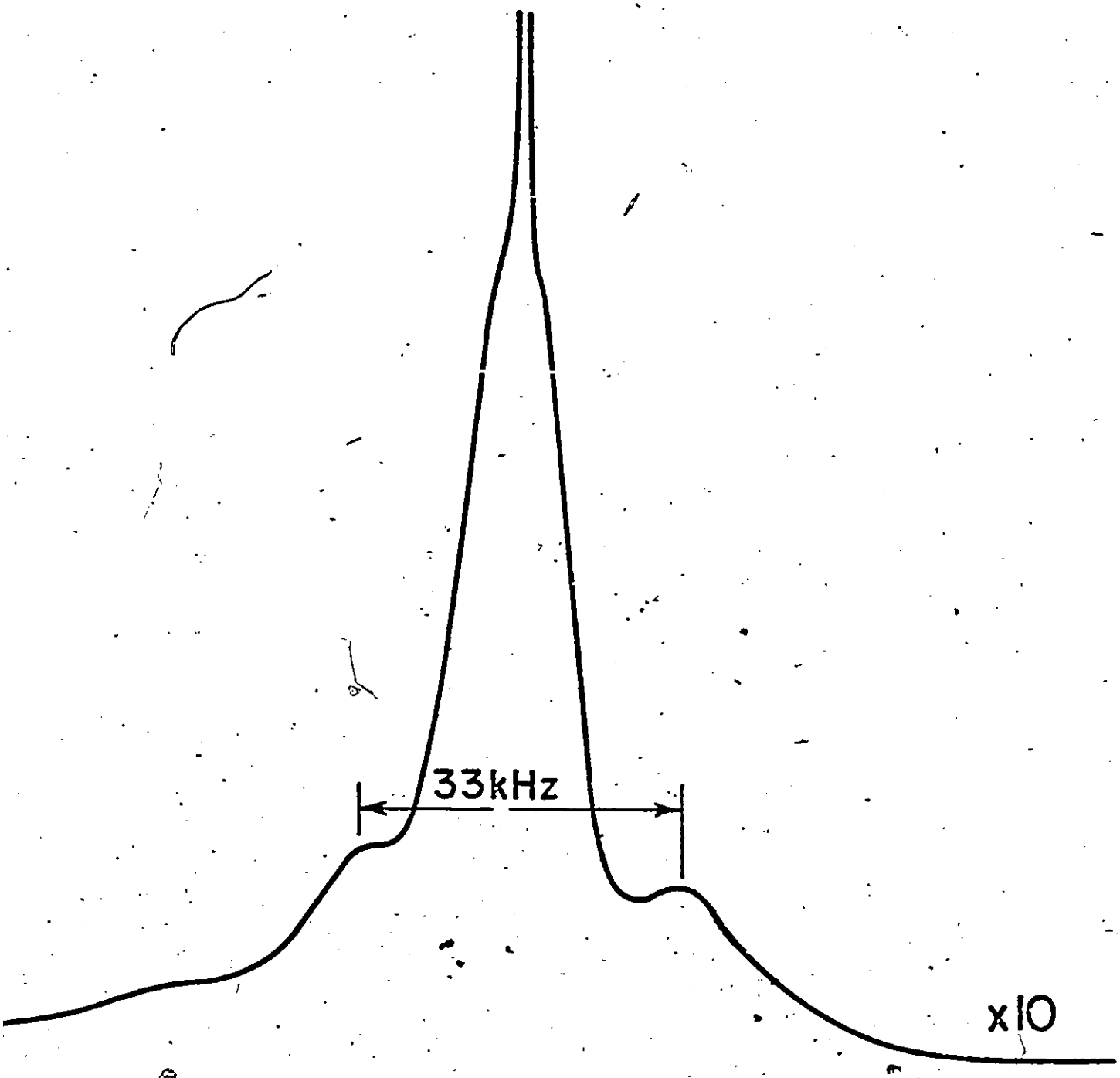

Fig.5-2 Pulsed 300-MHz ^1H NMR spectrum of solid $CF_3SO_3^-H_3O^+$ at 198 K. Pulse time 3 μs, 287 acquisitions.

molecular H_2O hydrate (see Chapter 2).

The infrared spectrum of liquid $CF_3SO_3^-H_3O^+$ shows the absence of any bands due to $-SO_3H$, consistent with an ionic monohydrate in the liquid state[200].

Kotz et al.[201] have studied the integrated intensities of the Raman bands due to CF_3 and SO_3^- groups with the progressive addition of H_2O to CF_3SO_3H; for values of the molar ratio $(H_2O)/(CF_3SO_3H) > 1$, they conclude that complete ionization of CF_3SO_3H to form the H_3O^+ salt occurs in the liquid state.

In the liquid $CF_3SO_3^-H_3O^+$, the H_3O^+ ion is stabilized by strong coulombic interactions with the $CF_3SO_3^-$ anion. This environment differs substantially from that for H_3O^+ in excess water where the corresponding interactions are through ion-dipole forces and H-bonding; in fact the melt can be viewed as a sort of lattice liquid, like a molten salt. The consequences of the large concentration of anions in the $CF_3SO_3^-H_3O^+$ melt, e.g. on the kinetics of the h.e.r., or at an anodically polarized electrode surface, will be considered below.

(ii) Purity of $CF_3SO_3^-H_3O^+$ and Stability of the Anion to Electrochemical Reduction

Satisfactory purity of the $CF_3SO_3^-H_3O^+$ (see the experimental section for details of its preparation) was checked by performing a cyclic-voltammetry experiment at a Pt electrode; both in aqueous solution made up from pyro-distilled water and in the liquid "monohydrate", the cyclic-voltammetry behaviour with respect to the surface processes of H deposition and ionization and surface oxide formation and reduction, indicated (Fig.5-3) very

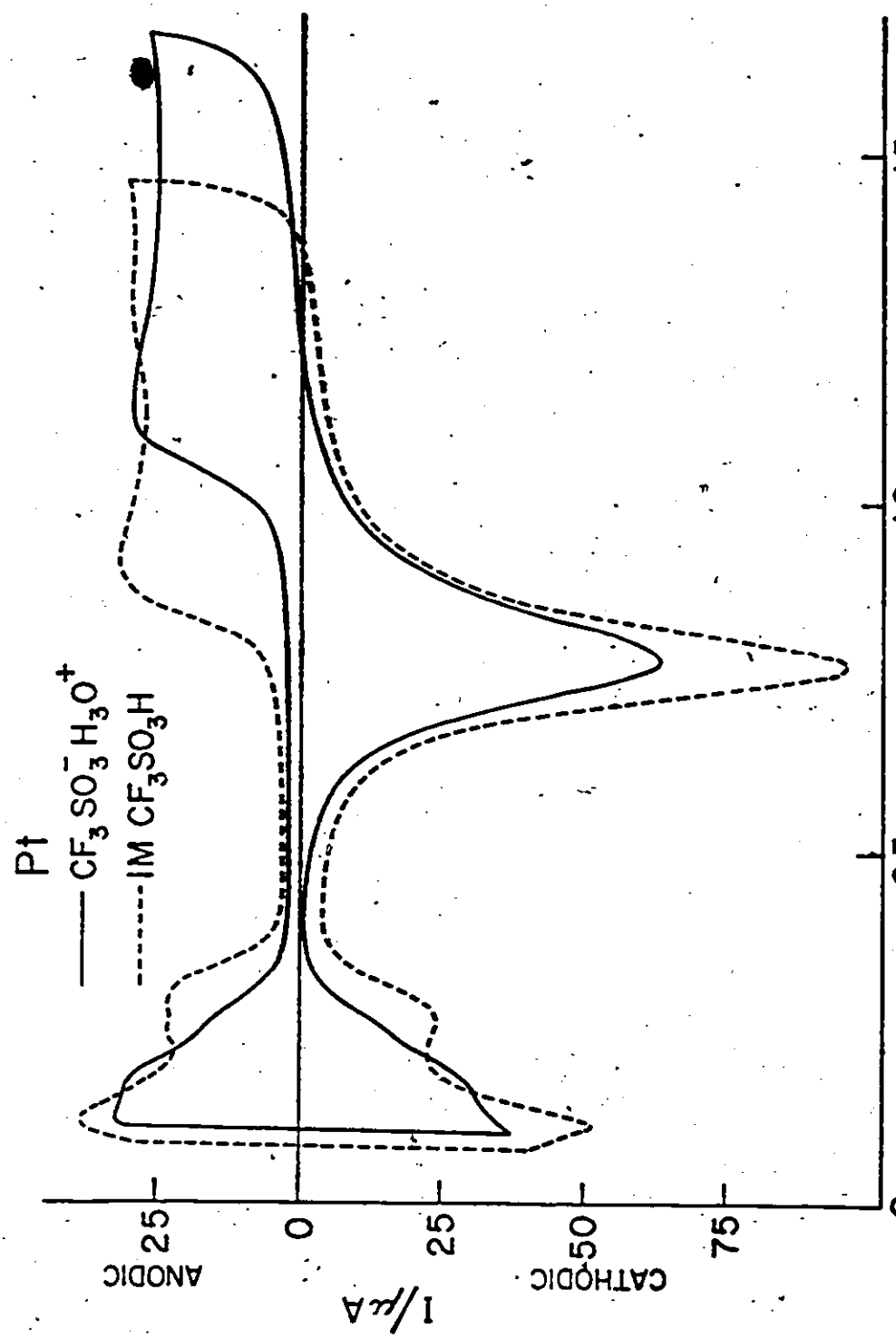

Fig.5-3 Cyclic voltammetry i vs V profiles for $CF_3SO_3^-H_3O^+$ and 1 M aqueous CF_3SO_3H at 313 K at a Pt electrode, Sqeep rate 0.092 $v.s^{-1}$.

satisfactorily clean solutions according to the relatively demanding criteria of solution (and surface) purity published previously[159]. The surface oxidation and O_2 evolution reactions at Pt in this monohydrate melt were investigated in some detail and the results are described in a later section.

With a sulfonic acid at catalytic cathodes there is the possibility that at potentials for H_2 evolution, some reduction of the acid to a sulfinic acid or a sulfide might occur and vitiate the kinetic results for H_2 evolution. That this was not the case was shown by taking cyclic-voltammograms before and immediately after a H_2 evolution kinetic run over a range of current densities, with and without stirring. The excellent initial cyclic-voltammogram (Fig.5-3), characteristic of a "clean solution", was retained after cathodic H_2 evolution at Pt from $CF_3SO_3^-H_3O^+$; no changes in the H-adsorption region with stirring, nor extra currents over the surface oxidation region, indicative of reoxidation of some reduced species in the solution or on the electrode surface, are observed.

(iii) Concentration Effects in the Measured Rates or Exchange Currents

Since we are really interested in the difference or ratio of electrochemical rate constants for discharge from H_3O^+ and "$H_9O_4^+$" corresponding to the respective rates measured, allowance must be made for the concentration difference of protons in the two types of solutions. Thus, since the density of $CF_3SO_3^-H_3O^+$ is 1.81 g cm^{-3}, the molarity of the liquid "monohydrate" at its melting point (309 K) is ca. 10.8 compared with 1.0 for the selected

solution in excess H_2O.

On account of well-known[1,202] "double-layer" effects in electrode kinetics, the rate constant ratio for H_2 evolution from these two systems cannot be derived from the measured rates simply by allowance, in direct proportion, for the ratio of H^+ concentration (10.8). For example, in dilute solutions, the η vs log i relations for the h.e.r. at Hg are independent[203] of H^+ concentration due to compensating effects between various concentration-dependent terms in the rate equation, especially through the diffuse-layer potential Ψ_1. However, at the higher concentrations involved in the present work, this compensation is incomplete so that a concentration correction has to be made in order to compare the factors other than concentration that lead to the observed difference of rates to be described below.

Thus, at the concentrations involved; 10.8 M and 1.0 M, the diffuse double-layer, (Ψ_1) effect originating from the log $[C_{H^+}]$ dependence of the Ψ_1 potential which arises in dilute solutions, becomes only a small factor, approaching constancy, in solutions stronger than ca. 0.2 M when specific adsorption is absent. The log i at constant η should increase with increase of C_{H^+} (rather than remain almost constant) if the symmetry factor $\beta = 0.5$, since, for concentrations > ca. 0.2 M , where $\Psi_1 \rightarrow$ constant,

$$\eta = RT/\beta F \log i + RT(1-\beta)/F\beta \log[C_{H^+}] + \text{constants} \qquad (5\text{-}18)$$

which gives

$$\left\{ \frac{d \log i}{d \log[C_{H^+}]} \right\}_{\eta} = 1 - \beta \qquad (5\text{-}19)$$

Hence log i would be expected to increase approximately by

$(1-\beta)\log 10.8$ due to the H^+ concentration difference, i.e. the i should increase 3.29 times with β taken as 0.5.

The above estimates of double-layer effects apply in the absence of specific adsorption of ions. However, in the acid hydrate, specific adsorption of $CF_3SO_3^-$ is almost certainly significant (a related anion adsorption effect can be seen, for example, when the cyclic-voltammetry i vs V profiles for the acid hydrate and the 1 M aq. solution are compared at Pt, Fig.(5-3)). This will lead to a different double-layer potential effect involving the inner-layer, Ψ_2, potential[202]. An exact calculation of such an effect is difficult[204] but all that is required here is the direction of the effect, kinetically, and an approximate estimate of its magnitude. Thus, if Ψ_2 is taken approximately (cf. ref.202) as

$\Psi_2 = \Psi_2^\circ - RT/F \log[C(CF_3SO_3^-)] = \Psi_2^\circ - RT/F \log[C_{H^+}]$, so that

$$\left[\frac{d \log i}{d \log[C_{H^+}]}\right] = 2\beta, \qquad (5\text{-}20)$$

an increase of current with increasing CF_3SO_3H concentration, larger than that predicted in the case where $\Psi_1 \rightarrow$ constant in strong solutions in the Frumkin treatment, would arise. Compared with the case considered earlier in this section for the absence of specific adsorption, it is seen that, when specific adsorption is significant, the rate increase with H^+ concentration would be larger than in the previous case, in fact, for $\beta = 0.5$, by the factor $(3.29)^2 = 10.8$, i.e. the original concentration ratio. (Such an effect of enhancement of h.e.r. rates at high hydrogen halide acid concentrations was in fact observed by Jofa[204]).

(iv) Behaviour at Hg Film Surfaces and Liquid Hg Pool Electrodes

The kinetic behaviour at Hg surfaces will be considered first, since at Ni and Pt, the interpretation of kinetic results is always complicated by the involvement of chemisorbed H and whether the H desorption step (either by chemical recombination or electrochemical desorption $MH_{ads} + H^+_{aq} + e = M + H_2 + H_2O$) is rate-controlling or not. At Hg, on the other hand, there is almost complete unanimity (at least among the Russian and Western workers) that the kinetics of the h.e.r. at Hg are controlled by a rate-limiting proton-discharge process prior to the H desorption step. In this case, therefore, the behaviour is uncomplicated by effects connected with potential-dependent coverage by chemisorbed H so that experiments using H_3O^+ or "$H_9O_4^+$" as proton sources should less ambiguously give information on the effects of the proton source on the H^+ dischage and H transfer kinetics, apart from possible complications due to co-anion adsorption, to be discussed below.

Fig.5-4 shows the Tafel relations for H_2 evolution at Hg film electrodes on Au at 313 K in 1 M aq. CF_3SO_3H and in $CF_3SO_3^-$ H_3O^+. In this case, the actual measured rates of H_2 evolution from the H_3O^+ electrolyte are actually slower but only by a factor of ca. 3.5 times than from the aqueous 1 M acid solution (cf. the results for Ni and Pt to be presented later). The considerations on double-layer effects given above indicate that the rate should increase by a factor of either about 3.29 or about 10:8, depending on specific adsorption, due to the 10.8-fold concentration ratio for the two types of solutions.

The observed decrease of rate (3.5 times) in going from 1 M

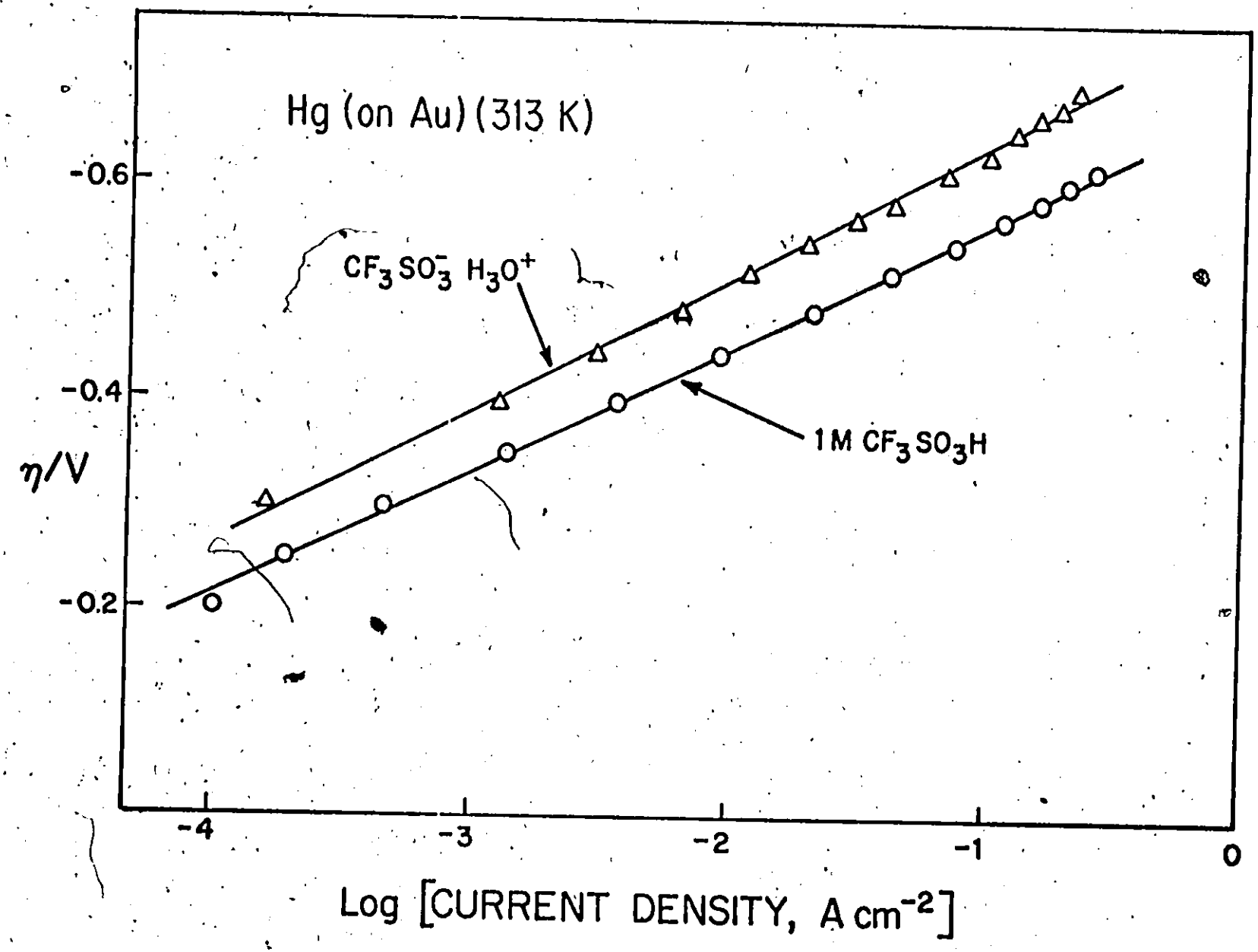

Fig.5-4 Overpotential vs log[current density] relations for the h.e.r. on Hg film surfaces on Au from $CF_3SO_3^-H_3O^+$ and 1 M aqueous CF_3SO_3H at 313 K.

aqueous solution to the 10.8 M acid hydrate cannot therefore be accounted for by the concentration difference nor by diffuse-layer or anion adsorption effects on the kinetics. In fact, there is a "slowness factor" for discharge from H_3O^+ compared with $H_9O_4^+$ in the 1 M aqueous solution of about 3.5 x 3.29 (= 11.5 times), or 3.5 x 10.8, i.e. 37.8 times for the cases considered above so that, on any basis, double-layer effects cannot account for the direction and magnitude of the observed rate ratio of 3.5 times.

The Tafel slopes for the h.e.r. at the Hg film electrodes (Fig.5-4) are very similar for proton discharge from 1 M aq. CF_3SO_3H and $CF_3SO_3^-H_3O^+$ solutions respectively (compare the Tafel slopes for discharge at Hg pool surfaces, below). These values correspond to those usually found in dilute acid solution.

Overpotential versus log [current density] measurements at the Hg film surface were made at various temperatures in order to evaluate the apparent[188,35] heats of activation $\Delta H^{\ddagger}$ for discharge from H_3O^+ and $H_9O_4^+$. The $\delta(\Delta H^{\ddagger})$ values are summarized in Table 5-1. These figures, with allowance for the effects of concentration differences discussed above, enable the apparent frequency factor ratios to be evaluated, as also shown in Table 5-1.

Table 5-1

Apparent Activation Parameters for the H.E.R. at Hg Film (Au) Electrodes in the Media Indicated.

-η/V	$\Delta H^{\ddagger}$ for $CF_3SO_3^-H_3O^+$ aq. kJ mol^{-1} (a)	$\Delta H^{\ddagger}$ for 1 M CF_3SO_3H kJ mol^{-1} (b)	$\delta(\Delta H^{\ddagger})$ kJ mol^{-1} (b) - (a)	Frequency factor ratio*
0.250	42.4	27.5	-14.9	14.6
0.300	43.9	32.3	-11.6	14.0
0.350	45.3	31.3	-14.0	16.4
0.400	46.8	28.5	-18.3	17.3

Note on Table 5-1: The $\Delta H^{\ddagger}$ values are substantially smaller than on pure liquid Hg and the corresponding h.e.r. currents are higher. This is because a Hg film electrode on Au has some dissolved Au in it but a reproducible surface behaviour was still found to result.

* Here and below this ratio refers to $A(H^+_{aq})/A(H_3O^+)$.

Over the range of overpotentials investigated, the heat of activation for proton discharge at Hg film electrodes from $CF_3SO_3^-H_3O^+$ is found to be ca. 15 kJ mol^{-1} larger than that for the 1 M CF_3SO_3H; on this basis alone then, the relative rates of the h.e.r. from these two media would be expected to be $i(H^+_{aq}) > i(H_3O^+)$. Thus it is evident that both apparent heats and entropies (or frequency factors) of activation contribute to the "slowness factor" noted in connection with the overpotential vs log [current densities] relation at Hg film electrodes.

Steady-state polarization measurements were also made for the h.e.r. at pure Hg pool electrodes in 1 M aqueous CF_3SO_3H and $CF_3SO_3^-H_3O^+$; the resulting Tafel plots at 313 K are shown in Fig.5-5.

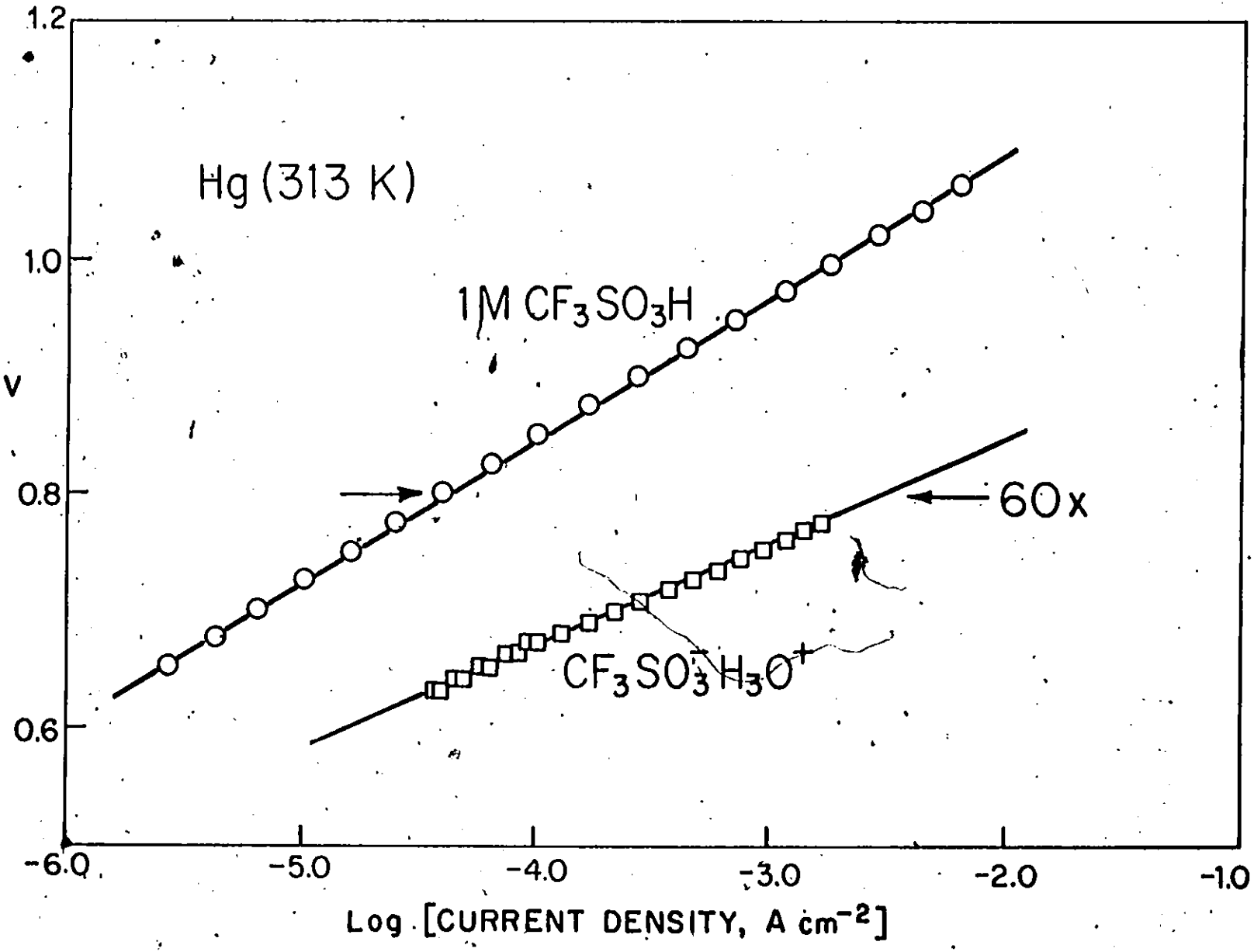

Fig.5-5 Overpotential vs. log[current density] relations for the h.e.r. on pure Hg pool electrodes from $CF_3SO_3^-H_3O^+$ and 1 M aqueous CF_3SO_3H at 313 K.

In contrast to the Tafel behaviour noted above for the Hg film (Au) electrode, the measured rate of reaction at pure Hg in the monohydrate $CF_3SO_3^-H_3O^+$ exceeds that in the 1M aqueous CF_3SO_3H by a factor of ca. 60 x at an overpotential of -0.8 V. This difference in rates is in the direction of the increase in rate of ca. 3.29 or ca. 10.8 to be expected as a result of concentration and anion adsorption effects on the rate of reaction.

However, Fig.5-5 shows that the difference in rate of reaction in 1 M aq. CF_3SO_3H and in $CF_3SO_3^-H_3O^+$ is very dependent on potential. This is due to the appreciably different Tafel slope, ca. 0.09 V in the monohydrate compared with the usually found slope of ca. 0.11 - 0.12 V in dilute aqueous acid solution. Consequently as the applied overpotential is lowered progressively, the rate of hydrogen evolution decreases more markedly for discharge from the molten monohydrate than from the 1 M CF_3SO_3H solution; the rates in the two media become equal at an overpotential of ca. -0.17 V. At lower potentials, the order of rates will be the reverse of that obtaining at the higher values of the overpotential shown in Fig 5-5.

This interesting difference in Tafel slopes found at pure Hg in the two media investigated is not observed in the case of the Hg film electrodes. The Hg film electrodes on Au substrates yielded reproducible surface behaviour for several hours after their preparation but exhibited lower hydrogen overpotentials than the Hg pool electrodes. Both these differences in behaviour arise because a Hg film electrode on Au has some traces of dissolved Au in it; the reproducible behaviour of the film

electrode suggests the presence of a constant surface composition of Au in Hg. Changes of the bulk properties in the Hg film due to the presence of dissolved Au are not likely to account for the observed differences from pure Hg electrodes.

Apparent heats of activation for the h.e.r. at pure Hg pool surfaces in $CF_3SO_3^-H_3O^+$ and 1 M aq. CF_3SO_3H are given in Table 5-2.

Table 5-2

Apparent Activation Parameters for the H.E.R. at Hg (pool) Electrodes in the Media Indicated.

V	$\Delta H^{\ddagger}$ for $CF_3SO_3^-H_3O^+$ kJ mol^{-1} (a)	$\Delta H^{\ddagger}$ for 1 M aq. CF_3SO_3H kJ mol^{-1} (b)	$\delta(\Delta H^{\ddagger})$ kJ mol^{-1} (b) - (a)	Frequency factor ratio*
0.0	84.0	56.4	-27.6	3.6×10^{-4}
-0.4	51.1	47.8	-3.3	5.3×10^{-2}
-0.6	39.2	43.5	+ 4.3	0.81
-0.8	24.3	39.3	15.0	20.4

* $A(H^+)/A(H_3O^+)$

At the higher overpotentials, the 1 M aq. CF_3SO_3H shows larger values of the heat of activation; however, as the potential is lowered to $\eta = 0$, the reverse relationship obtains. This change in relative magnitude of heats of activation results from the significantly different Tafel slopes for the h.e.r. in these two media, as mentioned above.

The apparent frequency factor ratios (Table 5-2) increase over ca. 5 decades on going from 0.0 to -0.8 V RHE; at the most

cathodic potentials, frequency factor ratios (> 1) comparable to those found for the Hg film (or Au) electrodes arise.

The potential dependence of these activation parameters will be considered in detail in a following section in relation to the temperature variation of the Tafel slope (and hence the transfer coefficient) and to the origin of the potential-dependence of the rates of electron transfer reactions.

(v) Behaviour at Ni Electrodes

Steady-state polarization measurements were made at reduced Ni electrode surfaces; an initially oxide-free Ni surface was achieved by firing and maintaining the electrodes in a hydrogen atmosphere in glass bulbs prior to use as cathodes.

Fig.5-6 shows the IR-corrected Tafel plots for cathodic hydrogen evolution at Ni electrodes from pure $CF_3SO_3^-H_3O^+$ and from 1 M aq. CF_3SO_3H.

The 1 M aq. solutions give the usual, almost linear Tafel plot for the h.e.r. on Ni with a slope $d\eta/d \log i$ of 2.3 x 1.69 RT/F, i.e. with a transfer coefficient of 0.59. The $CF_3SO_3^-H_3O^+$ system gives a non-linear IR-corrected plot (Fig.5-6) with an initial slope of ca. 2.3 x 2.1(2) RT/F. Because of the curvature of the plot for $CF_3SO_3^-H_3O^+$, comparison of the Tafel behaviour of the two acid systems gives, e.g. at 314 K, ratios of H_2 evolution current-densities which increase from ca. 3 x at $\eta = 0$ (the exchange current densities) to ca. 36 x at $\eta = -400$ mV.

These relative rates are in contrast to the order found for proton discharge at pure Hg surfaces described above (compare Fig.5-5).

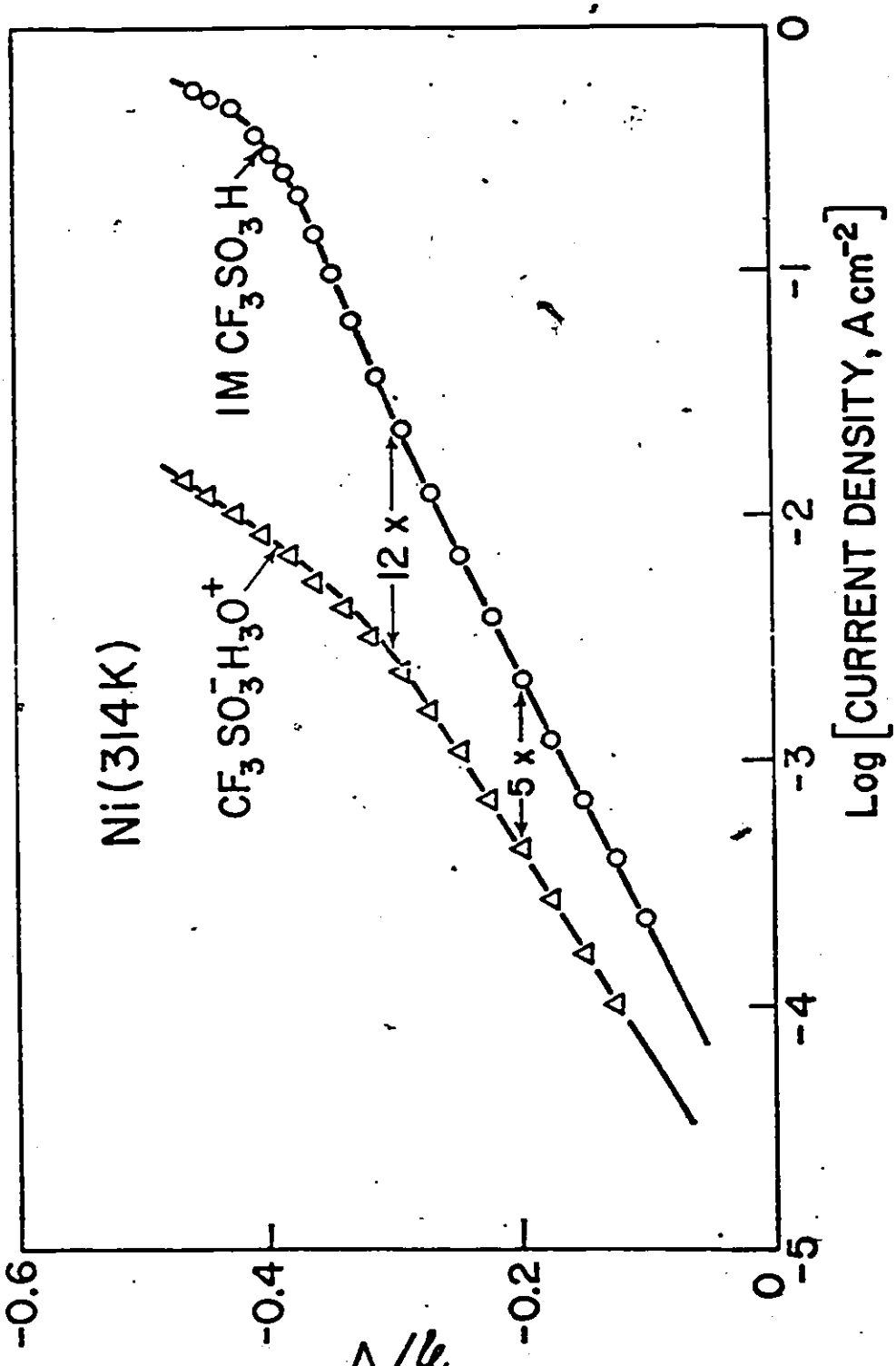

Fig.5-6 Overpotential vs log[current density] relations for the h.e.r. on a Ni electrode from $CF_3SO_3^-H_3O^+$ and 1 M aqueous CF_3SO_3H.

Noting again that the acid hydrate has a molarity of 10.8, the rate ratios mentioned above correspond to rate-constant ratios which increase from 32.4 to 389 assuming a reaction order $R = 2\beta$ (ca. 1) in $[H^+]$, using eqn.(5-20), i.e. large kinetic effects are involved with a substantial increase in the rate of the h.e.r. as the proton source is changed from H_3O^+ to the extensively hydrated "$H_9O_4^+$" in dilute aqueous acid solution.

Upon maintaining the Ni electrode for several minutes at potentials more cathodic than ca. -0.1 V RHE followed by stepping the potential to a value in the range -0.035 to -0.050 V RHE, net anodic currents were observed at these latter potentials which are nevertheless still cathodic to the RHE; this behaviour was found in both the monohydrate melt and dilute aqueous CF_3SO_3H. These anodic current transients decayed over a period of 10 - 100 s to yield steady-state cathodic currents corresponding to those found in the steady-state polarization measurements. This behaviour upon stepping the potential (to values cathodic to the RHE) cannot be due to a readjustment of surface coverage of adsorbed H, or to double-layer charging currents since both these processes occur on the sub-millisecond time scale. The anodic current transients are probably related to the formation of a three-dimensional hydride or surface hydride phase at Ni which has been found to develop on cathodic polarization in some media[205,206].

This hydride phase at Ni electrodes is associated with good electrocatalytic properties for H_2 evolution similar to those associated with the two-dimensional hydride surfaces at Pt and Rh. At these latter active metals, full coverage of strongly

bound H (or surface hydride) exists already at or even before the reversible hydrogen potential, although this strongly bound species is probably not directly an intermediate in the overall h.e.r. In the case of Ni on the other hand, full coverage by atomic H (or hydride formation) is not attained at the reversible potential.

At Ni and and Raney Ni Al-type electrodes in concentrated alkaline solution, Conway et al.[207] found characterisic time-dependent currents depending on whether measurements were made in the direction of increasing or decreasing overpotential in the range -0.02 to -0.10 V,and related this behaviour to the formation of a hydride of Ni.

In the present work in acidic solutions, this hysteresis effect was not encountered and hence steady-state polarization measurements at Ni could be made (cf. Fig.5-6).

The potential vs log [current-density] relations at Ni electrodes in 1 M CF_3SO_3H and in $CF_3SO_3^-H_3O^+$ at several temperatures are shown in Fig.5-7 and Fig.5-8.

In the aqueous medium, normal mean values of the activation energy varying from 43 to 58 kJ mol^{-1} with potential, are observed. However, in the acid hydrate, unusual but reproducible behaviour is observed: the apparent heat of activation is suprizingly small and shows some tendency to pass through zero to negative (apparent) values with increasing temperature. This may be due to temperature-dependent adsorption of the $CF_3SO_3^-$ anion at the Ni surface and/or H surface coverage. In addition, Ni hydride which is probably present at these potentials (see above)

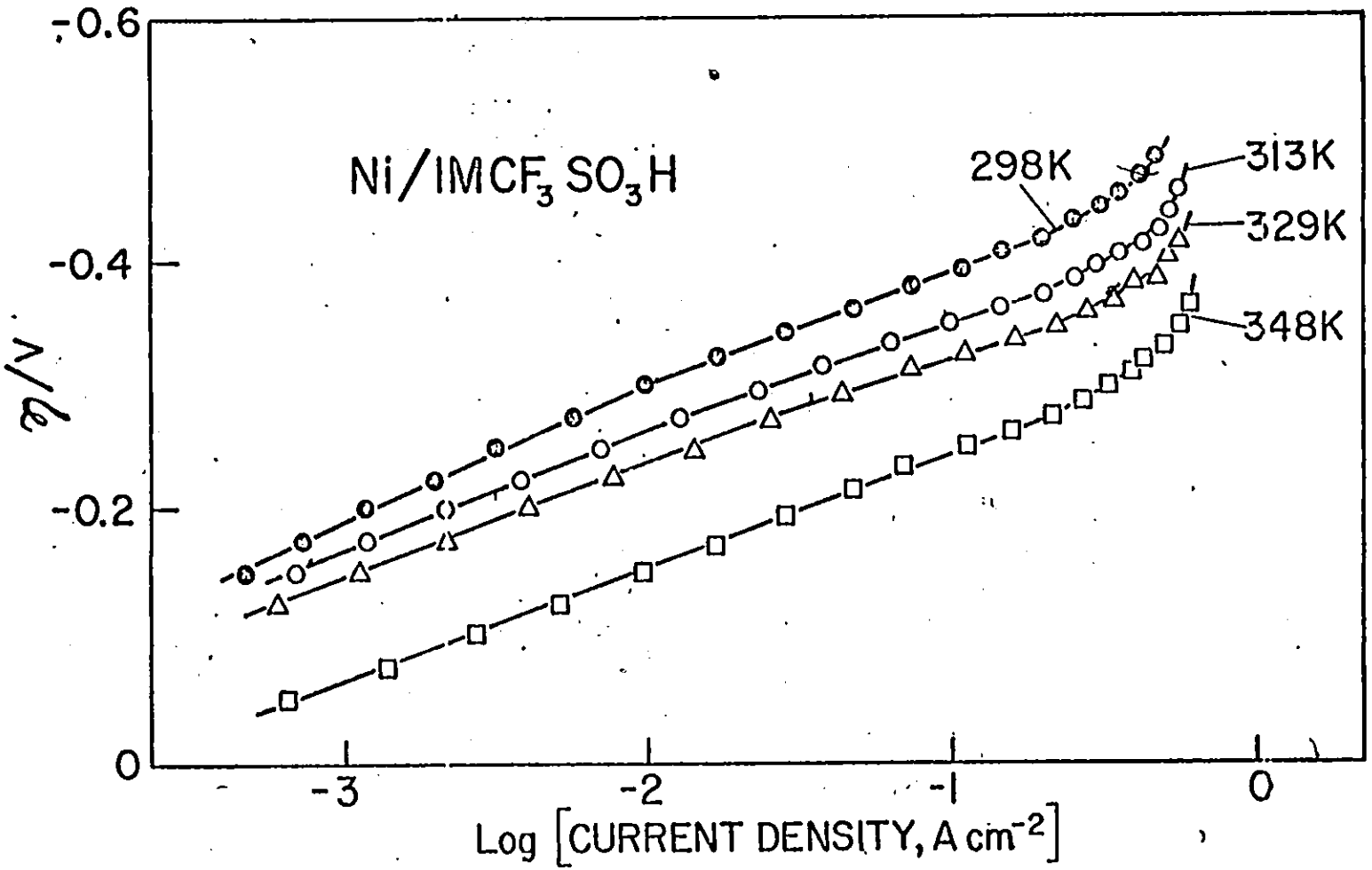

Fig.5-7 Overpotential vs log[current density] relations for the h.e.r. on a Ni electrode from 1 M aqueous CH_3SO_3H at four temperatures.

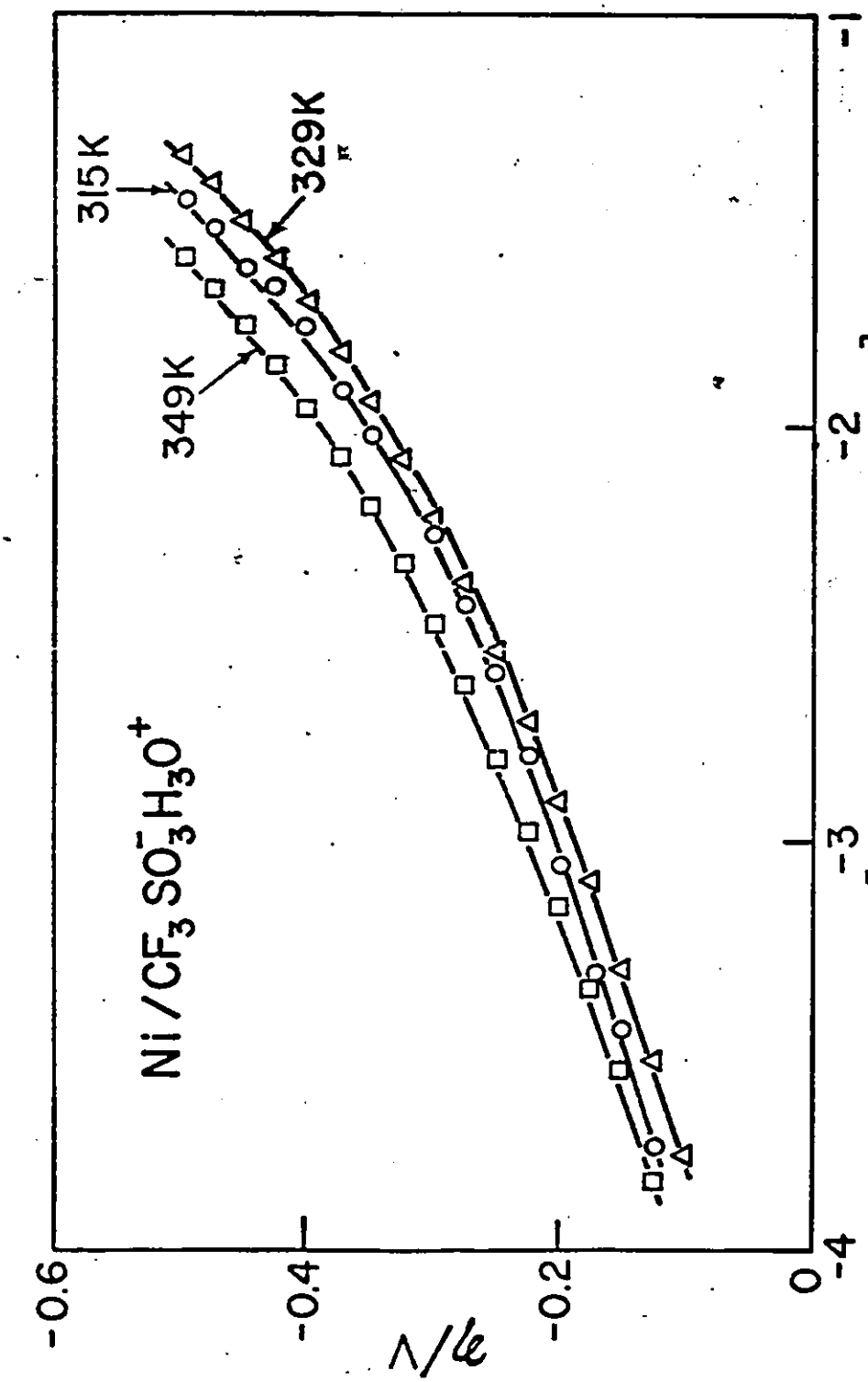

Fig.5-8 Overpotential vs log[current density] relations for the h.e.r. on a Ni electrode from $CF_3SO_3^-H_3O^+$ at three temperatures.

may well contribute to this unusual temperature-dependence of rate, in a manner analogous to that described in a previous section of this thesis for temperature-dependent H adsorption. Because of these complications, it is not possible to work out satisfactory ratios of frequency factors for the h.e.r. at Ni from the two types of proton source.

The occurrence of this maximum in rate with temperature was confirmed in several independent polarization runs. The effect of varying the temperature (whilst potentiostating the Ni electrode at -0.1 V) on the current that passes is shown in Fig.5-9. The maximum in the rate seems to occur at ca. 332 K and corresponds to the behaviour noted in the steady-state polarization measurements.

(vi) Behaviour at Pt Electrodes

Steady-state polarization measurements for the h.e.r. were also made at Pt electrodes; the Pt surface was conditioned just prior to each kinetic run by cycling the potential linearly between ca. 0.05 and 1.35 V RHE. This anodization pre-treatment yielded a reproducible, well defined and clean initial surface state, as discussed elsewhere[159].

Fig.5-10 shows the Tafel relations for the h.e.r. at Pt in the two systems. Again, the rates of the reaction are much smaller when H_2 is evolved from H_3O^+ in the melt than from $H_9O_4^+$ in the 1 M aq. CF_3SO_3H solution at the same temperature. Around η = 200 mV, the rate ratio is ca. 30 x. Correction for the concentration difference in the case of the recombination-controlled h.e.r. at Pt depends on the differential Tafel slope

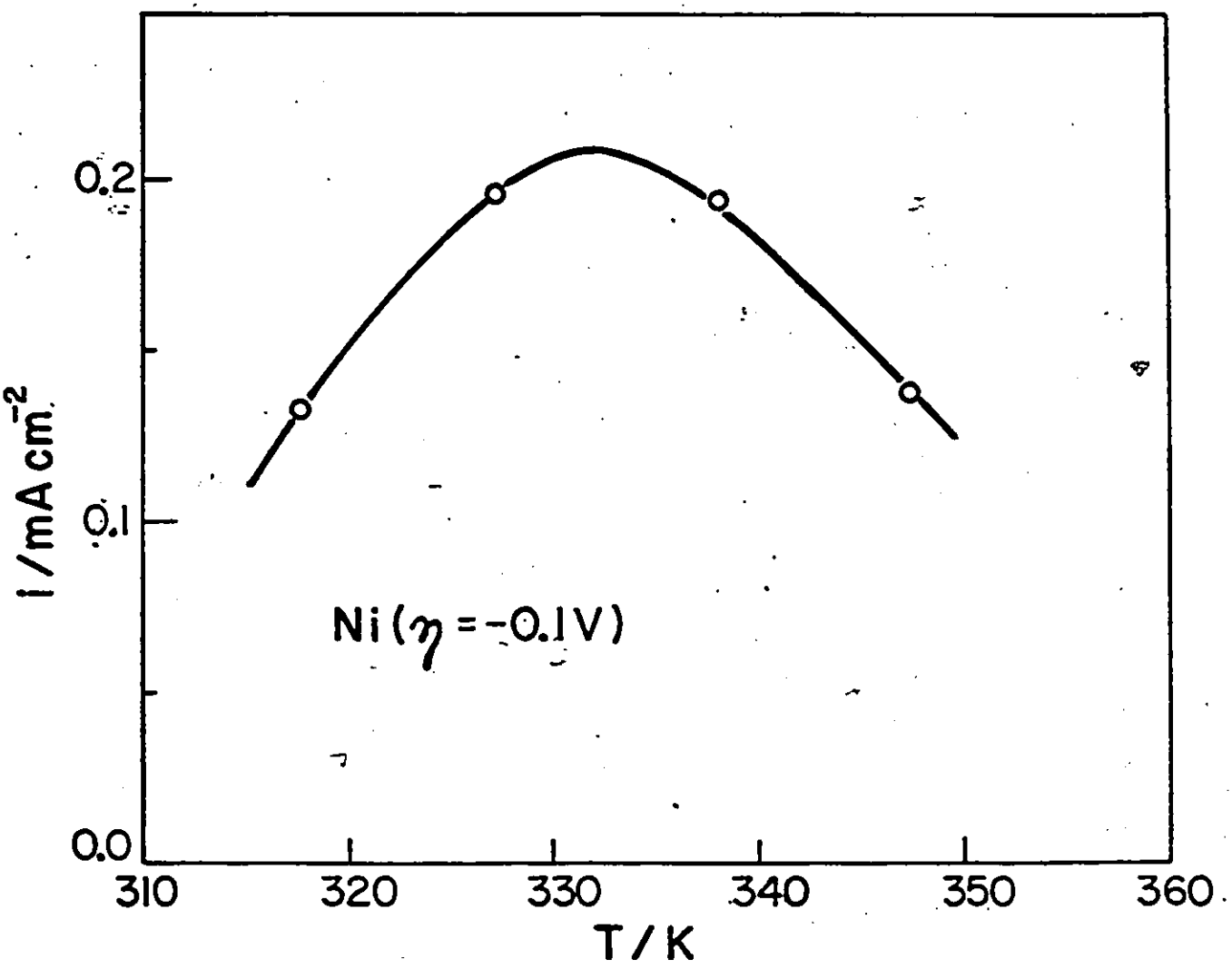

Fig.5-9 Effect of temperature on the current passed in the h.e.r. at a Ni electrode in $CF_3SO_3^-H_3O^+$ at -0.10 V RHE.

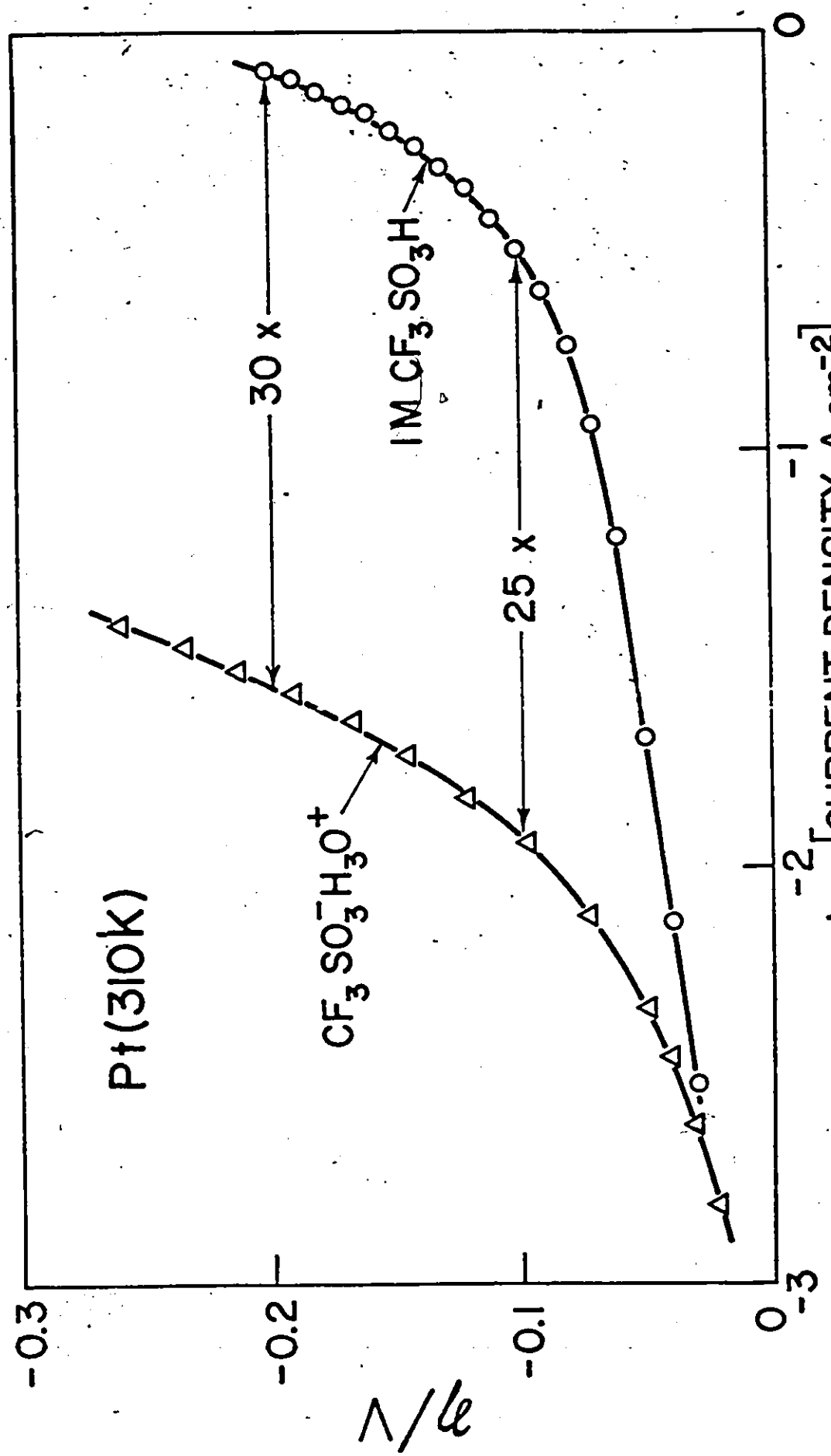

Fig.5-10 Overpotential vs log[current density] relations for the h.e.r. on a Pt electrode from $CF_3SO_3^-H_3O^+$ and 1 M aqueous CF_3SO_3H.

involved: at low θ_H, where b is ca. 0.029 V, the concentration correction in the rate involves $[C(H_3O^+)]^2$; towards the limiting current it involves $[C(H_3O^+)]^0$ (zero order of the process). Note that if the discharge step producing H_{ads} is at quasi-equilibrium, no Ψ_1 effect is involved in this case; however, concentration-dependent anion adsorption effects can affect the rate constant for MH + MH recombination and the H coverage.

Proton discharge from both solutions at Pt yield non-linear Tafel relations characterized by a low-slope region at smaller overpotentials. The curvature in these plots reflects a progressive change in mechanism as the magnitude of the cathodic overpotential is increased, as well as the desorption of anions at the more negative potentials, particularly in the case of the aqueous CF_3SO_3H solution. The cyclic-voltammogram for Pt in $CF_3SO_3^-H_3O^+$ shown in Fig.5-3 exhibits a compressed hydrogen underpotential deposition region (see this Chapter, Section 4,i) which is diagnostic of anion adsorption at this metal (see ref.208 for halide adsorption at Pt).

Surface coverage of kinetically active adsorbed H at Pt is also probably changing with potential. Conway et al.[185] have quantitatively evaluated the extent of so-called overpotentially deposited (OPD) H at hydrogen-evolving Pt electrodes in dilute aqueous acid and alkaline solutions using the open-circuit potential decay technique described in Chapter 4. Their analysis indicates that this loosely bound adsorbed H is the kinetically-involved intermediate in the h.e.r. at Pt, unlike the underpotentially deposited H which is present already at full coverage at the reversible potential.

The apparent activation energies for H_2 evolution from H_3O^+ and $H_9O_4^+$ at Pt are also quite different and depend in an unusual way on η (because of the curved Tafel relations in Fig.5-10). Based on a T range of 298.7 to 348 K for the 1 M aq solution and 308 to 358 K for the $CF_3SO_3^-H_3O^+$, the following apparent activation energies are found as shown in Table 5-3.

Table 5-3

Apparent Activation Parameters for the H.E.R. at Pt from the Media Indicated.

$-\eta$/V	$\Delta H^{\ddagger}$ for $CF_3SO_3^-H_3O^+$ kJ mol^{-1} (a)	$\Delta H^{\ddagger}$ for 1 M aq. CF_3SO_3H kJ mol^{-1} (b)	$\delta(\Delta H^{\ddagger})$ kJ mol^{-1} (b) - (a)	Frequency factor ratio
0.100	24.6*	4.7(5)*	-19.9	1.2×10^{-1}
0.150	26.3	6.9(4)	-19.3	1.7×10^{-1}
0.200	27.2	8.3(8)	-18.8	2.1×10^{-1}

* The values here do not decrease in the usually expected way[203] with increasing β because no linear Tafel region is observed.

For Pt, the apparent activation energies are seen to be substantially larger for H_2 evolution from H_3O^+ than from $H_9O_4^+$, but in this case the rates from H_3O^+ are significantly smaller than from $H_9O_4^+$. (See steady-state polarization behaviour in Fig.5-10).

The kinetic effects at Pt stem mainly from the differences of apparent activation energy. Relative to the H_2 electrode potentials in the two media, the potential ranges for

underpotential H chemisorption are similar, so there are no substantial differences of H chemisorption energy at Pt in the two media. Therefore the main effect originates as a kinetic "medium effect" arising principally from the activation energy difference. It should be mentioned, however, that the H atom recombination-controlled kinetics at Pt, when such a mechanism applies, e.g. at not too active electrodes, really involves a weakly bound H species rather than the three or four distinguishable strongly bound H states, resolvable in cyclic-voltammetry experiments. The apparent frequency factor ratios at Pt vary only weakly with potential, unlike the behaviour at the Hg pool electrodes seen above.

The completely different behaviour of the h.e.r. at Pt from that at pure Hg surfaces is consistent with the well known difference of mechanism of the h.e.r. at Pt where the kinetics are probably controlled by the H atom recombination step* (hence the approach to activation-controlled limiting currents in Fig. 5-10) rather than by proton discharge. Then the difference in proton discharge rates appears indirectly in the steady-state coverages by H in the two systems.

Additionally (cf. Fig.5-3) the adsorption of the $CF_3SO_3^-$ anion in the acid hydrate solution will have significant inhibiting effects on the adsorbed-H recombination-controlled kinetics. This is probably why there is such a large difference in the Pt case between the currents for H_2 evolution from H_3O^+

* At very active Pt electrodes, diffusion of generated H_2 away from the electrode controls the electrode kinetic behaviour.

and $H_9O_4^+$ solutions because the $CF_3SO_3^-$ anion concentration difference affects the adsorption of the electroactive adsorbed H species (cyclic-voltammetry at Pt indicates that the accessible charge for UPD of H decreases by ca. 45% on going from 1 M CF_3SO_3H to the monohydrate melt. In this case, therefore, the rate differences cannot be attributed simply to differences of facility of H^+ discharge from H_3O^+ or $H_9O_4^+$.

3. True Activation Parameters for the H.E.R. at Hg from 1M CF_3SO_3H and $CF_3SO_3^-H_3O^+$

The use of non-isothermal cell measurements in fixing, to a good approximation, the metal-solution potential difference (when the temperature is varied) was discussed in Section 1. In the present section, the use of this technique in order to investigate the potential-dependence of the true enthalpy and entropy of activation (i.e. at constant ϕ_{M-S}) for the h.e.r. at pure Hg electrodes in 1M CF_3SO_3H and in $CF_3SO_3^-H_3O^+$ will be described. A comparison of the "true" activation parameters in these two media will then be made, based on an approximate extra-thermodynamic procedure. From the foregoing material, it will have been seen that such a comparison is least ambiguous for the case of the Hg electrode.

We should note, at this point, that differences of "true" and "apparent" heats of activation for different conditions, e.g. for different metals, would be identical; however, when comparisons are made between different media, this is not the case since the H_R^o terms for the reaction in the two media are not necessarily identical.

(i) Results of Non-Isothermal Cell Measurements

Measurements of the hydrogen reference electrode potential in 1 M CF_3SO_3H and in $CF_3SO_3^-H_3O^+$ in non-isothermal cells were made relative to a reference temperature of 313.0 K (selected in view of the 309 K m.p. of $CF_3SO_3^-H_3O^+$). The neglect of the thermal liquid junction potential-difference and details of the experimental cell arrangement were discussed in Section 1 and Chapter 3. The importance of using of a salt-bridge thermocell was stressed in that discussion.

The thermal potential differences for the hydrogen electrode in 1 M CF_3SO_3H and $CF_3SO_3^-H_3O^+$ are shown in Fig.5-11. In this figure positive values correspond to the RHE establishing a potential more positive than that of the RHE at the reference temperature (313 K).

A polynomial least squares regression was performed on the V vs T data of Fig.5-11 and the associated coefficients are given in Table 5-4; no improvement was found on going to a third order power series.

Table 5-4

Regression Coefficients* for the Observed Thermocell Potential Differences for the RHE (relative to 313 K)

Solution	a_o/mV	a_1/mV K^{-1}	a_2/mV K^{-2}
1M CF_3SO_3H	-38.22	0.933	1.66×10^{-4}
$CF_3SO_3^-H_3O^+$	-44.03	1.072	5.84×10^{-2}

* $E = a_o + a_1(T - 273.15) + a_2(T - 273.15)^2$

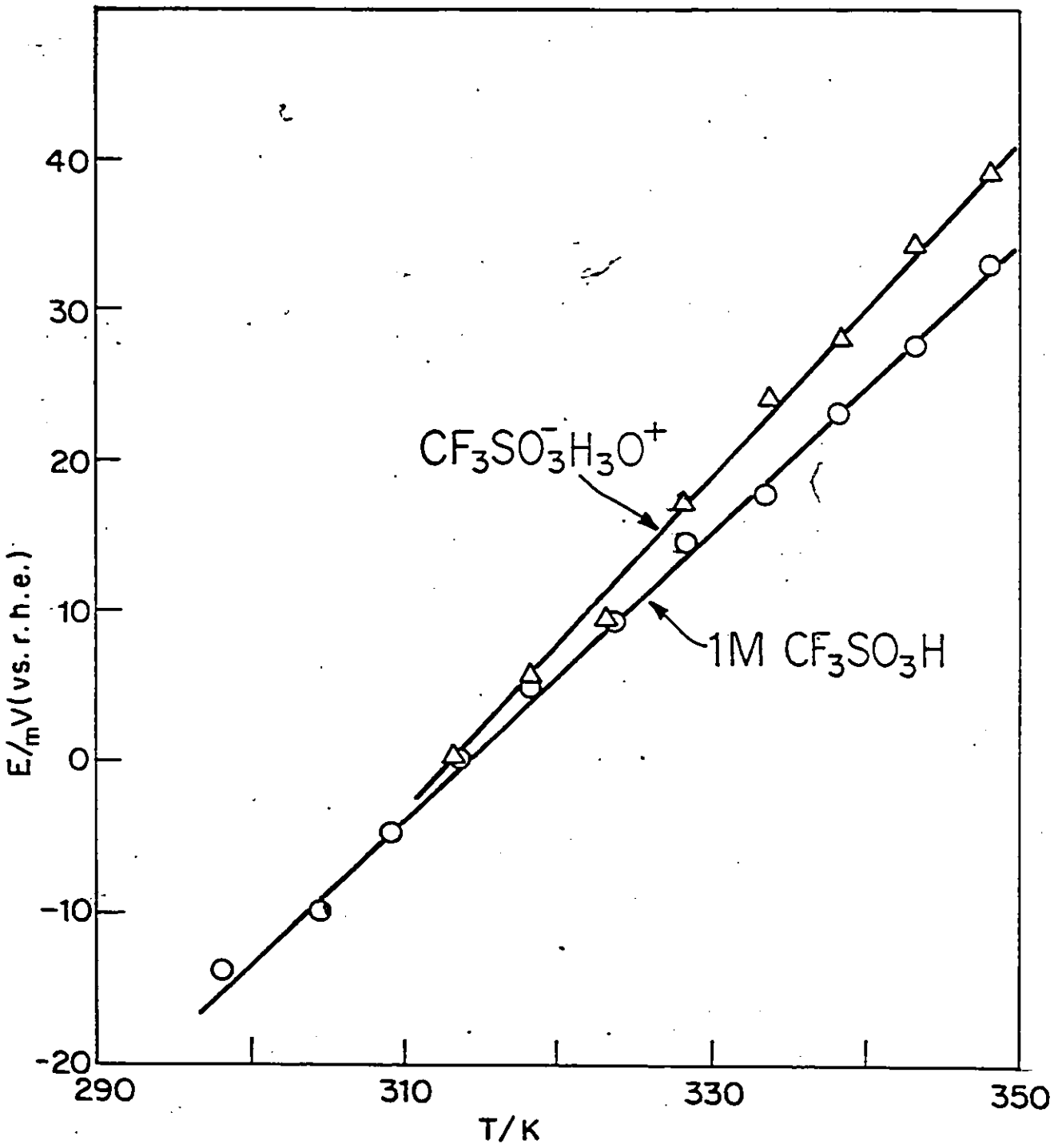

Fig.5-11 Non-isothermal cell potentials for the RHE in $CF_3SO_3^-H_3O^+$ and 1-M CF_3SO_3H relative to the RHE at 313 K.

The temperature coefficients of the h.e.r. reversible potential in each of the media are as follows: in $CF_3SO_3^-H_3O^+$, $dE/dT = 1.12$ mV K^{-1} (at 313 K), and in 1 M aq. CF_3SO_3H, $dE/dT = 0.95$ mV K^{-1} (at 313 K). For comparison in the case of dilute aqueous solution, dE^o/dT can be calculated[189] from $dE^o/dT = \Delta S^o/zF$ where $\Delta S^o = 1/2\ S^o(H_2) - \bar{S}^o(H^+) - S^o(e^-)$ using the best numerical estimates for $\bar{S}^o(H^+)$ and $S^o(e^-)$ and the well-known value for $S^o(H_2)$. Thus $\Delta S^o = 31/2 - (-4.5) = 20$ e.u., whence $dE^o/dT = +0.84$ mV K^{-1}. The experimentally determined value in 1 M CF_3SO_3H is somewhat larger as is the value for the monohydrate melt.

Thus for the steady-state polarization measurements at T > 313 K, in both 1M CF_3SO_3H and $CF_3SO_3^-H_3O^+$, the overpotential values observed must be reduced in magnitude (according to Fig.5-11) in order to refer them the scale of potential of the RHE maintained at 313 K.

An example of this procedure is shown in Fig.5-12 where Tafel lines are drawn for the h.e.r. at Hg (from 1 M CF_3SO_3H) at a reference temperature $T_1 = 313$ K and at a higher temperature $T_2 = 348$ K, the potential being referred to an H_2 electrode in the same solution at each of the respective temperatures. Application of the overpotential correction described above, leads to a shift of the Tafel line at 348 K to less negative overpotentials (according to Fig.5-11) so that the difference in rate on going from 313 K to 348 K in Fig.5-12 (at constant potential) is increased. The resulting Arrhenius plots at a given value of the "corrected" potential then yield larger activation energies, corresponding to the condition of

Fig.5-12 Illustration of the thermocell correction applied to steady-state polarization results for the h.e.r. at Hg from 1 M aqueous CF_3SO_3H: potentials for the 313 K data referred to the RHE (313 K); potentials for the 348 K data referred to the RHE (348 K) and transformed, according to the non-isothermal cell measurements, to the RHE (313 K) potential scale.

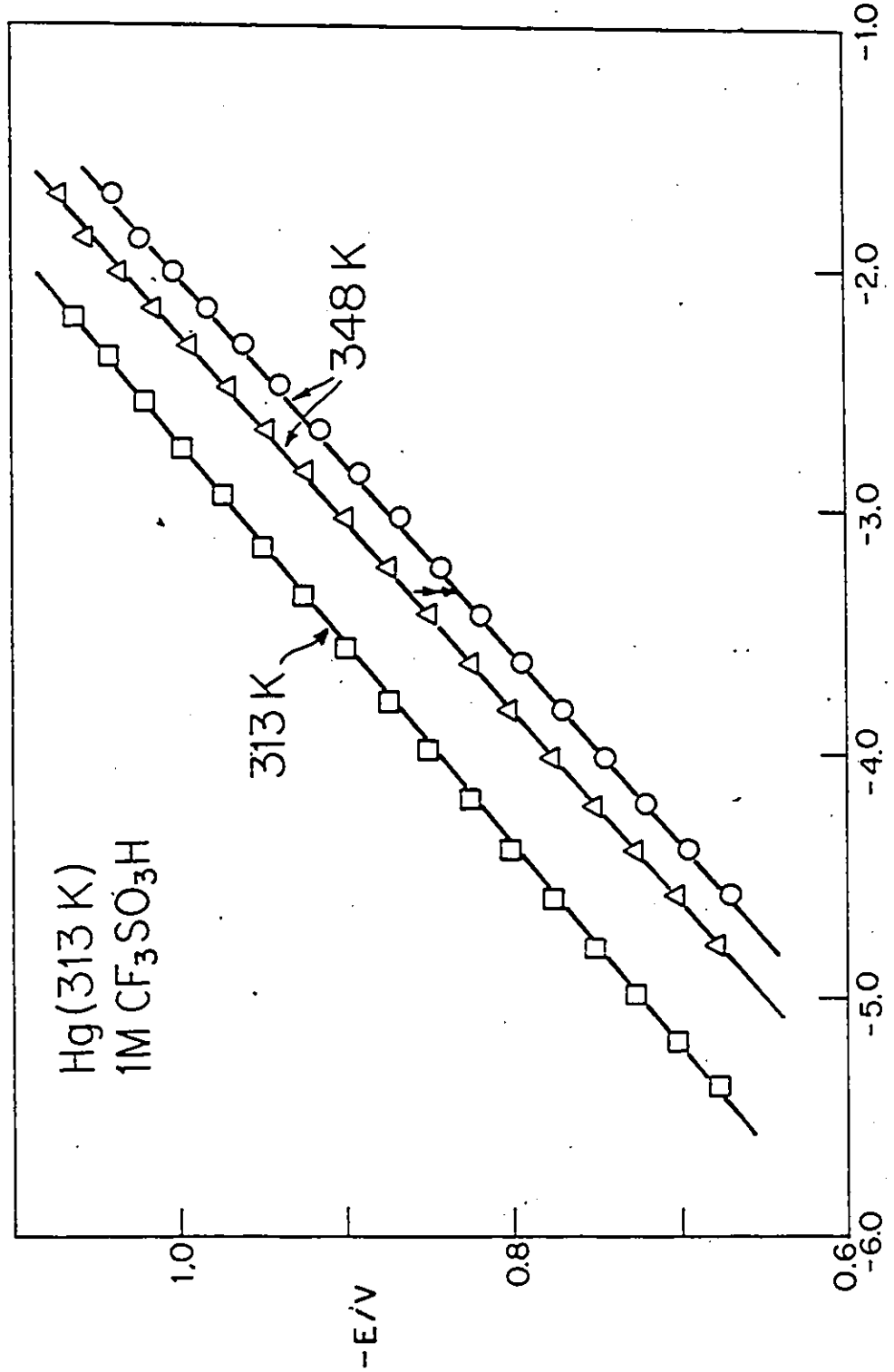
Hg(313 K)
1M CF_3SO_3H
313 K
348 K
-E/V
1.0
0.8
0.6
-1.0
-2.0
-3.0
-4.0
-5.0
-6.0
Log [CURRENT DENSITY, A cm^{-2}]

approximately constant interfacial potential difference, ϕ_{M-S}. These activation energies are, to a good approximation, the kinetically significant true quantities.

(ii) True Activation Parameters and Their Potential-Dependence

Following previously employed procedures[77] in the analysis of kinetics from Arrhenius plots, it is possible to obtain experimental relations between ln i_ϕ at various fixed electrode potentials, ϕ, and 1/T (see sub-section (i) above). In the usual way, the slopes give $\Delta\bar{H}_V^{o\ddagger}$ values at the respective ϕ values but also the logarithm of the electrochemical frequency factor A_ϕ can be obtained from the intercept of such plots at $1/T \to 0$. ln A_ϕ values as $f(\phi)$ then result as shown in Fig.5-13 while the corresponding $\Delta\bar{H}_V^{o\ddagger}$ values as $f(\phi)$ or $f(\eta)$ are shown in Fig.5-14.

The relative magnitude of the potential-dependent $\Delta\bar{H}_V^{o\ddagger}$ for the h.e.r. from 1 M aqueous CF_3SO_3H and $CF_3SO_3^-H_3O^+$ shown in Fig.5-14 depends strongly on potential. Near the reversible potential (313 K), the $\Delta\bar{H}_V^{o\ddagger}$ for proton discharge from the $CF_3SO_3^-H_3O^+$ is ca. 35 kJ mol^{-1} larger than for the 1M CF_3SO_3H; at -1.0 V, the reverse order obtains with a difference of ca. 18 kJ mol^{-1}. This behaviour parallels that found above for the apparent heats of activation; these true values of the enthalpy of activation are larger than the corresponding apparent quantities by ca. 22 and 15 kJ mol^{-1} for the h.e.r. from the $CF_3SO_3^-H_3O^+$ melt and 1 M aqueous CF_3SO_3H, respectively.

The slopes of the lines in Fig.5-14 reflect the effectiveness of the applied potential in reducing $\Delta\bar{H}_V^{o\ddagger}$ and hence in increasing the rate of reaction. Clearly the effect of

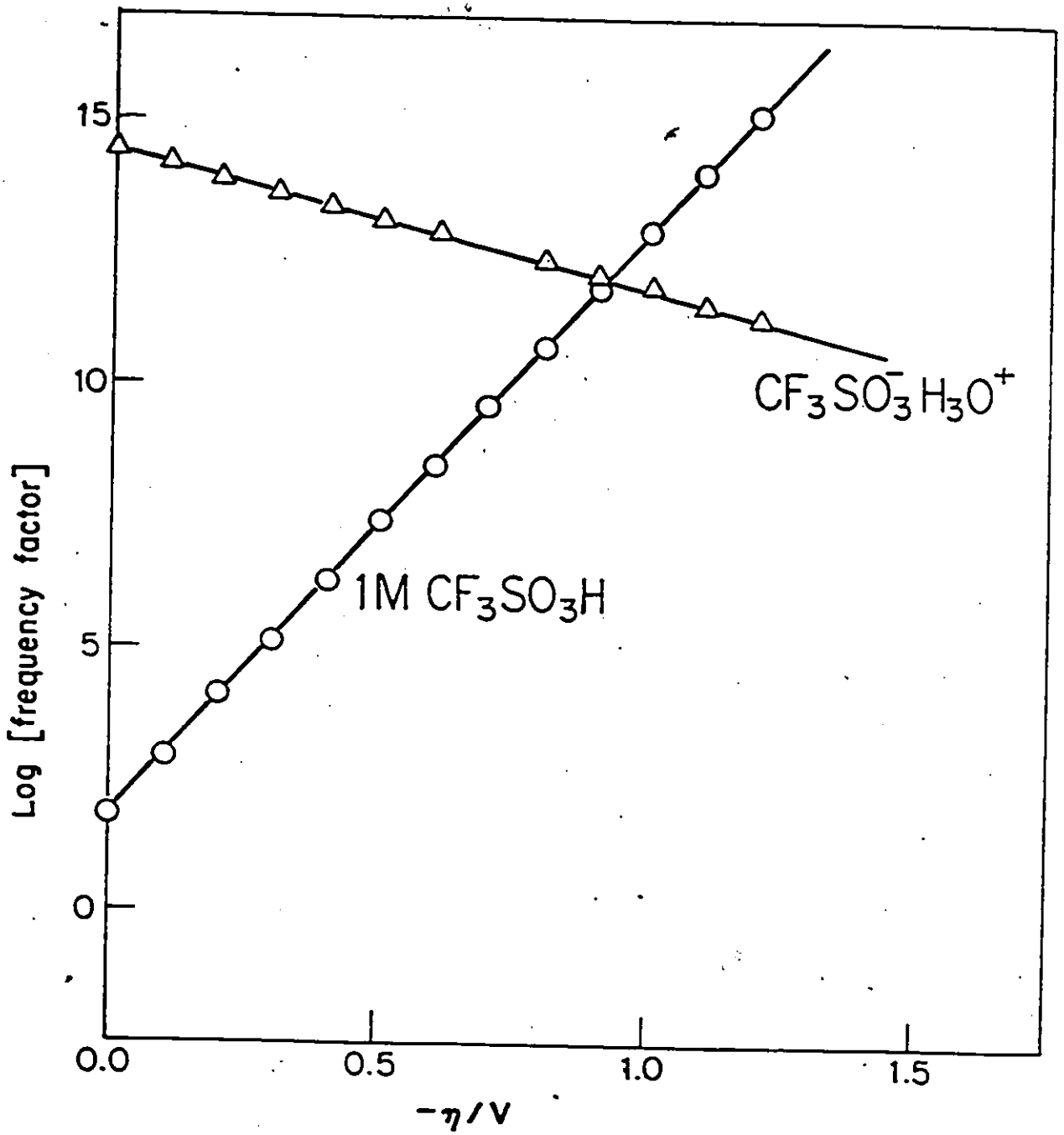

Fig.5-13 Potential-dependence of true log[frequency factor] values for the h.e.r. at Hg from $CF_3SO_3^-H_3O^+$ and 1 M aqueous CF_3SO_3H.

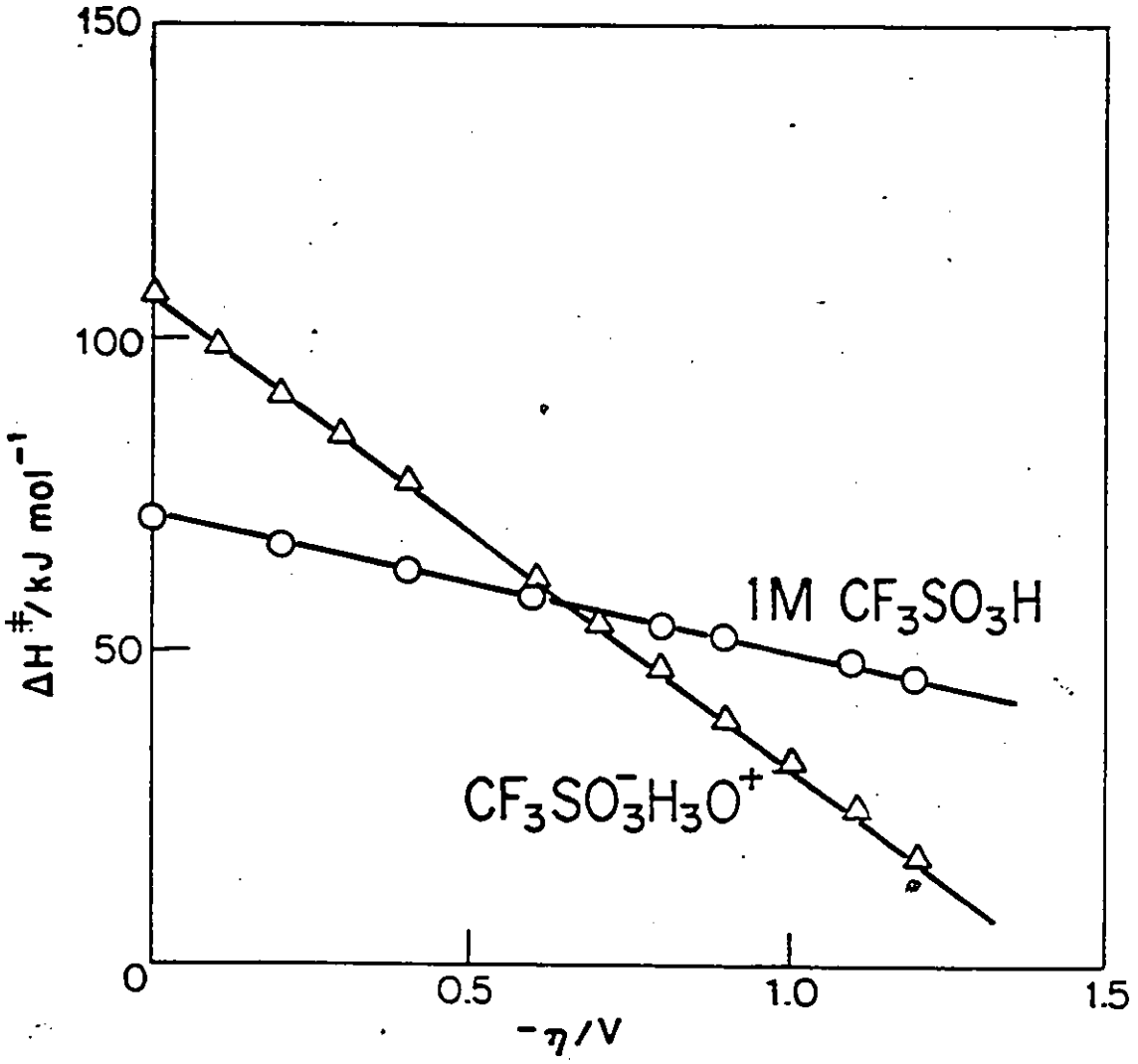

Fig.5-14 Potential-dependence of the true heat of activation for the h.e.r. at Hg from $CF_3SO_3^-$ H_3O^+ and 1 M aqueous CF_3SO_3H.

applied potential is more pronounced for hydrogen evolution at Hg from the monohydrate $CF_3SO_3^-H_3O^+$ than from the dilute aqueous CF_3SO_3H solution; this observation is in qualitative agreement with the relative magnitudes of the symmetry factors (= 2.3RT/bF) derived from the Tafel slopes, b.

The potential-dependence of the frequency factor (related to the entropy of activation) corresponding to the above values of $\Delta\bar{H}_V^{o\ddagger}$ shown in Fig.5-13 indicates that quite different behaviour evidently obtains in the two media.

In the 1 M aqueous CF_3SO_3H, log [frequency factor], and hence the entropy of activation $\Delta\bar{S}_V^{o\ddagger}$, becomes more positive with increasingly cathodic overpotential, and leads to increased rate of reaction. On the other hand, the entropy of activation decreases at more cathodic potentials for hydrogen evolution from $CF_3SO_3^-H_3O^+$, thereby tending to reduce the rate of reaction. Of course the overall rate of reaction increases with applied cathodic potential for the h.e.r. at Hg from both media (see Tafel relations in section 2(iv)) owing to the dominant effect of the potential-dependence of the enthalpic component (see Fig.5-14 and the above discussion) of the electrochemical free energy of activation.

It is of great interest that ln A_ϕ values are found to be potential-dependent, i.e. the entropy of activation, as well as the enthalpy of activation, is evidently potential-dependent. While this possibility was realized[74] as a formal consequence of a temperature-dependent transfer coefficient (see Chapter 2), this work is the first in which such an effect on $\Delta S^\ddagger$ has been

experimentally demonstrated in a direct way.

This result means that changes of electrode potential not only affect the energy of electrons at the Fermi level, and thus in the conventional way, modulate the rate through changes of energy of activation but they also change the entropy of activation. Therefore, the important conclusion from this part of the work is that changes of electrode potential have a direct effect on either or both the structure and configuration of the reactant and its transition state, and the solvational environment of these latter species. This is a major departure from conventional representations and ideas concerning the role of potential changes in electrode kinetics.

A detailed quantitative comparison and discussion of the kinetic behaviour in the two media will be given in a following section where the magnitude and direction of these changes in enthalpy and entropy of activation, the difference of the Tafel slopes, b, and the relation of the entropies of activation to the important question of the temperature dependence of b (cf. Chapter 2) will be examined.

The apparent frequency factor ratios for the h.e.r. at pure Hg in 1 M CF_3SO_3H and $CF_3SO_3^-H_3O^+$, based on the experimentally determined apparent enthalpies of activation, were given previously (cf. Table 5-2); the corresponding quantities derived from the true enthalpies of activation (Fig.5-14) will be related to the former frequency factor ratios by a factor dependent on the respective differences in apparent and true heats of activation in the two media. Thus, the frequency factor ratios at constant potential (at 313 K) derived from the true enthalpies

of activation are obtained by multiplying the apparent frequency factor ratios (Table 5-2) by the factor, f,

$$f = \exp[\delta(H^+_{aq}) - \delta(H_3O^+)]/RT \qquad (5\text{-}21)$$

where, e.g., $\delta(H^+_{aq})$ is the difference in true and apparent heats of activation in the 1 M aqueous solution and $\delta(H_3O^+)$ is the corresponding quantity for the melt; the other symbols have their usual significance. Inserting the values given previously in this section for $\delta(H^+_{aq})$ and $\delta(H_3O^+)$, in eqn.(5-21), yields $f = \exp[(15 - 22)/313R] = 6.8 \times 10^{-2}$ at 313 K for the h.e.r. at pure Hg in 1M CF_3SO_3H and $CF_3SO_3^-H_3O^+$.

The frequency factor ratios obtained by applying the transformation in eqn.(5-21) are intended to provide a comparison between the kinetic behaviour of the h.e.r. in the two media corresponding to proton discharge from unhydrated H_3O^+ in the melt and from "$H_9O_4^+$" in excess water in 1 M CF_3SO_3H. However, the choice of a particular <u>overpotential</u> (at a reference temperature, here taken as 313 K) at which to compare the activation parameters for proton discharge from these two media, will still involve some difference in absolute metal-solution potential difference, ϕ_{M-S}, in the respective media, e.g., at the reversible potential in either solution, a difference $\phi^R_{M-S}(H^+_{aq}) - \phi^R_{M-S}(H_3O^+)$. An approximate basis for a comparison, at constant ϕ_{M-S}, of the kinetics for the h.e.r. at pure Hg from 1 M CF_3SO_3H and $CF_3SO_3^-H_3O^+$ will be given in the following section.

(iii) <u>Comparison of the Results at Hg in CF_3SO_3H and $CF_3SO_3^-H_3O^+$</u>

It is of interest to compare true activation parameters for the h.e.r. at pure Hg from the two proton sources, under

conditions of equal ϕ_{M-S} in the respective solutions. The required information is not, however, directly obtainable from the experimental results without some discussion of the significance of activation parameters for single electrode processes and some unavoidable excursions into extra-thermodynamic considerations.

The approach adopted involves: a) estimating the difference in $\Delta H_V^{o\ddagger}$ at $\phi_{M-S} = 0$ in the two media, b) estimating the experimental potential, e.g. vs RHE, at which $\phi_{M-S} = 0$ in the 1 M aq. CF_3SO_3H and c) combining the results of a) and b) with the $\Delta H_V^{o\ddagger}$ data presented in Fig.5-14 above in order to select an appropriate potential at which to compare the activation parameters.

a) First we note, following Temkin[188], that the apparent heats of activation, $\Delta H_{\eta=0}^{\ddagger}$, involve the temperature variation of the absolute potential difference of the reversible H_2 electrode according to a relation

$$\Delta H_{\eta=0}^{\ddagger} = \Delta H_{\phi=0}^{\ddagger} - \beta \Delta H_R^o \qquad (5\text{-}22)$$

where $\Delta H_{\phi=0}^{\ddagger}$ is the "true" heat of activation of the studied electrode process at hypothetical zero metal/solution p.d., ΔH_R^o is the standard heat of reaction in the single electrode process $H_{aq}^+ + e = 1/2\ H_2$ at its reversible potential and β is the symmetry factor of the charge transfer process.

In the systems studied in the present work, we have essentially two media from which H is discharged or ionized: the H_3O^+ melt and the H_3O^+ ion in excess water, to be designated H_{aq}^+. Then the activation energies must be expressed as follows:

$$\Delta H^{\ddagger}_{\eta=0}(H_3O^+) = \Delta H^{\ddagger}_{\phi=0}(H_3O^+) - \beta\Delta H^{\circ}_R(H_3O^+) \qquad (5\text{-}23)$$

and

$$\Delta H^{\ddagger}_{\eta=0}(H^+_{aq}) = \Delta H^{\ddagger}_{\phi=0}(H^+_{aq}) - \beta\Delta H^{\circ}_R(H^+_{aq}) \qquad (5\text{-}24)$$

where the β's are the relevant symmetry factors.

We note first that the heat of reaction ΔH°_R for the H_2 electrode half-cell reaction will not be quite the same in the H_3O^+ melt as in water. The processes involved are

$$H_3O^+_{melt} + e = 1/2\ H_2 + H_2O\ (\text{in melt}) \qquad (5\text{-}25)$$

and

$$H^+_{aq} + e = 1/2\ H_2 + H_2O\ (\text{in } H_2O) \qquad (5\text{-}26)$$

From the experimentally observable difference $\Delta H^{\ddagger}_{\eta=0}(H_3O^+) - \Delta H^{\ddagger}_{\eta=0}(H^+_{aq})$ we could obtain the kinetically significant difference of "true" activation energies $\Delta H^{\ddagger}_{\phi=0}(H_3O^+) - \Delta H^{\ddagger}_{\phi=0}(H^+_{aq})$ if the difference δ of the two ΔH°_R terms in eqns.(5-23) and (5-24) can be estimated. δ obviously involves the heat transfer of H_3O^+ from the melt to water (1 M aq. CF_3SO_3H) together with the difference of heats of production of water in the melt (eqn.(5-25)) and in the dilute aqueous acid (eqn.5-26); this quantity was experimentally measured in the present work and its value is found to be -5.3 kJ mol^{-1} from a calorimetric experiment.

The heat of transfer of H_3O^+ from melt to water is not, however, directly measurable but the heat of dilution (dissolution) of $CF_3SO_3^-H_3O^+$ into water, which involves transfer both of H_3O^+ and the co-anion $CF_3SO_3^-$, is, however, measurable and was determined in a calorimetric experiment as -19.6 kJ mol^{-1}. This energy corresponds to separation of the cations and anions in the liquid lattice salt coupled with their hydration in excess water (cf. dissolution of a solid salt). Heats of solution of

solid salts are not normally separable into ionic components but we may suppose that a separate heat of transfer of H_3O^+ will involve a fraction of the above dilution energy (-19.6 kJ mol^{-1}) determined approximately by a reciprocal radius factor for the H_3O^+ (r_+) and $CF_3SO_3^-$ (r_-) ions and for water (r_w): $\{1 + [(r_+ + r_w)/(r_- + r_w)]^2\}^{-1}$. This gives a transfer energy for H_3O^+ of -12.8 kJ mol^{-1} so that with a reasonable estimate of the uncertainty in this figure and the above transfer energy of H_2O, the required enthalpy difference is found to be -18.1±4 kJ mol^{-1}.

Then the difference of heats of activation for the h.e.r. in the two media when $\phi_{M-S} = 0$ is $\Delta H^{\ddagger}_{\phi=0}(H_3O^+) - \Delta H^{\ddagger}_{\phi=0}(H^+_{aq}) = +25.8 \pm 6$ kJ mol^{-1}.

b) The potential, $V_{\phi=0}$, at which $\phi_{M-S} = 0$ at pure liquid Hg in 1 M aqueous CF_3SO_3H will now be estimated. Electrocapillary measurements at liquid Hg in an electrolyte solution enable the thermodynamically unambiguous potential of zero charge (p.z.c.) to be determined. However, at the p.z.c., a residual metal-solution potential difference exists, so that in general $V_{\phi=0}$ and the p.z.c. will differ. This interfacial field at the p.z.c. arises primarily from the residual orientation of dipolar solvent molecules; this effect has been investigated by means of the study of adsorption of neutral molecules at Hg.

Conway and Dhar[209] have investigated the role of oriented water molecules at Hg surfaces in a study of the adsorption of the non-polar flat and conformationally fixed molecule, pyrazine. From a consideration of Esin and Markov plots, it was concluded that no net water dipole orientation was present in aqueous

perchlorate solution at a Hg surface charge $q_M = -2$ μC cm^{-2} in the temperature range 293 - 323 K; this value of q_M corresponds to a potential of ca. 2 μC cm^{-2}/20 μF cm^{-2} = 0.1 V cathodic to the p.z.c. This relation may be expected to apply approximately in the dilute CF_3SO_3H solutions considered here since both the perchlorate and trifluromethanesulfonate anions are not significantly adsorbed at mercury[210,211].

By analogy with the Hg/1 M aq. $HClO_4$ interface at 313 K, the p.z.c. at Hg in 1 M aq. CF_3SO_3H is ca. -0.304 V RHE (313 K) so that the potential of zero field in 1 M aq. CF_3SO_3H is then ca. -0.304 - 0.1 = -0.40 V RHE (313 K).

c) In a previous section, we have evaluated the potential dependence of the true $\Delta\bar{H}_V^{o\ddagger}$ for the h.e.r. at pure Hg in 1 M CF_3SO_3H (cf. Fig.5-14). In b) above, we found $V_{\phi=0}(H^+_{aq})$ = -0.40 V RHE (313 K), which corresponds to $\Delta H^{\ddagger}_{\phi=0}(H^+_{aq})$ = +62.5 kJ mol^{-1}. From a) above, we have $\Delta H^{\ddagger}_{\phi=0}(H_3O^+) - \Delta H^{\ddagger}_{\phi=0}(H^+_{aq})$ = +25.8 kJ mol^{-1} so that $\Delta H^{\ddagger}_{\phi=0}(H_3O^+)$ = +25.8 + 62.5 = +88.3 kJ mol^{-1}.

Inspection of the data shown in Fig.5-14 indicates that $\Delta\bar{H}_V^{o\ddagger}(H_3O^+)$ = 88.3 kJ mol^{-1} at an overpotential in $CF_3SO_3^-H_3O^+$ solution at 313 K of ca. -0.23 V; this value then is an indirect estimate of $V_{\phi=0}$ in the monohydrate melt (313 K).

The above approximate values of $\Delta H^{\ddagger}_{\phi=0}$ for the h.e.r. at pure Hg in 1M aq. CF_3SO_3H and $CF_3SO_3^-H_3O^+$ together with the associated ratio of current densities at these potentials lead to a frequency factor ratio A(1M CF_3SO_3H)/A($CF_3SO_3^-H_3O^+$) of ca. 3.6 x 10^{-3}.

The relative effects on the observed current densities of these differences in heats of activation and ratios of frequency

factors for the h.e.r. at Hg will be considered in Section 5; the apparent activation parameters for the h.e.r. (Section 2) and for the desorption of strongly-bound H from Pt (cf. Section 4) will also be considered.

4. Kinetics of the Elementary H^+ Discharge Step

(i) Kinetics of H^+ Discharge at Pt in Relation to those for the H.E.R.

We have seen that the kinetics of the overall h.e.r. at Hg are controlled by the H^+ discharge step, while at other metals, e.g. Pt and Ni, potential- and coverage-dependent desorption of H is rate-determining. It is then of interest to examine the rate of the H^+ discharge step at one of these latter catalytic metals; however, a detailed kinetic study of this electrosorption/desorption step is difficult in the presence of large continuous faradaic currents (see Chapter 4 for a discussion of this problem).

The underpotential deposition (UPD) of strongly-bound H at Pt provides, however, an opportunity to examine unambiguously the elementary H^+ discharge step at this metal. At Pt, the H_{ads} which is involved as a kinetically significant intermediate in the desorption step(s) in the overall h.e.r. is probably not that which can be experimentally characterized as the strongly bound species by underpotential deposition techniques (charging curve evaluation or cyclic-voltammetry) or reflectivity measurements; rather, it is a species weakly bound on the complete monolayer of H which is known to be chemisorbed at clean Pt electrodes already at the H_2/H^+_{aq} reversible potential.

However, the step of underpotential deposition of H as a strongly bound chemisorbed species at Pt can be reliably studied as a separate electrode process by several transient electrochemical methods. In particular, the kinetics of H^+ discharge and adsorption can be followed by means of a.c. impedance measurements or by cyclic-voltammetry through evaluation of the reversibility parameter[158], s_o, for the reaction. [s_o is the maximum value of the sweep rate, s, in a cyclic-voltammetry experiment for which the electrosorption process just remains reversible in an experimentally demonstrable way.]

Angerstein-Kozlowska and Conway[158] have shown how s_o can be easily related to i_o, the exchange current density and thence to the standard rate constant, $\bar{k}_o$, for the surface electrosorption reaction at half-coverage, i.e. where the currents measured in cyclic-voltammetry are taken as the peak currents:

$$s_o = i_o/C_{rev} \qquad (5\text{-}27)$$

$$s_o = (2RT/zF)k^oC_{H^+}^{(1-\beta)} \qquad (5\text{-}28)$$

where C_{rev} is the maximum adsorption pseudocapacitance for adsorbed H measured under conditions, $s < s_o$, for which the surface process remains reversible. An interesting feature of the evaluation of s_o by means of cyclic-voltammetry is that the real area of the electrode surface is not a required quantity as it is for derivation of i_o. Hence, comparison of kinetic behaviour of one electrode preparation and another can be made without uncertainties in the "rate per real unit area" entering into the comparison; this is of considerable practical importance

in assessing the intrinsic electrocatalytic properties of electrode materials. However, at Pt, the real electrochemically significant area can in any case be determined accurately by measurement of the charge q_H for formation or desorption of the monolayer of strongly bound H. It should be noted that at Pt and other metals for which the required experiments can be unambiguously conducted, the strongly bound H is present in 4 or 5 states that can be distinguished as the monolayer of H is formed or desorbed; even on well prepared crystal surfaces of Pt, several states are still resolvable[212] which correspond probably to formation of successive lattice arrays as the ad-layer becomes extended to monolayer coverage.

In the present work, the kinetics of H UPD were evaluated by means of cyclic-voltammetry through the determination of s_o values; data were obtained for the most strongly bound state of the chemisorbed H at Pt.

The evaluation of s_o data is preferred from the anodic (H desorption) side of the voltammagrams, as complications due to the parallel H_2 evolution partial current on the cathodic side at the least positive potentials are avoided. Also some advantage exists regarding better control of anion adsorption effects in the aqueous medium. Comparison of the anodic and cathodic behaviour was given in Fig.5-3 above. Apparent activation energies were evaluated from the measured dependence of log s_o/T values on reciprocal temperature[158].

Potentials, V_p, of the peaks of the "IR"-compensated cyclic-voltammetry, I vs V curves were obtained and are plotted vs log s in Fig.5-15. Comparative kinetic behaviour of proton transfer

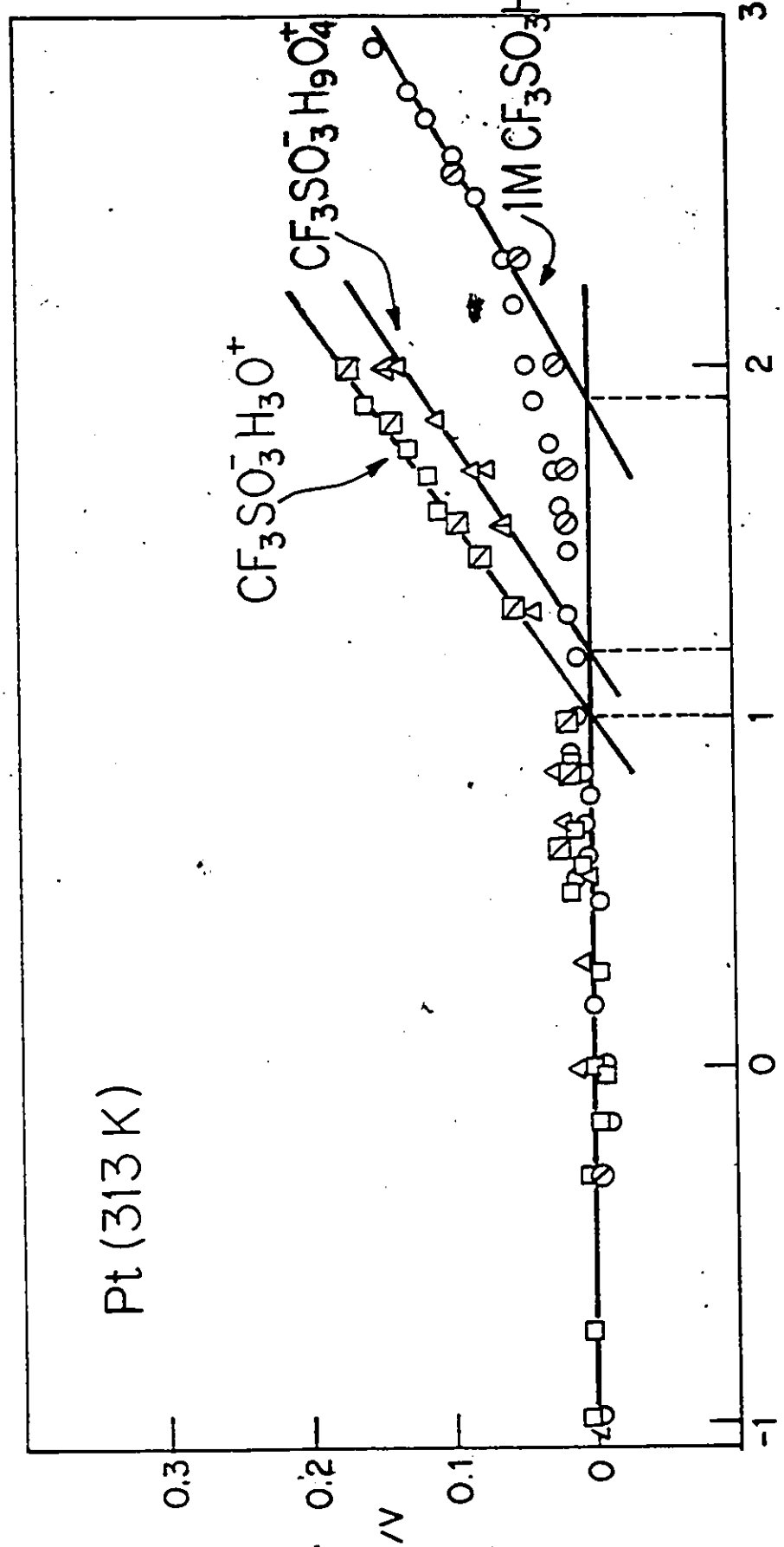

Fig.5-15 Tafel-type plots for desorption of strongly bound H from Pt in solutions of CF_3SO_3H at 313K.

from $CF_3SO_3^-H_3O^+$ (i.e. from the unhydrated H_3O^+ ion), $CF_3SO_3^-H_9O_4^+$ (from Eigen's "$H_9O_4^+$" species) and from CF_3SO_3H in excess water, as the 1 M aq. solution, is shown in this figure.

The plots of V_p vs log s show the expected[158] transition from reversible (V_p independent of s) to irreversible (V_p logarithmic in s) kinetic behaviour in the anodic ionization of adsorbed H. The log s_o value is based on extrapolation of the Tafel region of Fig.5-15, where V_p is logarithmic in s, to the line where V_p is independent of log s, i.e. where $s < s_o$. Experimentally, it is recognized (cf. ref.174) that a deviation of V_p behaviour from independence on log s to dependence on log s can arise from "IR" drop effects as well as from onset of kinetic irreversibility (see the treatment given in Chapter 4). However, deviations due to "IR" drop are not logarithmic in s ; the peak pseudocapacitance behaviour was shown in Chapter 4 also to be diagnostic of the presence of spurious "IR" losses. All the V_p data shown in Fig.5-15 have been acquired with compensation for "IR" drop effects which increase with s but the upper limit of the range of s values employed in the experiments was set as that for which the IR drop did not exceed ca. 0.05 V. The V_p potentials derived from the IR-compensated results were reproducible to better than 5 mV. The results shown in Fig.5-15 are based on two separate typical experiments as distinguished by the data symbols in this figure.

The significant aspect of these results is (Fig.5-15) that s_o increases with increasing extent of hydration, yet the proton concentration is decreasing: 10.8 M for $CF_3SO_3^-H_3O^+$; 6.8 M for

$CF_3SO_3H.4H_2O$ and 1 M for CF_3SO_3H in the nominal unimolar solution in excess water. This trend is shown graphically in the logarithmic plot in Fig.5-16. Eqn.(4-27) indicates that a plot of log s_o vs log C_{H^+} would be expected to have a slope of ca. +0.5; in fact the slope of the line in Fig.5-16 is -0.45. Since s_o increases, like i_o, with increasing reactant concentration, it is evident that the observed direction of changes of s_o, shown in Figs.5-15 and 5-16 can in no way be due to a trivial effect of concentration which would be in the opposite direction.

The exchange current-densities, i_o, related to s_o, were calculated from the peak pseudocapacitance values under reversible conditions (low sweep rate, $s \ll s_o$), using eqn.(5-15) with C_{rev} being referred to unit electrochemically significant real area based on the charge for full coverage of most strongly bound H, q_H, determined in the 1 M aq. acid solution. The standard rate constants, $\bar{k}_o$ were then calculated from the i_o data in the usual way. The s_o, i_o and $\bar{k}_o$ results are summarised in Table 5-5 below; because these quantities are derived from the variation of peak potentials with log s using the reversible peak pseudocapacitance, they refer to the kinetics of the H desorption process at half coverage of the state involved.

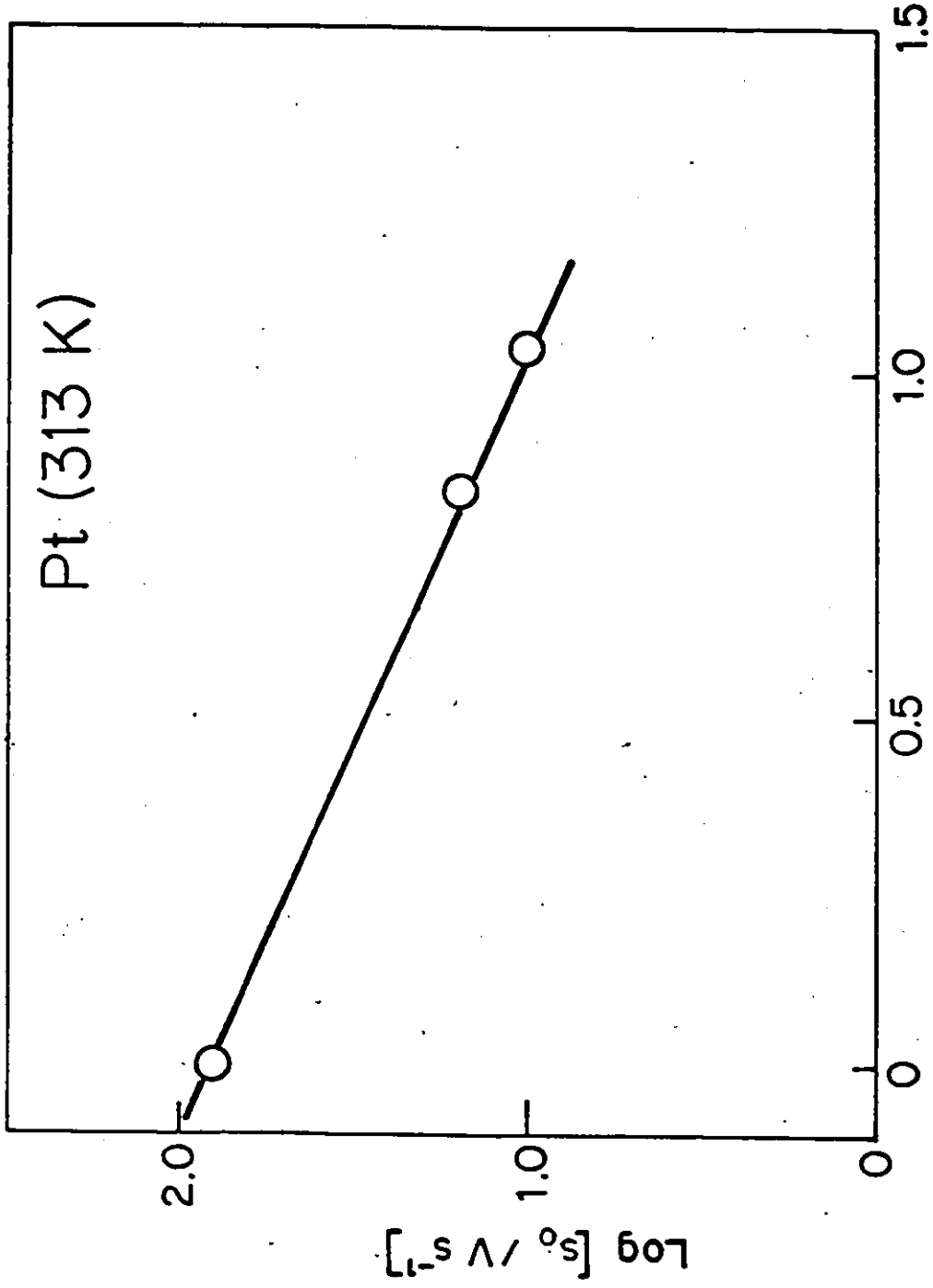

Fig.5-16 Dependence of log s_o on concentration of H_3O^+ for desorption of strongly bound H from Pt in solutions of CF_3SO_3H at 313 K.

Table 5-5

Values of s_o, i_o and $\bar{k}_o$ for H Desorption at Pt at 313 K from three States of Hydration of H^+

Solution	log s_o	log i_o	log $\bar{k}_o$	$\Delta H^{\ddagger}_{\eta=0}$/kJ mol^{-1}
$CF_3SO_3^-.H_3O^+$	1.01	-2.59	2.08	17
$CF_3SO_3^-.H_9O_4^+$	1.19	-2.41	2.36	--
1 M aq. CF_3SO_3H	1.91	-1.72	3.50	19.7

For H ionization from a UPD state at Pt (see Fig.5-17) the apparent $\Delta H^{\ddagger}_{\eta=0}$ values were derived by plotting log s_o/T (cf. ref.158) vs 1/T and are shown in Table 5-5. These heats of activation are again the apparent quantities since the s_o values are determined at the peak potential, i.e. for half coverage; the potential at which the peak in the cyclic-voltammetry profiles occurs under reversible conditions of sweep rate, is itself dependent on temperature, just as the reversible potential for the h.e.r. is temperature dependent, and hence the "apparent" nature of these activation parameters.

The log s_o and $\Delta H^{\ddagger}_{\eta=0}$ values in Table 5-5 result in an apparent frequency factor ratio, A(1M)/A(H_3O^+), of 1.5 x 10^2. In this case, where the difference, $\Delta \bar{H}_V^{o\ddagger}$(1M) - $\Delta \bar{H}_V^{o\ddagger}(H_3O^+)$ in heats of activation is only ca. 2.7 kJ mol^{-1}, the 8-fold increase in s_o on going from $CF_3SO_3^-H_3O^+$ melt to 1 M aqueous CF_3SO_3H results from this apparent frequency factor ratio. This behaviour is in contrast with that for the h.e.r. at Hg seen above where the relative rates in the two media were determined primarily by changes in the heats of activation.

Fig.5-17 Electrochemical Arrhenius plot for desorption of strongly bound H from Pt in $CF_3SO_3^-H_3O^+$ and 1 M aqueous CF_3SO_3H.

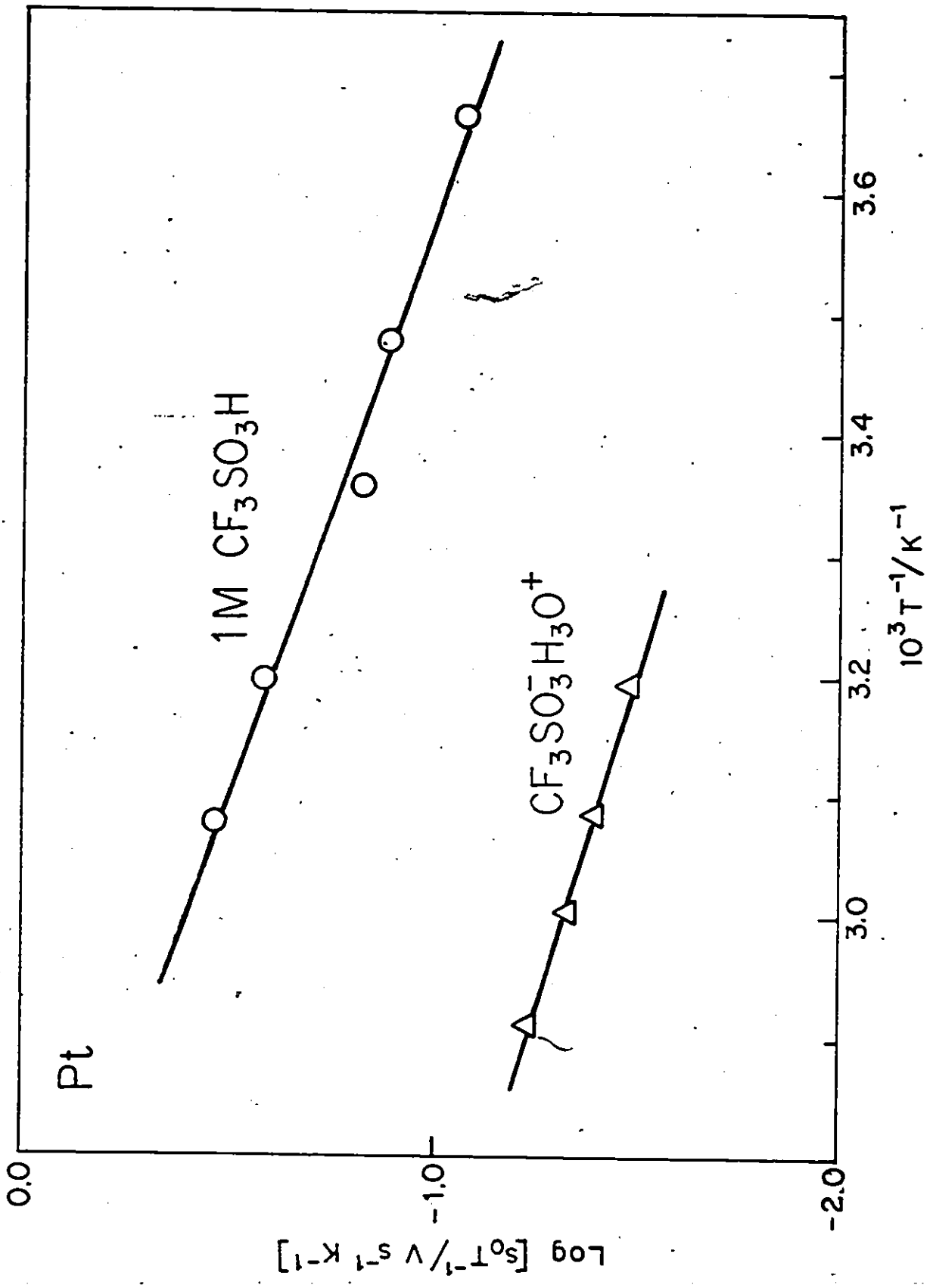
Pt
1M CF_3SO_3H
$CF_3SO_3^-H_3O^+$
0.0
-1.0
-2.0
3.0
3.2
3.4
3.6
$10^3 T^{-1}/K^{-1}$
Log $[s_o T^{-1}/V\ s^{-1}\ K^{-1}]$

(ii) H/D Kinetic Isotope Effects at Pt and Hg

H/D kinetic isotope effects in s_o and i_o were evaluated by comparing the log s_o and log i_o values for the various proton transfer processes investigated at a given temperature in the fully protic and fully deuteric electrolytes, the latter being prepared as described in the experimental section. For the d-solutions, potentials were measured against a reversible D_2 electrode in the same solution (cf. ref.73,75). Note that the apparent isotope effect thus evaluated involves a change of scale of the reference potential as discussed elsewhere[213]. Corrections can be made for this effect based on the $H_2/H_3O^+:D_3O^+/D_2$ potential difference[73,214] with correction for liquid junction potential.

Cyclic-voltammetry was used to determine the apparent H/D isotope effects for H^+ and D^+ transfer at Pt from the monohydrate/monodeuterate solutions and from the 1 M H_2O/D_2O solutions are shown in Figs.5-18 and 5-19. It is seen that for the former case, the apparent H/D kinetic isotope effect is quite small, ca. 1.5, while for the latter the effect is ca. 2.6.

In a recent paper, Marschoff[215] has studied the H/D kinetic isotope effect in the anodic desorption of strongly bound H from Pt by means of the method developed by Angerstein-Kozlowska and Conway[158] for the evaluation of kinetic parameters of surface processes from cyclic-voltammetry experiments. A ratio of s_o^H/s_o^D = 6.2 was found (apparently near 298 K) for desorption of H from Pt in 0.84 M H_2SO_4, compared with the value 2.6 (313 K) found in the present work in 1 M CF_3SO_3H. The difference in s_o^H/s_o^D may be

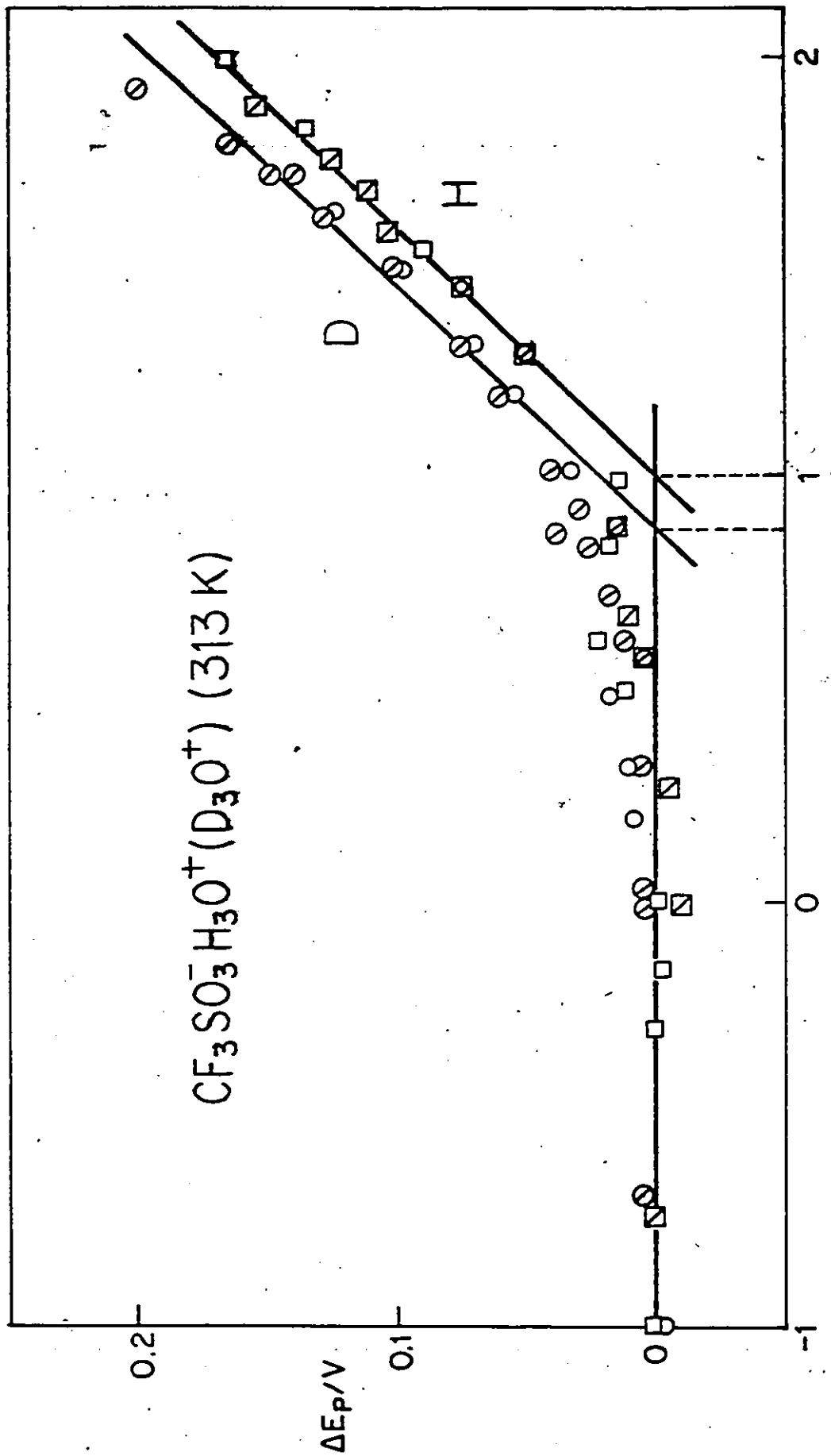

Fig.5-18 Tafel-type plots for desorption of strongly bound H (D) from Pt in $CF_3SO_3^-H_3O^+$ and $CF_3SO_3^-D_3O^+$ at 313 K.

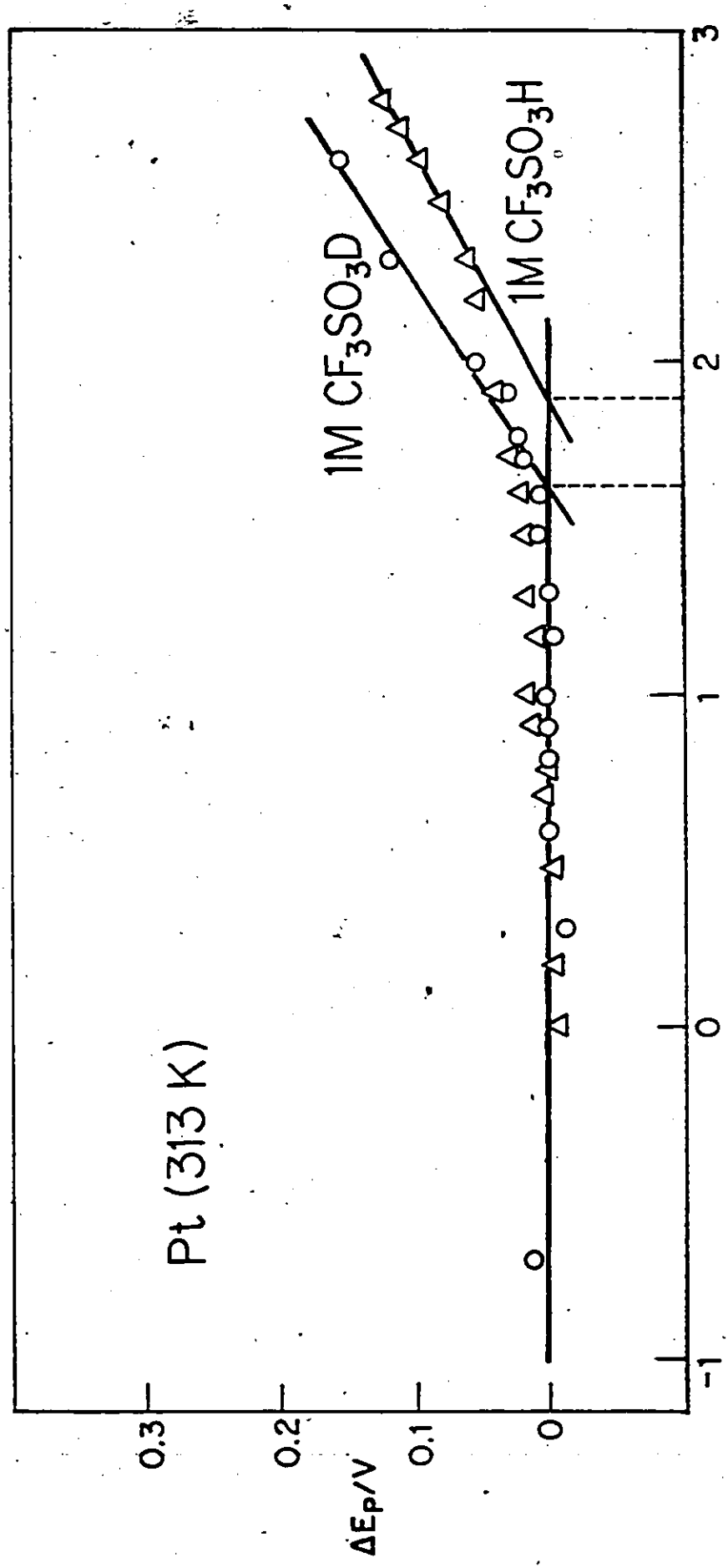

Fig.5-19 Tafel-type plots for desorption of strongly bound H_{ad}(D) from Pt in 1 M CF_3SO_3H (in H_2O) and 1 M CF_3SO_3D (in D_2O) at 313 K.

due in part to the different H^+_{aq} concentrations and temperatures (increasing T would lead to a reduction in s^H_o/s^D_o) employed in these two investigations. Some difference in s^H_o/s^D_o might be expected from the different properties of the $CF_3SO_3^-$ and SO_4^{2-} anions in these dilute aqueous solutions. Specific adsorption of SO_4^{2-} at Pt, where the p.z.c. is located in the H UPD region, leads to changes in the cyclic-voltammetry profile in this region, compared with the behaviour in solutions of relatively unadsorbed perchlorate ions; anion adsorption was considered in the work of Angerstein-Kozlowska and Conway[158] in the evaluation of s_o for surface processes at Pt. At Au surfaces where no UPD of H occurs, adsorption of SO_4^{2-} ions changes the double-layer charging behaviour and leads to a significantly more anodic potential for the onset of surface oxide formation[216]. The cyclic-voltammetry profile (Fig.5-3) in 1 M CF_3SO_3H exhibits an H-adsorption region similar to that observed previously in $HClO_4$ solutions, indicating a relatively small degree of specific adsorption of the $CF_3SO_3^-$ anion[158]. The competitive adsorption of $CF_3SO_3^-$ with SO_4^{2-}, PO_4^{3-} and ClO_4^- at Pt has been studied previously[217,218] by cyclic-voltammetry in dilute aqueous solution; it was concluded that $CF_3SO_3^-$ is adsorbed to approximately the same extent as ClO_4^-. Electrical double-layer capacitance studies at Hg have indicated that the $CF_3SO_3^-$ anion is not strongly adsorbed at this metal either[210,211].

It would be of interest to evaluate the effect of anion adsorption on the H/D kinetic isotope effect for desorption of H from Pt into dilute aqueous acid solution. Although in the $CF_3SO_3^-H_3O^+$ melt, anion adsorption is certainly indicated, it is

not possible to draw any meaningful general conclusions on the effect of anion adsorption on these H/D kinetic isotope effects owing to the drastic difference in the solution media involved on going from the monohydrate melt to dilute aqueous solution.

Figs.5-20 and 5-21 show the H/D isotope effect on the Tafel behaviour for the steady-state h.e.r. at pure Hg (where the proton discharge step is rate-determining) from $CF_3SO_3^-H_3O^+$ and 1 M aq. CF_3SO_3H. In the monohydrate/monodeuterate case the H/D kinetic isotope effect is ca. 2.6 while for the 1 M aq. CF_3SO_3H the effect is ca. 2.5. It is significant that similar Tafel slopes, b, are found for the h.e.r. at Hg in the $CF_3SO_3^-H_3O^+$ melt, i.e., no mass effect on b is found; this is the usual situation found at Hg in dilute acid (H or D) solution (cf. Fig.5-21) at ordinary temperatures.

In the monohydrate melt, H_3O^+ may be considered to be in very close contact with the electrode surface, especially at cathodic potentials; it is improbable, on electrostatic grounds, that the Hg electrode surface is fully covered by anions. In 1 M CF_3SO_3H, the Hg electrode surface can be considered (after BDM[70]) to be fully covered by water solvent dipoles with hydrated cations approaching only to the outer Helmholtz plane (O.H.P.) and with the possibility of specifically adsorbed (and hence partially de-solvated) anions; thus Bockris and Matthews[71], in their calculations on H^+ tunneling in H^+ discharge, treated H_3O^+ much like an alkali metal ion in the O.H.P. and therefore considered energy barriers with widths of ca. 0.3 - 0.4 nm (see Chapter 2). This model for aqueous H_3O^+ does not take the

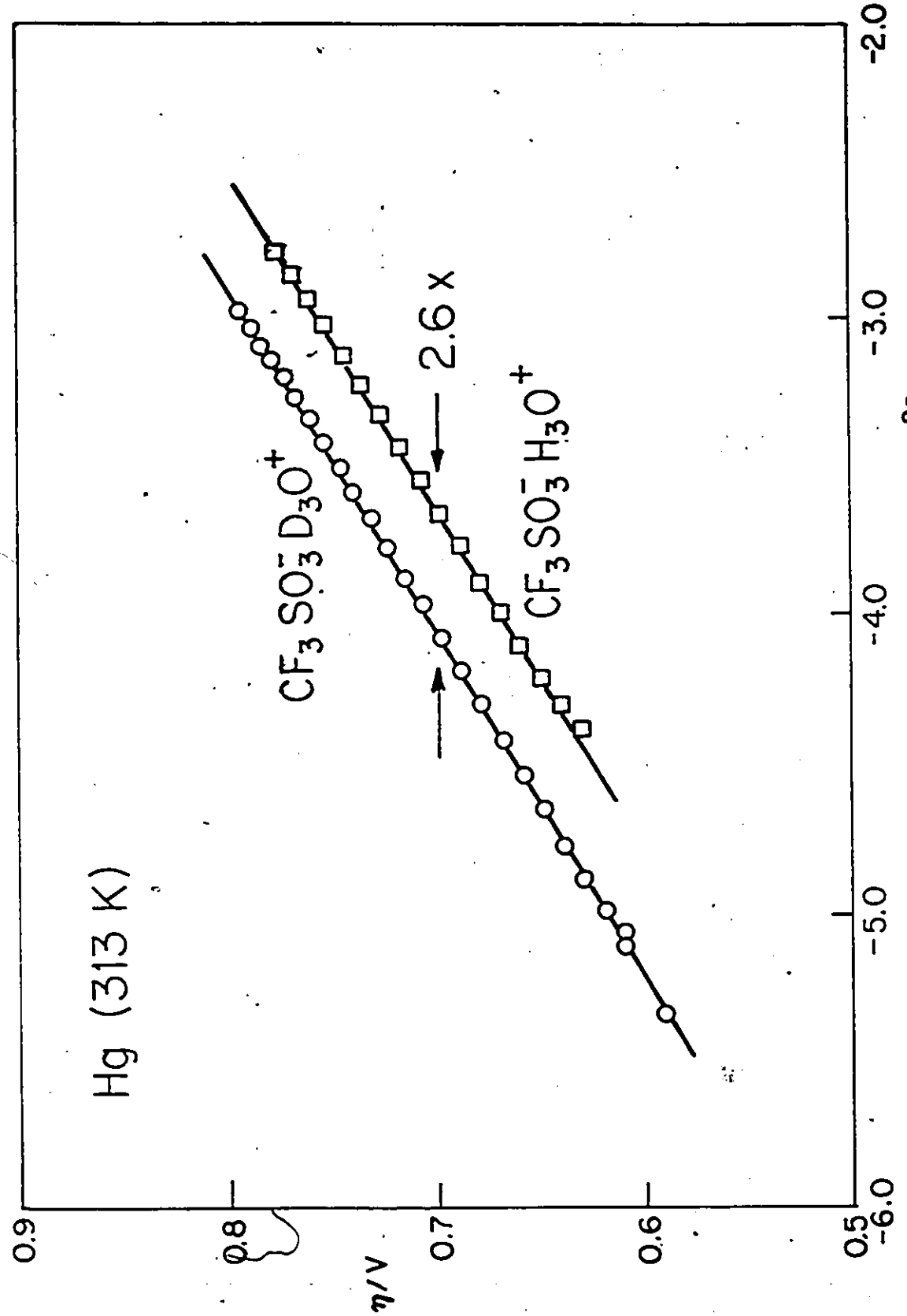

Fig.5-20 Overpotential vs log[current density] relations for the h.e.r. at Hg from $CF_3SO_3^-H_3O^+$ and $CF_3SO_3^-D_3O^+$.

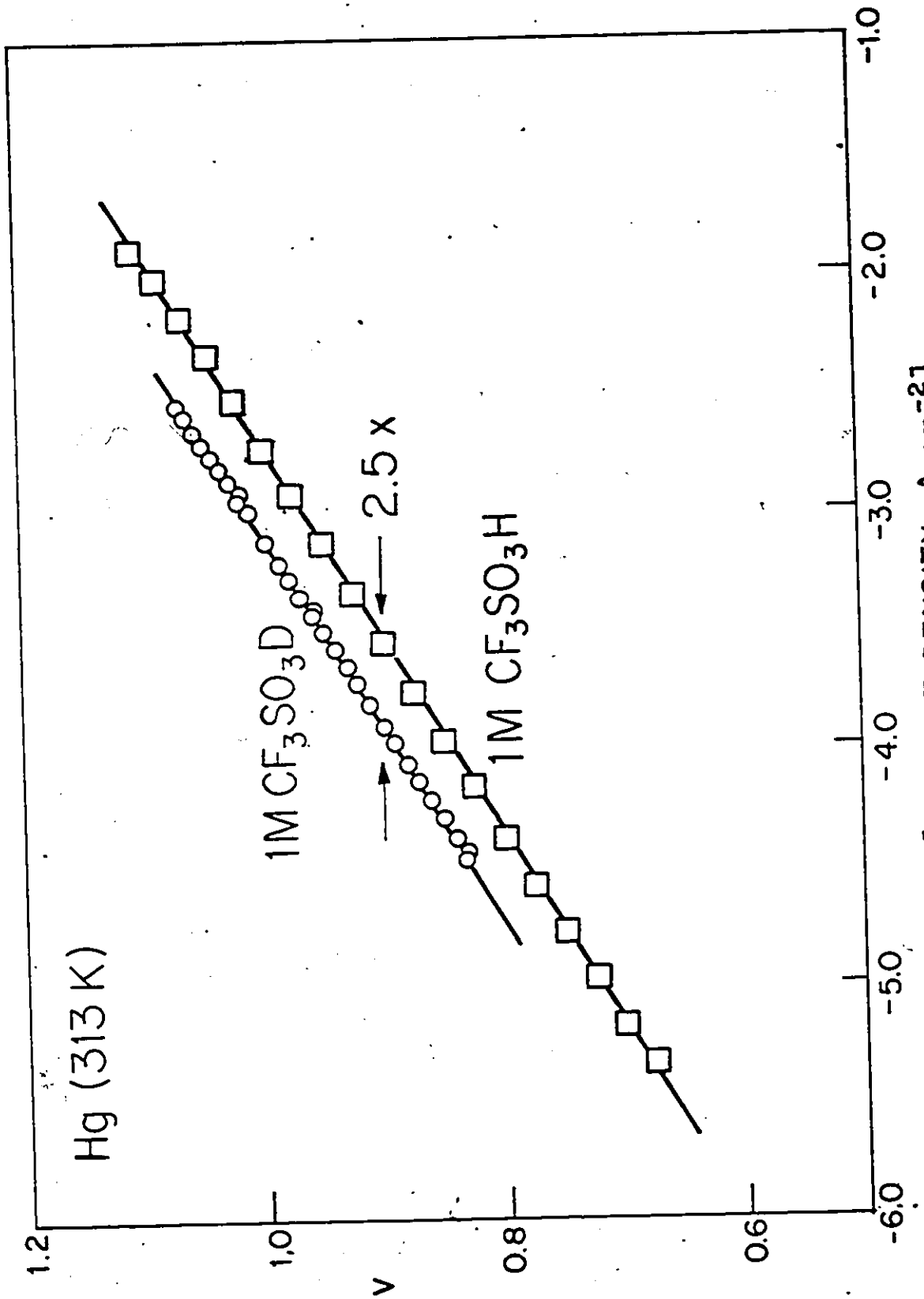

Fig.5-21 Overpotential vs log[current density] relations for the h.e.r. at Hg from 1 M aq. CF_3SO_3H and 1 M CF_3SO_3D (in D_2O).

special nature of the proton in aqueous acid solutions into account, which is responsible for the observed anomalous proton mobility in water[148]; in particular, a relatively small fluctuation in location of the proton amongst H_2O molecules about an H_3O^+ ion near an electrode surface could lead to much smaller distances of approach of H^+ to the electrode surface in the act of the discharge process[219]. The choice of barrier dimensions taken by Bockris and Matthews and hence, to some extent, their calculated results depend more on the particular model assumed for H_3O^+ in excess water, than on the use of the widely-used BDM model of the double-layer.

The calculation of Conway[72] (see Chapter 2) of the contribution of tunneling alone to H^+ discharge, involved narrower barriers, as are expected, e.g. in the $CF_3SO_3^-H_3O^+$ melt and resulted in a mass-dependent Tafel slope. The present results for b in the h.e.r. at Hg in $CF_3SO_3^-H_3O^+$ indicate the absence of a large H^+ tunneling component at 313 K. In the related H desorption process at Pt in $CF_3SO_3^-H_3O^+$ and $CF_3SO_3^-D_3O^+$, no H/D mass effect on the Tafel slope is indicated in the irreversible region of the ΔV_p vs log s plot (Fig.5-18).

Low temperature (< 150 K) experiments on the h.e.r. or H desorption reaction are expected to show better the effect of tunneling (see Chapter 2); this approach is currently being pursued in research in this laboratory. This work may allow verification of the conclusion[71], based on consideration of the potential-dependence of the H/D (and H/T) separation factor, that tunneling accounts for ca. 70% of the rate of the h.e.r. at Hg at room temperature.

5. Frequency Factors and Heats of Activation in Relation to Rates of H^+ Discharge

In the preceding sections, ratios of frequency factors and differences of heats of activation were given for the h.e.r. at Hg, Ni and Pt and the desorption of strongly bound H at Pt in the $CF_3SO_3^-H_3O^+$ melt and 1 M aq. CF_3SO_3H. The directions of the contributions of these two quantities in relation to the experimentally observed ratios of currents (or i_o values) in the two media, $i(H^+_{aq})/i(H_3O^+)$, are summarized in Table 5-6.

Table 5-6

Effect of Frequency Factor Ratios and Differences in Heats of Activation on $i(H^+_{aq})/i(H_3O^+)$

System	$\delta(\Delta H^{\neq})$*	$A(H^+_{aq})/A(H_3O^+)$*	$i(H^+_{aq})/i(H_3O^+)$*
h.e.r. Hg (low η)	>1	<1	>1
h.e.r. Hg (high η)	<1	>1	<1
h.e.r. Hg ($\phi_{M-S} = 0$)	>1	<1	>1
h.e.r. Hg film (on Au)	>1	>1	>1
h.e.r. Pt	>1	<1	>1
$PtH = Pt + H^+ + e^-$	<1	>1	>1
h.e.r. Ni**	<1	(>1)	>1

* Entries refer to the expected magnitude of $i(H^+_{aq})/i(H_3O^+)$

** At Ni in the monohydrate melt, the rate was found to pass through a maximum with temperature (see Section 2,v).

In the case of the h.e.r. from $CF_3SO_3^-H_3O^+$ and 1 M CF_3SO_3H, the relative rates in the systems shown in this table are deter-

mined primarily by the differences in heats of activation; in fact, except at the Hg film electrode, the frequency factor ratios make an opposing contribution to the relative rates. On the other hand, in the ionization of strongly bound H at Pt, $i(H^+_{aq})/i(H_3O^+) > 1$ as expected from the frequency factor ratio and not according to the difference in heats of activation. In the case of the h.e.r. at Ni, the rate of reaction in the 1 M aqueous CF_3SO_3H is greater than that in the monohydrate melt, although in the latter solution, the rate was found to pass through a maximum with increasing temperature; this behaviour may result from potential- and temperature-dependent anion adsorption and surface hydride formation (see Section 2,v).

The potential-dependence of the activation parameters for the h.e.r. at Hg in relation to the temperature-dependence of the Tafel slope, b, will be considered in the following section.

6. Potential-Dependence of $\Delta H^{\ddagger}$ and $\Delta S^{\ddagger}$ and the Temperature Dependence of b

The question of the effects of potential and temperature in relation to the Tafel slope, b, was considered in Chapter 2. It will be recalled that experimentally b is rarely represented with respect to its temperature-dependence by the relation $b = 2.3RT/\alpha F$ where α is a charge transfer symmetry factor, analogous to the Brønsted factor[108] in linear free energy relations, in the case of rate-controlling proton and/or electron transfer. In particular, b is often found to be independent of temperature or to contain a temperature-independent component, implying temperature-dependence of the symmetry factor (or transfer coefficient)

itself (see Chapter 2).

In the present section, the potential-dependence of the true enthalpy and entropy of activation for the h.e.r. at pure Hg (see above) in $CF_3SO_3^-H_3O^+$ and 1 M aq. CF_3SO_3H will be considered in relation to the temperature-dependence of b. Earlier results on the h.e.r. at Hg in aqueous[69] and methanolic[73,74] HCl will also be discussed.

(i) Quasi-Thermodynamic Representation of the Activation Process

The electrode reaction current-density i may be written formally as

$$i = Bc \exp[-\Delta\bar{G}_V^{o\ddagger}/RT] \qquad (5\text{-}29)$$

where B is a combination of constants, c an appropriate reactant concentration expression and $\Delta\bar{G}_V^{o\ddagger}$ the electrochemical free energy of activation[120]. Eqn.(5-29) has been written, for simplicity, without reference to surface coverage or site availability at the electrode interface, since these are factors that are not immediately involved in the discussion here. $\Delta\bar{G}_V^{o\ddagger}$ in eqn.(5-29) has usually been expressed as,

$$\Delta\bar{G}_V^{o\ddagger} = \Delta H^{o\ddagger} - T\Delta S^{o\ddagger} \mp \beta\Delta VF \qquad (5\text{-}30)$$

where ΔV is some shift of potential from a reference value, usually taken as hypothetical zero metal-solution potential difference; here and below, the upper and lower signs in the notation "$\pm$" (or"$\mp$") refer to anodic and cathodic processes respectively. In writing eqn.(5-30), the usual assumption is that the Brønsted principle[108] applies[112] to the shift of energy curves representing the course of the electrochemical particle and/or electron transfer process, through the change of Fermi

level by $\pm \Delta VF$ which affects the energy of the initial state and hence the $\Delta \bar{H}_V^{o\ddagger}$ (or $\Delta \bar{E}_V^{o\ddagger}$) of the reaction. When the relation for $\Delta \bar{G}_V^{o\ddagger}$ in eqn.(5-30) is substituted in eqn.(5-29), the supposed potential-dependence of i is obtained through the resulting exponential factor in $\pm \beta \Delta VF/RT$. This gives the usually reported form for the Tafel slope, $b = 2.3RT/\beta F$, which, however, is rarely observed experimentally, as we have remarked above.

Conway, MacKinnon and Tilak, in their paper in 1970[74], following an earlier suggestion of Agar[241], proposed that the electrode field might substantially influence the <u>entropy of activation</u> rather than, or as well as, the energy as usually assumed. They pointed out that, more generally, the Tafel slope should be regarded as originating from the total derivative w.r.t. potential of $\Delta \bar{G}_V^{o\ddagger}$. In order to illustrate this, we write the electrical energy factor, which modifies the free energy of activation by changing the Fermi level, as a fraction β (=0.5) of ΔVF. Then:

$$d(\Delta \bar{G}_V^{o\ddagger})/dV = d(\Delta \bar{H}_V^{o\ddagger})/dV - Td(\Delta \bar{S}_V^{o\ddagger})/dV \qquad (5\text{-}31a)$$

$$= \mp \beta F \qquad (5\text{-}31b)$$

Thus $\Delta \bar{S}_V^{o\ddagger}$ for the reaction may be potential-dependent, a situation that may well arise in structured solvents[220] such as water where hydrated ions are intimately associated[221] with the co-plane of oriented water molecules in the inner region of the double layer.

We write the two derivatives in eqn.(5-31a) as $\mp \beta_H F$ (from the $\Delta \bar{H}_V^{o\ddagger}$ term in $\Delta \bar{G}_V^{o\ddagger}$) and $\pm \beta_S F$ (from the $\Delta S^{o\ddagger}$ term). Then

$$d(\Delta \bar{G}_V^{o\ddagger})/dV = \mp(\beta_H + \beta_S T)F \qquad (5\text{-}32)$$

where positive values of β_H or β_S are taken as contributing to

an increase in rate with more favourable (anodic or cathodic) overpotential.

For a reaction in which electron transfer is rate-determining, the usual symmetry factor β, $d(\Delta\bar{G}_V^{o\ddagger})/d(VF)$ is written as $\mp\beta$. Therefore

$$\beta = \beta_H + \beta_S T \qquad (5\text{-}33)$$

Thus β is seen to have a T-independent component β_H (the term corresponding to the conventional behaviour) and a second component, $\beta_S T$, giving rise to the temperature-dependence.

From eqn.(5-33), introducing the Boltzmann factor 1/RT (cf. eqn.(5-29)), the Tafel slope is seen to be

$$b \equiv \pm 2.3RT/\beta F = \pm 2.3RT/(\beta_H + \beta_S T)F \qquad (5\text{-}34)$$

If $\beta_S TF$ is sufficiently larger than $\beta_H F$ as a limiting case, it is seen that

$$RT/\beta F = RT/\beta_S TF = R/\beta_S F \qquad (5\text{-}35)$$

or, as written earlier, $\beta(T) = \beta_S T$. Thus, this case can evidently arise, as was shown in ref.74, if, under certain conditions, increase of electrode potential has its principal effect on $\Delta\bar{S}_V^{o\ddagger}$ rather than on $\Delta\bar{H}_V^{o\ddagger}$ or $\Delta\bar{E}_V^{o\ddagger}$. We recognize here the problem that it is difficult to see how any electrode reaction should not be subject to the effect of changing the potential of the Fermi level, i.e. $\beta_H > 0$ would normally be expected. However, experimental cases exist[123,128] where b is independent of T so that β_H is apparently zero, and the main effect is evidently entropic. In relation to this conclusion, it is of interest that many thermodynamic and kinetic properties of aqueous systems are "entropy controlled" as much as "energy

controlled", a fact first noted by Butler[220] many years ago.

Since the transfer coefficient enters the rate equation in the numerator of the argument of the Boltzmann exponential, it is often more convenient to treat the potential-dependence of electrode reaction rates in terms of the reciprocal of the Tafel slope, b^{-1}, which elsewhere[123] was referred to as the "Lefat" slope; thus, from eqn.(5-34),

$$b^{-1} = \mp\beta F/2.3RT = \mp(\beta_H/T + \beta_S)F/2.3R \qquad (5\text{-}36)$$

so that b^{-1} is made up of a linear combination of a temperature independent term, β_S, and a temperature-dependent one, β_H/T.

We have seen that in the conventional treatment of potential-dependence of electrode reaction rates, it is assumed that $\Delta\bar{S}_V^{o\ddagger}$ is independent of potential, a result that is experimentally indicated in the work of Weaver[77,160] on outer-sphere redox reactions of Cr, V, Eu and Co complex ions in aqueous medium at the Hg electrode. The direct experimental examination of the potential-dependence of $\Delta\bar{S}_V^{o\ddagger}$, or of the corresponding electrochemical frequency factor, for atom + electron transfer reactions such as the H_2 evolution reaction (h.e.r.) has not yet been reported, but it is implicit, as we have noted above, in the form of the observed temperature-dependence of Tafel slopes[74]. The present results give information on this matter.

(ii) H.E.R. at Hg in $CF_3SO_3^-H_3O^+$ and 1 M aq. CF_3SO_3H

(a) Enthalpy of Activation, $\Delta\bar{H}_V^{o\ddagger}$

True heats of activation for the h.e.r. at Hg in $CF_3SO_3^-H_3O^+$ and 1 M aq. CF_3SO_3H were shown as a function of potential in

Fig.5-14. In both cases $\Delta\bar{H}_V^{o\ddagger}$ is seen to decrease linearly with applied potential as expected. The effectiveness of the applied potential in reducing $\Delta\bar{H}_V^{o\ddagger}$ can be characterized by the slopes of the lines in Fig.(5-14) through the quantity $\beta_H = \mp(\text{slope})/F$; the resulting β_H values are compared with the usual symmetry factor, β, derived in the conventional way from the Tafel slope b as recorded in Table 5-7:

Table 5-7

Enthalpic, Entropic and Net Activation Efficiencies for the H.E.R. at Hg

System	β_H	$10^4\beta_S/K^{-1}$	$\beta = \pm 2.303RT/bF$
1 M aq. CF_3SO_3H	0.22	+9.6	0.50
$CF_3SO_3^-H_3O^+$	0.77	-2.2	0.70

Clearly, in the dilute aqueous acid solution, $\beta_H < \beta$ so that the effect of potential on $\Delta\bar{H}_V^{o\ddagger}$ does not account at all completely for the observed "activation efficiency" expressed as $\beta = 0.5$ (Table 5-7) derived directly from the Tafel slope b. In the monohydrate, $\beta_H > \beta$ so that, in this case, some retarding factor must operate in order to reduce the "activation efficiency" from 0.77 (Table 5-7) to the value of 0.7 that is derived from the Tafel slope.

In the cases considered here (cf. Fig.5-14), the experimental potential-dependence of $\Delta\bar{H}_V^{o\ddagger}$ can be represented by,

$$\Delta\bar{H}_V^{o\ddagger} = \Delta H^{o\ddagger} \mp \beta_H \Delta V F \qquad (5\text{-}37)$$

which is of the form referred to above in the discussion of the temperature-dependence of the Tafel slope.

(b) Entropy of Activation, $\Delta\bar{S}_V^{o\ddagger}$

The potential-dependence of $\Delta\bar{S}_V^{o\ddagger}$ (proportional to log[A], the frequency factor) is evident from the variations of log[A] with potential shown in Fig.5-13. In the dilute acid solution (Fig.5-13), $\Delta\bar{S}_V^{o\ddagger}$ for the h.e.r. evidently increases linearly with potential while in the monohydrate melt $\Delta\bar{S}_V^{o\ddagger}$ decreases linearly with potential; the magnitude of the change in $\Delta\bar{S}_V^{o\ddagger}$ with potential is greater in the dilute acid solutions than in the H_3O^+ melt. In the $CF_3SO_3^-H_3O^+$ melt, this entropic factor has a negative effect on the rate, with increasing cathodic potential; the converse is true of the h.e.r. at Hg in the 1 M CF_3SO_3H.

The experimental potential-dependence (Fig.5-13) of $\Delta\bar{S}_V^{o\ddagger}$ can be represented by

$$\Delta\bar{S}_V^{o\ddagger} = \Delta S^{o\ddagger} \pm \beta_S \Delta VF \qquad (5\text{-}38)$$

where $\beta_S = \pm R/F \times$ (slope of lines in Fig.5-13); the resulting β_S values are shown in Table 5-7.

The incremental effect of potential on the "true" and "apparent" activation parameters is identical (cf. section 3), although a constant difference in magnitude occurs that is, of course, independent of potential. Clearly the observed slopes of these lines, and hence the associated β_H and β_S values do not arise trivially on account of the inclusion of the non-isothermal cell potential correction.

Entropy of activation values, $\Delta\bar{S}_V^{o\ddagger}$ at the reversible potential in the two media were determined from the intercepts of electrochemical Arrhenius plots taking B = zFkT/h in eqn.(5-29) and expressing reactant concentrations in mol cm^{-3}; the resulting

$\Delta\bar{S}_V^{o\ddagger}$ values appear in Table 5-8.

Table 5-8

Entropies of Activation at the Reversible Potential for the H.E.R. at Hg (313 K).

Medium	$\Delta\bar{S}_V^{o\ddagger}/JK^{-1}mol^{-1}$ *
1M aq. CF_3SO_3H	-190
$CF_3SO_3^-H_3O^+$	-203

* See Appendix 1.

(iii) The Entropy Factor in the Tafel Slope

Both $\Delta\bar{H}_V^{o\ddagger}$ and $\Delta\bar{S}_V^{o\ddagger}$ are found to be linear functions of potential and, significantly, it is seen that the "activation efficiency", based on $\Delta\bar{H}_V^{o\ddagger}$ alone, does not account satisfactorily for the value derived in the usual manner from the Tafel slope. It is evidently necessary to include the potential-dependence of $\Delta\bar{S}_V^{o\ddagger}$ in order to account for this discrepancy. In view of the appreciable potential-dependence of $\Delta\bar{S}_V^{o\ddagger}$, the usual implicit assumption that the latter quantity is constant seems not to apply in the systems considered here, and should be examined carefully in a given situation.

For the h.e.r. from the dilute aqueous CF_3SO_3H solution, this entropic component evidently contributes significantly towards increasing the "activation efficiency", while in the $CF_3SO_3^-H_3O^+$ melt, the entropic component acts in the opposite direction. The difference in magnitude and this reversal in sign of the direction of the potential-dependent entropic contribution

would seem to be associated with the drastic difference between the two solution media, and their structures, on going from dilute aqueous acid solution to the monohydrate melt (essentially a molten salt of H_3O^+). Certainly a difference of this kind might qualitatively be expected.

Taking account of the experimentally-determined linear dependence of both $\Delta\bar{H}_V^{o\ddagger}$ and $\Delta\bar{S}_V^{o\ddagger}$ on potential, corresponding to eqn.(5-32), the current in eqn.(5-29) becomes

$$i(V) = kF \exp[(-\Delta H^{o\ddagger} + T\Delta S^{o\ddagger})/RT] \cdot \exp[\pm(\beta_H + \beta_S T)VF/RT] \quad (5\text{-}39)$$

Thus the Tafel slope, b, is found to be of the form given in eqn.(5-32) and consequently the conventional symmetry factor actually has the form

$$\beta = \beta_H + \beta_S T \quad (5\text{-}40)$$

A plot of b^{-1} *vs* T^{-1} should yield information on β_H and β_S, provided, of course, that in a particular case, $\Delta\bar{S}_V^{o\ddagger}$ has the form given in eqn.(5-38) and $\beta_S \neq 0$; this is the case when linear Tafel behaviour obtains. The result of eqn.(5-39) and eqn.(5-40) can account for those cases where the symmetry factor, β, varies linearly (increasing or decreasing) with temperature, as well as for the conventional case, viz. when $\beta_S = 0$ or when $\beta_S >> \beta_H$.

The expected temperature-dependence of the Tafel slope resulting from the experimentally determined values of β_H and β_S for the h.e.r. at Hg in these two media is given by eqn.(5-34). In the low temperature limit, b becomes proportional to T, while at high T, b approaches a limiting value (*cf.* eqn.(5-34)). When β_S and β_H are of opposite sign, as in the case of the h.e.r. from the melt $CF_3SO_3^-H_3O^+$, a singularity in b *vs* T will arise when $\beta_H = T\beta_S$; practically, this region where $\beta > 0$ (or even negative!)

will occur at elevated temperatures and may not be accessible experimentally but may correspond to the limiting kinetic behaviour that has been called[104] "barrierless".

Conway, Mackinnon and Tilak[74] proposed the empirical relation

$$b = 2.3RT/\beta'F + K \qquad (5\text{-}40)$$

to describe the temperature-dependence of b for the h.e.r. at Hg(see Chapter 2 and Fig.2-11). It is of interest to compare the agreement of the experimental b values at various temperatures found in the present work with eqns.(5-34) and (5-40). Plots of b vs T (eqn.(5-40)) and b^{-1} vs T^{-1} (eqn.(5-34)) for the h.e.r. at Hg from the $CF_3SO_3^-H_3O^+$ melt are shown in Fig.5-22a,b; the analogous results for the h.e.r. at Hg from 1 M aqueous CF_3SO_3H are given in Fig.5-23a,b. The data presented in both these figures are equally well represented by the empirical eqn.(5-40) or by eqn.(5-34). However, it is significant that eqn.(5-34) arises from consideration of the experimental potential-dependence of the enthalpy and entropy of activation, i.e., eqn.(5-34) is a consequence of the kinetic model for the proton discharge (in the h.e.r. at Hg) process. Analysis of b values over a wider range of temperatures than that accessible in the present study (due to the 309 K m.p. of $CF_3SO_3^-H_3O^+$) is desirable in deciding which of eqns.(5-34) and (5-40) better represents the experimental dependence of b on temperature. In a following section, this question will be considered in relation to the previously reported temperature-dependence of the Tafel slope for the h.e.r. at Hg in aqueous[69] (270 - 360 K) and methanolic[73,75]

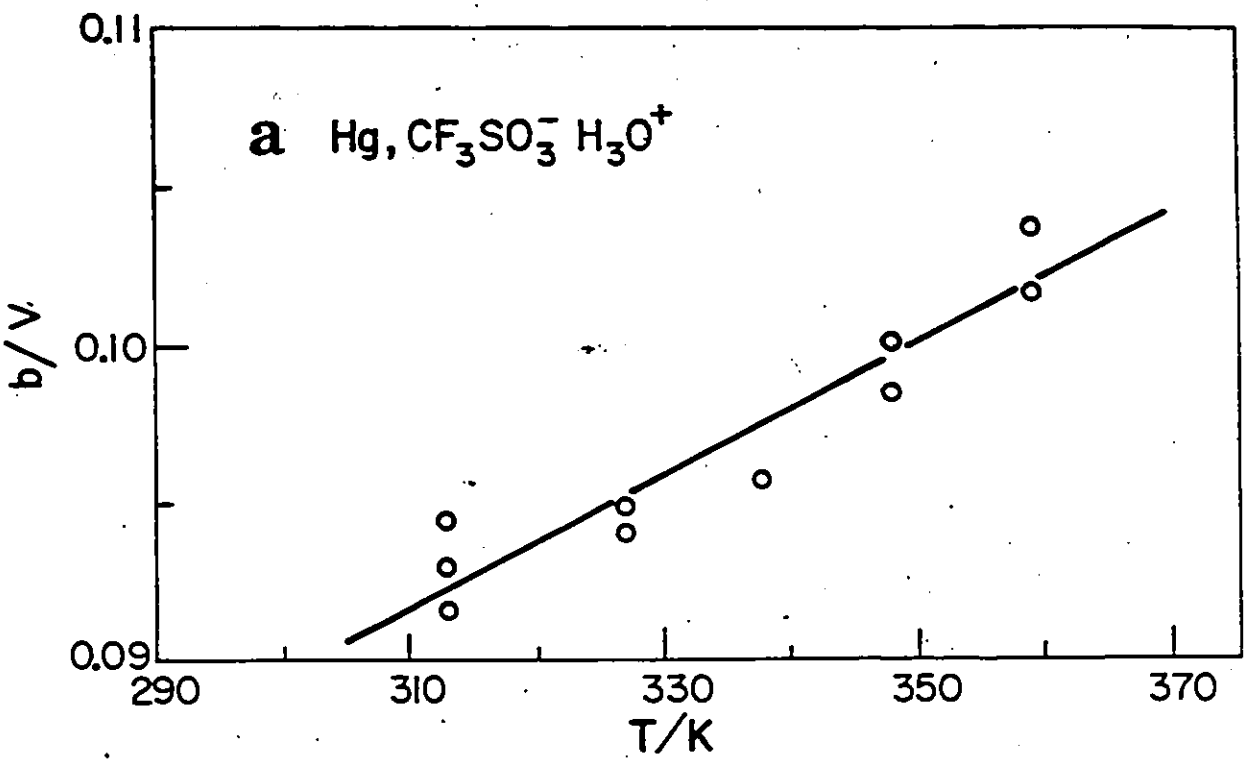

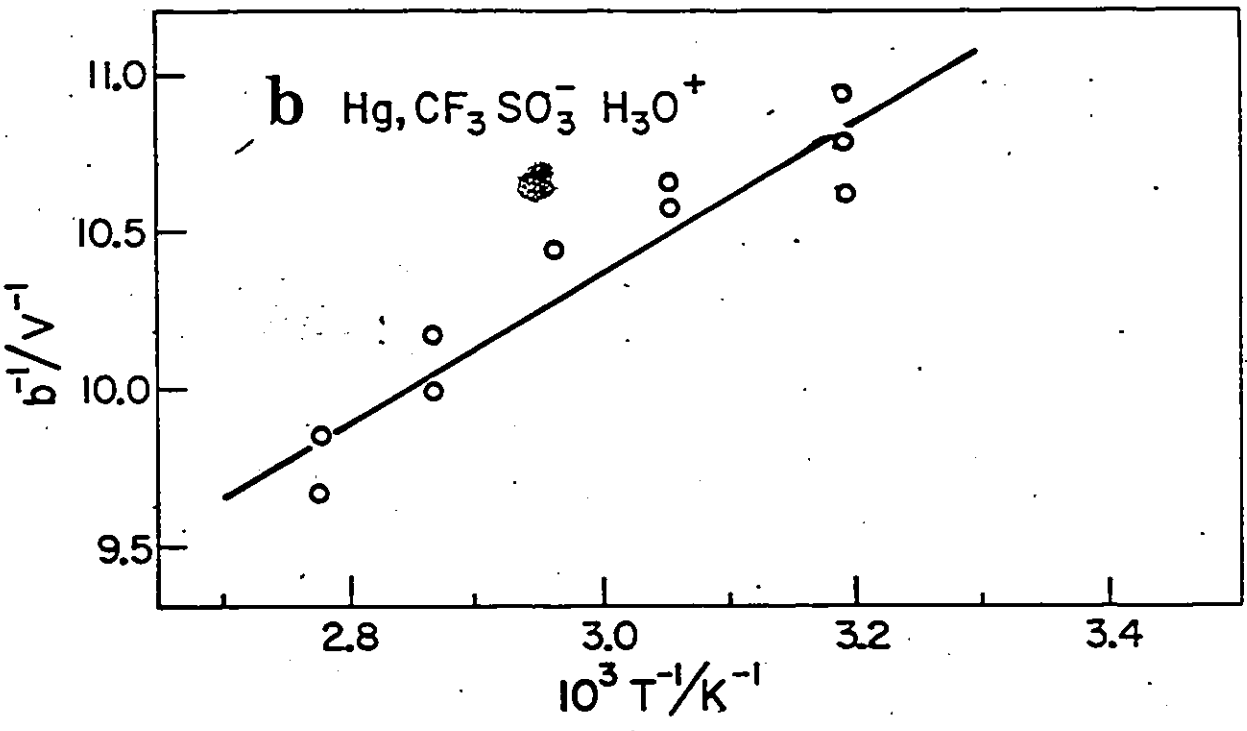

Fig.5-22 Temperature-dependence of the Tafel slope for the h.e.r. at Hg from $CF_3SO_3^-H_3O^+$: a) b vs T ; b) b^{-1} vs T^{-1}.

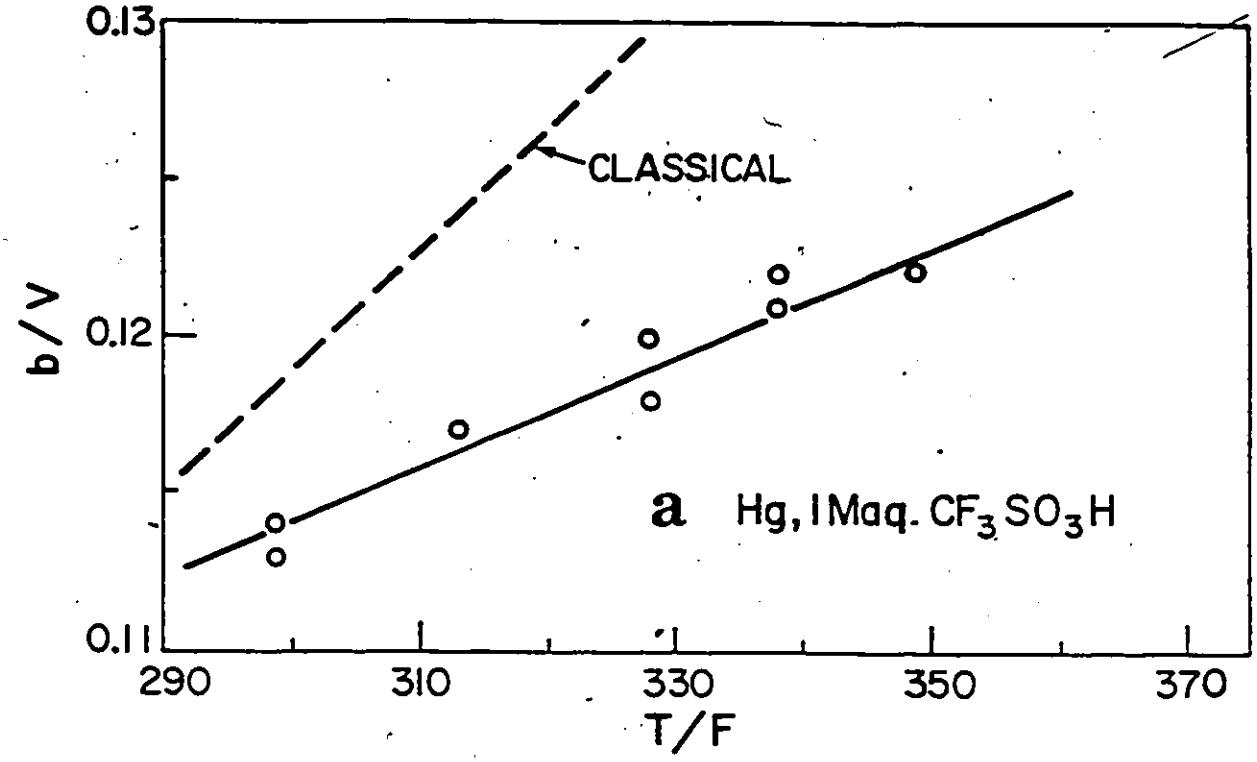

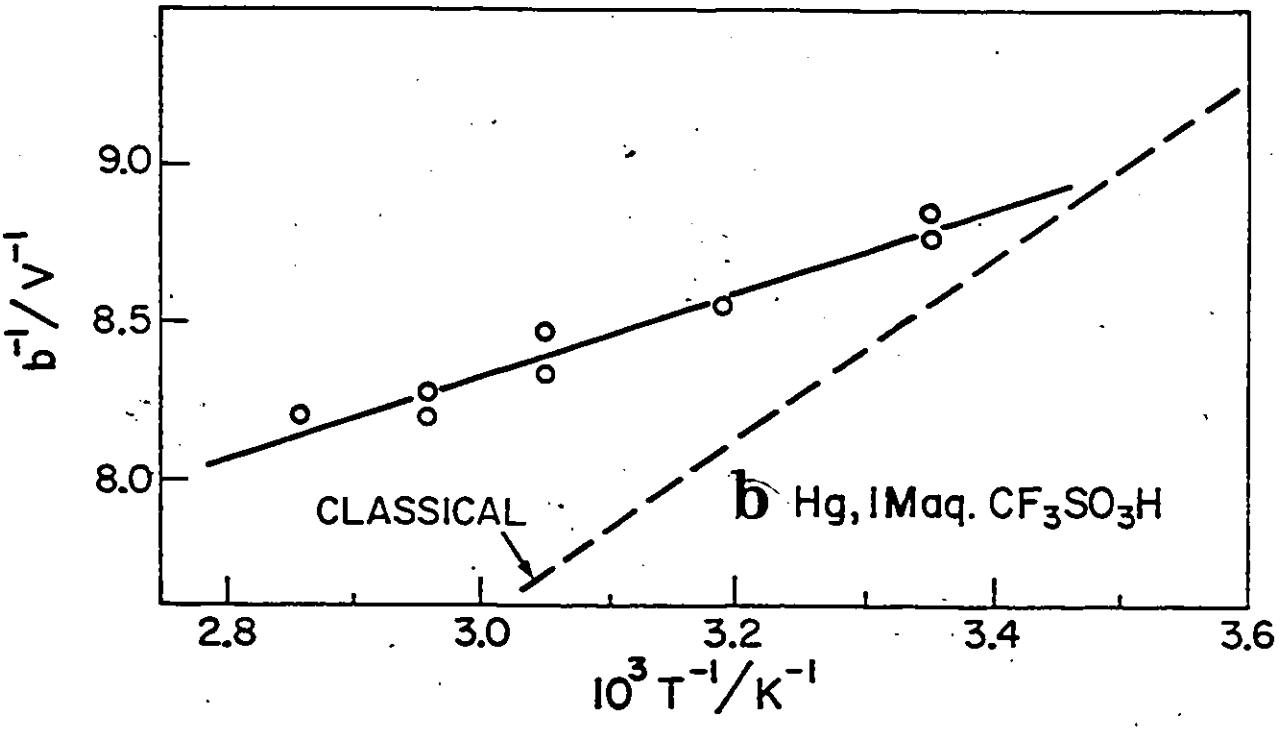

Fig.5-23 Temperature-dependence of the Tafel slope for the h.e.r. at Hg from 1 M CF_3SO_3H: a) b vs T ; b) b^{-1} vs T^{-1}.

(180 - 335 K) HCl over a greater range of temperature.

From the present results, a "non-conventional" temperature-dependence of the Tafel slope, and hence the symmetry factor, is expected to arise as a consequence of the significant contribution and the form of the potential-dependence of $\Delta\bar{S}_V^{o\ddagger}$ to the change in free energy of activation with applied potential.

Conway et al[74] reached this same conclusion, but from a different direction. In their study of the temperature-dependence of b, they showed how an apparent linear dependence of the symmetry factor, β, on temperature could result from a potential-dependent $\Delta\bar{S}_V^{o\ddagger}$ of the form given by eqn.(5-38) and now demonstrated experimentally in the present work. These authors suggested that the temperature-dependence of b might be explained in terms of electric field effects on the entropy of activation, e.g. through solvent orientation effects[70,222] in the inner region of the double-layer.

Qualitatively it can be seen how potential-dependence of the entropy of activation for proton discharge could arise: the environment of the transition complex for proton transfer and neutralization must be appreciably influenced by solvent dipole orientation in the double-layer field, the extent of which is known to be temperature- and potential-dependent in a correlated way. Thus the volume fractions of oriented water dipoles and hydrated protons in the double-layer can be shown[221] to be of comparable magnitude and both are dependent on electrode potential.

It is curious that these striking deviations of electrochemical kinetic behaviour from that expected conventionally have

not been recognized or treated in the recent quantum-mechanical approaches, e.g. of Levich, Kuznetsov and Dogonadze (e.g. see refs.51,81), to the interpretation of electrode reaction rates. The reasons for this may be traced to the emphasis which is placed in such treatments on quantal effects in the energy of the system and continuum modeling of the solution with neglect of the specific solvational-, and solvent-structure aspects that can lead, in aqueous media[132], to the important entropic factor in the kinetics.

(iv) Relation to Brønsted Behaviour for Homogeneous Proton Transfer

In the light of the above discussion of the temperature-dependence of β for electron/atom transfer, it would be of interest to examine the temperature-dependence of the Brønsted[6] coefficient α for homogeneous proton transfer reactions; unfortunately, the required values of α at several temperatures for a "well-behaved" system are unavailable. However, the dependence of $\Delta S^{\ddagger}$ on log K_a (or on ΔG_R°) for the homogeneous reaction provides a basis for comparison with the potential-dependence of $\Delta \bar{S}_V^{\circ\ddagger}$ for the h.e.r. In a kinetic study of the second de-protonation step of a series of intramolecularly H-bonded substituted malonic acids, Eyring et al[223] have found a linear Brønsted relation and a linear relationship between the enthalpy and entropy of activation for reactions of the type

$$AH^- + OH^- = A^{2-} + HOH \quad ; \qquad (5\text{-}41)$$

Thus, for such a series of homogeneous proton transfer reactions, the entropy of activation varies linearly with changes in ΔG_R° in a manner analogous to that found in the present work for the

potential-dependence (equivalent to changes in $\Delta G_R^o = -RT \ln K_a$) of $\Delta \bar{S}_V^{o\ddagger}$ for the h.e.r. at Hg. This variation in $\Delta S_R^{\ddagger}$, e.g. for reaction (5-41), may be expected to result in a temperature-dependence of α analogous to that discussed above for the electrochemical symmetry factor β.

Extension of the Brønsted relation to heterogeneous proton/electron transfer (Tafel behaviour) would seem to lead naturally to the possibility of a potential-dependent entropy of activation, in addition to the usually-assumed potential-dependent $\Delta \bar{H}_V^{o\ddagger}$; the observed temperature-dependence of β then follows limitingly as shown above.

(v) The sign of $\Delta \bar{S}_V^{o\ddagger}$

In the context of a particular reaction rate theory, the magnitude and sign of the entropy of activation are determined by the choice of standard state for reactant and activated complex[187,224] as well as by possible structural or electrostrictive changes (see also Appendix 1). For example, a standard state of 1 mol cm^{-3} for a bimolecular gas phase reaction yields $\Delta S^{\ddagger} \simeq 0$ for agreement with the collision theory; deviations in $\Delta S^{\ddagger}$ may then be interpreted in terms of changes in structural, steric and other factors involved in forming the activated complex. A number of reactions involving changes in state of charge exhibit entropies of activation which do not enable a unique choice between possible mechanisms to be made: (a) homogeneous nucleophilic substitution reactions[225] where the possible limiting $S_N2(1)$ and $S_N2(2)$ mechanisms may occur; (b) heterogeneous redox processes where inner- or outer-sphere

mechanisms operate[77]. In the inner-sphere case, specific adsorption of the reactant to form an anion-bridged intermediate is accompanied by the desorption of at least one water molecule, which results in a small net change in entropy, comparable to that for the alternate outer-sphere pathway[77]; (c) homogeneous electron transfer reactions which may proceed via inner- or outer-sphere routes[226].

Nonetheless it is interesting that the $\Delta\bar{S}_V^{o\ddagger}$ values for the h.e.r. are large and negative, as also deduced by Parsons and Bockris[48] for the h.e.r. at Hg from aq. HCl. According to general kinetic and solvational principles, this result is unexpected since, in a reaction involving loss of net charge, as in ion neutralization, the entropy change is expected to be dominated by electrostrictive factors and hence be positive. Actually for deposition of adsorbed H at Pt from H_3O^+ in acid solution the overall reaction entropy change is actually positive[227]. Normally, in homogeneous reactions involving extinction of charge, both the reaction entropy and the $\Delta\bar{S}_V^{o\ddagger}$ values are positive. The situation here with the h.e.r. is therefore unexpected in terms of electrostatic effects that are likely to be involved (see Appendix 1). A corresponding anomalously negative $\Delta V^{\ddagger}$ also arises[219]. Conway et al.[219] have suggested that this behaviour originates from a localization of the proton in the $H_9O_4^+$ complex[228] at the moment of proton transfer and neutralization so that a negative $\Delta V^{\ddagger}$ arises due to enhanced electrostriction. This effect which is particular to the proton in water, may cause the $\Delta\bar{S}_V^{o\ddagger}$ to be negative. However,

recently Conway et al.[229] have found similarly negative $\Delta\bar{S}_V^{o\ddagger}$ for anodic Br^- discharge at C in CH_3CN; this result suggests that this behaviour is not specific to the proton, but may be characteristic of coupled electron/atom transfer processes.

(vi) Models for the Potential-Dependence of $\Delta S^{\ddagger}$

(a) Energy and Entropy Change along the Reaction Coordinate

For homogeneous reactions, it is common to regard the course of entropy change from the initial to the final state of the reaction, through the transition state, as related to the course of the reaction "along the reaction coordinate" and the associated energy change. Thus in comparison of a series of similar reactions with regard to the relation between the free energy profiles and the linear free energy relationship, when the transition state "crossing region" becomes nearer to the initial state configuration, as the overall ΔG^o becomes more negative, the entropy of the transition state is regarded as becoming increasingly similar to that of the initial state. In this way, the entropy and configuration of the transition state has been regarded as taking some value intermediate between the entropy and configuration of the initial and final states. For some complex enzyme-catalysed reactions, Laidler and Banerjee[230] have made estimates of the entropy profile in relation to the enthalpy profile in the course of the reaction, sometimes for cases involving more than one step.

Applied in a simplistic way (Fig.5-24) to the effect of potential on reaction rates (through change of $\Delta\bar{G}_V^{o\ddagger}$), it would be found for the discharge step in the h.e.r. for example that with

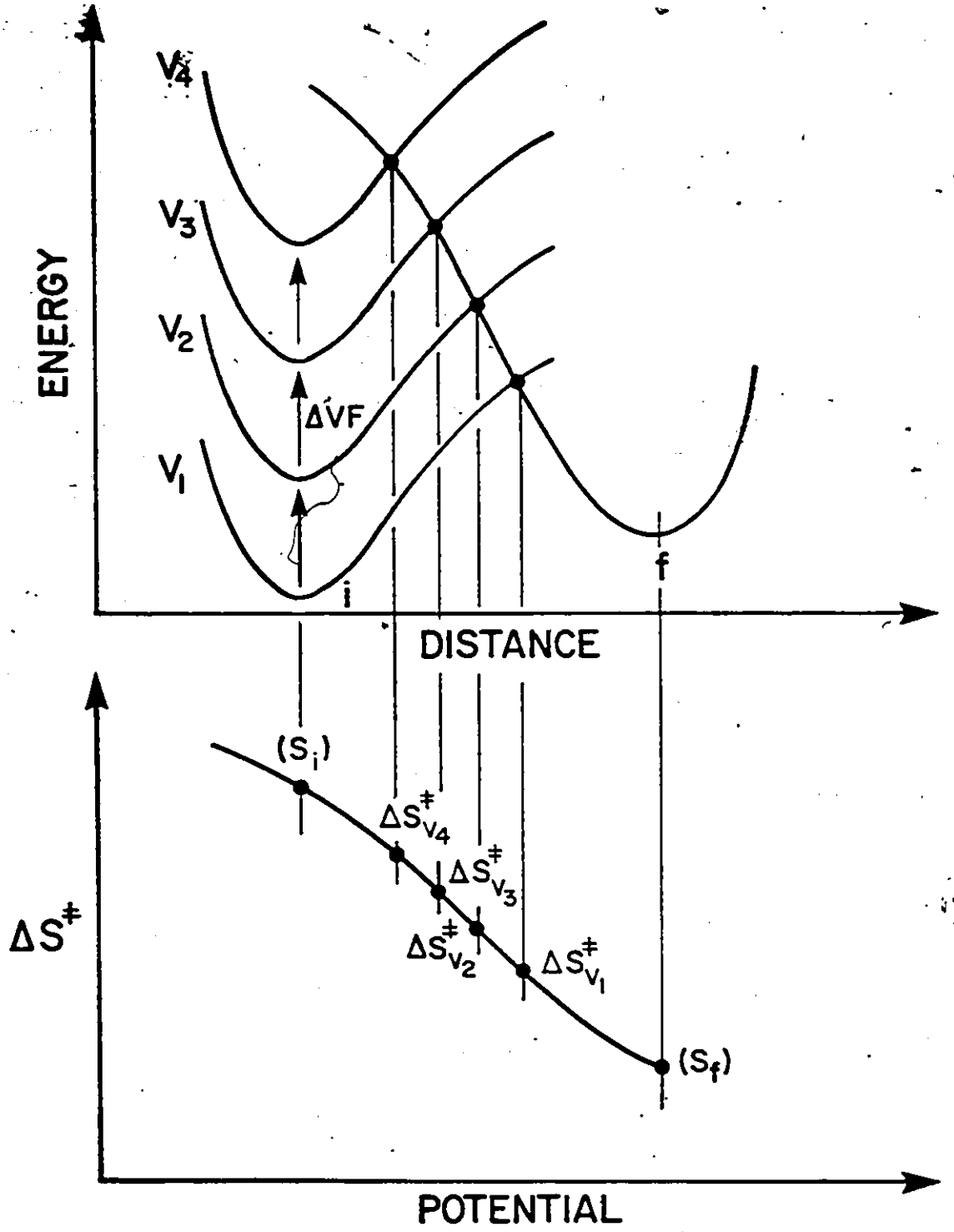

Fig.5-24 Schematic representation of effect of applied potential on heat and entropy of activation in heterogeneous electron transfer.

increasing overpotential, the transition state configuration would tend to become progressively more similar to that of the initial state, so that the corresponding entropy of activation would then be potential dependent. However, an important difference arises in the case of an heterogeneous electrochemical reaction: as potential changes, it is only the energy of electrons at the Fermi level that is changed, in the first approximation; the energy profile for the reactant species itself is usually assumed to be not materially changed as was discussed in sub-section (vii).

In the case of homogeneous reactions involving change of charge, it is usually possible from knowledge of the individual partial molar entropies of the ionic reactants, to evaluate the changes of entropy of the respective transition states, knowing the measured $\Delta S^{\ddagger}$ values from suitable kinetic measurements. However, in the case of an electrode reaction conducted at various potentials, it is not experimentally possible to evaluate the changes of reactant partial molar entropy in the double-layer as the potential is varied, so the approach conducted in the treatment of some homogeneous reactions cannot, unfortunately, be applied.

(b) State of Interaction of an Ion being Discharged with Polarized Solvent Dipoles in the Double-Layer

Near the potential of zero charge at Hg or at the potential of zero solvent dipole orientation[209] (for H_2O at $q_{Hg} = -2\ \mu C\ cm^{-2}$), reactant ions in the double-layer can experience maximum electrostatic interaction (orientation polarization of solvent by

the ion) with the surrounding medium adjacent to the electrode and thus acquire minimum entropy of solvation (maximum negative $\Delta S^{o}_{solvation}$). As the dipole polarization in the inner region of the double-layer increases with electrode potential, the entropy of solvation of ions in the double-layer will tend to become less negative because part of their solvation co-spheres will already be polarized by the field of the electrode surface charge (see schematic representation in Fig.5-25). Such an effect might be expected to lead to a less positive entropy change upon ion neutralization than for the zero-field situation. Such an effect may appear in the $\Delta S^{\neq}$ values derived from experiment but unfortunately it is very difficult to predict, even qualitatively, how such an effect of electrode charge would differentially affect the entropy of the transition state in relation to the entropy of the initial state. Also, in relation to the experimentally determined directions of change of $\Delta S^{\neq}$ with potential for the $CF_3SO_3^-H_3O^+$ melt and the 1 M aqueous CF_3SO_3H solution, it is not easy to account for the <u>different signs</u> of direction of the effects except to observe that in the case of the melt there is no inner layer of field-orientable solvent dipoles as there is in the dilute aqueous solution double-layer. However, for anodic discharge of Br^- in CH_3CN at C, in the complete absence of water, Conway et al.[229] have found that $\Delta S^{o\neq}_{V}$ also becomes more negative with increasingly favourable anodic potential; this behaviour parallels that found in the present work for the h.e.r. at Hg from the $CF_3SO_3^-H_3O^+$ melt.

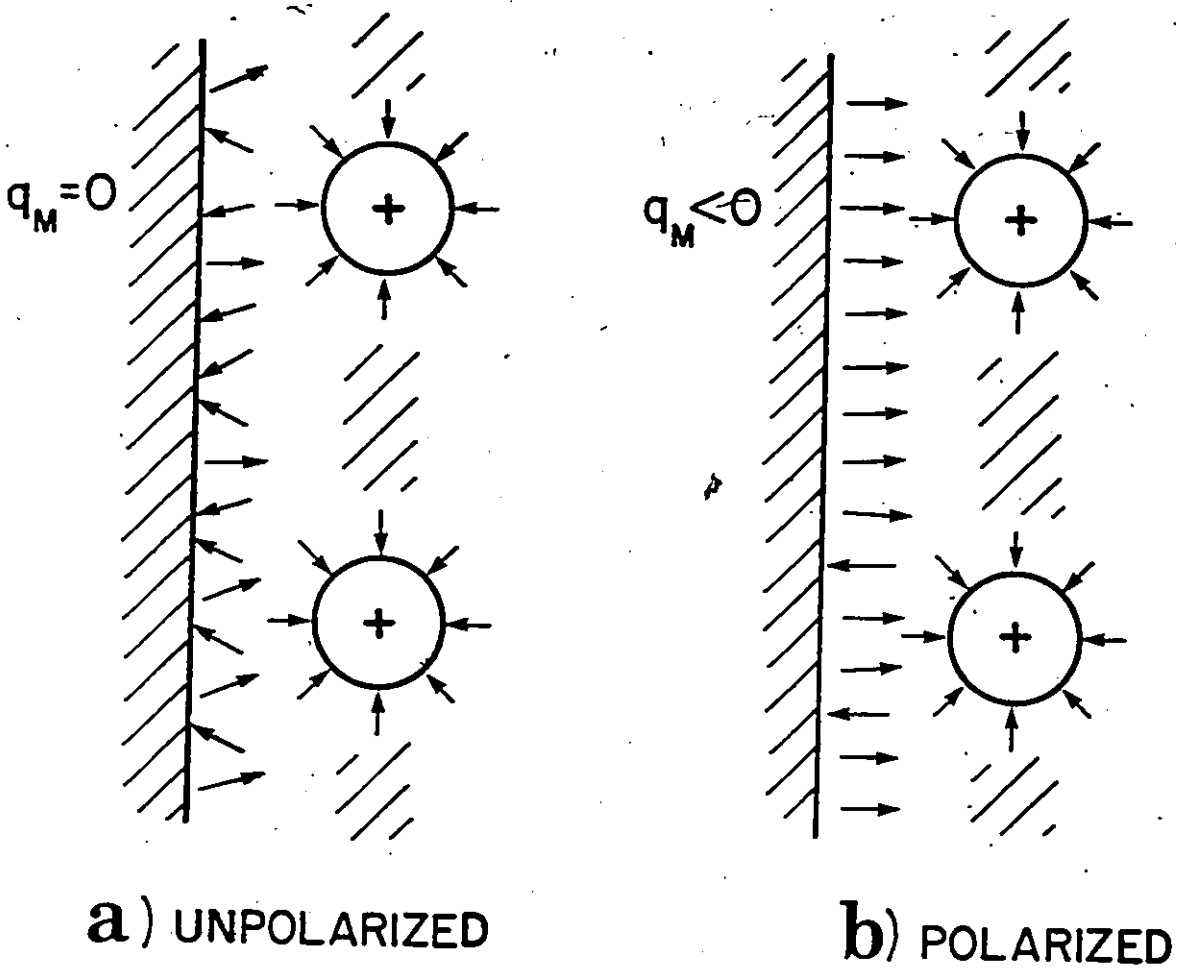

Fig.5-25 Schematic representation of the solvent dielectric polarization at an electrode surface accompanying ion neutralization.

(vii) The Potential-Dependence of $\Delta\bar{H}_V^{o\ddagger}$ and the Tafel Slope

We have referred above to the observed potential-dependence of $\Delta\bar{H}_V^{o\ddagger}$ (Fig.5-14) in relation to the Tafel slope and the effect of shifted Fermi level with potential which is associated with energic components, β_H, of the symmetry factor.

With regard to the measured dependence of $\Delta\bar{H}_V^{o\ddagger}$ on electrode potential, the question arises to what extent the chemical bond energy, e.g. of H chemisorbed on an electrode metal, may itself be dependent on the local electrode field in which the bond is situated. Moelwyn-Hughes[231] has given some polarizability data for polar diatomic molecules involving H. E.g. for HF, $\alpha_p = 0.30$ and for HCl, 1.74×10^{-24} cm^3. Taking a field of say 10^5 e.s.u., corresponding approximately to a rational potential of 1 V at Hg, we see that the polarization energy of an "M-H" bond in the double-layer at an appreciable overpotential will be only 0.09 kJ mol^{-1} for $\alpha_p = 0.3 \times 10^{-24}$ or 0.52 kJ mol^{-1} for $\alpha_p = 1.74 \times 10^{-24}$ cm^3, i.e. negligible. This corresponds with the recent observations from in situ-IR studies that chemisorption bond vibrational frequencies, e.g. for CO on Pt[232,233], vary with potential only by ca. 10 cm^{-1} V^{-1}, i.e. by ca. 0.1 kJ mol^{-1}.

An alternative estimate of this effect could be made on the basis of change of electronegativity χ of the metal M with changing electrode surface charge. Thus at relatively large surface charge-density of 20 μC cm^{-2}, the change of electron density per atom of the surface is ca. 0.1 with respect to the situation at the p.z.c. This is approximately equal to the net charge on e.g. the atoms of a C-H bond (dipole moment $\mu = 0.4$ D). χ will tend to become smaller with increasing cathodic potential.

However, since the $(\chi_M - \chi_H)^2$ in the Eley-Pauling relation[234] for chemisorption bonds constitutes itself only ca. 10% to the bond energy, it is unlikely that the change of electronegativity of M with electrode potential, and hence M-H bond energy, could be significant compared with the direct effect of V on the Fermi level.

(viii) Previous Work on the Temperature-Dependence of b in Relation to $\Delta\bar{H}_V^{o\ddagger}$ and $\Delta\bar{S}_V^{o\ddagger}$

We have seen in the present work on the h.e.r. at Hg how the potential-dependence of log[frequency factor] and hence $\Delta\bar{S}_V^{o\ddagger}$ results in an apparantly "anomalous" temperature-dependence of b. In this section this behaviour will be compared with previous work on the h.e.r. at Hg from acid solution and on the kinetics of O_2 reduction. "True" activation parameters were not derived from the experimental results in the studies to be considered below; the temperature-dependence of b in these works may be used to assess the representations for this dependence given in the empirical relation[74] eqn.(5-40) and in eqn.(5-34) which is indicated from potential-dependence of the activation parameters found in the present work. For a detailed survey of examples of the experimentally observed dependence of b on T, see the recent review by Conway in ref.123.

a) H.E.R. at Hg from Aqueous and Methanolic HCl

Post and Hiskey[69] studied the h.e.r. at Hg in 0.1 M aq. HCl; their values for the Tafel slope, b, as a function of temperature

are shown in detail in Fig.5-26. The results of Conway and Salomon[73,75] for the h.e.r. at Hg from 1 M HCl in methanol are also presented in this figure. As noted in Chapter 2, both these sets of experimental results differ significantly from the classical behaviour (dashed line in Fig.5-26) which is given by $b = 2.3\ RT/\beta F$, with β taken as 0.5; in this latter hypothetical conventional case, the b *vs* T line passes through the origin of the plot, while extrapolation of the apparently linear experimental data leads to a finite non-zero intercept as $T \to 0$. This behaviour led Conway, Mackinnon and Tilak[74] to propose the empirical relation, eqn.(5-40), to represent the "anomalous" temperature-dependence of b.

The experimental results for the potential-dependence of $\Delta\bar{S}_V^{o\neq}$ in the present work suggested the alternate form for b as f(T) in eqn.(5-34) (for which $b \to 0$ as $T \to 0$), i.e., b^{-1} should be linear in T^{-1} with a slope and an intercept related to β_H and β_S respectively. A plot of b^{-1} *vs* T^{-1} for the h.e.r. at Hg in aqueous[69] and methanolic[73,75] solutions is shown in Fig.5-27 along with the "conventional" behaviour (as above, dashed line). The data seem to fall on two straight lines, as expected from eqn.(5-34). In fact, lines drawn though the respective sets of results in Figs.5-26 and 5-27 represent the experimental behaviour equally well, despite the considerably larger range of temperatures used in these studies compared with that used in the present work in the $CF_3SO_3^-H_3O^+$ melt and 1 M aq. CF_3SO_3H systems. In order for a choice between eqns.(5-34) and (5-40) for the temperature-dependence of b to be made, investigations over an even greater range of temperature seem to be required; this

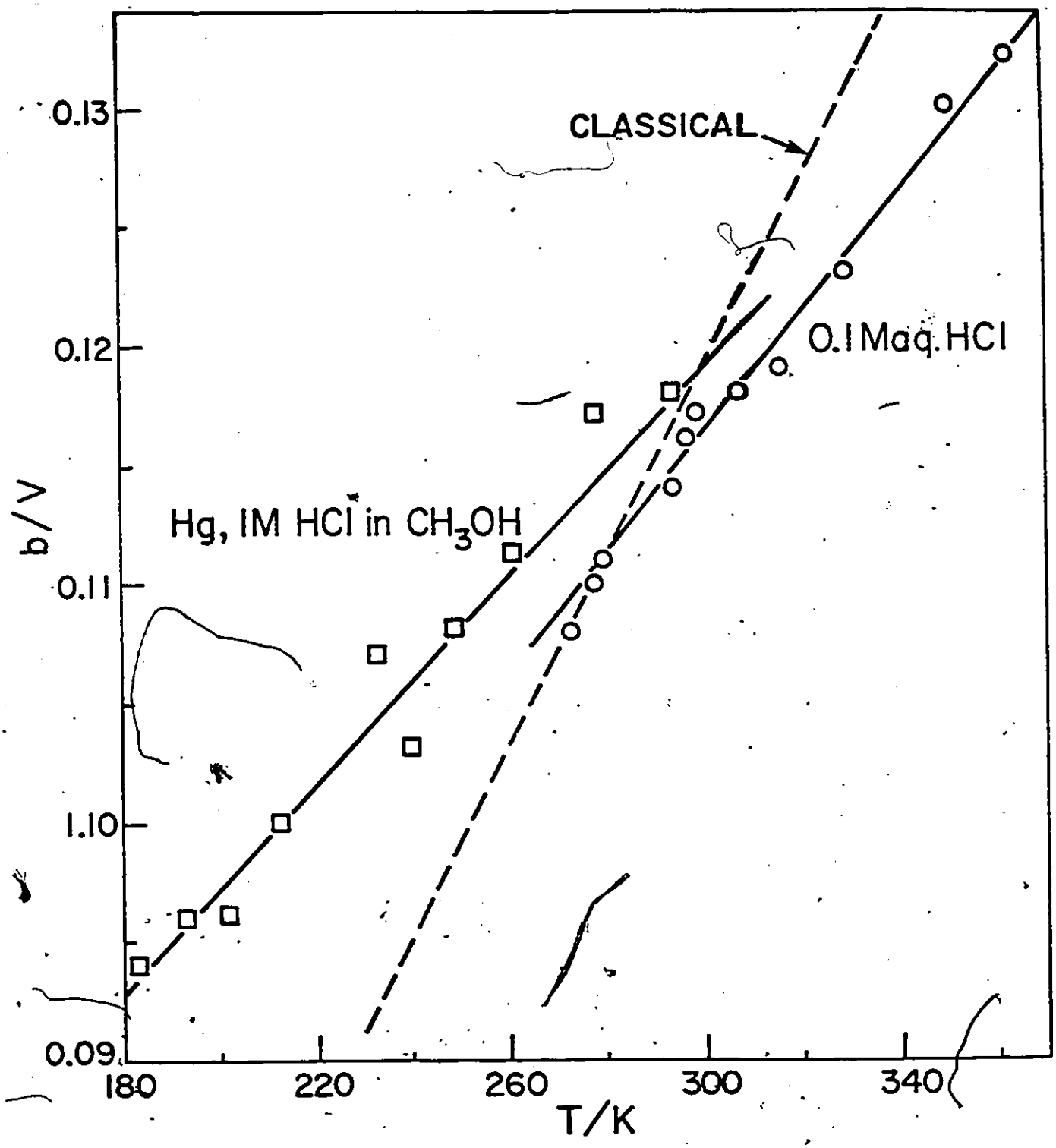

Fig.5-26 Temperature-dependence of b for the h.e.r. at Hg from aqueous[69] and methanolic[73,75] HCl.

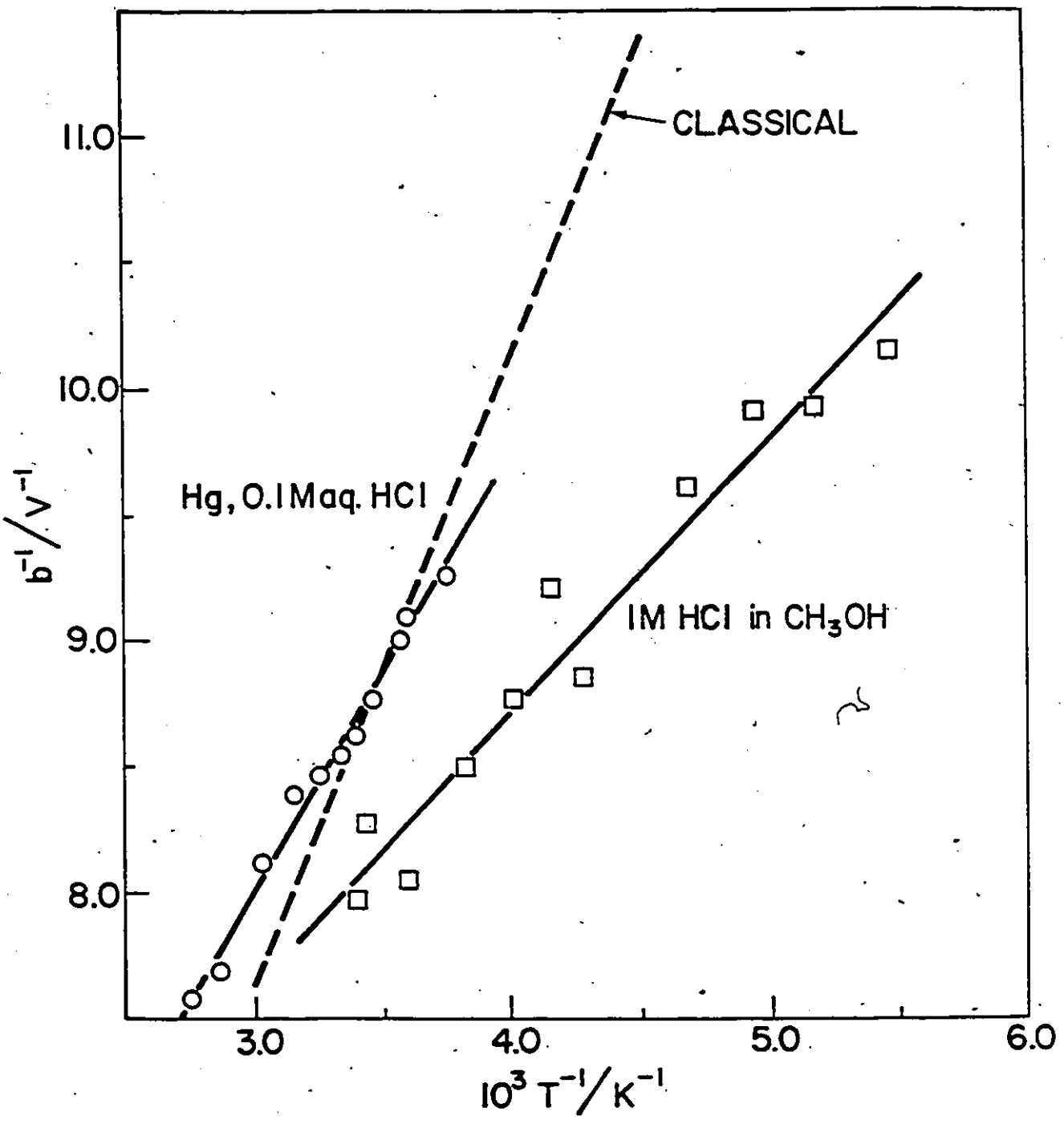

Fig.5-27 Dependence of b^{-1} on T^{-1} for the h.e.r. at Hg from aqueous[69] and methanolic[73,75] HCl.

approach is being pursued in ongoing research in this laboratory.

Examination of the b vs T behaviour expected from the β_H and β_S values found in the present work (according to eqn.(5-34)) shows that detection of the expected curvature in b vs T indeed requires consideration of a larger range of temperatures than that involved in the above work.

Values of β_H (= R/F x slope) and β_S (= R/F x intercept) for the h.e.r. at Hg in the above aqueous[69] and methanolic[73,75] HCl solutions can be derived from the slopes and intercepts of the b^{-1} vs T^{-1} relations in Fig.5-27, according to eqn.(5-34); the resulting values are shown in Table 5-9.

Table 5-9

β_H and β_S for the H.E.R. at Hg in Aqueous and Methanolic HCl Solutions* (refs.69,73,75)

System	β_H	$10^4 \beta_S/K^{-1}$	$\beta = \pm 2.303RT/bF$
0.1 M aq. HCl	0.35	+5.4	0.51
1.0 M HCl in CH_3OH	0.21	+9.7	0.50

* Derived from plots of b^{-1} vs T^{-1} (Fig.5-25) according to eqn.(5-34).

For both solutions, the resulting enthalpic β_H values do not account for the net "activation efficiency", β, of ca. 0.5 (298 K); the entropic β_S values are both positive and hence lead to the observed $\beta = \beta_H + T\beta_S = 0.5$ (298 K). This behaviour is similar to that found in the present work for the h.e.r. at Hg in 1 M aq. CF_3SO_3H in that $\beta_H < \beta$ and $\beta_S > 0$. The effect of going from aqueous to methanolic medium would seem to be to increase

the entropic factor β_S with a compensating change in β_H so that the net symmetry factor, β, remains constant (ca. 0.5); the difference in HCl concentration and Cl^- adsorption in these two media may also influence the values of β_H and β_S.

Thus, the behaviour of b as f(T) yields reasonable values of β_H and β_S, comparable to those derived from the analysis given in Section 5(ii) of the potential dependence of activation parameters.

b) Cathodic O_2 Reduction in H_3PO_4

Appleby[133] and later Yeager[128] found b to be constant with temperature for O_2 reduction at Os and Pt (see Chapter 2) in H_3PO_4; the temperature dependence of α (=2.3RT/bF) for O_2 reduction at Pt in H_3PO_4 was shown in Fig.2-12. In terms of enthalpic, α_H, and entropic, α_S, components of the transfer coefficient, this behaviour (Fig.2-12) corresponds to $\alpha_H < T\alpha_S$ over most of the temperature range (i.e. from Fig.2-12, extrapolation of α ($=\alpha_H + T\alpha_S$) to T = 0 yields α = 0.04). Thus, in this case, only a small enthalpic contribution to α seems to be indicated, while the entropic component $T\alpha_S$ is dominant in determining the net transfer coefficient α. This suggests that the exponential dependence of reaction rate on potential results primarily from the effect of applied potential on the entropy and not on the enthalpy (or energy) of activation. Although one can envisage that some change in $\Delta\bar{S}_V^{o\ddagger}$ might occur with potential, it is difficult to see, within the usual electrochemical Brønsted view, how a shift in the electron Fermi level of the metal, associated with a change of electrode potential, would not always result in

a significant change in energy of activation.

7. Anodic Processes at Pt in $CF_3SO_3^-H_3O^+$

At anodically polarized Pt electrodes in dilute aqueous acid solution, oxygen atoms from the H_2O solvent are incorporated into a growing surface oxide film or appear in evolved oxygen molecules. In the $CF_3SO_3^-H_3O^+$ melt, these anodic processes could conceivably involve oxygen from the $CF_3SO_3^-$ anion as well as, or alternatively from H_3O^+. Oxyanions (e.g. SO_4^{2-}, ClO_4^-) are known to be adsorbed and react anodically from concentrated aqueous solution at noble metal electrodes[235,235]. In addition to yielding specific decomposition products (e.g., persulfate, ClO_2, ...), labelling experiments show that these anions contribute oxygen atoms to the anodically produced oxygen gas. Thus it was of some interest to examine the source of O in O_2 evolution at Pt from the "anhydrous" $CF_3SO_3^-H_3O^+$ melt and the formation of a surface oxide film at Pt.

(i) Source of O in Evolved O_2

The source of O atoms in the O_2 evolved at Pt in $CF_3SO_3^-H_3O^+$ was determined by electrolysis of $CF_3S^{18}O_3^-H_3O^+$ prepared as described in Chapter 3.

A freshly prepared sample of the monohydrate, ^{18}O-labelled on the anion, was allowed to stand for 24 h (313 K) in order to examine if significant $^{18}O/^{16}O$ exchange between the $CF_3SO_3^-$ anion and H_3O^+ took place; this sample was then diluted with isotopically normal water and distilled (reduced pressure, 313 K). The water distillate was analyzed by negative ion mass spectrometry; the $^{16}O^-$ and $^{18}O^-$ ion intensities in the mass

spectrum indicated a ratio $^{16}O^-/^{18}O^-$ = 200:1; the signal attributed to $^{18}O^-$ also included residual background H_2O^- or OD^-. The positive ion mass spectrum of the water distillate indicated $H_2{}^{16}O^+/H_2{}^{18}O^+$ = 100:0.37 ; in this case the peak at m/e = 20 includes any residual background HF^+ and D_2O^+ ions. In view of the natural abundance (0.2 %) of ^{18}O, this result indicates that O-exchange between $CF_3SO_3^-H_3O^+$ and H_3O^+ in the melt is not significant. Nonetheless, the $CF_3S^{18}O_3^-H_3O^+$ was prepared from the labelled acid just prior to its use in the O_2 evolution experiments.

O_2 was evolved at a Pt anode (10 and 50 mA cm^{-2}) and the gas produced collected for analysis by positive ion mass spectrometry. Only the natural abundance of ^{18}O in the O_2 produced was found at the two current densities and hence the O atoms in the evolved O_2 originate from the H_3O^+ and not from the $CF_3SO_3^-$ anion. This is an interesting situation since this result indicates that the process involves the oxidation of a positive H_3O^+ ion at the positively charged anode surface; some cooperative mechanism of OH or O discharge from H_3O^+, e.g. involving anions in the melt, may operate and facilitate the otherwise electrostatically unfavourable direct oxidation of the H_3O^+ cation at the anode.

At oxygen evolving Pt and Ir anodes in dilute aqueous CF_3SO_3H, Miles et al.[237] found no interference from the anodic decomposition of the $CF_3SO_3^-$ anion; however, as noted above, the present $CF_3SO_3^-H_3O^+$ melt might be expected to show different behaviour from that in dilute aqueous solution. In the present

work in $CF_3SO_3^-H_3O^+$, no C- or F-containing gaseous products which might indicate the degradation of the $CF_3SO_3^-$ anion were found in the evolved O_2 samples.

(ii) Surface Oxide Formation at Pt

The formation of a thin surface oxide at Pt in $CF_3SO_3^-H_3O^+$ under potentiodynamic conditions is indicated in the cyclic-voltammogram of Fig.5-3; the onset of surface oxide deposition from the $CF_3SO_3^-H_3O^+$ melt occurs at a potential ca. 0.2 V RHE more positive than from 1 M CF_3SO_3H owing to anion adsorption effects. In this section, the growth law for surface oxide formation at constant potential at Pt from $CF_3SO_3^-H_3O^+$ will be examined briefly.

The quantity of oxide formed upon holding the potential in the region of surface oxidation for a time t_{ox} was determined by integration of the I vs V profile for reduction of the oxide film under cyclic-voltammetry conditions as described previously[208]. The potential programme used is shown in Fig.5-28: the oxide film is grown at potential V_{ox} (II, Fig.5-28) for times t_{ox} = 0.01 - 20 s and then is reduced in an analyzing cathodic sweep (s = 10 V s^{-1}, III); each oxide growth/reduction period is preceded by a surface equilibration potential arrest (I) at a potential just prior to the onset of surface oxidation and followed by a full conditioning cycle (10 V s^{-1}, IV)) between the potential limits V_C and V_A. The absence of surface roughening during the course of the oxide growth experiments was indicated from the invariant I vs V profile in the conditioning cycles.

The growth of Pt oxide at 1.251 V RHE in $CF_3SO_3^-H_3O^+$ obeys a

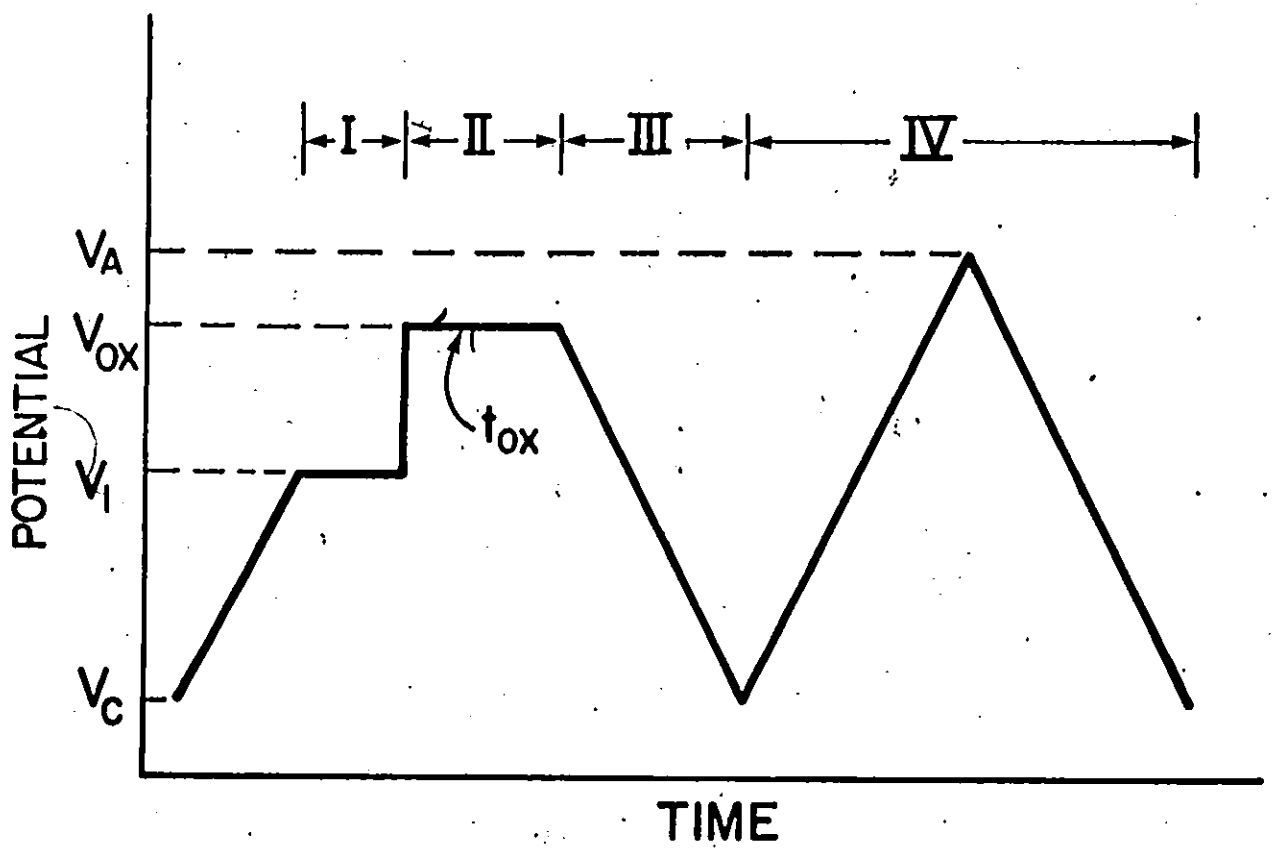

Fig.5-28 Potential-time programme for the study of the kinetics of growth of Pt oxide at constant potential, V_{ox}, for programmed periods of time, t_{ox}.

direct logarithmic law in growth time, t_{ox}, as shown in Fig.5-29. This behaviour parallels that found at Pt in dilute aqueous acid solution[208]. The region of the growth curve shown in Fig.5-29 lies below 210 $\mu C\ cm^{-2}$ ($\equiv$ 1 e^- per surface Pt atom) and hence corresponds to the formation of a sub-monolayer oxide film.

The studies of Rosenthal et al.[238] using ^{18}O-labelled water have shown that O_2 gas anodically evolved at Pt contains ^{18}O from the oxide layer on this metal. Although this result does not definitively demonstrate the participation of surface adsorbed oxygen atoms on Pt in the O_2 evolution reaction[239], the absence of ^{18}O in the O_2 gas produced at Pt from $CF_3SO_3^-H_3O^+$ in the present work strongly suggests that the O involved in the formation of the surface oxide film at Pt also originates from H_3O^+ ions.

It would be of interest to study the transition from sub-monolayer to thicker oxide film growth at Pt in this medium; in dilute aqueous acid, the growth curve (analogous to that in Fig.5-29) extends linearly well beyond the monolayer stage. In a recent radiotracer and <u>in situ</u> FT-IR study of the adsorption of $CF_3SO_3^-$ at Pt from solutions of the dilute aqueous acid, Zelenay et al.[240] have suggested that $CF_3SO_3^-$ may be incorporated <u>into</u> the growing oxide film, but further work in this area is required.

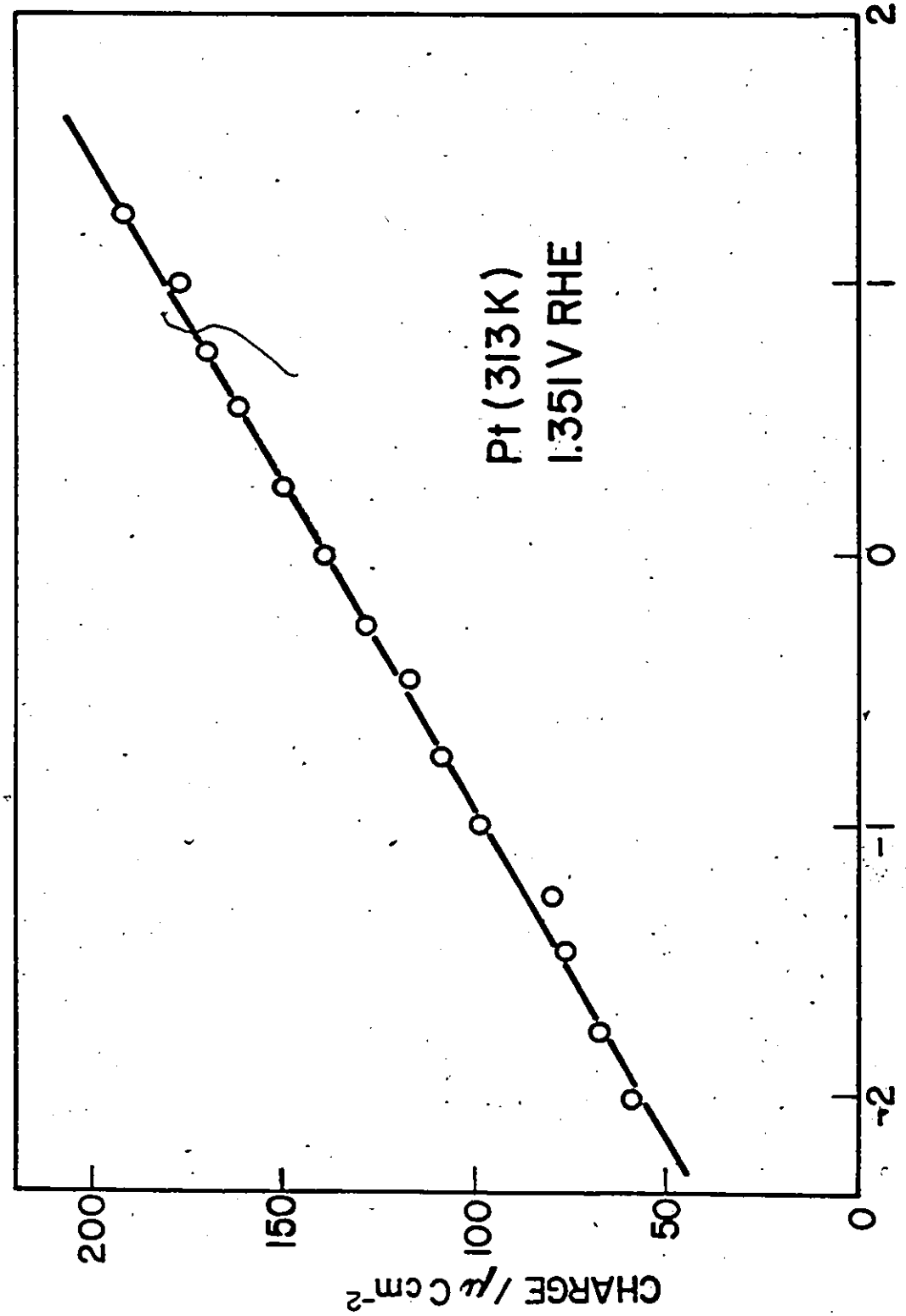

Fig.5-29 Oxide charge as a function of log[time] for growth of Pt oxide at constant potential, V_{ox}, as indicated in the figure.

APPENDIX 1

The entropies of activation treated above were derived from the intercepts, B, of electrochemical Arrhenius plots at constant metal-solution potential difference according to

$$\Delta S_V^{o\ddagger} = R[\ B - \ln(zFAc(1-\theta)kT/h)\ ] \qquad (A\text{-}1)$$

where c_b is the bulk concentration in mol cm^{-3} and θ is the coverage by H (or Br) assumed << 1 so that $1-\theta = 1$.

In the derivation of the rates of electrode processes according to activated-complex theory, a standard state of 1 mol cm^{-2} is usually taken for the activated complex, while quite another standard state is invoked for the unoccupied metal sites; thus the two surface "species" are treated differently. For consistency then, one might identify the quantity $1-\theta$ (for $\theta > 0$) with the concentration in mol cm^{-2} of bare metal sites, viz. $c_M \cong 1 \times 10^{15}/6.02 \times 10^{23} = 1.66 \times 10^{-9}$ mole cm^{-2}. Ignoring activity coefficient effects, then one should replace the $(1-\theta)$ in eqn.A1 with this number. This then will make the resulting entropies of activation more positive by an amount $-R \ln(1.66 \times 10^{-9}) = 168$ J K^{-1} mol^{-1}.

In a similar fashion, the concentration of reacting ion might alternatively be expressed in mol cm^{-2}; hence if reaction occurs from a solution layer of thickness δ adjacent to the electrode surface, the surface concentration then is approximately given by $c_s = c_b$ mol $cm^{-3} \times 1\ cm^2 \times \delta$ cm, which for $\delta = 2.0 \times 10^{-8}$ cm, yields $c_s = c_b \times 2.0 \times 10^{-8}$ mol cm^{-2}. This approach leads to entropies of activation more positive than

those calculated above by an amount $-R \ln(c_b \times 2.0 \times 10^{-8}/c_b) = 147 \text{ J K}^{-1} \text{ mol}^{-1}$.

When these corrections are applied to the results reported in the present work, entropy of activation values that are only slightly negative or even positive then result. Thus considerable caution should be exercised in rationalizing or interpreting the sign and/or magnitude of entropies of activation; an enlightened choice of standard states can enable certain contributions to the entropy changes (e.g. configurational entropy) to be effectively "tared off" so that any residual entropy change can then be interpreted in terms of specific molecular effects (e.g. electrostriction, structural factors, steric hindrance). Failing this, comparative results from an homologous series of electrochemical proton transfer reactants (as in work in progress in this laboratory on the h.e.r. from various solvents or proton sources) may allow some useful conclusions still to be drawn from the relative ordering of the respective values of the entropy of activation.

CONTRIBUTIONS TO ORIGINAL RESEARCH

A comparative study was made of the rates of the h.e.r. at Hg, Ni and Pt electrodes in the monohydrate melt $CF_3SO_3^-H_3O^+$ and in 1 M aqueous CF_3SO_3H. Large differences in relative rates and in *direction* of relative rates for the h.e.r. from these two media was found, depending on cathode metal and, in the case of Hg, where different Tafel slopes are obtained in the two media, also on electrode potential.

The kinetics electrochemical desorption of H at Pt was investigated in the $CF_3SO_3^-H_3O^+$ melt and in 1 M aqueous CF_3SO_3H by means of linear potential sweep cyclic-voltammetry. Criteria were described for assessing the possible interference of uncompensated solution resistance in the determination of s_o by the LPS technique of Angerstein-Kozlowska and Conway. The derived s_o values were found to be ca. 10 x larger for desorption in dilute 1 M acid solution solution than in the ca. 10.8 M monohydrate melt.

Apparent differences in heats of activation and frequency factor ratios for the h.e.r. and the desorption of H at Pt were derived from the temperature-dependence of rates in the $CF_3SO_3^-H_3O^+$ melt and in 1 M aqueous CF_3SO_3H.

By means of non-isothermal cell measurements, "true" activation parameters for the h.e.r. at Hg were derived as a function of potential; the true entropy of activation or the corresponding frequency factor for the proton discharge step in the cathodic h.e.r. is found to be appreciably potential-

dependent, and not constant as usually assumed. Possible origins of this significant entropic contribution to the potential-dependence of rates of coupled electron/atom transfer processes are proposed.

Implications of this potential-dependent entropy of activation in relation to the important question of the temperature-dependence of Tafel slopes were considered; a temperature-dependent Tafel slope of the form $b = \pm 2.3RT/(\beta_H + \beta_S T)$ was shown to be expected where β_H and $\beta_S T$ are enthalpic and entropic components, respectively, of the overall symmetry factor, β.

H/D kinetic isotope effects for the h.e.r. at Hg and for desorption of H at Pt in the monohydrate melt and in 1 M aqueous CF_3SO_3H were evaluated; the results did not show the large values of k_H/k_D or the isotope-mass dependent Tafel slopes which would indicate the presence of a significant or appreciable degree of proton tunneling.

In ^{18}O labelling experiments, the H_3O^+ ion in the monohydrate melt and <u>not</u> the $CF_3SO_3^-$ anion was shown to be the source of O in O_2 gas evolved at Pt from this medium. No evidence of gaseous decomposition products of the anion were found.

The growth of a thin surface oxide film at Pt in the $CF_3SO_3^-$ H_3O^+ melt was shown to follow linear log[time] growth kinetics. The anodic reaction of H_3O^+ in the $CF_3SO_3^-$ melt to form a surface oxide or oxygen gas is somewhat novel since, at least formally, it involves the oxidation of a positively charged ion.

REFERENCES

1. A.N. Frumkin in "Advances in Electrochemistry and Electrochemical Engineering", vol.3, P. Delahay and C. Tobias, Eds., Wiley Interscience, N.Y., 1963, p.287.
2. J.O'M. Bockris, in "Modern Aspects of Electrochemistry", vol.1, J.O'M. Bockris and B.E. Conway, Eds., Butterworths, London, 1954, p.180.
3. R.W. Gurney, Proc. Roy. Soc. (London), **A134**(1931)137.
4. H. Eyring, S. Glasstone, and K.J. Laidler, J. Chem. Phys.,**7**(1939)1053.
5. J. Horiuti, Okamoto, and Hirota, Sci. Pap. Inst. Physic. Chem. Res. Tokyo, **29**(1936)233.
6. R. Parsons, Trans. Faraday Soc., **47**(1951)1332.
7. D.C. Walker, Can. J. Chem., **45**(1967)807; Anal. Chem., **39**(1967)896.
8. T. Pyle and C. Roberts, J. Electrochem. Soc., 115(1968)247.
9. B.N. Kabanov, D.I. Leikis, I.G. Kiseleva, I.I. Astakhov, and D.P. Aleksandrov, Doklady Akad. Nauk SSSR, **144**(1962)1085.
10. B.E. Conway and M. Salomon, Electrochim. Acta, **9**(1964)1599.
11. A.N. Frumkin in "Advances in Electrochemistry and Electrochemical Engineering", vol.1, P. Delahay and C. Tobias, Eds., Wiley Interscience, N.Y., 1961.
12. B.E. Conway in "Modern Aspects of Electrochemistry", vol.7, B.E. Conway and J.O'M. Bockris, Eds., Plenum Press, N.Y., 1972.
13. B.E. Conway and D.J. MacKinnon, J. Phys. Chem., **74**(1970)3663.

14. J. Horiuti, 17-th Reunion, CITCE, Tokyo, 1966.

15. J. Tafel, Z. phys. Chem., 50(1905)641.

16. J.O'M. Bockris, J. Chem. Phys., 24(1956)817.

17. J. Horiuti and M. Ikusima, Proc. Imp. Acad. Tokyo, 15(1939)39.

18. E. Gileadi in ref.35, Chapter 8, p.262.

19. T. Langmuir, J. Am. Chem. Soc., 40(1918)1361,1403; ibid, 54(1932)2798.

20. B.E. Conway and E. Gileadi, Trans. Faraday Soc., 58(1962)2493.

21. S. Srinivasan and E. Gileadi, Electrochim. Acta, 11(1966)321.

22. J.G.N. Thomas, Trans. Faraday Soc., 57(1961)1603.

23. E. Gileadi and B.E. Conway, J. Chem. Phys., 39(1963)3420.

24. J.A.V. Butler, Proc. Roy. Soc. (London), A157(1936)423.

25. T. Erdey-Gruz and M. Volmer, Z. phys. Chem., 150(1930)203; 162(1932)53.

26. M.W. Breiter, J. Electrochem. Soc., 109(1962)549.

27. S. Schuldiner, J. Electrochem. Soc., 109(1962)550.

28. B.E. Conway and D.M. Novak, J. Electroanal. Chem., 136(1982)191.

29. H.J.T. Ellingham and A.J. Allmand, Trans. Faraday Soc., 19(1924)748.

30. K.F. Bonhoeffer, Z. phys. Chem., A113(1924)199.

31. J.O'M. Bockris, Trans. Faraday Soc., 43(1947)417.

32. B.E. Conway and J.O'M. Bockris, J. Chem. Phys., 26(1957)532.

33. S. Trasatti, J. Electroanal. Chem., 39(1972)163.

34. A.T. Kuhn, C.J. Mortimer, G.C. Bond, and J. Lindley, J.

Electroanal. Chem., 34(1972)1

35. B.E. Conway "Theory and Principles of Electrode Processes", Ronald Press Co., N.Y., 1964.

36. P. Ruetschi and P. Delahay, J. Chem. Phys., 23(1955)195.

37. B.E. Conway, E. Beatty, and P.A.D. de Maine, Electrochim. Acta, 7(1962)39.

38. R. Parsons, Trans. Faraday Soc., 54(1958)1053.

39. M.I. Temkin, Zhur. Fiz. Khim., 15(1941)296.

40. S. Trasatti, J. Electroanal. Chem., 33(1971)351; J. Chem. Soc. Faraday I, 68(1972)229.

41. W. Libby, J. Phys. Chem., 56(1952)863.

42. N.S. Hush, J. Chem. Phys., 28(158)962;Trans. Faraday Soc., 57(1961)557.

43. R.A. Marcus, J. Chem. Phys., 24(1956)966,979; 26(1957)867; Can. J. Chem., 37(1959)155.

44. V.G. Levich and R.R. Dogonadze, Dokl. Akad. Nauk. SSSR, 124(1959)123.

45. For a review, see V.G. Levich in "Advanced Treatise of Physical Chemistry", vol.9B, H. Eyring, D. Henderson, and J. Jost, Eds., Academic Press, N.Y., 1970, p.986; and R.A. Marcus, Ann. Rev. Phys. Chem., 15(1964)155.

46. R.R. Dogonadze and A.M. Kuznetsov in "Comprehensive Treatise of Electrochemistry", vol.7, B.E. Conway, J.O'M. Bockris, E. Yeager, S.U.M. Khan, and R.E. White, Eds., Plenum Press, N.Y., 1983, p.173.

47. J. Horiuti and M. Polanyi, Acta Physicochim. SSSR, 2(1935)505.

48. R. Parsons and J.O'M. Bockris, Trans. Faraday Soc., **47**(1951)914.

49. B.E. Conway and J.O'M. Bockris, Can. J. Chem., **35**(1957)1124.

50. A.R. Despic and J.O'M. Bockris, J. Chem. Phys., **32**(1960)389.

51. R.R. Dogonadze, A.M. Kuznetsov, and V.G. Levich, Elektrokhimiya, **3**(1967)739.

52. R. Corkum and J.B. Milne, Can. J. Chem., **56**(1978)1832.

53. T. Gramstad and R.N. Hazeldine, J. Chem. Soc., (1947)4069.

54. T.G. Balicheva, V.I. Ligus, and Y.Y. Fialkov, Zh. Neorg. Khim., **18**(1973)3195.

55. F.P. Bowden, Proc. Roy. Soc. (London), **A125**(1929)446; **A126**(1929)107.

56. F.P. Bowden and R. Rideal, Proc. Roy. Soc. (London), **A120**(1928)59.

57. R.W. Gurney and E.U. Condon, Phys. Rev., **33**(1929)131.

58. For a review see M. Eigen, Disc. Faraday Soc., **24**(1957)25.

59. L. De Broglie, Ann. Phys., **10**(1925)22.

60. R.P. Bell, Proc. Roy. Soc. (London), **A139**(1933)436; **A48**(1935)241.

61. E. Wigner, Z. physik. Chem., **B19**(1933)203.

62. C. Eckart, Phys. Rev., **35**(1930)1303.

63. R.P. Bell, Trans. Faraday Soc., **55**(1959)1.

64. C.E.H. Bawn and G. Ogden, Trans. Faraday Soc., **30**(1934)432.

65. M.P. Appleby and G. Ogden, J. Chem. Soc., (1936)163.

66. B. Topley and H. Eyring, J. Am. Chem. Soc., **55**(1933)5058.

67. St. G. Christov, Z. Electrochem., **62**(1958)567.

68. St. G. Christov, Z. phys. Chem., **212**(1959)40; **214**(1960)40;

Electrochim. Acta, 4(1961)306.

69. B. Post and C.F. Hiskey, J. Am. Chem. Soc., 72(1950)4203; 73(1951)161.

70. J.O'M. Bockris, M.A.V. Devanathan, and K. Muller, Proc. Roy. Soc. (London), A274(1963)55.

71. J.O'M. Bockris and D.B. Matthews, J. Chem. Phys., 44(1966)298.

72. B.E. Conway, Can. J. Chem., 37(1959)178.

73. M. Salomon and B.E. Conway, Disc. Faraday Soc., 39(1965)223.

74. B.E. Conway, D.J. MacKinnon, and B.V. Tilak, Trans. Faraday Soc., 66(1970)1203.

75. B.E. Conway and M. Salomon, J. Chem. Phys., 41(1964)3169.

76. R.P. Bell, "The Tunnel Effect in Chemistry", Chapman and Hall, London, 1980.

77. M.J. Weaver, J. Chem. Phys., 83(1979)1748.

78. R.J. Marcus, B.J. Zwolinski, and H. Eyring, J. Phys. Chem., 58(1954)432.

79. E. Sacher and K.J. Laidler, Trans. Faraday Soc., 59(1963)396.

80. E. Sacher and K.J. Laidler in "Modern Aspects of Electrochemistry", vol.3, B.E. Conway and J.O'M. Bockris, Eds., Plenum Press, N.Y., 1964, Chap.1.

81. R.R. Dogonadze, A.M. Kuznetsov, and V.G. Levich, Electrochim. Acta, 13(1968)1025.

82. M. Falk and P.A. Giguere, Can. J. Chem., 35(1957)1195.

83. For a review of the state of the oxonium ion see P.A. Giguere, J. Chem. Educ., 56(1976)571.

84. R.R. Dogonadze and A.A. Kornyshev, J. Chem. Soc. Faraday Trans. II, 70(1974)1121.

85. L.I. Krishtalik, Electrochim. Acta, 13(1968)1045.

86. T. Ackermann, Disc. Faraday Soc., 24(1957)180.

87. L.I. Krishtalik, V.M. Tsionsky, and G.E. Titova, J. Res. Inst. Catalysis, Hokkaido Univ., 22(1974)101.

88. Y.I. Kharkats and J. Ulstrup, J. Electroanal. Chem., 65(1975)555.

89. R.R. Dogonadze and A.M. Kuznetsov, Prog. Surf. Sci., 1(1975)1.

90. A.A. Ovchinnikov, V.A. Benderskii, S.D. Babanko, and A.G. Krivenko, J. Electroanal. Chem., 91(1978)321.

91. A.M. Kuznetsov, J. Electroanal. Chem., 159(1983)241.

92. M. Falk and T.A. Ford, Can. J. Chem., 44(1966)169.

93. R.E. Moore, O. Ferral, G.W. Koeppe, and A.J. Kresge, J. Am. Chem. Soc., 93(1971)1.

94. J. Saveant and D. Tessier, Disc. Faraday Soc., 74(1982)57.

95. P.D. Tyma and M.J. Weaver, J. Electroanal. Chem., 111(1980)195.

96. M.J. Weaver and F.C. Anson, J. Phys. Chem., 80(1976)1861.

97. K.M. Joshi, W. Mehl, and R. Parsons in "Electrochemical Society Symposium on Electrode Processes", E. Yeager and P. Delahay, Eds., John Wiley, N.Y.

98. J.O'M. Bockris, I.A. Ammar, and A.K.M.S. Huq, J. Chem. Phys., 26(1958)109.

99. F.P. Bowden and F. Grew, Disc. Faraday Soc., 1(1947)86.

100. L.I. Krishtalik, Usp. Khim., 34(1965)1831; J. Electroanal.

Chem., **100**(1979)547.

101. L.I. Krishtalik, T.V. Ivanova, and D.V. Kohoulina, Elektrokhimiya, **9**(1973)200.
102. G.E. Titova and L.I. Krishtalik, Elektrokhimiya, **13**(1977)897.
103. L.I. Krishtalik and G.E. Titova, Elektrokhimiya, **13**(1977)1118.
104. L.I. Krishtalik, Faraday Disc., Chem. Soc., **74**(1982)205.
105. S.U.M. Khan in "Modern Aspects of Electrochemistry", vol.15, R.E. White, J.O'M. Bockris and, B.E. Conway, Eds., Plenum Press, N.Y., 1983.
106. D.P. Wilkinson and B.E. Conway, in course of preparation.
107. R.P. Bell, "The Proton in Chemistry", Chapman and Hall, London, 1973.
108. J.N. Brønsted and K.J. Pederson, Z. phys. Chem., **108**(1924)185.
109. J. Horiuti and M. Polanyi, Acta Physicochem. U.R.S.S., **2**(1935)505.
110. R.P. Bell, Proc. Roy. Soc. (London), **A154**(1936)414.
111. J.N. Brønsted and N.L. Ross-Kane, J. Am. Chem. Soc., **53**(1931)3024.
112. A.N. Frumkin, Z. phys. Chem., **160**(1932)116.
113. B.E, Conway in "Progress in Reaction Kinetics", G. Porter, Ed., Pergamon Press, Oxford, 1967, Chap.10, p.399.
114. R.P. Bell, J.A. Fendley, and J.R. Hulett, Proc. Roy. Soc. (London), **A235**(1956)453.
115. E.D. Sprague and F. Williams, J. Am. Chem. Soc.,

93(1971)787.

116. E.D. Sprague, J. Phys. Chem., 81(1977)516.

117. L.R.C. Barclay, D. Griller, and K.U. Ingold, J. Am. Chem. Soc., 96(1974)3011; G. Brunton, D. Griller, L.R.C. Barclay, and K.U. Ingold, J. Am. Chem. Soc., 98(1976)6803.

118. U. Stimming and W. Schmickler, J. Electroanal. Chem., 150(1983)125.

119. U. Frese, T. Iwasita, W. Schmickler, and U. Stimming, submitted for publication, July 1984.

120. Bauer, J. Electroanal. Chem., 16(1968)419.

121. N.S. Hush, Trans. Faraday Soc., 57(1961)557.

122. B.E. Conway and J.C. Currie, J. Phys. Chem., 125(1978)257.

123. B.E. Conway in "Modern Aspects of Electrochemistry", B.E. Conway and J.O'M. Bockris, Eds., Plenum Press, N.Y., 1984, in press.

124. H.P. Stout, Trans. Faraday Soc., 41(1945)64.

125. J.O'M. Bockris and R. Parsons, Trans. Faraday Soc., 45(1949)916.

126. J.O'M. Bockris, R. Parsons, and H. Rosenberg, Trans. Faraday Soc., 46(1950)918.

127. J. Horiuti, A. Matsuda, M. Enyo, and H. Kita in "First Australian Conference on Electrochemistry", Sydney/Hobart, 1963, p.21.

128. E. Yeager, D. Scherson, and B. Simic-Glavaski, Extented Abstracts of the Spring Meeting of the Electrochemical Society, San Francisco, 1983, p.1043.

129. B.E. Conway and D.M. Novak, J. Chem. Soc., Faraday Trans. I,

75(1979)2454; **77**(1981)2341.

130. A.K. Vijh and B.E. Conway, Chem. Rev., **67**(1967)623.

131. D. Gilroy and B.E. Conway, Can. J. Chem., **46**(1968)875.

132. B.E. Conway, "Ionic Hydration in Chemistry and Biophysics", Elsevier Publ. Co., Amsterdam, 1981, Chapters 3 and 23.

133. A.J. Appleby, J. Electrochem. Soc., **117**(1970)1157; see also J. Electroanal. Chem., **27**(1970)325; **24**(1970)97.

134. L.I. Krishtalik in "Comprehensive Treatise of Electrochemistry", vol.7, B.E. Conway, J.O'M. Bockris, E. Yeager, S.U.M. Khan, and R.E. White, Eds., Plenum Press, N.Y., 1983, p.107.

135. H. Goldschmidt, Z. Elektrochem., **15**(1909)4; **20**(1914)475.

136. M. Bagster and T.M. Cooling, J. Chem. Soc., (1920)693.

137. R. Richards and M. Smith, Trans. Faraday Soc., **47**(1951)1261.

138. S.Kakiuchi, I. Shono, J. Matsu, and K.J. Kigoshi, J. Phys. Soc. Japan, **7**(1952)102; J. Chem. Phys., **19**(1951)1009.

139. E.R. Andrew and R. Bersohn, J. Chem. Phys., **18**(1950)159.

140. B.E. Conway and D.F. Tessier, Int. J. Chem. Kin., Laidler Festchrift Volume, **13**(1981)925.

141. S. Luzzati, Acta Cryst., **4**(1951)239; **6**(1953)157.

142. A. Yoon and S. Carpenter, Acta Cryst., **12**(1959)17.

143. J.B. Spencer and J.-O. Lundgren, Acta Cryst., **B29**(1973)1923.

144. J.-O. Lundgren, R. Tellgren, and I. Olovsson, Acta Cryst., **B34**(1978)2945.

145. R. Beckey in "Proceegings of the Fourth International Congress on Electron Microscopy", Springer, Berlin, 1958; Z. Naturforsch., **15A**(1960)822.

146. P. Kebarle and E.W. Godbole, J. Chem. Phys., 39(1963)1131; see also B. Knewstubb and A. Tickner, ibid, 38(1963)464.

147. T. Suhrmann and W. Wiedersich, Z. Electrochem., 57(1950)93; Z. Anorg. Chem., 273(1953)166.

148. B.E. Conway, J.O'M. Bockris, and H. Linton, J. Phys. Chem., 24(1956)834.

149. K. Sherman, Chem. Rev., 11(1932)98.

150. I. Sokolov in "Hydrogen Bonding Symposium, Ljubłana", P. Hadzi, Ed., Pergamon Press, Oxford, 1959, p.402.

151. S. Lengyel and B.E. Conway, in "Comprehensive Treatise of Electrochemistry", vol.7, B.E. Conway, J.O'M. Bockris, E. Yeager, S.U.M. Khan, and R.E. White, Eds., Plenum Press, N.Y., 1983, p.339.

152. B.E. Conway and M. Salomon in "Chemical Physics of Ionic Solutions", B.E. Conway and R.G. Barradas, Eds., Wiley, N.Y., 1965, Chap.24.

153. E. Wicke, M. Eigen, and T. Ackermann, Z. phys. Chem. N.F., 1(1954)340.

154. M. Pssynskii, Acta Physicochim, URSS, 8(1938)835; T. Ulich, Z. Elektrochem., 36(1930)497; Z. phys. Chem., 108(1934)141.

155. B.E. Conway, J. Solution Chem., 7(1978)721.

156. M.M. Lister, S.C. Nyburg, and R.B. Poyntz, J. Chem. Soc., Faraday Trans. I, 70(1974)685.

157. F.H. Halliwell and S.C. Nyburg, Trans. Faraday Soc., 59(1963)1126.

158. H. Angerstein-Kozlowska and B.E. Conway, J. Electroanal. Chem., 95(1979)1.

159. B.E. Conway, H. Angerstein-Kozlowska, W.B.A. Sharp, and E. Criddle, Anal. Chem., 45(1973)1331.

160. E.L. Yee, R.J. Cave, K.L. Guyer, P.D. Tyma, and M.J. Weaver, J. Am. Chem. Soc., 101(1979)1131.

161. J.O'M. Bockris, B.E. Conway, and W. Mehl, J. Sci. Inst., 33(1956)400.

162. M. Breiter, Electrochim. Acta, 7(1962)25.

163. T.H. Ridgway and H.B. Mark, Jr. in "Comprehensive Treatise of Electrochemistry", R.E. White, J.O'M. Bockris, B.E. Conway, and E. Yeager, Eds., Plenum Press, N.Y., 1984, p.99; M.C.H. McKubre and D.D. Macdonald, ibid, p.1.

164. J. Mozota, B. Barnett, D.F. Tessier, H. Angerstein-Kozlowska, and B.E. Conway, Anal. Chim. Acta, 183(1981)191.

165. B.E. Conway, Lijun Bai, and D.F. Tessier, J. Electroanal. Chem., 161(1984)39.

166. J.M. Saveant and D. Tessier, Faraday Discussion, Chem. Soc. (London), 74(1982)57.

167. B.E. Conway and Lijun Bai in "Proceedings of the 5th Hydrogen Energy Conference, Toronto Canada" Publ. Permagon Press, N.Y., July 1984, p.879.

168. D. Britz, J. Electroanal. Chem., 88(1978)309.

169. K.A. Tellefsen, unpublished results.

170. P. Stonehart, H. Angerstein-Kozlowska, and B.E. Conway, Proc. Roy. Soc. (London), A310(1969)541.

171. N.R. de Tacconi, A.J. Calandra, and A.J. Arvia, Electrochim. Acta, 18(1973)571.

172. A.J. Calandra, N.R. de Tacconi, R. Pereiro, and A.J. Arvia,

Electrochim. Acta, 19(1974)901.

173. H. Angerstein-Kozlowska, W. Halliop, and B.E. Conway, in course of publication.

174. L. Rouillier and E. Laviron, J. Electroanal. Chem., 157(1983)193.

175. E. Laviron, J. Electroanal. Chem., 101(1979)1; 34(1972)463; 35(1972)333; 39(1972)1; E. Laviron, Bull. Soc. Chim. France, (1967)3717; E. Laviron, Electrochim. Acta, 16(1971)409.

176. H. Angerstein-Kozlowska, J. Klinger, and B.E. Conway, J. Electroanal. Chem., 75(1977)45.

177. S. Beaudoin, R. Vallot, and L.T. Yu, C.R. Acad. Sci. (Paris), 285C(1977)5.

178. C.F. Curtiss and J.O. Hirschfelder, Proc. Natl. Acad. Sci. U.S.A., 38(1952)235.

179. D. Edelson, J. Chem. Ed., 52(1975)642.

180. D.D. Warner, J. Phys, Chem., 81(1977)2329.

181. C.W. Gear, CACM, 14(1971)176; 14(1971)185.

182. B.E. Conway and P.L. Bourgault, Trans. Faraday Soc., 58(1962)593.

183. B.V. Tilak and B.E. Conway, Electrochim. Acta, 21(1976)745.

184. B.V. Tilak, C. Rader, and B.E. Conway, Electrochim. Acta, 22(1977)1167.

185. B.E. Conway and Lijun Bai, in course of publication.

186. J. Mozota, B.E. Conway, and D.F. Tessier, Anal. Chim. Acta, 141(1982)383.

187. S. Glasstone, K.J. Laidler, and H. Eyring, "The Theory of Rate Processes", McGraw-Hill Book Company, N.Y., 1941.

188. M.I. Temkin, Zhur. Fiz. Khim., 22(1948)1081.

189. D.J. MacKinnon, Ph.D. thesis, University of Ottawa, 1969.

190. E.A. Guggenheim, J. Phys. Chem., 33(1929)842; 34(1930)1540.

191. C.M. Criss and M. Salomon in "Physical Chemistry of Organic Solvent Systems", A.K. Covington and T. Dickinson, Eds., Plenum Press, N.Y., 1973, Chap.2.

192. E.D. Eastman, J. Am. Chem. Soc., 50(1928)292.

193. J.N. Agar in "Advances in Electrochemistry and Electrochemical Engineering", vol.3, P. Delahay, Ed., Wiley Interscience, N.Y., 1963, p.31.

194. A.J. de Bethune, T.S. Licht, and N. Swendeman, J. Electrochem. Soc., 106(1959)616.

195. D.D. Macdonald in "Modern Aspects of Electrochemistry", B.E. Conway and J.O'M. Bockris, Eds., Plenum Press, N.Y., 1975.

196. A.A. Seys and A.A. Van Haute, NACE, 1973.

197. A.J. de Bethune, H.O. Daley, N.A. Swendeman Loud, and G.R. Salvi, J. Electrochem. Soc., 114(1967)578.

198. M.A.V. Devanathan and M. Selvaratnan, Trans. Faraday Soc., 56(1960)1820.

199. D.G. Russel and J.B. Senior, Can. J. Chem., 52(1974)2975.

200. T.G. Balicheva, V.I. Ligus, and Yu. Ya. Fialkov, Russian J. Inorg. Chem., 18(1973)1701

201. R. Kotz, S. Clouser, S. Sarangapani, and E. Yeager, J. Electrochem. Soc., 131(1984)1097.

202. D.C. Grahame, Chem. Rev., 41(1947)441.

203. A.N. Frumkin, Z. phys. Chem., A164(1933)121.

204. I.A. Jofa, Acta Physicochim. URSS, 10(1939)903; 10(1939)326.

205. H. Jarmolowicz and M. Smialowski, J. Cat., 1(1962)165.

206. B. Baranowski and M. Smialowski, J. Phys. Chem. Solids, 12(1959)206; B. Baranowski, Z. Szklarska-Smialowski, and M. Smialowski, Second International Congress on Catalysis, Paris, 1960, paper 115.

207. B.E. Conway, H. Angerstein-Kozlowska, M.A. Sattar, and B.V. Tilak, J. Electrochem. Soc., 130(1983)1825.

208. D.M. Novak and B.E. Conway, J. Chem. Soc., Faraday Trans. I, 77(1981)2341.

209. B.E. Conway and H.P. Dhar, Croatica Chemica Acta, 45(1973)109.

210. E.R. Gonzalez and S. Srinivasan, Electrochim. Acta, 27(1982)1425.

211. E.R. Gonzalez, R. Naranjo, K.-L. Hsueh, and S. Srinivasan, Electrochim. Acta, 28(1983)165.

212. F.G. Will, J. Electrochem. Soc., 112(1965)451.

213. E. Langer, Z. Elektrochem., 44(1938)43.

214. G.N. Lewis and T.C. Doody, J. Am. Chem. Soc., 55(1933)3504.

215. Marschoff, J. Electroanal. Chem., 167(1984)281.

216. B. Barnett, Ph. D. Thesis, U. of Ottawa, 1981.

217. G.W. Walker and R.T. Foley, paper 491 presented at the Electrochemical Society Meeting, Minneapolis MN, May 1981.

218. G.W. Walker, Ph.D. Dissertation, The American University, Washington D.C., 1981.

219. B.E. Conway and J.C. Currie, J. Electrochem. Soc., 125(1978)252.

220. J.A.V. Butler, Trans. Faraday Soc., 33(1937)229.

221. B.E. Conway, J. Electroanal. Chem., **123**(1981)81.

222. S.L. Marshall and B.E. Conway, J. Chem. Phys., **81**(1984)923.

223. E.M. Eyring, L.D. Rich, L.L. McCoy, R.C. Graham, and N. Taylor, in "Advances in Chemical Physics", vol.21, Wiley-Interscience, N.Y.; M.H. Miles, E.M. Eyring, W.W. Epstein, and R.E. Ostlung, J. Phys. Chem., **69**(1965)467.

224. K.J. Laidler, "Theories of Chemical Reaction Rates", McGraw-Hill, N.Y., 1969.

225. K.J. Laidler and R. Martin, Int. J. Chem. Kin., **1**(1969)113.

226. H. Taube, "Electron Transfer Reactions of Complex Ions in Solution", Academic Press, N.Y., 1970.

227. B.E. Conway, H. Angerstein-Kozlowska, and W.B.A. Sharp, J. Chem. Soc., Faraday Trans. I, **74**(1978)1373.

228. M. Eigen and L. de Maeyer, Proc. Roy. Soc. (London), **A247**(1958)505.

229. B.E. Conway, D.F. Tessier, and D.P. Wilkinson, in course of publication.

230. K.J. Laidler and D.K.Banerjee, Can. J. Biochem., **61**(1983)1201.

231. E.A. Moelwyn-Hughes, "Physical Chemistry", Cambridge University Press, 1947.

232. J.W. Russel, M. Severson, K. Scanlon, and J. Overant, J. Phys. Chem., **88**(1984)1275.

233. W.G. Golden, K. Kunimatsu, and H. Seki, J. Phys. Chem., **88**(1984)1275.

234. D.D. Eley, Disc. Faraday Soc., **8**(1950)34.

235. C.H. Lee, A. Riga, and E. Yeager, in "Mass Transport

Phenomena in Ceramics", A.R. Copper and A.H. Heuer, Eds., Plenum Press, N.Y., 1974, pp.489-499.

236. T.R. Beck and R.M. Moulton, J. Electrochem. Soc., 103(1956)247.

237. M.H. Miles, E.A. Klaus, B.P. Gunn, J.R. Locker, W.E. Serafin, and S. Srinivasan, Electrochim. Acta, 23(1978)521.

238. K.I. Rosenthal and W.I. Veselovskii, Dokl. Akad. Nauk SSSR, III(1956)637.

239. M.R. Tarasevich, A. Sadkowski, and E. Yeager in "Comprehensive Treatise of Electrochemistry", vol.7, B.E. Conway, J.O'M. Bockris, E. Yeager, S.U.M. Khan, and R.E. White, Eds., Plenum Press, N.Y., 1983, p.

240. P. Zelenay, M.A. Habib, and J.O'M. Bockris, J. Electrochem. Soc., 131(1984)2464.

241. J.N. Agar, Trans. Faraday Soc., 1(1947)81